

Mutations that Affect the Bidirectional Electron Transfer in Photosystem I

by

Syed Lal Badshah

A Dissertation Presented in Partial Fulfillment  
of the Requirements for the Degree  
Doctor of Philosophy

Approved November 2014 by the  
Graduate Supervisory Committee:

Kevin Redding, Chair  
Ian Gould  
Petra Fromme

ARIZONA STATE UNIVERSITY

December 2014

## ABSTRACT

Photosystem I (PSI) is a multi-subunit, pigment-protein complex that catalyzes light-driven electron transfer (ET) in its bi-branched reaction center (RC). Recently it was suggested that the initial charge separation (CS) event can take place independently within each ec2/ec3 chlorophyll pair. In order to improve our understanding of this phenomenon, we have generated new mutations in the PsaA and PsaB subunits near the electron transfer cofactor 2 (ec2 chlorophyll). PsaA-Asn604 accepts a hydrogen bond from the water molecule that is the axial ligand of ec2<sub>B</sub> and the case is similar for PsaB-Asn591 and ec2<sub>A</sub>. The second set of targeted sites was PsaA-Ala684 and PsaB-Ala664, whose methyl groups are present near ec2<sub>A</sub> and ec2<sub>B</sub>, respectively. We generated a number of mutants by targeting the selected protein residues. These mutations were expected to alter the energetics of the primary charge separation event.

The PsaA-A684N mutants exhibited increased ET on the B-branch as compared to the A-branch in both *in vivo* and *in vitro* conditions. The transient electron paramagnetic resonance (EPR) spectroscopy revealed the formation of increased B-side radical pair (RP) at ambient and cryogenic temperatures. The ultrafast transient absorption spectroscopy and fluorescence decay measurement of the PsaA-A684N and PsaB-A664N showed a slight deceleration of energy trapping. Thus making mutations near ec2 on each branch resulted into modulation of the charge separation process. In the second set of mutants, where ec2 cofactor was target by substitution of PsaA-Asn604 or PsaB-Asn591 to other amino acids, a drop in energy trapping was observed. The quantum

yield of CS decreases in Asn to Leu and His mutants on the respective branch. The  $P_{700}$  triplet state was not observed at room and cryogenic temperature for these mutants, nor was a rapid decay of  $P_{700}^{+}$  in the nanosecond timescale, indicating that the mutations do not cause a blockage of electron transfer from the ec3 Chl. Time-resolved fluorescence results showed a decrease in the lifetime of the energy trapping. We interpret this decrease in lifetime as a new channel of excitation energy decay, in which the untrapped energy dissipates as heat through a fast internal conversion process. Thus, a variety of spectroscopic measurements of PSI with point mutations near the ec2 cofactor further support that the ec2 cofactor is involved in energy trapping process.

## ACKNOWLEDGEMENTS

First of all I thank my supervisor Dr. Kevin Redding for his guidance and cooperation throughout my Ph.D. work. Without his support, it was not possible.

I would like to thanks to my committee members, Prof. Ian Gould and Prof. Petra Fromme for their time and support.

I am thankful to members of our Lab, Patricia Baker, Zahid Khan, Michael McConnell, Kiera Reifschneider, Trevor Kashey, and John Cowgill for all of the help when I started working on this project. A large portion of my understanding of isolating and purifying Photosystem I protein comes from Michael McConnell and Patricia Baker.

I would also like to thank Dr. Su Lin for showing me how to set up time-correlated single photon counting and ultrafast transient absorption spectroscopic instruments and analyzing the data.

I am thankful to Dr. Art van der Est and his students Reza Siavashi, Sam Mula of Brock University, Canada for doing EPR on our PSI samples. I would also like to thank Prof. John Golbeck and his students Junlei Sun and Michael Gorka at the Pennsylvania State University, USA for analyzing our samples on Optical transient spectroscopy. Thanks to Prof Gary Hastings and his student Nan Zhao of Georgia State University, USA for doing FTIR of our samples. I also appreciate the help of Dr. Fabbrice Rappaport of Institut de Biologie Physico-Chimique, France, in analyzing our PSI samples in-vivo by transient optical spectroscopy.



I must acknowledge the National Science Foundation for supporting this research through a grant awarded to Dr. Redding. I am also thankful to Fulbright Commission; US Department of State for their student scholarship.

## TABLE OF CONTENTS

	Page
LIST OF TABLES.....	xii
LIST OF FIGURE.....	xiv
LIST OF SYMBOLS/ NOMENCLATURE.....	xix
CHAPTER	
1. INTRODUCTION.....	1
1.1. Photosystems.....	1
1.2. Light Harvesting Complexes.....	1
1.3 Light Harvesting Complex I.....	3
1.4 Light Harvesting Complex II.....	5
1.5 Photosystem I.....	6
1.6 Light Harvesting Pigments of Photosystem I.....	10
1.6.1 Chlorophyll a.....	10
1.6.2 Chlorophyll b.....	10
1.6.3 Carotenoids.....	10
1.7 Red chlorophylls.....	11
1.8 Types of Electron Transfer in Photosystem I.....	12
1.8.1 Linear Electron Flow.....	12
1.8.2 Cyclic Electron Flow.....	13

CHAPTER	Page
1.9 Excitation Energy Transfer and Trapping in PSI.....	15
1.9.1 Diffusion/Migration Limited Model.....	16
1.9.2 Trap Limited Model.....	16
1.9.3 Transfer to the Trap Limited Model.....	16
1.10 Theoretical Description of Electron Transfer.....	17
1.10.1 Normal Regime.....	17
1.10.2 Activationless Regime.....	18
1.10.3 Inverted Regime.....	18
1.11 Role of Protein Environment.....	19
1.11.1 Electronic Coupling.....	19
1.11.2 Free Energy.....	19
1.11.3 Reorganization Energy.....	20
1.12 Bi-directionality of Electron Transfer in Photosystem I.....	20
1.13 Primary Charge Separation in Photosystem I.....	26
1.14 Aims and Objectives.....	28
2.1 INTRODUCTION.....	35
2.2 MATERIAL AND METHODS.....	41
2.2.1 Genetic Manipulation of Mutants.....	41
2.2.2 Crude Membrane Preparation.....	42
2.2.3 Immunoblot Analysis.....	42

CHAPTER	Page
2.2.4 Spectroscopic Estimation of PSI ( $P_{700}$ ).....	44
2.2.5 Growth Analysis.....	45
2.2.6 Transient Optical Spectroscopy of <i>In Vivo</i> PSI.....	45
2.2.7 Isolation of H6-PSI.....	46
2.2.8 Ultrafast Transient Absorption Spectroscopy.....	47
2.2.9 Time-Resolved Fluorescence.....	48
2.2.10 Electron Paramagnetic Spectroscopy.....	49
2.2.11 Low-Temperature EPR.....	50
2.3 RESULTS.....	49
2.3.1 Immunological and Spectroscopic .....	49
2.3.2 Growth of PSI Mutants Strains.....	54
2.3.3 In Vivo Transient Absorption Spectroscopy.....	57
2.3.4 Femtosecond Transient Absorption Spectroscopy.....	61
2.3.5 Time-Resolved Fluorescence Decay.....	62
2.3.6 Room-Temperature Transient EPR Spectroscopy.....	65
2.3.7 Low-Temperature Transient EPR Spectroscopy.....	70
2.3.8 Out of Phase Echo Envelope Modulation.....	73
2.3.9 Measurement of $^3P_{700}$ Triplet by TR-EPR at Low- Temp.....	76
2.4 DISCUSSION.....	79
2.4.1 Charge Separation at Room Temperature.....	81
2.4.2 Change in the Spectrum of $P_{700}$ and the RC Chl(s).....	82

CHAPTER	Page
2.4.3 Charge Separation at Low-Temperature.....	83
2.5 CONCLUSIONS.....	89
2.6 SUPPLEMENTARY INFORMATION.....	90
2.61 <i>In Vivo</i> Transient Absorption Spectroscopy.....	90
3.1 INTRODUCTION.....	99
3.2 MATERIALS AND METHODS.....	105
3.2.1 Genetic Manipulations.....	105
3.2.2 Crude Membrane Preparation.....	106
3.2.3 Growth Assays.....	106
3.2.4 Isolation of H <sub>6</sub> -PSI particles.....	107
3.2.5 Immunoblot Analysis.....	108
3.2.6 Spectroscopic Estimation of PSI (P <sub>700</sub> ).....	109
3.2.7 Time-resolved Optical Spectroscopy of PSI Particles.....	111
3.2.8 Electron Paramagnetic Resonance (EPR) Spectroscopy.....	112
3.2.9 Ultrafast Transient Absorption Spectroscopy.....	113
3.2.10 Time-Resolved Fluorescence.....	114
3.2.11 Static Fourier Transformed Infrared Difference.....	115
3.3 RESULTS.....	115
3.3.1 Biochemical Characterization.....	115
3.3.2 Spectroscopic Estimation of PSI (P <sub>700</sub> ).....	118

CHAPTER	Page
3.3.3 Growth Characteristics.....	123
3.3.4 Kinetics at 390 nm in Living Cells.....	126
3.3.5 Nanosecond Kinetics at 480 nm .....	127
3.3.6 Charge Recombination.....	133
3.3.7 Low Temperature Transient EPR Spectra of $P_{700}^{++}PhQ^{--}$ .....	138
3.3.8 Room Temperature Transient EPR Spectroscopy.....	142
3.3.9 Observation of $P_{700}$ Triplet.....	145
3.3.10 Ultrafast Transient Absorption Spectroscopy.....	147
3.3.11 Time-Resolved Fluorescence .....	156
3.3.12 FTIR Spectroscopy .....	162
3.3.12.1 FTIR Difference Spectra of WT PS1.....	162
3.3.12.2 Double Difference Spectrum of Two WT.....	163
3.3.12.3 . FTIR Difference Spectra of Asp .....	165
3.3.12.4 FTIR Difference Spectra of Lys.....	172
3.3.12.5 FTIR Difference Spectra of Leucine.....	178
3.4 DISCUSSION .....	180
3.5 CONCLUSIONS.....	188
3.6 SUPPLEMENTARY INFORMATION.....	188
3.6.1 Room Temperature Absorbance Spectroscopy.....	188
4.1 INTRODUCTION.....	190

CHAPTER	Page
4.2 MATERIALS AND METHODS.....	195
4.2.1 Genetic Manipulations.....	195
4.2.2 Isolation of H <sub>6</sub> -PSI Particles.....	196
4.2.3 Time-Resolved Optical Spectroscopy.....	197
4.2.4 Quantum Yield of Charge Separation.....	199
4.2.5 EPR Spectroscopy.....	200
4.2.6 Ultrafast Transient Absorption Spectroscopy.....	201
4.2.7 Time-Resolved Fluorescence.....	201
4.3 RESULTS.....	202
4.3.1 Nanosecond Kinetics at 480 nm.....	204
4.3.2 Charge Recombination .....	207
4.3.3 Quantum Yield of Charge Separation.....	213
4.3.4 Room Temperature Transient EPR Spectroscopy.....	214
4.3.5 Low-Temperature TREPR Spectra of P <sub>700</sub> <sup>•+</sup> PhQ <sup>•-</sup> .....	219
4.3.6 Ultrafast Transient Absorption Spectroscopy.....	225
4.3.7 Time-Resolved Fluorescence.....	237
4.4 DISCUSSION.....	242
4.4.1 The ec2 Cofactor as a Primary Electron Donor.....	242
4.4.2 Absence of <sup>3</sup> P <sub>700</sub> .....	243
4.4.3 Models of Excitation Energy Decay.....	244
4.4.4 Difference in the Lifetimes.....	246

CHAPTER	Page
4.4.5 New Channel.....	248
4.5 CONCLUSIONS.....	250
4.6 SUPPLEMENTARY INFORMATION.....	251
5.0 SUMMARY.....	267
REFERNCES.....	271



## LIST OF TABLES

Table	Page
1.1 Table of Mutants.....	34
2.1 Quantification of PS1 in Membranes from Different Mutants.....	51
2.2 Fitting Parameters of <i>In Vivo</i> Transient Optical Data.....	58
2.3 Global Fitting parameters of RT-EPR.....	69
S2 Supplementary Tables.....	90
S2.1 Lifetimes of Energy Equilibration in Antenna.....	90
3.1 Quantification of P <sub>700</sub> Bleaching.....	120
3.2 Ratio of Slow: Fast Decay at 390 nm in Living Cells.....	127
3.3 Rates and Amplitudes of Decay Components at 480 nm.....	130
3.4 Rates and Amplitudes of Decay Components in the ns-s at 820 nm.....	135
3.5 DADS of WT and Mutant PSI.....	152
3.6 Difference of Fast and Slow Excitation Energy.....	158
3.7 Stretching Frequencies of P <sub>700</sub> of WT PSI.....	163
4.1 Rates and Amplitudes at 480 nm.....	205
4.2 Rates and Amplitudes of Decay Components in the ns-s at 820 nm.....	211
4.3 Quantum Yield of Charge Separation.....	231
4.4 Three Components of DADS.....	240
S4 Supplementary Tables.....	251

Table	Page
S4.1 Rates and Amplitudes of Decay Components in the ns at 480 nm.....	251
S4.2 Rates and Amplitudes of Decay Components in the ns-s at 820 nm.....	252
S4.3 Quantum Yield of Charge Separation Calculated at 703 nm.....	253

## LIST OF FIGURES

Figure	Page
1.1 Model of <i>C. reinhardtii</i> PSI-Core Complex.....	5
1.2 Schematic Diagram of PSI Subunits.....	9
1.3 Cyclic Electron Flow Between PSI.....	14
1.4 Reaction Center of Photosystem I.....	31
1.5 Sequence alignment of PS1 helix 9 of PsaA and PsaB.....	32
1.6 Sequence Alignment of PS1 Helix 10 of PsaA and PsaB.....	33
2.1 Reaction Center of PSI.....	39
2.2 Immunoblot of PsaA-A684 and PsaB-A664 mutants.....	53
2.3 Light Induced DS of PsaA-A684 and PsaB-A664 mutants.....	54
2.4 Growth Test of PsaA-A684 mutants.....	56
2.5 Growth Test of PsaB-A664 mutants.....	57
2.6 Decay of Flash Induced Absorption Changes at 395 nm.....	60
2.7 DADS of Energy Equilibration.....	63
2.8 Decay Associated Fluorescence Emission Spectra.....	66
2.9 Room Temperature X-band Spin Polarized Transient EPR Spectra.....	70
2.10 Spin Polarized Transient EPR Spectra.....	72
2.11 Simulations of Q-Band EPR Spectra.....	75
2.12 Time Dependence of the OOP-ESEEM.....	75
S2.0 Supplementary Figures.....	87

Figure	Page
S2.1 Sequence Alignment of PS1 Helix 10 of PsaA and PsaB.....	91
S2.2 Position of Alanine Residue Between ec2 and ec3 Chlorophyll.....	92
S2.3 Normalized Light Induced Difference Spectra.....	93
S2.4 Absorption Spectra of PSI.....	94
S2.5 Transient Absorption DS at Different Delay Times.....	95
S2.6 DADS of WT (A), PsaA-A684N (B) and PsaB-A664N.....	96
S2.7 Kinetic Traces at 680, 695 and 730 nm.....	97
S2.8 X-Band TR-EPR Spectra at 80 K.....	98
3.1 X-Band TR-EPR Spectra at 80 K.....	104
3.2 Western Blot of PsaA-N601 and PsaB-N587 Transformants.....	118
3.3 Normalized Light Induced Difference Spectra of $P_{700}$ of ec2 <sub>A</sub> .....	121
3.4 Normalized Light Induced Difference Spectra of $P_{700}$ of ec2 <sub>B</sub> .....	122
3.5 Growth on Solid Media.....	124
3.6 Growth on Solid Media.....	125
3.7 Time-resolved Optical Spectroscopic Kinetics at 480 nm.....	131
3.8 Time-resolved Optical Spectroscopic Kinetics at 480 nm.....	132
3.9 $P_{700}^{+}$ Reduction kinetics Monitored at 810 nm.....	138
3.10 $P_{700}^{+}$ Reduction Kinetics Monitored at 810 nm.....	136
3.11 Low Temperature Spin Polarized X-Band Transient EPR Spectra.....	141
3.12 Spin Polarized X-Band Room Temperature Transient EPR of WT.....	143
3.13 Spin Polarized X-Band Room Temperature Transient EPR.....	144

Figure	Page
3.14 Comparison of the Triplet Spectra of PSI.....	146
3.15 Transient Absorption Difference Spectra.....	153
3.16 Transient Absorption Difference Spectra.....	154
3.17 Normalized Decay Associated Difference Spectra.....	155
3.18 TCSPC of WT PSI Particle.....	159
3.19 Decay Associated Spectra (DAS) of PSI Particles.....	160
3.20 Decay-Associated Spectra (DAS) of PSI Particles.....	161
3.21 FTIR Difference Spectra of WT-A and WT-B.....	164
3.22 Double Difference Spectrum of WT.....	165
3.23 FTIR Difference Spectra of PsaA-N601D.....	168
3.24 FTIR Difference Spectra of PsaA-N601D.....	169
3.25 FTIR Difference Spectra of PsaB-N587D.....	170
3.26 FTIR Difference Spectra of PsaB-N587D.....	171
3.27 FTIR Difference Spectra of PsaA-N601K.....	175
3.28 FTIR Difference Spectra of PsaA-N601K.....	176
3.29 FTIR Difference Spectra of PsaB-N587K.....	177
3.30 FTIR Difference Spectra of PsaB-N587K.....	178
3.31 FTIR Difference Spectra of PsaA-N601L .....	180
3.32 Proposed Models of Excitation Energy Decay.....	187
S3.1 Room Temperature Absorbance Spectra of PSI Particles.....	189
4.1 Arrangement of Electron Transfer Cofactors in RC of PSI.....	194

Figure	Page
4.2 Transient Absorbance Difference Traces at 480 nm.....	206
4.3 Transient Absorbance Difference Traces at 820 nm.....	212
4.4 The Amount of Stable Charge Separation.....	214
4.5 Spin Polarized X-Band Room Temperature Transient EPR.....	217
4.6 Spin Polarized X-Band room Temperature Transient EPR.....	218
4.7 Low Temperature Spin Polarized X-Band Transient EPR.....	223
4.8 Low Temperature Spin Polarized X-Band.....	224
4.9 Transient Absorption Difference Spectra.....	232
4.10 Energy Trapping Component of DADS.....	233
4.11 Non Decaying Component of Normalized DADS.....	234
4.12 Energy Trapping Component of DADS.....	235
4.13 Long Lived Component of DADS.....	236
4.14 Decay Associated Fluorescence Spectra.....	241
4.15 Proposed Models of Excitation Energy Decay.....	246
S4 Supplementary Figures.....	254
S4.1 Room Temperature Absorbance Spectra of WT.....	254
S4.2 Transient Absorbance Difference Traces at 480 nm.....	255
S4.3 Transient Absorbance Difference Traces at 820 nm.....	256
S4.4 Comparison of the Spin Polarized Transient X-Band EPR.....	257
S4.5 Spin Polarized Transient EPR Spectra of Chl Triplet States.....	258
S4.6 Spin Polarized Transient EPR Spectra of Chl Triplet States.....	259

Figure	Page
S4.7 Transient Absorption Difference Spectra of PSI Trimers.....	260
S4.8 Energy Trapping Component from DADS.....	261
S4.9 Long Lived Component from DADS.....	262
S4.10 Kinetics of WT; PsaA-N601L and PsaB-N587L .....	263
S4.11 Kinetics of WT, PsaA-N604H and PsaB-N591H.....	264
S4.12 Decay Associated Fluorescence Spectra.....	265
S4.13 Decay Associated Fluorescence Spectra.....	266

## LIST OF ABBREVIATIONS

Symbol	Definition
PSII.....	Photosystem II
PSI .....	Photosystem I
NADP <sup>+</sup> .....	Nicotinamide adenine dinucleotide phosphate (Oxidized form)
NADPH.....	Nicotinamide adenine dinucleotide phosphate (Reduced form)
ADP .....	Adenosine dinucleotide phosphate
ATP .....	Adenosine trinucleotide phoasphate
Pi .....	Inorganic Phosphate
Cyt <b><i>b</i>6<i>f</i></b> .....	Cytochrome <i>b6f</i>
Fd .....	Ferredoxin
Cyt-c.....	Cytochrome c
RC .....	Reaction Center
EET .....	Excitation Energy Transfer
ET.....	Electron Transfer
CS .....	Charge Separation
CR .....	Charge Recombination
ec.....	Electron transfer Cofactor
Pc .....	Plastocyanin
NPQ .....	Non photochemical quenching
DADS.....	Decay associated difference spectra
DAS.....	Decay associated spectra
OOP-ESEEM .....	Out of phase electron spin echo envelope modulation
EPR.....	Electron paramagnetic resonance spectroscopy



FTIR..... Fourier transform infra-red spectroscopy  
RT.....Room temperature  
TR .....Time-resolved  
JTS..... Joliot type spectrophotometer  
TCSPC..... Time correlated single photon counting  
IRF.....Instrument response function

## 1. INTRODUCTION

Photosynthesis means “synthesis with light”. It is the process by which light energy is harvested for the production of nicotinamide adenine dinucleotide phosphate (NADPH) and adenosine triphosphate (ATP) through splitting of water into protons, oxygen and electrons in the light reaction. The NADPH and ATP are utilized for carbon dioxide fixation into reduced sugar in the Rubisco complex in the dark reaction. In photosynthesis, water is split by the oxygen evolving complex (OEC) of Photosystem II (PSII), whose mechanism is not yet fully established. The electrons are transported from PSII to PSI via the cytochrome *b<sub>6</sub>f* complex and plastocyanin. The electrons transferred from PSI to ferredoxin are utilized by ferredoxin NADP<sup>+</sup> reductase (FNR) enzyme for the reduction of NADP<sup>+</sup> to NADPH, which is used for the reduction of CO<sub>2</sub> into carbohydrates. The protons generated establish a proton gradient across the membrane. ATP synthase used this proton gradient for the synthesis of ATP from ADP and P<sub>i</sub> (1).

### 1.1 Photosystems

In Oxygenic photosynthesis, there are two membrane-bound Photosystems. These are Photosystem II (PSII) and Photosystem I (PSI). Photosystem II is type II RC where mobile quinones are the terminal electron acceptor. Photosystem I (PSI) is a type I RC, where the iron-sulfur cluster acts as a terminal electron acceptor.

### 1.2 Light harvesting complexes

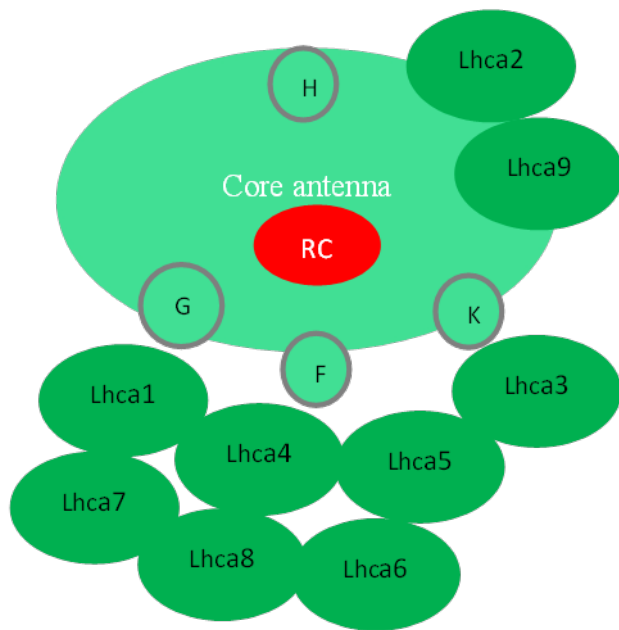
Nature has mastered the efficient capture of sunlight energy by densely packing pigments in the core antenna and external antenna called light-harvesting complexes. The initiation of light capture and its regulation takes place in these complexes. The absorbed energy is transferred in the time range of tens to hundreds of ps to the reaction center (RC). The excitation energy is trapped in the form of a charge-separated state has a lifetime from nanoseconds to milliseconds. This transient charge-separated state generates an electrochemical potential, which is used to drive other biological processes. The main function of light harvesting complexes is to capture the high number of incoming solar photons. Thus, LHC enhances the ability of the RC, by increasing the absorption surface area almost 100 fold and enhancing the turnover rate of charge separation of RC by providing excitation energy to it. Through this efficient harvesting mechanism, different organisms attain the ability to live in low light conditions. The photosynthetic pigments like chlorophylls, linear tetrapyrroles (i.e. bilins) and carotenoids (e.g.  $\beta$ -carotene and lutein in plants, fucoxanthin and peridinin in certain algae) perform the light harvesting function. These pigments have high molar extinction coefficients. Furthermore, they are present at high concentration; for example, the effective concentration of chlorophyll *a* is 0.25 M in LHCII and 0.5 M in PSI. The spatial and energetic landscape of the pigments in photosynthetic complexes is important for high quantum efficiency (2). Quantum efficiency is the number of electrons produced per the number of photons absorbed by the photosystem (3). The high efficiency is made possible due to: a) fast energy transfer, b) avoidance of quenching, c) maximization of charge separation. According to the Förster theory of energy transfer, the rate of excitation energy transfer depends upon the distance

between donor and acceptor. The shorter the distance between the two pigments, the faster the energy transfers; proper orientation is also necessary. At the lower limit of 1.5 nm distance ( $R$ ) between the two pigments, the transfer rate is directly proportional to  $R^{-6}$ . A decrease in the distance between the neighboring pigments results in the delocalization of excitation energy over them. If the pigments are too close then quenching causes conversion of excitation energy to heat, lowering the quantum efficiency. Naturally the protein puts the chlorophylls and carotenoid molecules at a proper distance and geometry that is appropriate for fast energy transfer but not for excited state quenching. Proteins tune the energy levels of pigments by controlling its wavelength for maximum absorption. Simultaneously their vibrations (phonons) can couple to the electronic transition of chlorophylls/carotenoids to broaden the absorption spectra and helps in uphill and downhill type of energy transfer. Energy transfer occurs spontaneously from higher energy absorbing pigments towards lower energy absorbing pigments. This downward flow of energy in the photosynthetic complexes is called the deep funnel model, which is present in phycobilisomes (external antenna) of cyanobacteria. In the antenna complexes of green algae and plants, the pigments are isoenergetic, and energy transfer process between pigments is fast (4).

### 1.3 Light harvesting complex I

LHCI is the external antenna of PSI. There are nine light harvesting antenna (Lhca) polypeptide antennas in *C. reinhardtii* PSI-LHCI (Figure 1.1) (5, 6). This complex is larger than that of the PSI-LHCI complex of plants. A projection map developed at 15-Å resolution by electron microscopy showed that the nine Lhca are present in two half rings

around one side of PSI. Lhca2 and Lhca9 are the red-most antenna complexes and are lightly connected to the PSI core complex in a 1:1 ratio (7). The land plant PSI-LHCI structure at 3.3 Å resolution revealed 4 Lhca attached on one side of the PSI core (8, 9). There are two extra Lhca 5 and 6 identified in *Arabidopsis thaliana* (A.t), but a combination of both is present in a small amount as compared to other Lhca (10). In *C. reinhardtii*, the LHCI is accumulated even when PSI is deleted by removing *psaB* gene, so a decrease in PSI amount has no effect on the LHCI. The Lhca1 and Lhca4 to Lhca8 bind to PSI firmly, while Lhca2, Lhca3 and Lhca9 are loosely attached and lost during the purification process (7). This phenomenon causes problems in poorly accumulated PSI mutant due to stability issues. We faced such problems for most of the mutants, and it causes difficulty to obtain proper signals from ultrafast transient absorption spectroscopy. The variability in the number of Lhca attached to PSI causes variation in the lifetime of excitation energy transfer and energy trapping in *C. reinhardtii* PSI complex (11).



**Figure 1.1.** Model of *C. reinhardtii* PSI-Core complex (7).

#### 1.4 Light harvesting complex II (LHCII)

LHCII is considered the world's most abundant light harvesting antenna protein. They are photosynthetic complexes that absorb the initial excitation energy and transfer it to PSII via its core antenna. At high light conditions, the extra energy absorbed is dissipated as heat through a process called non-photochemical quenching in order to protect the RC and to avoid the production of harmful radicals (12). There are six light harvesting complex b (Lhcb), which are present in various combinations. Lhcb1, Lhcb2 and Lhcb3

make the major trimeric LHCII complex. Lhcb4 (CP29), Lhcb5 (CP26) and Lhcb6 (CP24) are connected to the core of PSII in the form of a complex. The combination and association of these antennas vary in different plants. During state transition, a few trimeric LHCII complexes move from PSII to PSI at high light conditions. (13). Recent investigations have shown that during normal light conditions the LHCII acts as an antenna for both PSI and PSII in plants. Further, the LHCII acts as a better light-capturing complex than that of LHCI for PSI (14). The 2.7Å crystal structure of spinach major LHC II shows that there is one monomer in a single icosahedral proteoliposome assembly, and each monomer has 14 chlorophyll molecules. In these 14 molecules, 8 are chlorophyll *a* and 6 are chlorophyll *b* molecules. The latter is present at the periphery and in between monomers, which help in efficient energy transfer between chlorophylls among the monomers. Each monomer contains four carotenoids molecules(15). In *C. reinhardtii* the chlorophyll *a/b* ratio is slightly lower than that of the plants LHCII and due to this reason its spectrum is blue shifted. There is a minimum of six LHCII trimers per the dimeric core of PSII in *C. reinhardtii*, which is higher than plants PSI (12).

## 1.5 PHOTOSYSTEM I

The PSI core protein coordinates about 100 chlorophylls and 20  $\beta$ -carotenes. The primary and tertiary structure is highly conserved between green algae and plants. There are 14 subunits present in green algae and plants; these include PsaA to PsaL and PsaN to PsaO. The PsaP subunit is present only in plants. In cyanobacteria, there are 12 subunits of PSI.

The PsaA and PsaB subunits are the largest subunits with a molecular weight of 82-83 kDa (Figure 1.2). They have low amino acid sequence identity and together form a heterodimer that is the core of PSI. The carboxyl termini of each subunit has five transmembrane  $\alpha$ -helices that form the RC and surround the pigment molecules involved in electron transfer. The N-terminal portion of PsaA/B consists of six transmembrane  $\alpha$  helices and mainly binds core antenna pigments. Together PsaA and PsaB bind 85 chlorophylls of the core antenna. The remaining 11 chlorophylls are bound to other subunits, including PsaL, K, J, M and X. The chlorophylls form two layers, one on the stromal and one on the luminal side; there are also a few chlorophylls between the two layers. The position and orientation of the core antenna chlorophylls in PSI are almost similar from cyanobacteria to plants.

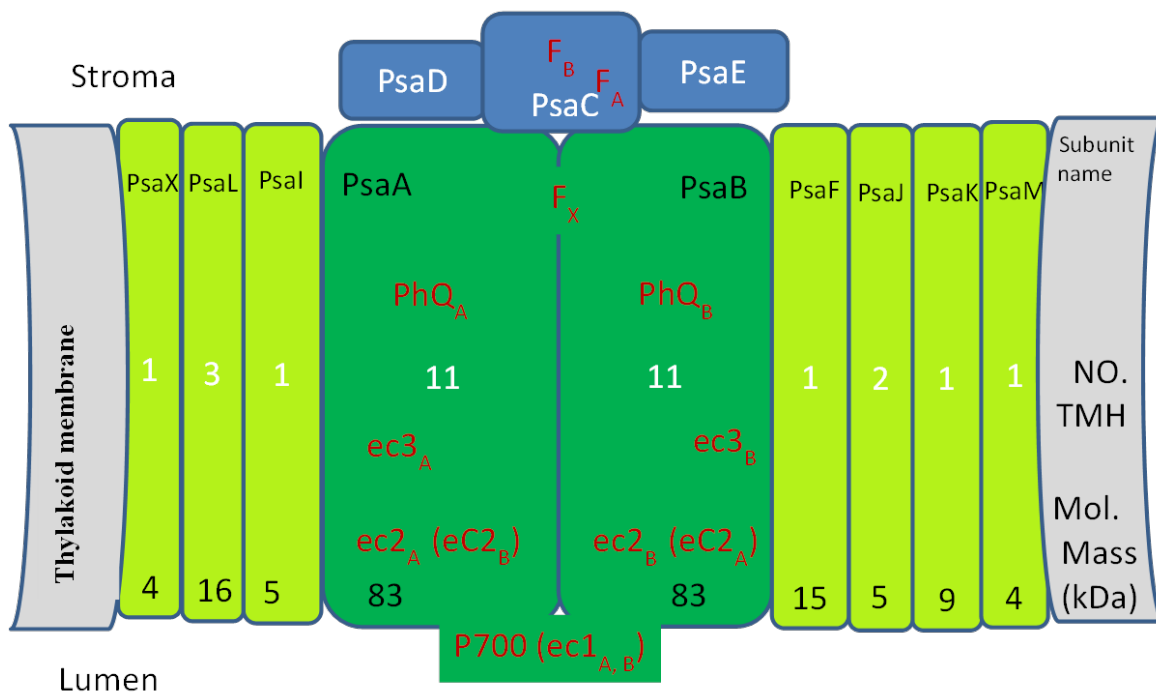
The PsaF and PsaN help in binding plastocyanin for optimal electron transfer to P700 (16). The PsaF helps in electrostatic interaction with plastocyanin (17) while, in *A. thaliana*, lack of PsaN subunit showed a decrease of approximately 50 % P<sub>700</sub> reduction activity (18). PsaJ is a hydrophobic subunit near PsaF that stabilizes it in the correct conformation for binding to plastocyanin (19). PsaH, I, L, O and P make a cluster on one side and interact with LHCII during the state transition phenomenon (20). PsaG and PsaK help in interaction with different Lhca proteins. PsaL plays a role in the trimerization of PSI in cyanobacteria, and its deletion causes prevention of the trimerization (8, 9, 21-24).

The RC of PSI contains six chlorophyll *a* molecules, two phylloquinone (PhQ) and three iron-sulfur clusters. These pigments are arranged in a pseudo-C2



symmetry, making two similar branches emanating from the dimeric  $P_{700}$ . There is a pair of ec2 and ec3 chlorophyll and a phylloquinone (PhQ) molecule on each side. The two branches meet at the first iron sulfur cluster, known as  $F_X$ . There are two additional iron-sulfur clusters, called  $F_A$  and  $F_B$ , present in the PsaC subunit, which is a peripheral subunit bound at the PsaA/PsaB interface on the stromal side. The cofactors of RC interact with various amino acids in the protein via different interactions.  $P_{700}$  is a dimer of chlorophyll *a* molecules, which are approximately 3.6 Å apart and perpendicular to the membrane plane. The A-side chlorophyll *a* ( $P_A$ ) is a C-13 epimer of chlorophyll *a*, called chlorophyll *a'*. It makes two hydrogen bonds, one with the threonine residue of protein and another with a water molecule, while  $P_B$  has no hydrogen bonding interactions. Due to this asymmetry in H-bonding and other factors like *Chl a'*, the protein environment around  $P_{700}$ , the spin density distribution is mostly on  $P_B$  (25). Histidine acts as a fifth ligand to the central magnesium of each chlorophyll of  $P_{700}$  (21, 26, 27). The ec2 cofactor are the proposed as primary electron donors (11, 28, 29). The axial ligand of ec2 is a water molecule that makes a hydrogen bond to a nearby asparagine residue from the polypeptide that surrounds the opposite branch of the RC mostly. The central magnesium of ec3 is bound to a methionine, whose sulfur atom donates a coordinate covalent bond. The central magnesium atom of *Chl a* is a hard Lewis acid, which makes a coordinate covalent bond with a hard Lewis base. This hard Lewis base includes nitrogen or oxygen of amino acids like histidine, glutamine and asparagine. The sulfur of methionine is exception, which is a soft Lewis base, making this an unusual choice (30, 31). The ec3 chlorophyll also accepts a hydrogen bond from a tyrosine residue on each branch. The

next cofactor is PhQ, which accepts a hydrogen bond from a backbone amide of a leucine residue. Each PhQ is also in a  $\pi$ -stacking interaction with a tryptophan side chain. The final cofactor at the junction of the two branches is F<sub>X</sub>, a [4Fe4S] cluster which ligates two cysteine thiolates from PsaA and PsaB subunits (8, 21).



**Figure 1.2.** Schematic Diagram of PSI subunits and the number of trans-membrane helices in them.

## 1.6 LIGHT HARVESTING PIGMENTS OF PSI

The main pigments of PSI include Chlorophyll *a*, *b*, and Carotenoids. These are discussed as follows:

### 1.6.1 Chlorophyll *a*

Chlorophyll *a* is the sole chlorophyll present in PSI and PSII. The absorption spectrum of *Chl a* in pyridine shows two major absorption bands. These are the Soret band at 443 nm and the  $Q_Y$  band at 671 nm. The weaker  $Q_X$  band is not very prominent. The fluorescence emission peaks at 677 nm and has a Stokes shift of  $132\text{ cm}^{-1}$  as compared to the  $Q_Y$  band. There is also a small vibronic band at 737 nm and its relative intensity to the major peak is 0.15 (32).

### 1.6.2 Chlorophyll *b*

Chlorophyll *b* is present in light-harvesting complexes of the PSI and PSII of green algae and plants. The absorption spectra of *Chl b* shows that the Soret band is at 473 nm while the  $Q_Y$  band is at 656 nm and has quite different intensities. The fluorescence spectrum of chlorophyll *b* shows that it has a maximum peak at 662 nm and has a Stokes shift of  $161\text{ cm}^{-1}$  and also has an obvious vibronic band at 721 nm and a relative intensity of 0.19, represented (32).

### 1.6.3 Carotenoids

The function of  $\beta$ -carotene is light harvesting and protection under excessive light and it quenches the triplet state of chlorophyll ( $^3\text{Chl}$ ). The  $\beta$ -carotene absorbs in the visible region between 450 to 525 nm region. Smaller conjugated carotene mutant PSI were

unable to quench this energy from  $^3\text{Chl}$ . As a result, the formation of singlet oxygen  $^1\text{O}_2$  is unavoidable, which causes damage to PSI. (32).

## 1.7 RED CHLOROPHYLLS

Chlorophylls absorbing at longer wavelength than the  $P_{700}$  are called red chlorophylls. The spectral characteristics of these chlorophyll molecules include absorption at the red edge of the spectrum with broad bandwidth due to high electron-phonon coupling. In *Thermosynechococcus elongatus* these *Chl a* molecules are denoted as C-708, C-715 and C719. These chlorophylls are present either in dimeric form or lying very close to one another in the protein environment (33). The red chlorophylls are present either in the core antenna of PSI of cyanobacteria or the LHCI of higher plants (Lhca3 and Lhca4) and algae. Energy trapping in the absence of red chlorophylls is trap limited in the PSI RC. The influence of red chlorophylls on energy trapping lifetime is four times larger than that of PSI with increase in the size of its external antenna (34). The energy trapping process in PSI containing red chlorophylls is trap limited, and these chlorophylls slow down the process by 60% (35). In the case of *C. reinhardtii* PSI, these are present in Lhca2 and Lhca9; these subunits are loosely attached to PSI and fall off during isolation. The absorption maxima of these antennas carrying red chlorophylls are between 707 and 715 nm and are referred to as red forms (36-38). The red chlorophylls increase the absorption range of the antenna of PSI and can provide protection against high light by dissipating energy as heat (36, 39). The longest decay of excited state red chlorophyll is about 100 ps, so they have little effect on the quantum efficiency of PSI (34). The cyanobacterium *Arthrospira platensis* has the red most chlorophylls, which also form the

most stable PSI trimer; it absorbs at 740 nm and fluoresces at 760 nm at low temperature (38, 40).

## 1.8 TYPES OF ELECTRON TRANSFER IN PHOTOSYNTHESIS

Oxygenic phototrophs can use two types of electron flow. The cyclic flow of electrons generates ATP while linear electron transfer makes NADPH, as well as ATP.

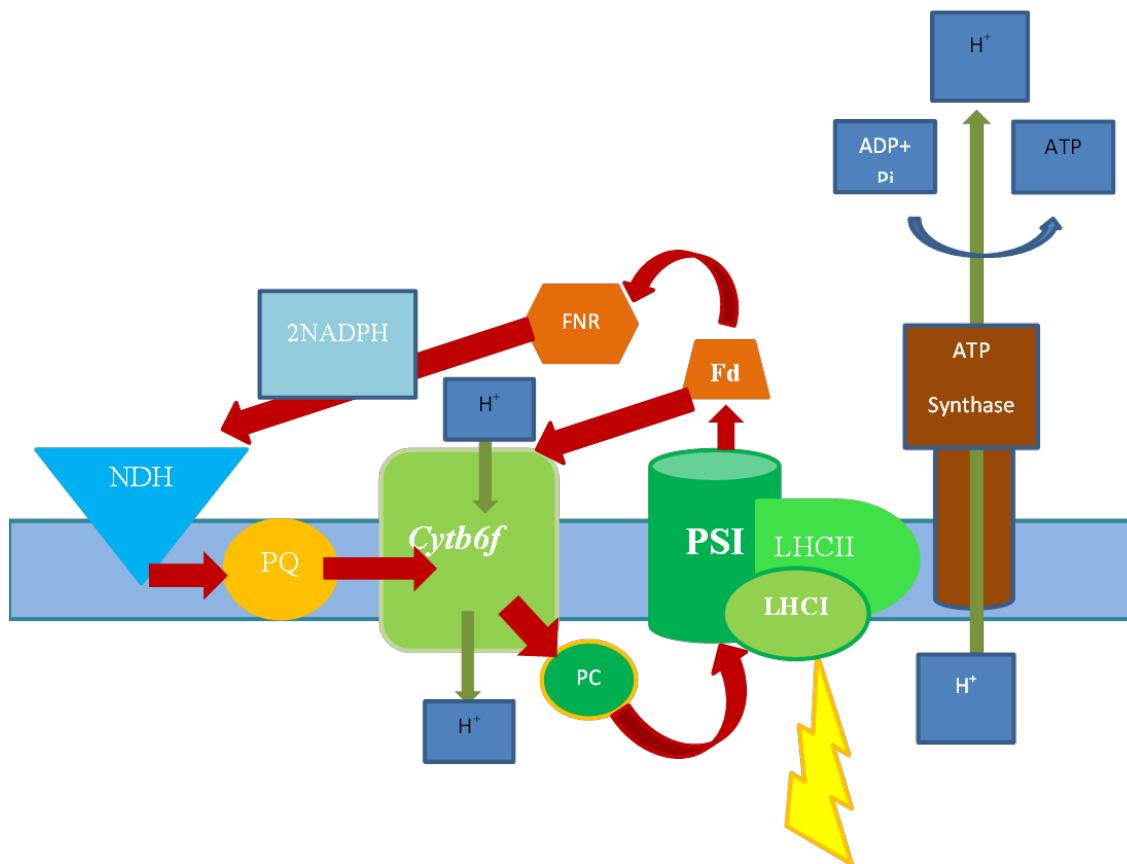
### 1.8.1 Linear Electron flow (LEF)

During normal illumination, the oxidation of water at the oxygen evolving complex (OEC) produces electrons along with protons and oxygen. The electron transfer occurs in a number of steps between tyrosine Z and different cofactors of the PSII RC. These cofactors include P680, chlorophyll D, pheophytin and quinone ( $Q_A$ ) on the D1, and the quinone B ( $Q_B$ ) of the D2 branch. The excitonic energy trapped on the PSII RC from the antenna is used for this electron transfer. The  $Q_B$  quinone is re-oxidized by cytochrome *b6f*. Light-driven charge separation in PS1 results in oxidation of  $P_{700}$  and reduction of ferredoxin (Fd). Plastocyanin, a water-soluble electron carrier, oxidizes Cyt *f* of cytochrome *b6f* and reduces  $P_{700}^+$  of PSI. Fd transfers an electron to the Ferredoxin-NADP<sup>+</sup>-reductase (FNR), which uses it for the reduction of NADP<sup>+</sup> to NADPH. The protons generated at the OEC are transferred from the luminal to the stromal side through ATP synthase, and this electromotive force produces ATP from Adenosine diphosphate (ADP) and inorganic phosphate ( $P_i$ ). In the membrane, the doubly reduced plastoquinone also gets protons from the stromal side and then gives the electron to the *Cyt-b6f*

cofactors, while the protons are released on the luminal side using the Q cycle. This process is also functional in CEF. Thus during LEF, ATP and NADPH are produced (41).

### 1.8.2 Cyclic Electron Flow (CEF)

Cyclic electron flow occurs between PSI and *Cyt-b6f*, where PSI forms a super-complex with the mobile LHCII and the associated *Cyt-b6f*. During the CEF, only ATP is generated. This ATP is consumed for the formation of reduced sugars from the absorbed CO<sub>2</sub> in rubisco complex. The CEF is well established in cyanobacteria, algae and C4 plants in the past but recently its role has also been recognized in C3 plants. The CEF becomes functional in various stress conditions like decreased CO<sub>2</sub> levels, high light conditions, dark-to-light shifts and drought. There are three predicted paths of CEF (Figure 1.3): 1) Ferredoxin donates its electron via FNR to NADP<sup>+</sup>, then to the NAD(P)H dehydrogenase complex, and finally to the plastoquinone pool. 2) Ferredoxin gives an electron to the plastoquinone pool using a newly discovered protein of ferredoxin-plastoquinone oxidoreductase. 3) Ferredoxin interacts directly with *Cyt-b6f* and donates an electron to *Cyt-c'* as shown in figure 4. A decrease in CEF results in reduced acidification of thylakoid lumen and a decline in non-photochemical quenching (NPQ) (41, 42).



**Figure 1.3.** Cyclic electron flow between PSI, FNR, *Cyt-b6f* and plastocyanin and other protein components. Fd= Ferredoxin; FNR= ferredoxin NADP<sup>+</sup> reductase; NADPH = nicotinamide adenine dinucleotide phosphate; NDH= NADP<sup>+</sup> dehydrogenase; PQ=Plastoquinone; Cytb6f+ Cytochrome b6f; PC= Plastocyanin; LHCII = Light harvesting complex II; LHCI = light harvesting complex I; ATP= Adenosine triphosphate; ADP = Adenosine triphosphate; Pi= inorganic phosphate. The red arrows indicate the path of electron transfer and the dark green arrows indicate the flow of protons across the membrane.

## 1.9 EXCITATION ENERGY TRANSFER IN PSI

The natural photosynthetic complexes have evolved efficient excitation energy transfer mechanisms. To be successful there are three rules that must be followed: 1) the excited pigment must not be quenched. 2) The excitation energy must be transferred to the primary electron donor. 3) The primary electron transfer must be irreversible as much as possible. The rate of excitation energy transfer (EET) depends upon the distance between the donor and acceptor pigments, as well as their orientation. The shorter the distance between the two pigments, the faster the energy transfer. According to the Förster equation, a distance of 1.5 nm between the centers of two pigments is optimal for energy transfer and the transfer rate scales with  $R^{-6}$  (1, 4). Placing two pigments too close together is also not suitable and causes concentration quenching, in which excitation is lost, resulting in characteristics like a decrease in excited state lifetime and a drop in quantum efficiency. The protein environment also plays an important role in modulating the pigments maximum absorption level and wavelength region. After absorbing a photon, the protein vibrations (phonons) couple with electronic transitions of pigments that expand the absorption spectra. This permits the uphill and downhill energy transfer on the excited energy transfer landscape (4). The bulk chlorophylls of the antenna absorb maximally at 680 nm. EET between two pigments in the antenna occurs with a time constant of approximately 100-200 fs, but in the red forms it is 2-10 ps; thus, the red forms slow down EET. The EET from the core to the RC and its trapping in RC occurs with a lifetime of 20-40 ps. There are different mechanisms proposed for the excitation



energy transfer to the trap, followed by conversion of the energy into primary charge separation. These include the following:

#### 1.9.1 Diffusion/migration-limited model

According to this model, EET to the primary electron donor occurs by diffusion and is limited by the time it takes to reach the primary donor. Trapping is irreversible, and there is no chance for this excitation energy to go back into the antenna.

#### 1.9.2 Trap-limited model

According to this model, the excitation energy visits the trap in the RC several times before trapping into the CS state. In the case of green algae *C. reinhardtii* PSI, it is generally accepted that CS is trap limited. The ultrafast transient absorption spectroscopic data and time-resolved fluorescence data are explained well by the trap limited model, as the equilibration of excitation energy in the antenna is very fast (43). Experimentally, it is observed that energy transfer and equilibration occurs around two ps timescale (11).

#### 1.9.3 Transfer to the trap-limited model

This model suggests that first the energy equilibration occurs in the core antenna and then it is transferred to the RC only once, where charge separation occurs. This model considers the distance between the core antenna and RC as an important factor because the rate of excitation energy depends upon the distance. The distance between the core antenna and RC is large, as in PSI it is more than 16 Å and approximately 20 Å in PSII. It may be possible that the spectral and spatial equilibration of excitation energy in the antenna occurs on the same time line. But once the excitation energy is equilibrated then

its transfer from the core antenna to the P<sub>700</sub> in the RC is a slow process (4). This model describes the energy transfer in cyanobacteria very well. Different theoretical approaches have been used to describe the excitation energy transfer and trapping in photosynthetic complexes. Fitting of steady state and time-resolved spectra predicts an intrinsic CS lifetime of 0.9 ps<sup>-1</sup> in PSI. The excitonic coupling theory also proposes that the CS process is between the trap limited model and transfer to the trap limited model (44). A highly predictive approach of site energy estimation based on quantum-chemistry and electrostatic calculations predict that energy transfer in PSI should be asymmetric, and most of the long wavelength chlorophylls are present on the PsaA side. There is an increased transfer of excitation energy towards the A-branch that results into increased CS on the A-side, making electron transfer in PSI asymmetric. At physiological temperature the excitation energy is transferred to the ec2 chlorophylls, which is the proposed primary electron donor on each branch. However, at cryogenic temperature it was predicted that the excitation energy will be transferred to the P<sub>700</sub> instead of ec2 chlorophylls (45).

#### 1.10 THEORITICAL DESCRIPTON OF ELECTRON TRANSFER IN PHOTOSYNTHESIS AND PARAMETERS AFFECTED BY MUTATION

Electron transfer in photosynthesis can be explained based on Marcus's theory of electron transfer for inorganic reactions in solutions. After excitation energy transfer from the antenna to the reaction center, the primary electron transfer event can be represented by the following rate equation

$$K(ET) = \frac{2\pi}{\hbar} \tilde{V}_e^2 FC$$

Where  $\tilde{V}_e^2$  is the electronic coupling matrix between the electron donor and acceptor, FC is the Franck-Condon factor, and  $\hbar$  is the reduced Planck or Dirac constant. In the above equation, the different parameters are described by the following mathematical expressions:

$$\hbar = h/2\pi$$

$$\tilde{V}_e^2 = \tilde{V}_e^{\circ 2} \exp(-\beta d)$$

$$FC = (4\pi\lambda KT)^{-\frac{1}{2}} \exp[-(-\Delta G^\circ - \lambda)^2 / 4\lambda KT]$$

There are three different regimes for the dependence of the rate upon the free energy difference:

#### 1.10.1 Normal regime

When  $-\Delta G^\circ < \lambda$ , this process behaves like a thermally activated reaction. The electron transfer reactions in this region are endergonic or slightly exergonic, and the rate of electron transfer ( $K_{ET}$ ) is lower than the activationless regime.

#### 1.10.1 Activationless regime

This is when  $-\Delta G^\circ = \lambda$ , the early electron transfer events in photosynthesis occur in this regime. The  $K_{ET}$  in this region is very fast. The FC factor is maximum, and there is very little dependence on temperature.

#### 1.10.2 Inverted regime

When  $-\Delta G^\circ > \lambda$ , this is called the Marcus inverted region, and it corresponds to highly exergonic reactions. Here both the Franck-Condon factor and rate of electron transfer ( $K_{ET}$ ) decrease again. This is usually used to explain the slow rate of charge recombination as compared to the forward electron transfer reaction and the lack of temperature effect in photosynthetic processes (46, 47).

## 1.11 ROLE OF PROTEIN ENVIRONMENT

The protein bath regulates the function of the reaction center through the following four parameters: 1) Overall geometry of the cofactors, including spatial orientations and distances between them, 2) Electronic coupling between cofactors, which is a function of the  $\beta$  factor, 3) Free energy difference of the electron transfer reaction ( $\Delta G^\circ$ ), which comes from the redox potentials of the cofactors, 4) reorganization energy of the reaction ( $\lambda$ ), which is a function of the vibration modes of the protein bath and cofactors along with solvent interactions of the medium (47). The latter three factors are as follow:

### 1.11.1 Electronic coupling ( $H_{AB}$ )

Electronic coupling depends upon the distance between the two cofactors and the medium of interaction between them. Point mutations can alter this parameter by changing the distance between two cofactors or their spatial orientation, or by making the environment more hydrophobic or hydrophilic.

### 1.11.2 Free energy ( $\Delta G^\circ$ )

Point mutations can affect the free energy ( $\Delta G^\circ$ ) of electron transfer reactions, by altering the reduction potential ( $E_h$ ) of electron transfer cofactors via various mechanisms. These include 1) Modification of the ligands attached to the central metal of the cofactor. 2) Conformational restraints imposed upon cofactor geometry; cofactor metal-ligand geometry, such as bonds and angles; changing the hydrogen bonding between the cofactor and the protein environment and the strength of an existing hydrogen bond. 3) Altering the hydrophobicity and electrostatic environment of the cofactor within the protein pocket.

#### 1.11.3 Reorganization energy ( $\lambda$ )

Reorganization energy is the amount of energy required to distort the geometry of reactants into the products without electron transfer actually taking place. It depends upon the size of the reacting groups. For example, in the case of electron transfer between two chlorophylls, reorganization energy does not change structural or vibrational frequencies to a great extent upon oxidation and reduction. Thus, the reorganization energy for electron transfer from one *Chl* to another should be small and could be a few tenths of an electron volt. In the case of two different molecules like chlorophyll and a quinone, its value may reach 1.5 eV (1).

#### 1.12 BI-DIRECTIONALITY OF ELECTRON TRANSFER IN PSI

From the last two decades, there has been intense research done on electron transfer in PSI. Some of the conclusions are still under debate and new work is ongoing to unravel the activity of the two branches. Electron transfer activity in the two branches of PSI was first monitored in spinach PSI particles where the semiphyllquinones generated decays

with half-life of 25 and 150 ns (48). The activity of ET in the two branches of PSI was also observed in *Chlorella sorokiniana* cells. The decay of two equal semiphylloquinone populations at 377 nm and electrochromic band shift sense by the nearby carotenes at 480 and 515 nm decays with two half-life of 18 and 160 ns suggest that either the PhQ are in two different states or both branches are competent for ET (49). In vivo analysis of *C. reinhardtii* point mutation of tryptophan that is pi stacking with PhQ to phenylalanine showed two decay lifetimes that are modulated individually. The PsaA-W693Y decrease the rate of ET from  $\text{PhQA}^{\bullet-}$  towards  $\text{F}_X$  several fold slow and same is the case of PsaB-W673Y that decrease the rate on B-side. The PsaA-W693Y/PsaB-W673Y double mutant has effect on both fast and slow phase of ET from  $\text{PhQ}_{A/B}$ . This showed the activity of two branches, working independently (50). One of the main factors of 10 fold difference between the rate of electron transfer from  $\text{PhQ}_A$  and  $\text{PhQ}_B$  towards  $\text{F}_X$  is the strength of an amide hydrogen bond between the respective PhQ and leucine of PsaA-L722 and PsaB-L706. In *C. reinhardtii* PSI, mutation of the leucine to bulky amino acids like tyrosine and threonine showed that they weaken this hydrogen bond interaction between the amide nitrogen and oxygen of carboxyl group of PhQ through steric clashes. The side chain of these bulky amino acids pushes the PhQ and thus destabilized the semiphylloquinone radicals, which in turn affect the electron transfer rates. It has been found that PsaB-L706Y mutant increases the decay of semiphylloquinone from 24 ns to 10 ns while the PsaA-L722Y/T speeds up from 250 ns to 180 ns. The relative amplitude of decay associated spectrum of semiphylloquinone showed that these mutations also affect the distribution of electron transfer across the two branches. The normal ratio of

PhQ<sub>A</sub><sup>-</sup>/PhQ<sub>B</sub><sup>-</sup> of WT is 0.65:0.35 and was shifted to 0.50: 0.50 in PsaA-L772Y/T and 0.80:0.2 in PsaB-L706Y mutant. The fluorescence detected magnetic resonance (FDMR) spectroscopy of the <sup>3</sup>P<sub>700</sub> triplet states showed that there is possibility of interquinone electron transfer between the two branches by using back reaction through F<sub>X</sub> (51). Replacement of PsaA-L722 to tryptophan also decreases the strength of the hydrogen bond between the amide bond nitrogen of leucine and C4 carbonyl oxygen of PhQ<sub>A</sub>. This change in protein and PhQ interaction caused a change in free energy as a result rate of ET becomes 3 fold faster than in WT (52).

The ec3 chlorophyll is the primary electron acceptor in all the proposed CS models and its role in bidirectional ET is studied in both cyanobacteria and green algae by several mutagenesis studies. Removal of hydrogen bond between ec3 cofactor and the nearby tyrosine in PsaA-Y696F and PsaB-Y676Y mutants PSI provided the evidence that a redistribution of excitation energy for CS between the two branches occurs. The transient absorption spectroscopy showed an increase in the amplitude of fast phase in PsaA-Y696F while the opposite phenomenon occurs in PsaB-Y676F mutant on B-branch. A similar effect was also observed through room temperature transient EPR spectroscopy of these mutants. The earlier 135-225 ns spectra of PsaA-Y696F have small amplitude, where ET occurs on the B-side. The PsaB-Y676F have opposite effect having an increase flow of ET on the A-branch and a larger amplitude at 135 ns is present (53). The methionine ligand of central Mg atom of ec3 chlorophyll has been replaced with several other amino acids in *Synechocystis* sp. PCC 6803 and *C. reinhardtii* PSI. Pulse EPR spectroscopic analysis of PsaA-M688H and PsaB-668H mutants from *Synechocystis*

sp. PCC 6803 showed ET activity in both branches. The PsaA-M688H mutant generates both  $P_{700}^{++} \text{PhQ}_A^{\bullet-}$  and  $P_{700}^{++} \text{PhQ}_B^{\bullet-}$  RPs, presumably by modifying the energetics of  $\text{ec3}_A$ . As a result, CS on the B-side becomes more favorable than CS on the A-side. PsaB-M668H mutation has minor effect and is similar to WT in generation of RPs (54). Time and spectral dependence of the electron spin echo showed the difference between the two radical pairs. The inter-spin distance between  $P_{700}^{++}$  and  $\text{PhQ}^{\bullet-}$  is  $25.43 \pm 0.01 \text{ \AA}$  for  $P_{700}^{++}\text{PhQ}_A^{\bullet-}$  and  $24.25 \pm 0.01 \text{ \AA}$  for  $P_{700}^{++}\text{PhQ}_B^{\bullet-}$  (54). Transient optical spectroscopy with a ns time resolution at 480 nm showed that in PsaA-M688H, 57% amplitude of CS is from A-side ET while in PsaB-M668H has 48%. The decrease in stable CS results in fast charge recombination. (31) . In another set of *ec3* mutants, where methionine was replaced with asparagine, the quantum yield of CS is decreased in both PsaA-M688N and PsaB-M668N mutants as compare to WT but the inhibitory effect is more in PsaA-M688N. Room temperature transient EPR showed that ET from  $\text{PhQ}_A$  towards  $F_X$  is faster in PsaA-M688N while the B-branch mutation has no perturbation in kinetics of ET from  $\text{PhQ}_B$  towards  $F_X$ . Simulation of the RT-EPR showed that the lifetime of the  $P_{700}^{++}\text{ec3}_A^{\bullet-}$  RP has increased in the PsaA-M688N mutant. Low temperature transient X, Q and W band EPR showed that the spin polarization pattern is also modified for  $P_{700}^{++}\text{PhQ}_A^{\bullet-}$  in PsaA-M688N and simulation of this data showed an increase in the lifetime of  $P_{700}^{++}\text{ec3}_A^{\bullet-}$  RP (55). The transient W-band EPR spectrum of  $P_{700}^{++}\text{PhQ}^{\bullet-}$  was unaltered in the PsaB-M688N mutant, presumably due to the strong dominance of A-side ET in this mutant; conversely, the spectrum of the PsaA-M688N mutant was noticeably different. These differences includes a shift in the sine decay trace of ESEEM towards



higher frequency showing an increase involvement of  $P_{700}^{+\bullet}PhQ_B^{\bullet-}$  and a 30 fold decrease in the 80 K transient spectrum of  $P_{700}^{+\bullet}PhQ^{\bullet-}$ . Charge recombination between  $P_{700}^{+\bullet}$  and  $(F_A/F_B)^{\bullet-}$  is slow in PsaA-M688N as compared to B-side mutant and WT. These results indicate that ec3 cofactor is energetically modified in such a way that its redox properties are similar to  $PhQ_A$ . This is possible only when asparagine of PsaA-M688N makes a hydrogen bond with the C=O group of  $PhQ_A$ ; however the EPR spectrum with methyl hyperfine coupling magnitude does not support this view. The out of phase electron-electron dipolar electron spin echo envelope modulation (ESEEM) data of PsaB-M668N showed an approximate distance similar to that of X-ray crystallography of  $P_{700}^{+\bullet}PhQ_A^{\bullet-}$  RP. Thus in PsaA-M688N mutation, the excitation energy is diverted towards B-branch and we can observe the two sides RP's which we cannot detect easily in WT due to higher dominance of A-side ET in cyanobacterial PSI (56). Theoretically it was predicted that PsaA-M688N and PsaB-M668N exists in different conformation that leads to different hydrogen bond strength between amide of asparagine and carbonyl oxygen of  $PhQ$ . There is higher probability that a hydrogen bonding is formed when ec3 is in charged state and due to this hydrogen bonding the experimentally investigated slowing of ET from ec3 to  $PhQ$  happened in PsaA-M688N. Thus there is a possible inherent asymmetry in the protein environment of ec3 on the two branches (57).

The role of the  $P_{700}$  dimer as the main energy trapping molecule and primary electron donor in the classical model of charge separation has been tested by several spectroscopic methods in combination with mutagenesis studies. Upon oxidation of  $P_{700}$ , the spin density in the cation radical is mostly located on the  $P_B$  Chl. This asymmetry was

attributed to the presence of a hydrogen-bonding network interacting with P<sub>A</sub> and its near P<sub>B</sub> (58, 59). In the *C. reinhardtii* PsaA-T739A mutant, which could remove the hydrogen bond from the threonine hydroxyl group to the 13<sup>1</sup>-keto group of P<sub>A</sub>, modifies the electron-phonon environment of P<sub>700</sub>. Analysis of this mutant PSI by nanosecond pump-probe spectroscopy revealed no effect on directionality of ET. Thus this initial study showed that P<sub>700</sub> is not directly involved in primary charge separation. FTIR spectroscopy showed that there is a modification in electronic ground state of P<sub>700</sub> and positive charge redistribution of 14-18% to A-side chlorophyll (60).

The ec2 cofactors are next to P<sub>700</sub> on each branch. The theoretically calculated  $E_m$  of ec2<sub>A</sub> (ground state) is 833 mV and ec2<sub>B</sub> is 815 mV and it is 220 to 250 mV higher than that of P<sub>700</sub> (ground state) (61). The ec2 chlorophyll influences the  $E_m$  of P<sub>700</sub> through steric and electrostatic interactions. The methyl ester of the chlorophyll on ec2<sub>A</sub> and ec2<sub>B</sub> are in different direction and make these chlorophylls rotamers. The distance between the carbonyl O atom of ec2<sub>A</sub> and the central Mg of P<sub>A</sub> is 5.4 Å while the corresponding distance on the B side is 7.1 Å. Due to this decrease in distance the methyl ester group of ec2<sub>A</sub> interacts with P<sub>A</sub><sup>+</sup> and stabilizes it through electrostatic interaction, resulting in lower  $E_m$  value for P<sub>A</sub> as compare to P<sub>B</sub>. Although there is no H-bonding interaction between the methyl ester group of ec2 with the neighboring protein residues in PsaA or PsaB but 180° rotation of these methyl ester group in C13<sup>2</sup>-C13<sup>3</sup> axis shift the charge density from A side chlorophyll to B side from 27.9:72.1 to 22.4: 77.6 and spin density shift from 22.4: 77.6 to 15.1: 84.9 respectively. Thus making a bulky mutation near ec2 could influence not only ec2 itself but also P<sub>700</sub> (25).

### 1.13 PRIMARY CHARGE SEPARATION IN PSI

PSI is an ideal natural nanosystem that could be mimic in artificial photosynthetic material. Understanding the origin and kinetics of primary charge separation is also an important part of photosynthesis study to understand the energy trapping process and its 100% quantum efficiency. Modeling of ultrafast transient absorption spectroscopy of *C. reinhardtii* PSI predicted that the energy trapping process is three times faster than previously observed and the early charge separation processes occur in 6-9 ps. This study suggested the role of ec2 as a primary electron donor or somehow involved in primary electron transfer step by acting as primary electron acceptor in the form of ec2-ec3 dimer and P700 as primary electron donor (62). The role of P<sub>700</sub> in primary CS was discussed in bi-directionality of ET study in PsaA-T739A mutant that breaks the hydrogen bond with P<sub>A</sub>. This mutation have no effect on directionality and suggesting its role as a secondary electron donor (60). Femtosecond transient absorption spectroscopic (TAS) measurements on different mutants around P<sub>700</sub> from *C. reinhardtii* including PsaA-T739V; PsaA-W679V and PsaB-H656C showed that they have no effect on primary charge separation. The target modeling of ultrafast transient spectroscopy provides the rates of different radical pair (RP) formation, where only the rate constants of secondary radical pairs and also their back reactions are modified in these mutants as compared to WT (29). Independent primary charge separation between ec2-ec3 chlorophylls on each branch was also supported by an analysis of the PsaA-Y696F and PsaB-Y676F mutants, which disrupts H-bond to ec3<sub>A</sub> and ec3<sub>B</sub>, respectively. Ultrafast transient absorption spectroscopy showed a decrease in the rate of primary charge separation in both of the

mutants. Target modeling of this spectroscopic data showed that the effect is only on primary RP which is  $ec2^+ec3^-$  and in a second step  $ec2^+$  is reduced by  $P_{700}$  (11). The role of  $ec2$  as primary electron donor is challenged based on theoretical electrostatic measurement and quantum chemical treatment, which showed that  $ec2$  should have a less negative redox potential than  $ec3$  in the excited state and thermodynamically ET from  $ec2$  toward  $ec3$  is not possible (63).

Excitation of *Synechocystis* PCC 6803 PSI with a 20 fs duration pulse at 720 nm wavelength initiated ET by giving two bands in 100 fs, in which the 660 nm band was assigned to  $ec3^{*-}$  and 705 nm to  $P_{700}^{*+}$ . The primary charge separation according to this study is  $P_{700}^{*+}ec3^-$  and this is for the first time that such a fast energy trapping into CS was reported in 60% of the PSI sample. However there are shortfalls in this analysis such as decrease in the bleaching band of 705 nm representing  $P_{700}^{*+}$  from 4 to 50 ps time scale in the difference spectra. However, after the  $P_{700}^{*+}$  cation radical is formed, it should exist for milliseconds and a decrease in its bleaching is not possible unless it is reduced. There is possibility that the red chlorophylls spectrum is considered as the evolution of  $P_{700}^{*+}$  (64). In another study on *Synechocystis* PCC 6803 PSI with a 25 fs duration pulse at 620, 700 and 720 nm central excitation wavelength, a similar 100 fs lifetime of  $P_{700}^{*+}ec3^-$  formation is reported. The only difference in using the different wavelength excitation is that at 670 and 700 nm the bulk antenna chlorophyll excitation is high as compared to the 720 nm (65). A slow decay of fluorescence is observed in the transient fluorescence spectra of PsB-M664H, and PsA-M664S mutant PSI particles effecting  $ec3_B$  cofactor in *C. reinhardtii*. This decrease showed modulation in the energy trap

where  $ec3$  is the primary electron acceptor. Based on modeling of the above data and sample with pre-oxidized  $P_{700}$  form WT and mutants proposed a fast charge recombination to the ground state from  $ec2^+ec3^-$  and  $ec2$  as primary electron donor. The positive charge on  $P_{700}$  shifts the equilibrium of excitation energy toward the excited antenna from the primary RP of  $ec2^+ec3^-$  (28). Another approach to disentangle the antenna and early charge separation dynamics is to use visible/mid-Infrared Pump-Probe spectroscopy with femtosecond time resolution. Studies of *Synechococcus elongatus* PSI trimers showed a very early signature of a cationic state, that is a band with a charge transfer character and evolution of this signal is beyond the instrument time resolution of 0.2 ps, thus it could be possibly the red chlorophylls that are populated early during energy equilibration in the antenna and stay for longer time due to equilibration of excitation energy between the RC and these red chlorophylls. An increase in the intensity of these bands are observed at 0.8-1 ps and 7-40 ps, the initial increase in intensity was assigned to the formation of  $ec2^+$  and the later to  $P_{700}^+$ . Fitting of this data into a kinetic model support the view that  $ec2^+ec3^-$  is a primary radical pair and  $P_{700}^+ec3^-$  as a secondary RP step. The presence of red chlorophyll clearly dampens the assignment of exact lifetime to the rise time of primary RP in cyanobacteria, therefore it is necessary to use a PSI particles free from red chlorophylls (66).

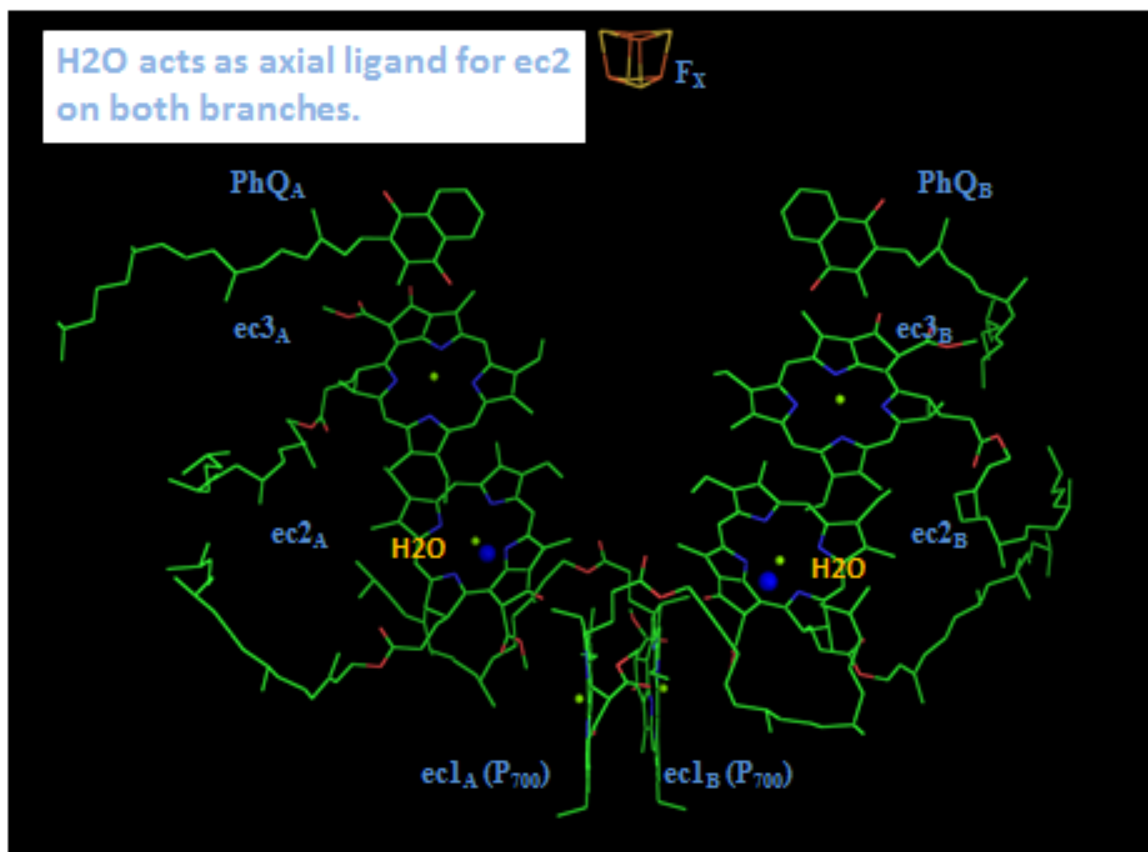
#### 1.14 AIMS AND OBJECTIVES

In order to study the site of primary charge separation and the base root of directionality, we selected the  $ec2$  chlorophylls as a target for mutagenesis. These chlorophylls are proposed as the primary donor of electron transfer but need further

investigation to confirm this hypothesis (11, 29, 62). If one examines the crystal structure of PSI from *T. elongatus*, there is a water molecule that acts as a fifth ligand to the central Mg atom of ec2 and there is no direct linkage from the protein (Figure 1.4). The water molecule donates a hydrogen bond to an asparagine from the opposite branch polypeptide. That is, the central Mg of ec2<sub>A</sub> or eC2-B (crystal structure nomenclature) makes coordinate bond with the oxygen of water by accepting the lone pair of electron from the oxygen of water, while the carboxyl oxygen of the asparagine side chain from helix 9 (Figure 1.5) of PsaB accepts a hydrogen bond from the same water molecule. Thus, the interaction of each ec2 Chl with the “opposite side polypeptide” is rather indirect. For that reason and to avoid unnecessary confusion, we prefer to use the nomenclature that names the cofactor according to which branch it is in (i.e. ec2<sub>A</sub> and ec2<sub>B</sub>), not according to which polypeptide coordinates the water molecule serving as its axial ligand (i.e. eC2-B and eC2-A).

For a second target for mutagenesis, we chose an alanine residue whose methyl group is near the ec2 *Chl* on the opposite side of the macrocycle to that of the axial ligand. This alanine (or mutants of it) may also influence the nearby ec3 chlorophyll, as it lie in between ec2 and ec3 chlorophyll on each branch shown in the figure 2.1 and figure S2.1. These alanine residues found in helix 10 of both PsaA and PsaB are highly conserved among cyanobacteria, algae and plants, so it is reasonable to expect that their position in PS1 will be the same as that seen in the crystal structure of *T. elongatus* (21) shown in (Figure 1.6). Although this residue has no direct interaction with the chlorophyll molecules, its methyl group is directed towards ec2 chlorophyll and therefore

after mutation it would become the  $\beta$ -methylene group of a new side chain, directing new functional groups to the vicinity of ec2 (and ec3). This project on bi-directionality of electron transfer in photosystem I is carried out by making mutants of amino acid residue close to ec2, (Table 1.1). After making these mutants, the level of accumulation of PS1 by the mutants was measured by spectroscopic and other biochemical methods. The effect of mutation on the primary trap on each branch was measured *in vivo* by monitoring the decay of semiphylloquinone, decay of the electrochromic band shift that is caused by the formation of electric field due to  $P_{700}^+PhQ^-$ , and also the charge recombination between terminal iron sulfur cluster and  $P_{700}^+$ . The electron transfer activity was also studied by room temperature and low temperature EPR. Ultrafast transient absorption spectroscopy was used to analyze the early electron transfer events and effects on the  $P_{700}^+PhQ^-$  difference spectra. Any loss of excitation energy and energy trap lifetime modulation due to mutation was monitored by time-resolved fluorescence spectroscopy.



**Figure 1.4.** Reaction Center of Photosystem I, representing the cofactor involved in ET on the two branches. The P<sub>700</sub> is composed of ec1<sub>A</sub> and ec1<sub>B</sub> chlorophylls. On each branch is a pair of chlorophylls (ec2<sub>A</sub>ec3<sub>A</sub> or ec2<sub>B</sub>ec3<sub>B</sub>) and a phylloquinone (PhQ<sub>A</sub> or PhQ<sub>B</sub>). The F<sub>x</sub> cluster is shared by PsaA and PsaB, while the two terminal iron-sulfur clusters (F<sub>A</sub> and F<sub>B</sub>) are bound by PsaC subunit. Water molecule (blue circles) acts as a fifth ligand to the Mg atom of ec2 chlorophyll on each branch (21).




## Helix # 9



```

C.r PsaA      588 AWDHVFLGLFWMNSLSIVIFHFSWKMQS
S.e PsaA      592 GWDHVFLGLFWMNSLSIVIFHFSWKMQS
A.t PsaA      587 AWDHVFLGLFWMYNAISVVIFHFSWKMQS
Clustal Consensus .*****:.*:*****
  
```

## Helix # 9



```

C.r PsaB      573 AYDAFYLA VFWMLNTIGWVTFYWHWKHL
S.e PsaB      579 AWD AFYLA MFWMLNTLGWLT FYWHWKHL
A.t PsaB      572 AWD AFYLA VFWMLNTIGWVTFYWHWKHI
Clustal Consensus *: * *****:*****: ** :*****:
  
```

**Figure 1.5.** Sequence alignment of PS1 helix 9 of PsaA and PsaB in *Chlamydomonas reinhardtii* (*C.r*), *Synechococcus elongatus* (*S.e*) and *Arabidopsis thaliana* (*A.t*). Key: Red: negatively charged. Cyan: small, hydrophobic, aromatic, not Y. Blue: acidic. Magenta: basic. Green: hydroxyl, amine, amide, basic. Gray: others. "\*": identical. ":": conserved substitutions (same color group). ".": semi-conserved substitution (similar shapes).

## Helix # 10

<i>C.reinhardtii</i>	<i>PsaA</i>	666	SAYGLIFLGAHFVWAFSLMFLE
<i>S.elongatus</i>	<i>PsaA</i>	670	SAYGIMFLAGHFVFAFSLMFLE
<i>A.thaliana</i>	<i>PsaA</i>	665	SAYGLEFFLGAHFVWAFSLMFLE
<i>Clustal Consensus</i>			****: **: :****:*****

## Helix # 10

<i>C.reinhardtii</i>	<i>PsaB</i>	646	SVWAWTFLFGHLIYATGFMFLI
<i>S.elongatus</i>	<i>PsaB</i>	651	SVWAWMFLFGHLVWATGFMFLI
<i>A.thaliana</i>	<i>PsaB</i>	644	SVWAWMFLFGHLVWATGFMFLI
<i>Clustal Consensus</i>			***** *****: :*****

**Figure 1.6.** Sequence alignment of PS1 helix 10 of PsaA and PsaB in *Chlamydomonas reinhardtii*; *Synechococcus elongatus*; and *Arabidopsis thaliana*. Key: "\*": identical. ":": conserved substitutions (same color group). ".": semi-conserved substitution (similar shapes).

**Table 1.1:** Site of mutation, where ec2 on each branch is targeted to study energy trapping and primary charge separation.

<b>PsaA-Asn604 and PsaB-Asn591</b>	<b>PsaA-Ala684 and PsaB-Ala664</b>
<b>Asp</b>	<b>Cys</b>
<b>His</b>	<b>Asp</b>
<b>Lys</b>	<b>His</b>
<b>Leu</b>	<b>Ile</b>
<b>Tyr</b>	<b>Asn</b>

## CHAPTER NO 2

### 2.1 INTRODUCTION

Photosystem I (PSI) is one of the two multi-subunit, pigment-protein complexes that drive the initial processes of light utilization in oxygenic photosynthesis. The PSI complex includes redox cofactors comprising the reaction center (RC), as well as approximately 100 chlorophyll (Chl) *a* molecules that compose the core antenna. The RC cofactors are arranged in two pseudo-symmetric branches, spanning the membrane from the chlorophyll *a* dimer P<sub>700</sub>, and then splitting into two branches with ec2 and ec3 chlorophylls and phyloquinone (PhQ) on each branch, and then a single iron-sulfur cluster, F<sub>X</sub>. All of these are bound by a heterodimeric assembly of the PsaA and PsaB subunits. There are two additional iron-sulfur clusters on the stromal side called F<sub>A</sub> and F<sub>B</sub>, and they are bound by the extrinsic PsaC subunit (Figure 1) (8, 21). Various investigators have studied electron transfer (ET) along the two branches, and there is consensus that both branches are active for electron transfer, but that electron transfer to F<sub>X</sub> was ~10-fold faster from PhQ<sub>B</sub> than from PhQ<sub>A</sub> (67).

In the last two decades, there has been intense research done on electron transfer in PSI. Some of the conclusions are still under debate, and new work is ongoing to unravel the activity of the two branches. Electron transfer activity in the two branches of PSI was first observed in spinach PSI particles, in which the semiphyloquinone signal showed a biphasic decay with lifetimes of 25 and 150 ns (48). *Chlorella sorokiniana* cells also exhibited this biphasic decay, with half-lives of 18 and 160 ns, suggesting that either

the active PhQ existed in two different states or both branches were competent for ET and that the rates of ET were different between the two quinones (49). *In vivo* analysis of *C. reinhardtii* mutants in which tryptophan residues that  $\pi$ -stack with PhQ were changed to phenylalanine showed that these substitutions modulated the two decay lifetimes individually. The PsaA-W693F mutation decreased the rate of ET from  $\text{PhQA}^{\bullet-}$  to  $\text{F}_X$  and the PsaB-W673F that reduce the rate on B-side (50). One factor contributing to the  $\sim 10$ -fold difference between the rates of electron transfer from  $\text{PhQ}_A$  and  $\text{PhQ}_B$  to  $\text{F}_X$  is the strength of an hydrogen bond to the O-4 of the PhQs from a peptide N of a nearby Leu residue. Mutation of this leucine to tyrosine and threonine was thought to weaken this interaction through steric clash, thus destabilizing the semiphylloquinone. The PsaB-L706Y mutant increased the rate of decay of  $\text{PhQ}_B^-$  from 24 ns to  $\sim 10$  ns, while the PsaA-L722Y/T increased the rate of decay of  $\text{PhQ}_A^-$  from 250 ns to 180 ns (51).

The ec3 chlorophyll is the primary electron acceptor in all the proposed CS models. A number of mutagenesis studies probed the role of this cofactor in bidirectional ET in both cyanobacteria and green algae. Removal of the hydrogen bond between ec3 and the nearby tyrosine in PsaA-Y696F and PsaB-Y676F mutants PSI caused an increase in the amplitude of the fast phase in PsaA-Y696F, while the opposite phenomenon was seen with the PsaB-Y676F mutant (53). In *Synechocystis* sp. PCC 6803 and *C. reinhardtii* PSI, the methionine ligand to ec3 on each branch has been substituted with several amino acids. The mutations effect on A-branch is more prominent than that of the B-branch in terms of kinetics and inhibition of ET (31, 55, 56, 68-71). Theoretically it was predicted that PsaA-M688N and PsaB-M668N exists in a different conformation that leads to

different hydrogen bond strength between amide of asparagine and carbonyl oxygen of PhQ. There is a higher probability of hydrogen bond formation when ec3 is in charged state and due to this hydrogen bonding, the experimentally investigated slowing of ET from ec3 to PhQ happened in PsaA-M688N. Thus, there is a possible inherent asymmetry in the protein environment of ec3 on the two branches (72).

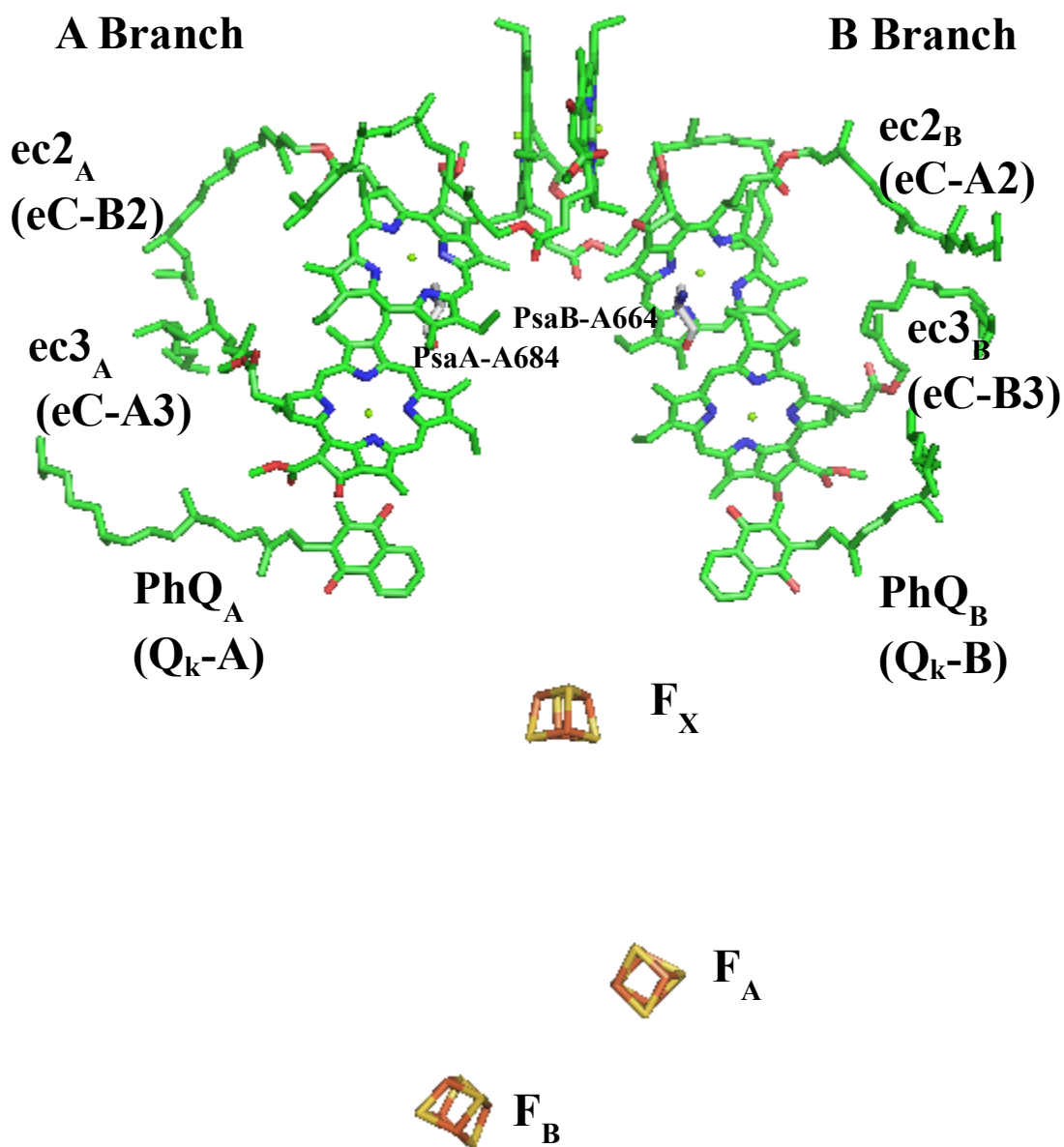
The origin and kinetics of primary charge separation in PSI are important to understand the energy trapping process and its 100% quantum efficiency. It is predicted from mathematical modelling of time-resolved fluorescence and absorption spectroscopy of PSI that ec2 is part of the energy trapping and CS process. Initially, modeling of ultrafast transient absorption spectroscopy of *C. reinhardtii* PSI predicted the involvement of ec2 in primary electron transfer, perhaps as the primary electron donor (62). The role of P<sub>700</sub> in primary CS was challenged based on an analysis of the effects of the PsaA-T739A mutation, which breaks a hydrogen bond to P<sub>A</sub> but has no effect on directionality (60). Femtosecond transient absorption spectroscopic (TAS) measurements on different mutants around P<sub>700</sub> from *C. reinhardtii* also showed that they have only affect secondary ET step (29). Ultrafast transient absorption spectroscopy of the PsaA-Y696F and PsaB-Y676F mutants showed a decrease in the rate of primary charge separation in both mutants. Target modeling of this spectroscopic data predicted that the effect is only on formation of the primary RP (i.e.  $ec2^+ec3^-$ ); in a second-step  $ec2^+$  is reduced by P<sub>700</sub> (11). A slow decay of fluorescence in PsaB-M664H and PsaB-M664S mutant PSI particles from *C. reinhardtii* also points towards a change in the efficiency of the energy trap. Model based fitting of this data proposed that the mutation near ec3 or

$P_{700}$  in the oxidized state shifts the equilibrium toward the antenna side from  $ec2^+ec3^-$  state, suggesting  $ec2$  as a primary electron donor. (28). The cationic state signature is always observed during excitation and equilibration of antenna in *T. elongatus* PSI. Its intensity increases in two-time step, first between 0.8-1 ps and second at 7-40 ps. The initial increase in intensity is predicted to be the formation of  $ec2^+$  and the later to  $P_{700}^+$ . Kinetic modelling support the view that  $ec2^+ec3^-$  is the major primary radical pair and  $P_{700}^+ec3^-$  is the major secondary RP. The presence of red chlorophylls dampens the assignment of exact time of formation and decay of primary electron donor, in cyanobacteria; it is therefore necessary to use PSI particles free from red chlorophylls. In this way the early cation formation that absorb in the far-red region can easily be observed (66). The role of  $ec2$  as primary electron donor is challenged based on theoretical electrostatic measurement and quantum chemical treatment, which showed that  $ec2$  should have a less negative midpoint potential ( $E_m$ ) than  $ec3$  in the excited state and thermodynamically ET from  $ec2$  toward  $ec3$  is not possible (63).

In order to study the site of primary charge separation and the base root of directionality, we sought to modify the  $ec2$  chlorophyll site on each branch. We choose alanine residues PsaA-Ala684 and PsaB-Ala664 for mutation. These alanine residues are found on helix 10 of both PsaA and PsaB and are highly conserved among all oxygenic phototrophs (Figure S2.1), so we expect that their position in PSI of *C. reinhardtii* will be the same as shown in the crystal structure of *T. elongatus* PSI (21). Each of these Ala residues is located on the opposite side of the  $ec2$  chlorophyll macrocycles from the water molecule serving as the axial ligand to the  $ec2$  Mg(II), with the  $\beta$ -methyl group directed towards

the ec2 chlorophyll. It is also close to the edge of the neighboring ec3 Chl (Figurer 2.1 and S2.2). Substitution of these alanine residues is expected to place new functional groups close to the ec2/ec3 pair, perhaps affecting the coupling between the two chlorophylls and/or the energetics of charge separation between the two chlorophylls. This work was undertaken by making a number of different substitutions of the alanine residues on each branch and measuring the levels of expression of PSI in the mutants by spectroscopic and immunoblotting methods. Mutants expressing sufficient PSI were selected for further study of ET using different transient spectroscopic methods.





**Figure 2.1.** Reaction center of Photosystem I from *T. elongatus* showing position of alanine on each branch near ec2 chlorophyll. The  $P_{700}$  is composed of  $ec1_A$  and  $ec1_B$  chlorophylls. On each branch is a pair of chlorophylls ( $ec2_A ec3_A$  or  $ec2_B ec3_B$ ) and a phylloquinone ( $PhQ_A$  or  $PhQ_B$ ). The  $F_X$  cluster is shared by PsaA and PsaB, while the two terminal iron-sulfur clusters ( $F_A$  and  $F_B$ ) are bound by PsaC subunit.

## 2.2 MATERIALS AND METHODS

### 2.2.1 Genetic manipulations

A total of five pairs of mutants of Ala substitution in *psaA* and *psaB* genes of PSI were created via a previously described PCR method (73) and introduced into two background strains of *C. reinhardtii* in which either the *psaA* exon-3 or *psaB* had been deleted (60). These strains also have the FUD7 chloroplast mutation, which is a deletion of the *psbA* gene encoding the D1 core polypeptide of PSII and results in no PSII, and the nuclear *P71* mutation, which causes a decrease in the total amount of LHCII. In A-branch PsaA-A684 was substituted by cysteine, aspartic acid, histidine, isoleucine and asparagine; whereas similar substitutions were made at PsaB-A664 site. The respective plasmid for the specific site was mixed with tungsten particles and bombarded on *C. reinhardtii* cells spread on agar plates containing Tris-acetate phosphate (TAP) with 75 µg/mL spectinomycin and 100 µg/mL ampicillin, using a home-built gene gun with a helium gas at a pressure of approximately 450 psi. The plates were kept in the dark and colonies appeared after 7 days. These colonies were passaged alternately on 300 µg/mL spectinomycin and 100 µg/mL streptomycin every 14 days. The transformants were checked for *psaA* or *psaB* genes and homoplasmicity by isolating the plasmid DNA and amplification via PCR. These strains were used primarily for *in vivo* analyses.

A second set of background strains had the *P71* nuclear mutation but lacked the FUD7 mutation: PBC12-5 (*psaAΔ*) and PBC 18-6 (*psaBΔ*). These backgrounds also have a hexahistidine tag on exon 1 of the *psaA* gene (74). The plasmids were shot in the same way as described. PSI was isolated from these strains for *in vitro* studies.

### 2.2.2 Crude membrane preparation

One liter of each transformant cells was grown under room light ( $81 \mu\text{Einstein m}^{-2} \text{s}^{-1}$ ) and temperature ( $23^\circ\text{C}$ ) in Tris-acetate phosphate (TAP) media. The cells were harvested by centrifuging at  $3500 g$  for 5 minutes at  $4^\circ\text{C}$ , the supernatant was discarded and the pellet was washed with cell resuspension buffer (0.3 mM sucrose; 25 mM HEPES having pH 7.5 with KOH; 5 mM  $\text{MgCl}_2$ ; 5 mM  $\text{CaCl}_2$  ) and recentrifuged at  $3500 g$  for 5 minutes at  $4^\circ\text{C}$ . The washed cell pellet was suspended in thylakoid resuspension buffer (0.3 mM sucrose; 25 mM HEPES having pH 7.5 with KOH; 10 mM EDTA) and French pressed at 3000 psi. The broken cells or crude thylakoid membrane were washed with thylakoid resuspension buffer and centrifuged at  $40000 g$  for 10 -15 minutes at  $4^\circ\text{C}$  twice by collecting the green residue and discarded the lower white starch material. Storing buffer which contains 25 mM HEPES-KOH (pH 7.5); 10 mM EDTA; 1 mM phenylmethylsulfonyl fluoride (PMSF); 10 % Glycerol was added to the pellet. The sample was homogenized with a chilled homogenizer and 1X protease inhibitor buffer (50 mM EDTA; 10 mM Benzamide-HCl; 500  $\mu\text{g/mL}$  Pepstatin A; 200  $\mu\text{g/mL}$  Leupeptin; 100  $\mu\text{M}$  E-64; 100 mM  $\epsilon$ -aminocaproic acid). The crude thylakoid membranes were stored at  $-80^\circ\text{C}$  for later use after flash freezing in liquid nitrogen in aliquots for  $P_{700}$  estimation through spectroscopy and immunoblot analysis.

### 2.2.3 Immunoblot analyses

For immunoblot analyses, 20  $\mu\text{g/mL}$  of chlorophyll containing crude thylakoid membranes of WT and mutants were taken and an equal volume of 2X Lamelli buffer

(4% SDS; 20% Glycerol; 125 mM Tris-HCl having pH 6.8; 4 M Urea) was added to it and dissolved by vortexing. The sample was diluted by 1X Lamelli buffer, so that it has the final concentration of 0.5 µg of chlorophyll containing sample. Each sample was heated at 50 °C for 30 minutes in water a bath then vortexed briefly and spun at 25000 g for 10 minutes. The supernatant was collected for later usage. 10 µL of sample was added in wells of 4-10 % Tricine gel. The gel was run at constant voltage of 90 V with 110-125 mA expected current at start and 15 mA at end for 4 hours in 1X MES ( (2-[N-morpholino] ethanesulfonic acid))-SDS ( sodium dodecyl sulfate) running buffer (pH 7.3). The protein was transferred to the pre-soaked polyvinylidene difluoride (PVDF) membrane [Millipore Corporation, USA] using transferring buffer (1X Tris-glycine SDS; 20 % methanol) in immunoblot transferring assembly cell at constant voltage of 30 V for 3 hours at 4 °C. The blotted membrane was placed in mixture of TBST ( 20 mM Tris-HCl pH 7.5; 500 mM NaCl; 0.05 % Tween 20) along with 5 % non-fat skim milk (NFDM) and 1 mM sodium azide for overnight at 4 °C to block empty protein binding sites on membrane. The blot was placed in a primary α- PsaA antibody solution (TBST+ 1% NFDM + 1° antibodies that are diluted in a ratio of 1:2000) and shake gently at room temperature for one and half hour. The blot was washed with TBST three times for a total of fifteen minutes on shaker. The blotted membrane was then placed in secondary antibody solution (TBST+ 1% NFDM and 2° antibody which is made by 2 µL HRP complex [Goat anti-rabbit IgG conjugated to horseradish peroxidase (BIO-RAD Laboratories, Hercules, CA) and used at 1: 10, 000] and shake gently at room temperature for one hour. The blot was then washed with TBST three times for a total of

15 minutes on shaker. Supersignal West Femto maximum sensitivity substrate (equal volume mixture of stable peroxide solution and luminal/enhancer solution) by Thermo scientific IL, USA was used as chemiluminescent that makes a conjugated complex with the protein-antibodies complex and glow. The blot image was probed with Omega Molecular Imaging System (ULTRA LUM, California, USA) (74).

#### 2.2.4 Spectroscopic estimation of PSI ( $P_{700}$ )

Spectroscopically the amount of PSI accumulation in each mutant was measured using Joliot type spectrophotometer called JTS-10 (Bio-logic), which can measure the light-induced changes in crude thylakoid membranes with a time resolution of 10  $\mu$ s. For PSI estimation, a sample of 20  $\mu$ g/ml of Chl containing CTM was taken and 40  $\mu$ M of dibromothymoquinone (DBMIB) was added to inhibit or slow down the cyclic electron flow from cytochrome *b<sub>6</sub>f*. A 10  $\mu$ M of Carbonyl cyanide p-[trifluoromethoxyl]-phenyl-hydrozone (FCCP) to disrupt the proton gradient if present in the crude thylakoid membranes, 5 mM Sodium ascorbate was used as a reducing agent to reduce the oxidized  $P_{700}$ . For excitation, a frequency-doubled Nd:YAG laser (Continuum Electro-Optics, Inc., Santa Clara, CA) emitting 33 mJ pulses at 532 nm (6 ns duration) was used for the oxidation of  $P_{700}$  of PSI. The laser flash has enough energy to saturate the sample. The oxidation of sample was probed with 700 and 810 nm weak actinic flashes from JTS-10 spectrophotometer. The sample was measured in the absorbance mode where a baseline of 20 s was measured initially and then in the illumination period a single laser flash was given to oxidize the  $P_{700}$ . Measuring flashes commenced 250  $\mu$ s after the laser flash and continued for 18 s, long enough for the bleaching signal to recover entirely. The

transients were recorded at wavelength of 675, 680, 685, 690, 695, 700, 705, 740 and 810 nm by using interference filters. The lowest bleaching point of the transients was taken for wavelength from 675 to 705 nm while at 740 and 810 nm the positive peak was taken for calculation as at 740 nm and beyond  $P_{700}^{+}$  absorb. From these transients, a light minus dark difference spectrum was plotted for  $P_{700}$ .

#### 2.2.5 Growth Assays

Cells were grown in 20-25 mL TAP liquid culture overnight and on the next day the cells were counted. 10  $\mu$ L of  $2 \times 10^6$  cells was spotted on TAP and TBP plates. The TAP plates were placed in dark and variable light conditions of 2, 20 and 80  $\mu$ Einstein  $m^{-2} s^{-1}$  of light intensity, which was measured with a LI-COR Photometer (Model LI-250 Light Meter). One set of TBP plates were placed in microaerobic conditions using anaerobic gas generator pouch system with indicator (BD GasPak EZ, Becton, Dickinson and company, USA), and another was placed at 80  $\mu$ Einstein  $m^{-2} s^{-1}$  in normal air conditions.

#### 2.2.6 Transient Optical Spectroscopy of in vivo PSI

Spectroscopic measurements were performed in whole cells of *C. reinhardtii* using a home built spectrophotometer as reported previously (50). The absorption changes were probed by using short laser flashes. The probe light in the visible region ( $\lambda > 410$  nm) is generated through a frequency-tripled Nd:YAG laser (Surelite II; Continuum) pumping a computer controlled optical parametric oscillator (OPO, Panther; Continuum). For probe measurements in the UV region, the output of the OPO is frequency doubled. The pump-probe delay was controlled through a home built pulse programmer. The cells sample was

loaded in a 2.5 mm optical path cuvette and placed close to the detector diodes to avoid scattering. The temporal resolution of the setup is approximately 5 ns before the instrument function deconvolution. The samples were excited at 700 nm of actinic excitation that has intensity around 1 mJ per pulse of 7 ns duration. This excitation source is created through a dye laser (LDS 698) pumped by a frequency doubled ND: YAG laser (Brilliant: Quatel) (51). The data was fitted through Origin Lab software.

#### 2.2.7 Isolation of H<sub>6</sub>-PSI particles

WT and mutants strains were grown in 6 L flasks using 5 L of TAP medium with constant stirring and bubbling with filtered air under light condition of 81  $\mu\text{Einstein m}^{-2} \text{s}^{-1}$  and approximately 23 °C. The cells were harvested during the early logarithmic phase by centrifugation at 3500 g for 5 minutes at 4 °C, washed with cell resuspension buffer (0.3 mM sucrose, 5 mM MgCl<sub>2</sub>, 5 mM CaCl<sub>2</sub>, 25 mM HEPES-KOH (4-(2-hydroxyethyl)-1-piperazineethanesulfonic acid), pH 7.5) and centrifuged again. The cells were suspended in thylakoid resuspension buffer (0.3 mM sucrose, 10 mM EDTA, 25 mM HEPES-KOH, pH 7.5) and broken by passage through a French pressure cell at 3000 psi. The broken cells were washed with thylakoid resuspension buffer and centrifuged at 40000 g for 10-15 minutes at 4 °C twice by collecting the green residue and discarded the lower white starch material and upper supernatant. Crude thylakoid membranes were homogenized in cold thylakoid resuspension buffer at approximately 6 mg Chl mL<sup>-1</sup> and stored at -80 °C after flash freezing in liquid nitrogen. Crude thylakoid membranes (CTM) at 0.4 mg Chl mL<sup>-1</sup> (PBC12-5 background strains) or 0.2 mg Chl mL<sup>-1</sup> (PBC18-6 background strains) were solubilized by dropwise addition of 10% w/v  $\beta$ -D-

dodecylmaltoside ( $\beta$ -DM) to a final concentration of 0.1%, and the sample was stirred gently for 30 minutes at 4 °C in the dark. After sample was centrifugation at 64000 g for 25 minutes at 4 °C to remove unsolubilized material, the supernatant was loaded onto a Ni-NTA (Invitrogen) column pre-equilibrated with solubilization buffer containing 0.03 %  $\beta$ -DM. The column was washed with solubilization buffer containing 0.03 %  $\beta$ -DM and 2 mM imidazole until the efflux was clear. The H<sub>6</sub>-tagged PSI was eluted from the column with elution buffer (300 mM imidazole and 40 mM 2-(*N*-morpholino) ethane sulfonic acid MES-NaOH, pH 6). The eluate were concentrated in Amicon Ultra-15 centrifugal filters with 100 K molecular weight cutoff (Millipore Ltd. Ireland) and washed with storage buffer (40 mM CaCl<sub>2</sub>, 40 mM MgCl<sub>2</sub>, 0.03%  $\beta$ -DM, 10% glycerol, 10 mM Tricine, pH 8) to remove imidazole several folds during concentration. The sample was concentrated to a final concentration 2.5-3 mg Chl ml<sup>-1</sup>. Glycerol was added to a final concentration of 20%. Samples were stored in 100  $\mu$ L aliquots by flash freezing in liquid nitrogen at -80 °C.

#### 2.2.8 Ultrafast Transient Absorption Spectroscopy

The sample was excited with a laser light of 700 nm excitation with a full width at half maximum (FWHM) of 0.15 ps and was probed with a white light continuum over a broad wavelength region from 601 to 750 nm. The pump and probe light was placed at the magic angle (54.7°). Intensity of the excitation light was adjusted low enough to avoid annihilation. Measurements were performed in is the Q<sub>Y</sub> transition region of Chlorophyll *a* of PSI. Data was collected from 0.9 ps before time zero and 2 nanosecond after the



excitation pulse. Circular rotating cuvette with a path length of 1.2 mm was used, for which the speed of the rotation was set so that the laser shot hit fresh open (reduced  $P_{700}$ ) PSI particles and to avoid the accumulation of long-lived intermediates state. The optical density of the sample was approximately 1 OD in the  $Q_Y$  region at 676 nm. For stability of PSI and to avoid aggregation issues, the buffer consists of 10 mM Tricine, 0.4 M  $MgCl_2$ , 0.4 M  $CaCl_2$ , 10% glycerol, 0.03%  $\beta$ -DM as a detergent. 40 mM of sodium ascorbate and 50  $\mu$ M of phenazine methosulfate were used as redox agents in order to keep the reaction center in an open state during measurements.

#### 2.2.9 Time-resolved fluorescence

Time correlated single photon counting (TCSPC) was performed to measure the kinetics of energy trapping in PSI mutant samples. The sample was excited with a Titanium-Sapphire (Ti:S) laser (Spectra-Physics, Millennia pumped Tsunami) at 420 nm with a 130 fs pulse duration and 4 MHz repetition rate. Fluorescence emission was collected at a  $90^\circ$  geometry setting and detected using a double-grating monochromator (Jobin-Yvon, Gemini-180) and a microchannel plate photomultiplier tube (Hamamatsu R3809U-50). The polarization of the emission was set at a magical angle of  $54.7^\circ$  relative to that of the excitation. The data acquisition was done using a single photon counting card (Becker-Hickl, SPC-830). The typical instrument response function (IRF) had a full wavelength half maximum (FWHM) of 35 ps, measured from the scattering of sample at 420 nm. The excitation power was 12.1  $\mu$ W at the sample to avoid singlet-singlet annihilation. A time window of 3.3 ns was used, and measurements were done from 680 to 740 nm with 10-nm spacing. The PSI particles were diluted to an OD of  $0.5\text{ cm}^{-1}$  at the Chl *a*  $Q_Y$  region at

676 nm with a buffer containing 10 mM Tricine (pH 8), 0.4 M MgCl<sub>2</sub>, 0.4 M CaCl<sub>2</sub>, 10 % glycerol, 0.03 %  $\beta$ -DM, 20 mM sodium ascorbate, and 50  $\mu$ M phenazine methosulfate. Global analysis was performed with ASUFIT 6.1 software. The decay-associated spectra (DAS) of fluorescence emission are the wavelength dependent pre-exponential part,  $A_i(\lambda)$ , from the multi-exponential fluorescence decay components, from the equation  $F = \sum A_i(\lambda) \exp(-t/\tau_i)$  and is related to specific exponential lifetime,  $\tau_i$ .

#### 2.2.10 Electron Paramagnetic Resonance (EPR) Spectroscopy

Low temperature (80 K) X-band (9 GHz) and Q-band (35 GHz) time/field transient EPR data sets were measured with a modified Bruker ER 200D-SRC spectrometer with an ER 041 X-MR X-band or an ER 051QR Q-band microwave Bridge. A Flexline ER 4118 X-MD-5WI dielectric resonator was used at low temperature. Light excitation was made using a Continuum Surelite Nd:YAG laser operating at 10 Hz, 4.0 mJ/pulse and 532 nm. The temperature of the bath was controlled using an Oxford Instruments CF9335 gas flow cryostat. The transient EPR signal was recorded in direct-detection mode with a home built broadband amplifier (bandwidth 500 MHz) and was digitized through a LeCroy LT322 500 MHz digital oscilloscope. PSI samples were treated with 1mM sodium ascorbate and 50  $\mu$ M phenazine methosulfate (PMS) and the samples were frozen in the dark.

Room temperature X-band EPR measurements were performed with a modified Bruker ESP 200 spectrometer equipped with a home built, broadband amplifier

(bandwidth >500 MHz). A flat cell and a rectangular resonator were used, and the samples were illuminated using a Q-switched, frequency-doubled Continuum Surelite Nd: YAG laser working at 10 Hz, 4.0 mJ/pulse and 532 nm. In order to bring the  $P_{700}$  in the reduced state before the excitation flash, 1 mM sodium ascorbate and 50  $\mu$ M PMS were used as electron donor and mediator.

#### 2.2.11 Low Temperature (80 k) Pulse EPR Experiments

The effect of mutation on the respective light induced  $P_{700}^{+}PhQ^{-}$  RP geometry, its polarization pattern and contribution of each RP in the PSI sample was measured with Pulse EPR experiment. The out of phase echo modulation curves were collected at 80 K using an X-band Bruker Eleksys E580 X-band spectrometer. The echo was generated using the following timing sequence: laser flash ( $h\nu$ ) —  $\tau_L$  —  $(\pi/2)_X$  —  $\tau$  —  $(\pi)_X$ . In this pulse sequence,  $(\pi/2)_X = 8$  ns and  $(\pi)_X = 16$  ns microwave pulses applied in the x-direction in rotating frame. The time delay between the two microwave pulses was changed in 4 ns steps, starting from 64 ns. The echo intensity was integrated over a 48 ns window centered at the maximum echo at  $2\tau$  after the first microwave pulse. The time delay between the excitation laser pulse and initial microwave pulse ( $\tau_L$ ) was 400 ns. A Continuum Surelite Nd:YAG laser operating at 532 nm, 10 Hz and 4.0 mJ/pulse of energetic pulse was used to excite the sample to generate RP's. The chlorophyll concentration of PSI samples was 1 to 2 mg/mL. For the reduction of the sample, sodium ascorbate and phenazinemethosulfate (PMS) was added to the PSI samples in a final concentration of 50 mM and 5  $\mu$ M. In order to adequately reduce the sample so that no

$P_{700}^+$  is left, all the samples were dark adapted for 20 minutes on ice and then frozen in the dark.

## 2.3 RESULTS

### 2.3.1 Immunological and spectroscopic quantitation of PSI

We estimated the amount of PSI accumulated in each mutant by measuring the level of PsaA polypeptide in thylakoid membranes via immunoblotting. Serial dilutions of WT extract into extracts from PSI-null strains were made to make a standard curve. At least two independent transformants of each mutant were analyzed to account for minor variations in expression. The amount of PsaA accumulated in the PsaA-Ala684 substitution mutants was in the following order: WT > PsaA-A684C > PsaA-A684N > PsaA-A684I > PsaA-A684D > PsaA-A684H. The order was the same in the B-branch mutants: WT > PsaB-A664C > PsaB-A664N > PsaB-A664I > PsaB-A664D > PsaB-A664H (Figure 2.2). In general substitutions at the PsaB-Ala664 site were somewhat better tolerated than at the PsaA-Ala684 site (with Asp being a possible exception).

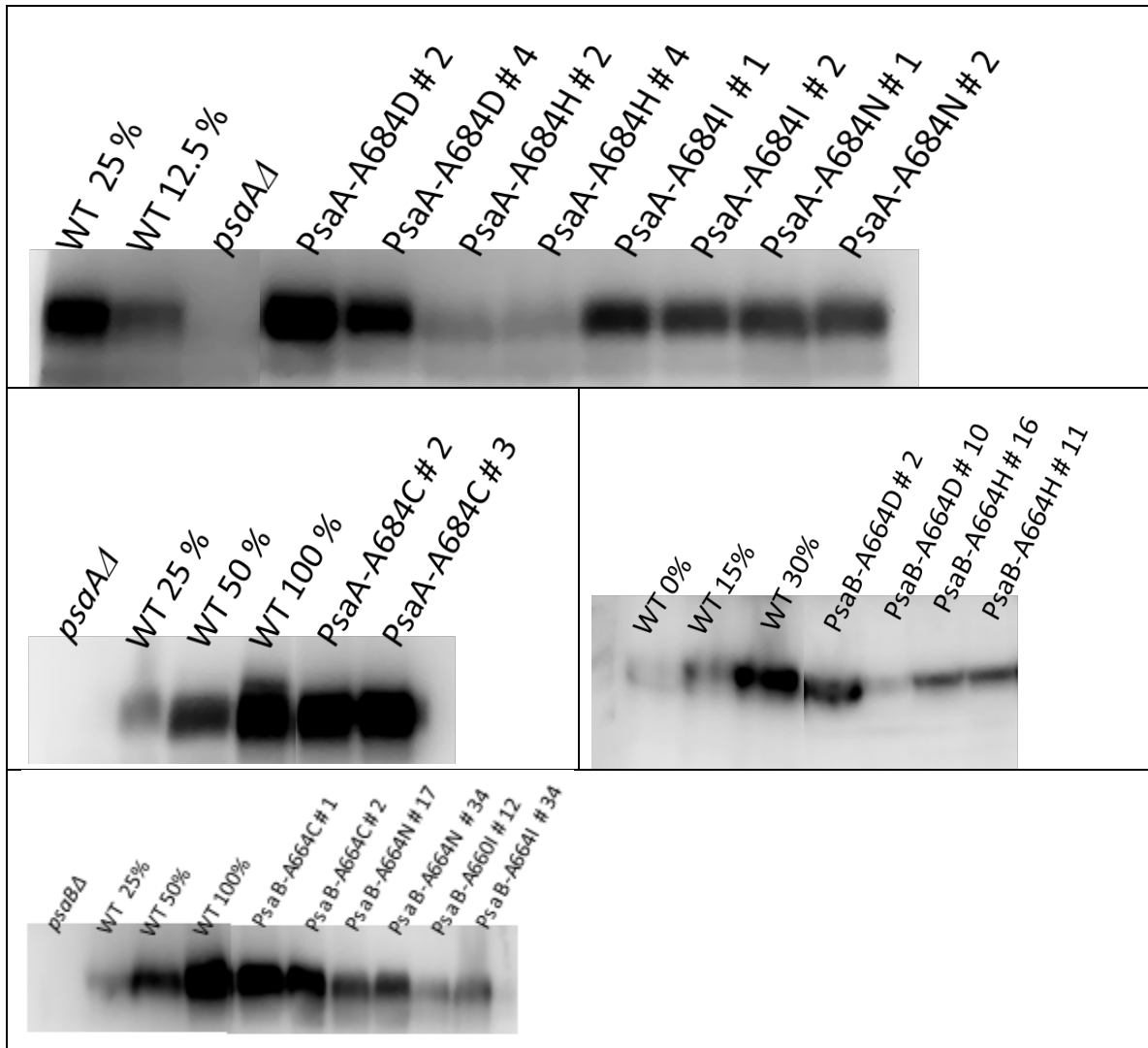
We used  $P_{700}$  photobleaching in thylakoid membranes as an independent method to quantify the accumulation of photoactive PSI. The two methods agreed remarkably well (Table 2.1). A laser flash was used to oxidize  $P_{700}$  due to generation of the  $P_{700}^+(F_A/F_B)^-$  state, which recombines in 50-100 ms (75, 76). If performed at several wavelengths, a  $P_{700}^+ - P_{700}$  difference spectrum can be constructed from the transients (Figure 2.3). In *C. reinhardtii* the maximum bleaching of  $P_{700}$  occurs at 696 nm and the extinction coefficient value of  $100 \text{ mM}^{-1} \text{ cm}^{-1}$  (77) was used to calculate the amount of  $P_{700}$ . The data was normalized based on the maximum amount of bleaching in WT (Table

1). In general, the relative amount of P<sub>700</sub> photobleaching was about equal to the relative amount of PsaA estimated from immunoblots. The exceptions were PsaA-A684D, and PsaA-A684I, PsaB-A664C, which seemed to exhibit only about 25-40% the amount of expected P<sub>700</sub> photobleaching, while no activity was detected in either of the His substitution mutants (PsaA-A684H and PsaB-A664H). In the PsaA-A684D and PsaA684N mutants, there is an increase in the width of the DS, primarily due to a shift of the blue edge. Conversely, the DS in the PsaA-A684I and PsaB-A664D mutants is narrower, primarily due to a shift of the red edge (Figure S2.3).

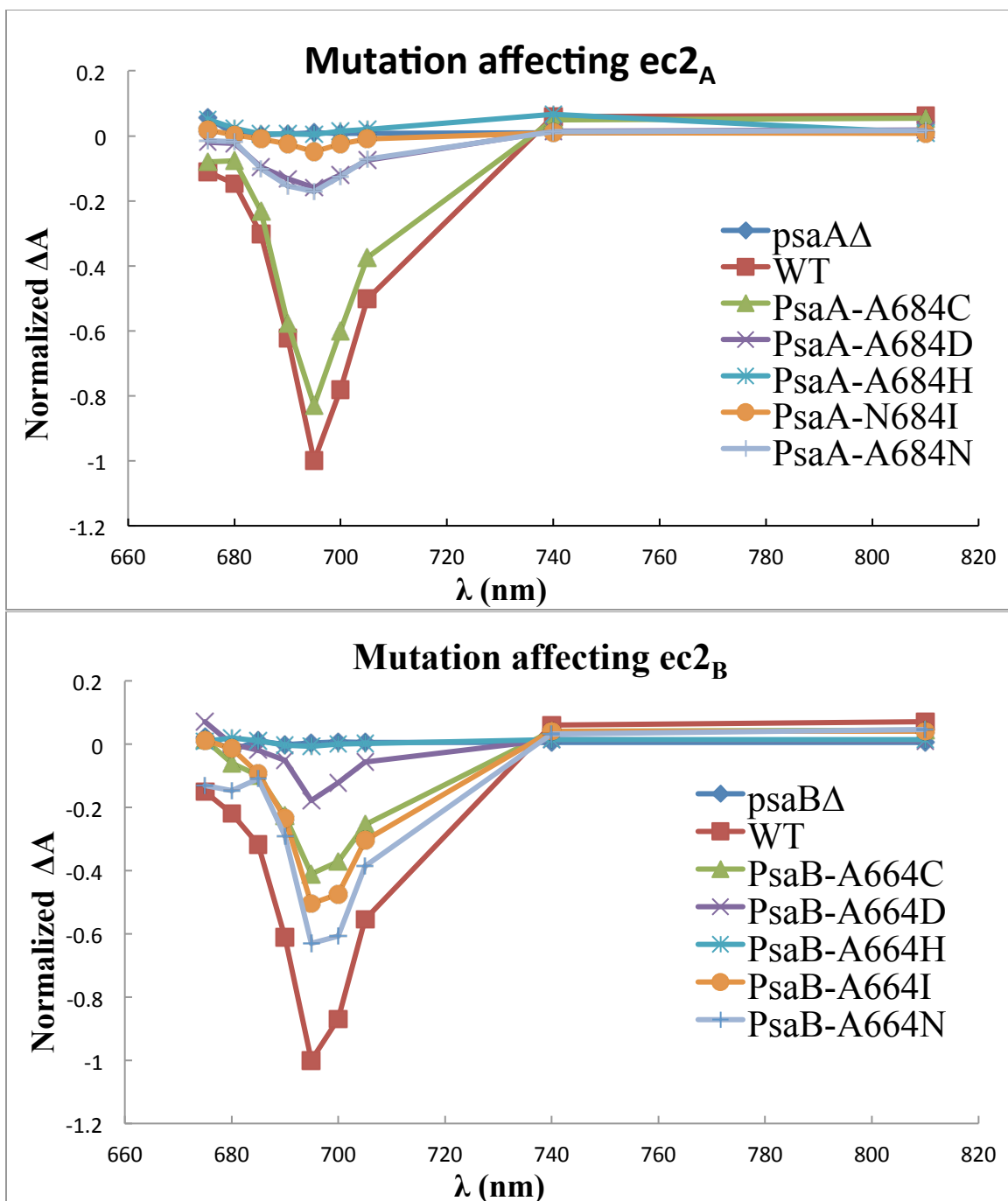
**Table 2.1.** Quantification of PS1 in membranes from different mutants.

Sample	P <sub>700</sub> level (% WT) <sup>1</sup>	PsaA amount (% WT) <sup>2</sup>	Sample	P <sub>700</sub> level (% WT) <sup>1</sup>	PsaA amount (% WT) <sup>2</sup>
WT	100.0 ± 16.3	100	WT	100.0 ± 9.4	100
PsaA-A684C	85.5 ± 11.0	91.5 ± 7.7	PsaB-A664C	35.1 ± 12.0	91.0 ± 14.1
PsaA-A684D	6.8 ± 1.3	24.6 ± 4.6	PsaB-A664D	10.1 ± 12.2	9.0 ± 9.9
PsaA-A684H	0.0 ± 0.0	4.9 ± 0.6	PsaB-A664H	0.0 ± 0.0	8.5 ± 0.7
PsaA-A684I	5.1 ± 0.8	18.2 ± 0.8	PsaB-A664I	48.2 ± 7.9	35.5 ± 2.1
PsaA-A684N	17.7 ± 2.8	19.3 ± 0.6	PsaB-A664N	63.7 ± 4.2	57.5 ± 0.7

1. The maximum bleaching at 695 nm was used for estimation of total amount of PSI, using the known extinction coefficient of P<sub>700</sub> in this species (100,000 mM<sup>-1</sup> cm<sup>-1</sup>; (77)), and was normalized to chlorophyll in each membrane preparation. (The 100% value for WT was 54 mM/g Chl)
2. The quantity of PsaA subunit relative to chlorophyll in each membrane preparation was quantified by densitometry as shown in Figure 2.



**Figure 2.2.** Immunoblots of PsaA-684 and PsaB-A664 mutants, for the detection of PsaA subunit of PSI. 0.5 $\mu$ g of chlorophyll containing protein of PSI with a volume of 10 $\mu$ L of sample were loaded on 4-10% Tricine gel with a constant voltage of 90V for 4 hour.

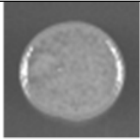
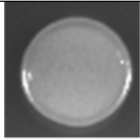
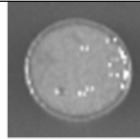
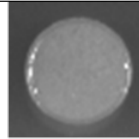
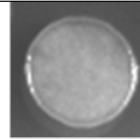
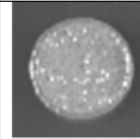
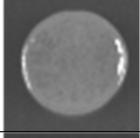
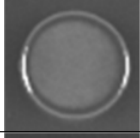
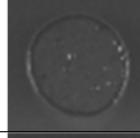
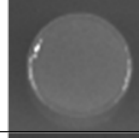
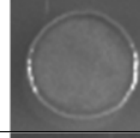
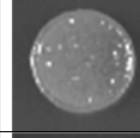
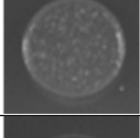
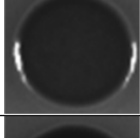
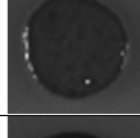
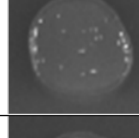
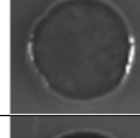
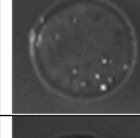
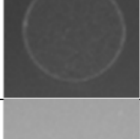
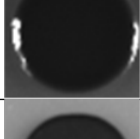
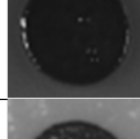
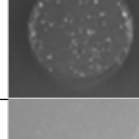
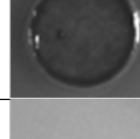
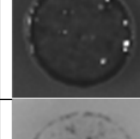

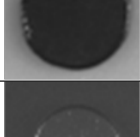
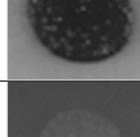
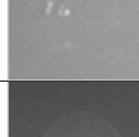

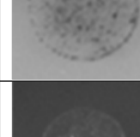



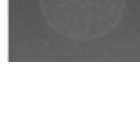
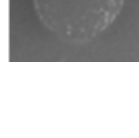
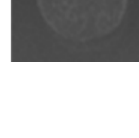


**Figure 2.3.** Light induced difference spectra of P<sub>700</sub> of different mutants affecting ec2<sub>A</sub> (A) or ec2<sub>B</sub> (B). The maximum bleaching at 695 nm was used for normalization and estimation of total amount of PSI.



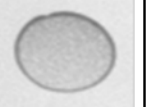


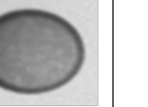



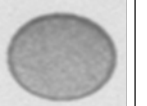

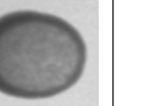

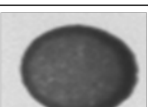
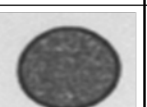



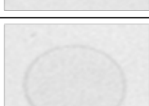

















### 2.3.2 Growth of PSI mutant strains

Based on the results in the PSII deficient strains, all of the mutants except for the His substitutions were introduced into strains that had PSII, low antenna, and the His<sub>6</sub>-tagged *psaA* exon 1 (74). Growth of the transformants was assessed in media containing or lacking a carbon source (acetate) under different illumination intensities. As seen before, WT *C. reinhardtii* grew slowly in the dark with a carbon source, and their growth accelerated with increasing light (Figure 2.4 and 2.5). Contrariwise, the PSI-deficient mutants grew in the dark at the same rate, but their growth was inhibited with increasing light; they were unable to grow without a carbon source. All of the mutants behave either like WT or intermediate between WT and the PS1-deficient parental strains. Bot of the Cys substitution mutants (PsaA-A684C and PsaB-A664C) were almost indistinguishable from WT, which is unsurprising given their high levels of PS1 accumulation. The Asp and Ile substitution mutants in either subunit (PsaA-A684D/I and PsaB-A664D/I) were incapable of photoautotrophic growth in air, but were able to grow photosynthetically under microaerobic conditions with elevated CO<sub>2</sub> (~5%). This phenotype has been seen before with mutants that accumulate low levels of PSI (78). The Asn substitution mutants (PsaA-A684N and PsaB-A664N) were intermediate in phenotype, with somewhat slower photoautotrophic growth in air than the transformants expressing WT *psaA* or *psaB*. As expected based on its lower accumulation of PSI, the PsaA-A684N strain grew more poorly.



Media (int)	<i>psaA</i> Δ	WT-A	PsaA-A684C	PsaA-A684D	PsaA-A684I	PsaA-A684N
TAP (0)						
TAP (2)						
TAP (20)						
TAP (80)						
TBP (80)						
TBP -O <sub>2</sub> (80)						

**Figure 2.4.** Growth on solid media of WT and Alanine mutants near *ec2<sub>A</sub>* of PSI. Colonies of *C. reinhardtii* were grown under heterotrophic (acetate, no light), various mixotrophic conditions (acetate with low, medium and high light) and phototrophic (no acetate but high light and anaerobic conditions).

Media (int)	<i>psaBΔ</i>	WT-B	PsaB-A664C	PsaB-A664D	PsaB-A664I	PsaB-A664N
TAP (0)						
TAP (2)						
TAP (20)						
TAP (80)						
TBP (80)						
TBP -O <sub>2</sub> (80)						

**Figure 2.5.** Growth on solid media of WT and Alanine mutants near *ec2<sub>B</sub>* of PSI. Colonies of *C. reinhardtii* were grown under heterotrophic (acetate, no light), various mixotrophic conditions (acetate with low, medium and high light) and phototrophic (no acetate but high light and anaerobic conditions).

### 2.3.3 *In vivo* transient absorption spectroscopy

Effects of the mutations upon directionality of ET within PS1 can be assessed by following the decay of the semiphylloquinone at 395 nm, a wavelength at which the DS of P<sub>700</sub> is negligible. Depending upon CS occurring on the A- or B-branch, either P<sub>700</sub><sup>•+</sup>PhQ<sub>A</sub><sup>•-</sup> or P<sub>700</sub><sup>•+</sup>PhQ<sub>B</sub><sup>•-</sup> will be generated. The P<sub>700</sub><sup>•+</sup>PhQ<sub>A</sub><sup>•-</sup> RP decays in ~200 ns, while P<sub>700</sub><sup>•+</sup>PhQ<sub>B</sub><sup>•-</sup> decays in ~20 ns (49, 50, 79, 80). Based on the estimated amount of PS1 by immunoblot and P<sub>700</sub> photobleaching, we eliminated substitution mutation for which either the PsaA or PsaB mutant accumulated active PS1 at <10% of the WT level. This method left us with the three substitutions: Asn, Cys, and Ile. We used diagnostic wavelengths at 395 nm (phyllosemiquinone) and monitored absorbance from 5 ns to 100 ms after the pump flash. As seen before (50, 53, 67), we observed biphasic decay of the absorbance at 395 nm, which is primarily due to the Phyllosemiquinone (Figure 2.6). In the WT control strain, the ratio of fast decay (22 ns) to the slow decay (252 ns) was about 0.9 (Table 2.2). We can take this ratio as a relative measure of the usage of the two branches. As these mutations are much closer to ec2 (and ec3) than to the PhQ of the targeted branch, the predicted effect of the mutation would be a change of the relative amplitude of the two kinetic components describing the semiquinone decay (and not their rates).

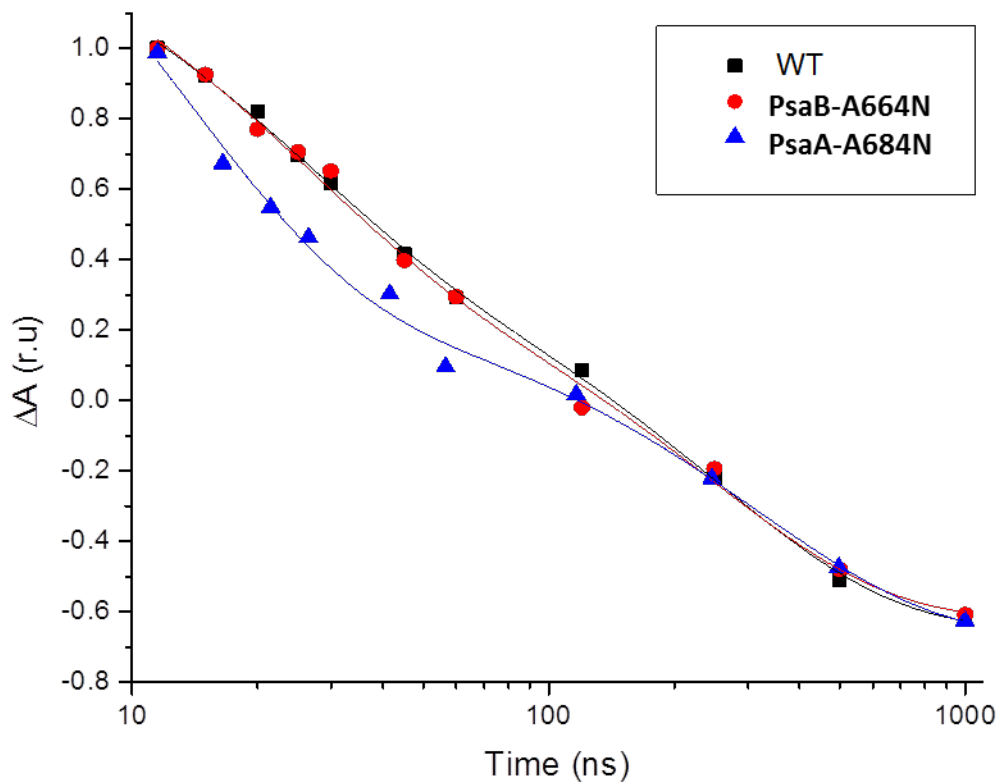
The PsaA-A684N mutant exhibited an overall faster decay with an increase of 25% in the fast phase amplitude. PhQ<sub>B</sub><sup>•-</sup> decays in 13 ns and a minor component of ET occurs through A-branch. The PhQ<sub>A</sub><sup>•-</sup> decays in 314 ns. Thus in PsaA-A684N most of the CS occurs on B-branch and the lifetime of PhQ<sub>B</sub><sup>•-</sup> is also

decreased. The ratio of fast to slow decay is 1.8 in this mutant. The PsaB-A664N has also increased in the fast phase by 5-6 % in amplitude. The decay time of 22 ns is like WT but the slower phase (244 ns) decays a few ns faster than the WT, as shown in figure 6. The ratio of fast to slow phase in PsaB-A664N is unity, which is also close to that of WT.

The *in vivo* spectroscopy allowed us to focus our attention on the mutants that appeared to have an effect upon the directionality of electron transfer within PS1. Based on them, we decided to study the Asn substitution mutants further. However, as we have no independent way of assessing the amount of PS1 *in vivo*, we were unable to distinguish between a lower yield of charge separation on one and an increase on the other branch at this level of analysis. Therefore, it was necessary to purify PS1 from the mutants in order to gain a more in-depth view of the consequences of these mutations. PS1 particles were purified from the His<sub>6</sub>-tagged strains expressing WT, PsaA-A684N, and PsaB-A664N PS1 for the biophysical analyses described below.

**Table 2.2** Fitting parameters of *in vivo* transient optical data.

Strain	Lifetime of fast phase $\tau$ (ns)	Lifetime of slow phase $\tau$ (ns)	(Ratio of fast/slow)
WT	22	252	0.9
PsaA-A684N	13	316	1.8
PsaB-A664N	22	244	1.0



**Figure 2.6.** Decay of flash-induced absorption changes at 395 nm (primarily due to PhQ<sup>-</sup>) presented as a semi-log plot. The solid lines represent the fit of a biexponential decay function to the experimental data, while the solid symbols are the data for WT (black squares), PsaA-A684N (blue triangles), and PsaB-A664N (red circles).

#### 2.3.4 Femtosecond transient absorption spectroscopy

In order to investigate primary charge separation (CS) and subsequent ET events, femtosecond transient absorption spectroscopy was used in a spectral window of 610 - 750 nm and time window of 2 ns. These mutations have no effect on the overall absorbance of the PSI particles (Figure S 2.4). Figure S2.5 shows the transient absorption DS at selected delay times after excitation at 700 nm, which preferentially excites the PS1 RC (11). In all samples, the excitation energy transfer (EET) in the RC/antenna chlorophylls is completed in 2-3 ps as shown by a small shift in the bleaching band towards the blue, this shows that energy is in equilibration between long wavelength chlorophylls and the average antenna chlorophylls. Thus the later DS from 3 ps to 2 ns mostly report on energy transfer and electron transfer events with the formation of different radical pairs (RP), as previously reported (11, 29, 62, 81). Formation of RPs takes place in tens of ps, with the DS evolving in less than ~100 ps to the final spectrum, which is assigned to the  $P_{700}^{++}PhQ^-$  RP. The mutant PS1s exhibit significant difference in spectral shape around 100 ps in the transient DS. PsaA-A684N showed absence of the 682 nm shoulder, while there is decrease in it in the PsaB-A664N as compare to WT.

The data obtained from the femtosecond transient absorption spectroscopy was analyzed with a combined approach of singular value decomposition (SVD) and global fitting (see Methods for details). Figure S2.6 shows quality of the fit and kinetics at selected wavelengths. This analysis unravels the time-resolved events in the form of time-independent spectra and wavelength-independent kinetic traces (82). The global

analyses provide information about the lifetime of three main components: energy equilibration, energy trapping and the non-decaying component ( $P_{700}^{+}PhQ^{-}$ ). All of the samples exhibited very similar lifetimes of energy trapping with 26.5 ps for WT, 25.6 ps for PsaA-A684N and 23 ps in PsaB-A664N, (Figures 2.7B and S2.5, Table S2.1). In Figure 2.7C, the long-lived components are compared. The main differences between the DADS can be observed in the wavelength region between 635 and 688 nm. The small bleaching band centered at ~656 nm in WT PSI becomes a small peak centered at ~650 nm in the two mutants. The relative intensity of the pair of (-)/(+) peaks at 680/684 nm in WT is noticeably affected by both mutations. In contrast, the major bleaching band ~695 nm is not observably affected by either mutation. The 635-688 nm region is of great importance in the  $P_{700}$  difference spectrum, as the 682-684 nm region is considered to be where the ec2 and ec3 chlorophylls contribute (83), while ec1<sub>A</sub>/ec1<sub>B</sub> are primarily responsible for the major bleaching band and increased absorption in the NIR.

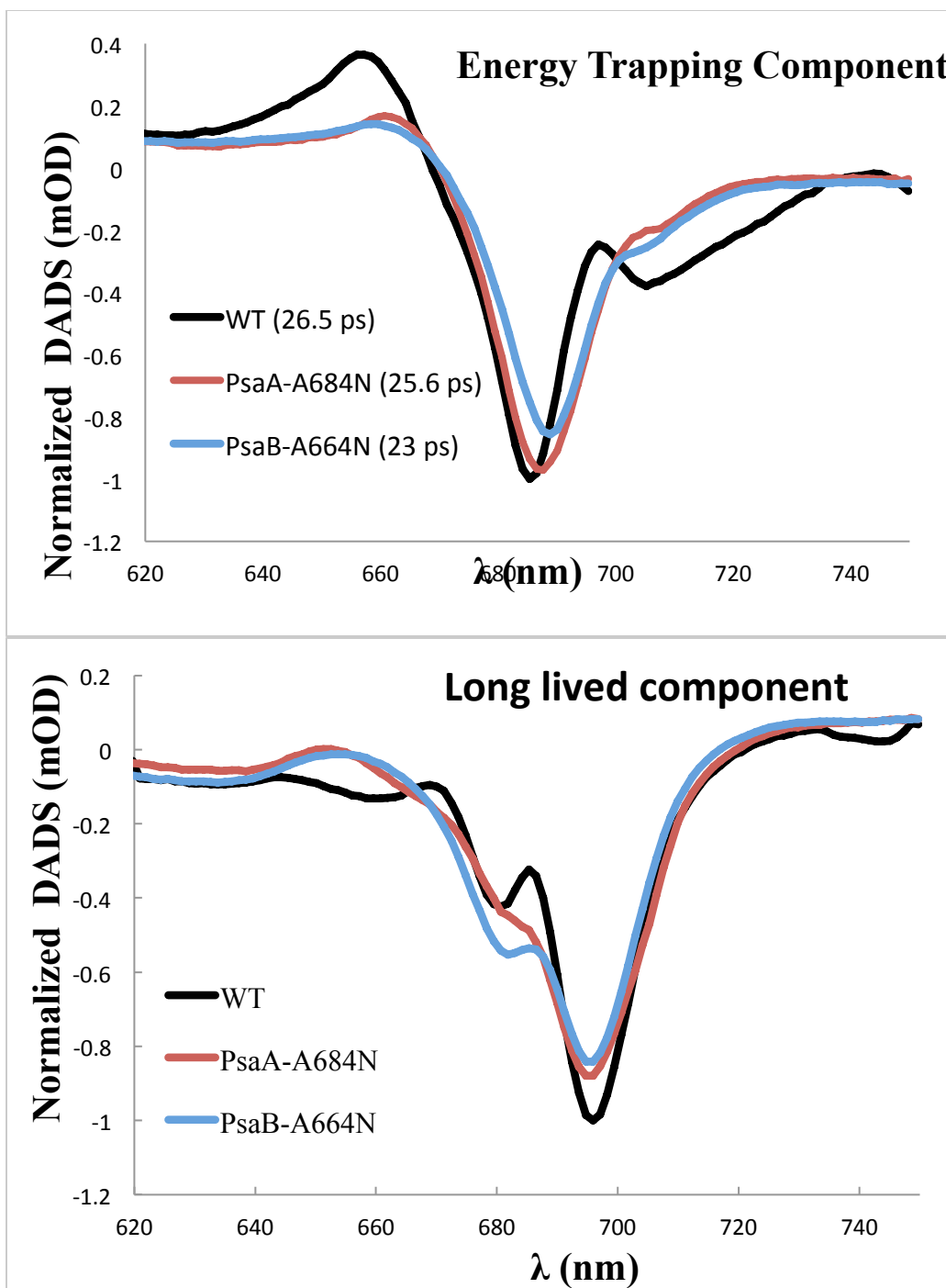


Figure 2.7. DADS of energy equilibration (A), energy trapping (B), and the long-lived component (C) calculated from the datasets of WT (black), PsaA-A684N (red), and PsaB-A664N (blue) PSI.

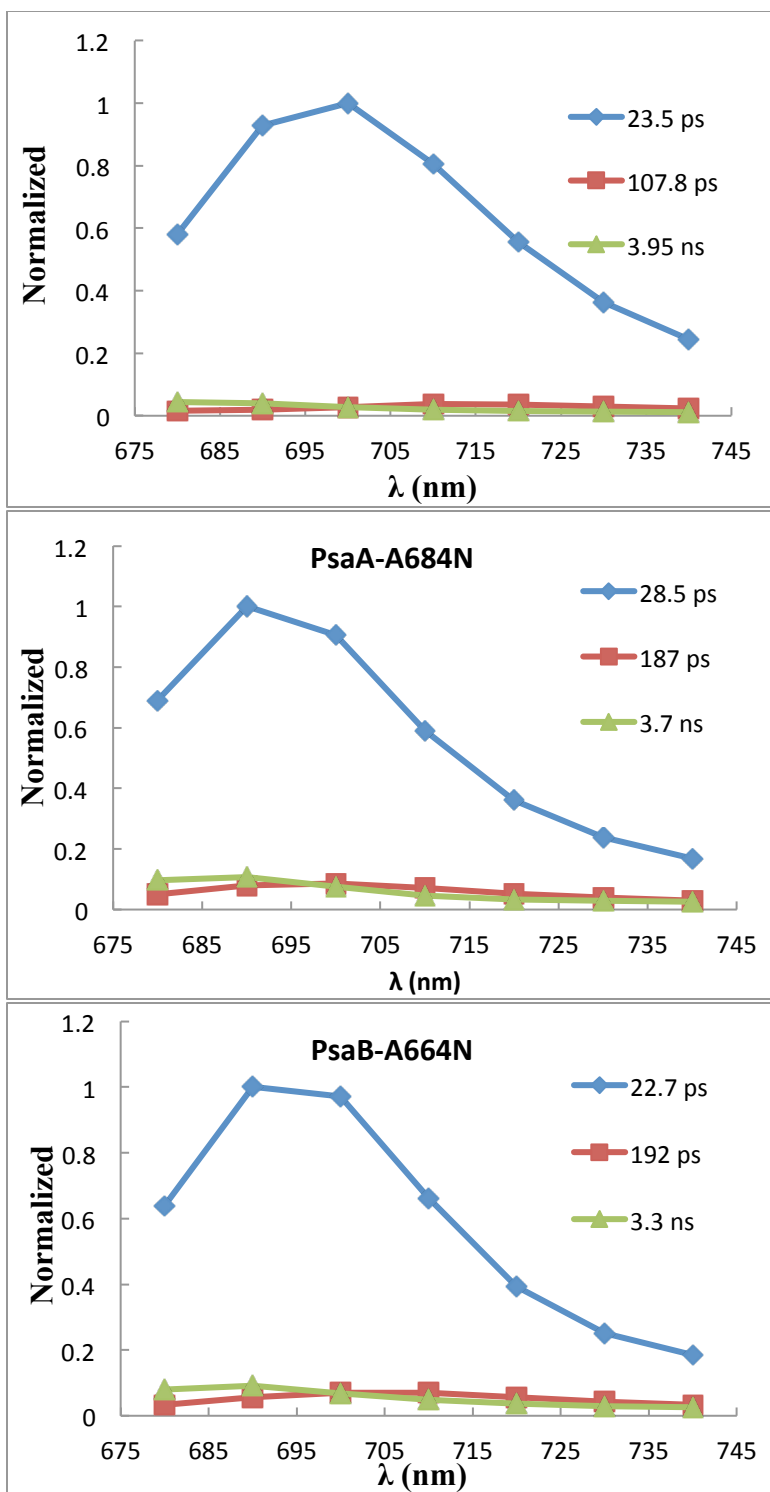


### 2.3.5 Time-resolved fluorescence decay

Time-resolved fluorescence of WT, PsaA-A684N and PsaB-A664N PS1 was performed to investigate the effect of the mutations on the energy trapping process. After exciting the sample with a laser flash at 420 nm, the absorbed energy can decay by different pathways: 1) charge separation to create a stable RP state; 2) charge separation followed by fast charge recombination back to the excited state (thus extending the lifetime of the excited state); 3) emission of energy in the form of fluorescence from the singlet excited state 4); or decay of the excited state to the ground state (with emission of heat), sometimes via a triplet state. Excitation of pigments not coupled to an open RC (e.g. uncoupled LHCI or free chlorophylls) will result in emission of fluorescence at a slow rate, giving rise to a long lifetime (typically 2-5 ns). Pigments that are coupled to an active RC will exhibit much faster decays, due to rapid charge separation.

In WT PSI, the time-resolved fluorescence was best fitted with three components. The fastest component has the dominant amplitude with a lifetime of 23-24 ps and the DAS peaks at 700 nm. This is the energy-trapping component assigned to primary CS (Figure 2.8). There are also two minor components of fluorescence decay, which have very small contributions in terms of the amplitude in the decay-associated fluorescence spectra. The slowest component (3-4 ns) is attributed to decay of the excited state in uncoupled antenna or free chlorophylls. The one with an intermediate lifetime of 100-200 ps is attributed to slow excitation energy transfer from the peripheral antenna (i.e. LHCI to PSI core), as has been observed before in PSI from *C. reinhardtii* (84). In PsaB-A664N, the

trapping lifetime is similar to WT. In PsaA-A684N, the lifetime of energy trapping is increased by about 20%, which is consistent with a somewhat slower rate of CS, as kinetics of excited state decay is trap-limited (35, 43).



**Figure 2.8.** Decay-associated fluorescence emission spectra of WT (A), PsaA-A684N (B), and PsaB-A664N (C) PS1 obtained from a 3-component fit using global analysis of

kinetic traces. The measurements were performed at room temperature using excitation at 420 nm.

### 2.3.6 Room-temperature transient EPR spectroscopy

Time-resolved X-band EPR spectroscopy at ambient temperature was used to study forward electron transfer in the PSI samples. Transient EPR signals were recorded at different magnetic field positions, and EPR spectra were constructed for 220 ns, 360 ns and 1000 ns after the laser flash. In Figure 2.9, the positive signal represents microwave absorptive spin polarization (A) while negative signals are emissive spin polarization (E). At the initial time point, the spin-polarized signal is largely from  $P_{700}^{++}PhQ^{\bullet-}$ , while the emissive signal seen at the end is due to  $P_{700}^{++}FeS^{\bullet-}$ , and primarily arises from  $P_{700}^{++}$  (53, 85, 86). Since ET from  $F_X^{\bullet-}$  to the terminal  $F_A/F_B$  clusters in PS1 from *C. reinhardtii* is estimated to take place in about 100-200 ns (87), it is kinetically unresolved, and ET from  $PhQ_A^{\bullet-}$  to  $F_X$  and the late EPR spectrum is, therefore, largely due to the  $P_{700}^{++}(F_A/F_B)^{\bullet-}$  state. In addition, this technique is unable to resolve the fast ET step from  $PhQ_B^{\bullet-}$  to  $F_X$  (~20 ns), which means that the early spectrum of 220 ns will arise from a mixture of states:  $P_{700}^{++}(F_A/F_B)^{\bullet-}$  mainly due to B-side ET and  $P_{700}^{++}PhQ_A^{\bullet-}$  almost purely due to A-side ET. There are two important consequences of these facts: (1) the shape of the earliest spectrum will be sensitive to the population of states in the mixture, which is a function of directionality of ET, and (2) the subsequent ET observed as the  $P_{700}^{++}PhQ^{\bullet-}$  evolves into a pure  $P_{700}^{++}FeS^{\bullet-}$  spectrum will be almost solely due to forward ET from  $PhQ_A$ . The initial transient spectrum in WT PS1 resembles the low-temperature spectrum of  $P_{700}^{++}PhQ_A^{\bullet-}$  (due to A-side ET), but it is distorted due the presence of  $P_{700}^{++}FeS^{\bullet-}$  (due to

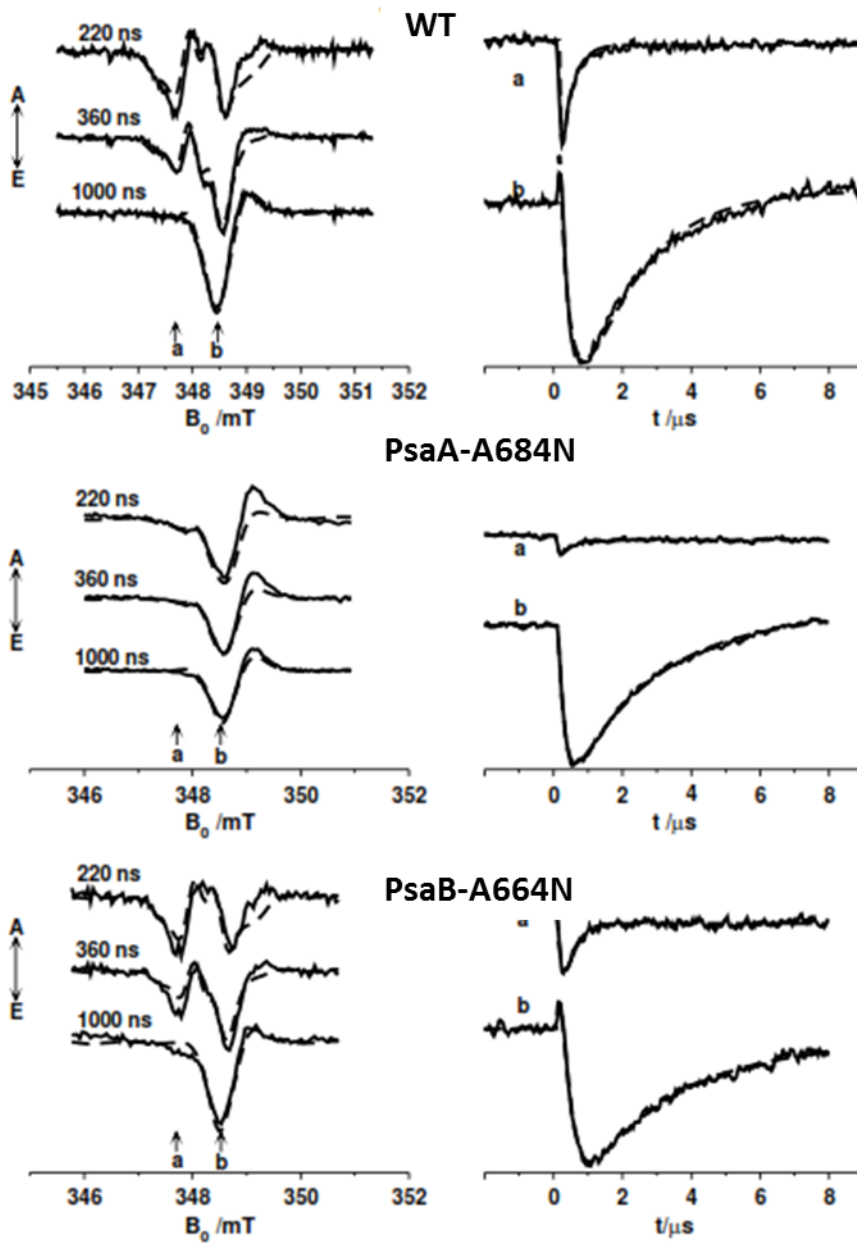
B-side ET). At later times, the  $P_{700}^{+}FeS^{-}$  increasingly dominates until it is the only species seen at 1  $\mu$ s. The transient spectra from the PsaB-A664N PSI mutant are very similar to WT.

In the PsaA-A684N PSI mutant, even the earliest spectrum looks like the later spectrum, which is of the  $P_{700}^{+}FeS^{-}$  state. There is very little evolution of the spectrum from 220 ns to 1000 ns, indicative of very little A-side ET. This is seen most clearly in the right panel, which shows very little drop at field position **a** or rise at position **b** in the sub- $\mu$ s time scale, unlike the WT or PsaB-A664N mutant. Thus, the  $P_{700}^{+}FeS^{-}$  state seen early on in the PsaA-A684N mutant must have been produced largely by B-side ET. The initial absorptive pattern at position “b” for PsaB-A664N representing  $P_{700}^{+}PhQ_A^{-}$  is unaffected and looks similar to that of WT, but the later emissive part has decreased amplitude by 15% as compared to WT.

Simulation of the whole time/field data set of each sample (dashed lines in Figure 2.9) was performed to extract the lifetimes and fractions of the kinetic components. In WT, the calculated ratio of the fast and slow decay components (i.e.  $PhQ_B^{-}:PhQ_A^{-}$ ) is 0.51:0.49 and the lifetime of the slow component is 200 ns, if one assumes a 20-ns lifetime for the fast component (Table 2.3). In the PsaA-A684N mutant, the fraction of the fast component is increased to 0.7 from 0.51, without a change in the lifetime of the slow component. For PsaB-A664N, the fraction of fast component is 0.31 (Table 2.3), with a slight increase in the lifetime of the slow component (240 ns).

**Table 2.3.** Global fitting parameters for decay components of different RP's from room temperature X-band transient EPR spectroscopy

<b>Strain</b>	<b>Fraction of fast component (Decay of <math>\text{PhQ}_\text{B}^-</math>)</b>	<b>Lifetime of slow phase <math>\tau</math> (ns)</b>	<b>Lifetime of fast phase <math>\tau</math> (ns)</b>
WT	0.51	200	20 (assumed)
PsaA-A684N	0.70	200	20 (assumed)
PsaB-A664N	0.31	240	20 (assumed)



**Figure 2.9.** Room temperature X-band spin polarized transient EPR spectra of the  $P_{700}^{+}\text{PhQ}_A^{-}$  and  $P_{700}^{+}\text{FeS}^{-}$  radical pairs (left panels) and calculated time dependent transients (right panels).

### 2.3.7 Low-temperature transient EPR spectroscopy

Below the glass transition temperature ( $\sim 80$  K), the RP formed upon excitation of PS1 is  $P_{700}^{+\bullet}\text{PhQ}_A^{\bullet-}$  and the contribution from the  $\text{PhQ}_B$  is negligible (88). Due to thermodynamic reasons, electron transfer from  $\text{PhQ}_A^{\bullet-}$  to  $F_X$  is impossible at low temperature (85). At X-band frequencies, all of the PS1 samples exhibited the E/A/E polarization pattern previously observed (Figure 2.10A) (89-91), where E represents emission, and A represents absorption. In WT PS1, there is a small shoulder on the low-field side of the central absorptive peak, which arises primarily from hyperfine coupling (hfc) of the 2-methyl protons of  $\text{PhQ}_A^{\bullet-}$  (89, 92). Due to H-bonding with O-4 of PhQ, electron spin density is more concentrated at C-2, and this position lies on the principal axis of the  $\text{PhQ}^{\bullet-}$  g-tensor (91). Thus, we can observe the partially resolved methyl hfc in the central absorptive region of  $P_{700}^{+\bullet}\text{PhQ}_A^{\bullet-}$  spectrum of WT PS1 (91). The spectrum of PsaB-A660N is quite similar to that of the WT. However, there are minor differences in the intensity and position of the methyl hfc position on the polarized absorption spectrum of  $P_{700}^{+\bullet}\text{PhQ}^{\bullet-}$ .

The spectrum of PsaA-A684N is markedly different from that of WT PS1. The 2-methyl hfc shoulder is rather distinct, showing an increase in coupling from the 2-methyl protons. At the high-field side of the central absorptive feature there is the appearance of another unusual shoulder in the PsaA-A684N spectrum. This shoulder can be explained in a number of ways. Firstly, the low-temperature EPR of PsaA-A684N may represent a mixture of  $P_{700}^{+\bullet}\text{PhQ}_A^{\bullet-}$  and  $P_{700}^{+\bullet}\text{PhQ}_B^{\bullet-}$ . Presumably, the spectrum of the  $P_{700}^{+\bullet}\text{PhQ}_B^{\bullet-}$  RP would possess such a feature. Secondly, this shoulder could arise from a  $P_{700}^{+\bullet}\text{FeS}^{\bullet-}$  RP



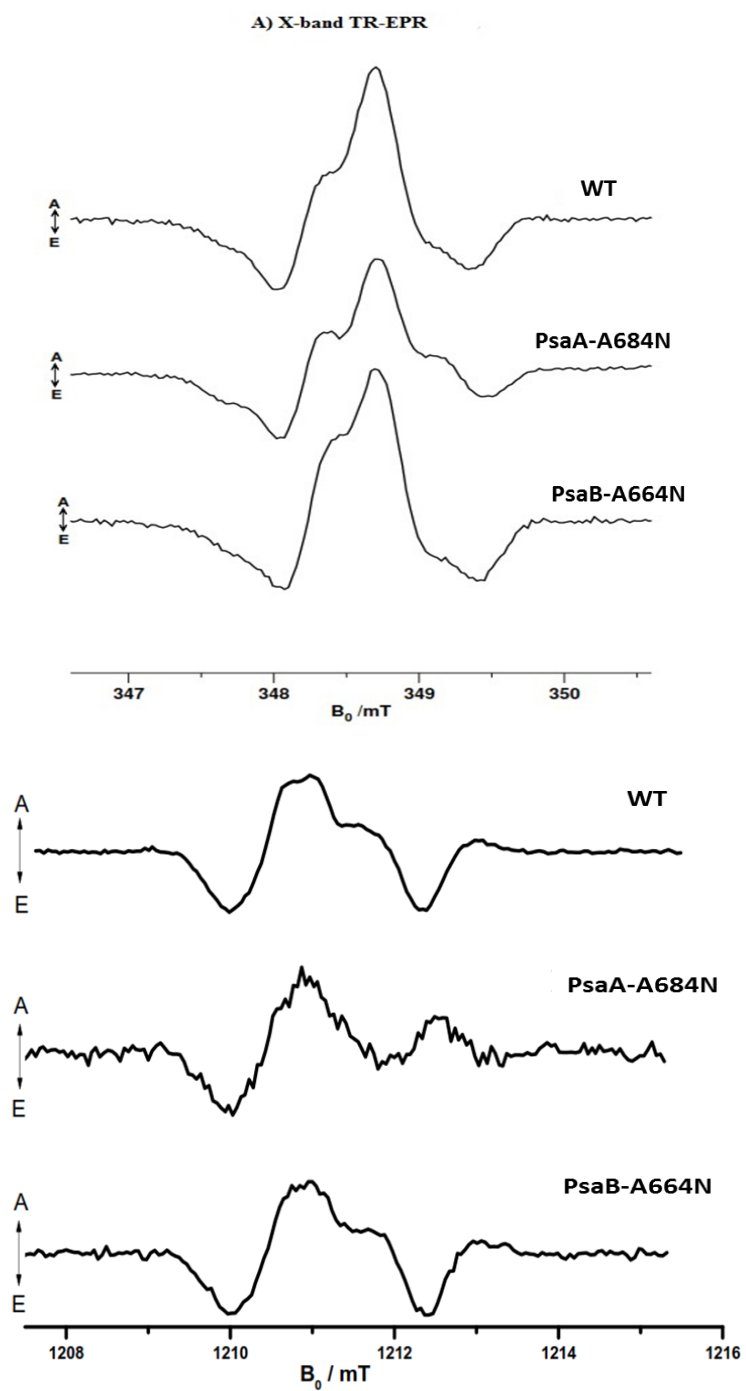
due to an increase in forward ET from  $\text{PhQ}_\text{A}^{\bullet-}$  at 80K in the mutant. It has been argued that some ET from  $\text{PhQ}_\text{A}$  to  $\text{F}_\text{X}$  can occur at low temperature, forming some  $\text{P}_{700}^{++}\text{FeS}^{\bullet-}$  (85, 93). At the high-field side of the central absorptive feature there is the appearance of another unusual shoulder in the PsaA-A684N spectrum. This shoulder can be explained in a number of ways. Firstly, the low-temperature EPR of PsaA-A684N may represent a mixture of  $\text{P}_{700}^{++}\text{PhQ}_\text{A}^{\bullet-}$  and  $\text{P}_{700}^{++}\text{PhQ}_\text{B}^{\bullet-}$ . Presumably, the spectrum of the  $\text{P}_{700}^{++}\text{PhQ}_\text{B}^{\bullet-}$  RP would possess such a feature. Secondly, this shoulder could arise from a  $\text{P}_{700}^{++}\text{FeS}^{\bullet-}$  RP due to an increase in forward ET from  $\text{PhQ}_\text{A}^{\bullet-}$  at 80K in the mutant. It has been argued that some ET from  $\text{PhQ}_\text{A}$  to  $\text{F}_\text{X}$  can occur at low temperature, forming some  $\text{P}_{700}^{++}\text{FeS}^{\bullet-}$  (85, 93). The amount of this ET from  $\text{PhQ}_\text{A}$  to  $\text{F}_\text{X}$  is minor and so is the ratio of  $\text{P}_{700}^{++}\text{F}_\text{X}^{\bullet-}$  to  $\text{P}_{700}^{++}\text{PhQ}_\text{A}^{\bullet-}$  in WT. In the EPR spectrum of PsaA-A684N, the intensity of  $\text{P}_{700}^{++}\text{PhQ}_\text{A}^{\bullet-}$  would be decreased while that of  $\text{P}_{700}^{++}\text{FeS}^{\bullet-}$  would be increased, producing this shoulder. The third explanation of this shoulder is that the PsaA-A684N mutation changes parameters of the  $\text{P}_{700}^{++}\text{PhQ}_\text{A}^{\bullet-}$  RP (e.g. orientation) due to perturbation of the environment of  $\text{P}_{700}^{++}\text{PhQ}_\text{A}^{\bullet-}$ . For the last two explanations, one would have to invoke indirect effects or long-range interactions to explain why a mutation near  $\text{ec2}_\text{A}$  would affect the ET or structural properties of  $\text{PhQ}_\text{A}$ .

In order to analyze the contribution of different RPs in a more detailed way, we repeated the low-temperature transient EPR experiments at higher magnetic field and microwave frequency (Q-band; Figure 2.10B). WT PS1 exhibits the E/A/A/E/A polarization pattern (where E=emissive and A=absorptive) seen before in cyanobacterial PS1 (91, 94). In this spectrum the lower field part of the central absorptive peak represents the spin

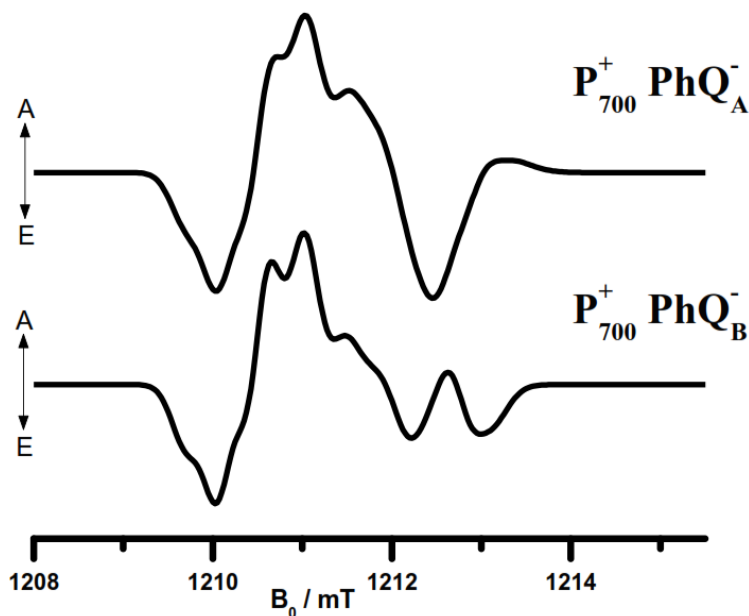
polarization of the semiphylloquinone (primarily  $\text{PhQ}_\text{A}^{\bullet-}$  in WT PS1), while the higher field part has strong contributions from  $\text{P}_{700}^{++}$ . There are two emissive bands, one on each side of the absorptive peak. The Q-band spectrum of PsaB-A664N PS1 is very similar to that of WT PS1.

The low-temperature transient Q-band EPR spectrum from the PsaA-A680N mutant is very different from that of WT PS1. Firstly, the small shoulder due to hfc from the 2-methyl protons near 1211 mT is mostly missing. Even more starkly, the emissive peak at 1212.5 mT has been replaced with an absorptive peak. We can explain this difference in the Q-band spectrum using the same explanations discussed above. As mentioned, the last two explanations invoke changes of  $\text{PhQ}_\text{A}$  due to indirect or long-range effects, and are not very appealing, as they rely upon a coincidental phenomenon and are therefore difficult to test. After chemical reduction of the FeS clusters, a flash-induced EPR spectrum with the same polarization pattern as that of PsaA-A680N was observed in the PsaA-L722T mutant from *S. 6803* at low temperature, and it was assigned to  $\text{P}_{700}^{++}\text{PhQ}_\text{B}^{\bullet-}$  (94). We tested the hypothesis that the spectrum seen in the PsaA-A680N mutant at low temperature represents the  $\text{P}_{700}^{++}\text{PhQ}_\text{B}^{\bullet-}$  RP by calculating theoretical EPR spectra for the  $\text{P}_{700}^{++}\text{PhQ}_\text{A}^{\bullet-}$  and  $\text{P}_{700}^{++}\text{PhQ}_\text{B}^{\bullet-}$  RPs (see Figure 2.11). The match is surprisingly good, as the calculated spectrum of the  $\text{P}_{700}^{++}\text{PhQ}_\text{B}^{\bullet-}$  RP recapitulates the two major changes seen in the in the spectrum of the PsaA-A684N mutant: the decrease of the high-field portion of the central absorptive feature and the appearance of a new emissive peak at high field. Thus, one can explain the changes in the low-temperature transient EPR spectra of the

PsaA-A680N mutant by changes in directionality of ET within PS1 without having to invoke indirect effects of the mutation upon the PhQ<sub>A</sub> cofactor.



**Figure 2.10.** Spin polarized transient EPR spectra of PSI from WT, PsaA-A684N, and PsaB-A664N mutants of *C. reinhardtii* at X-band (A) and Q-band (B) frequencies, measured at 80 K.



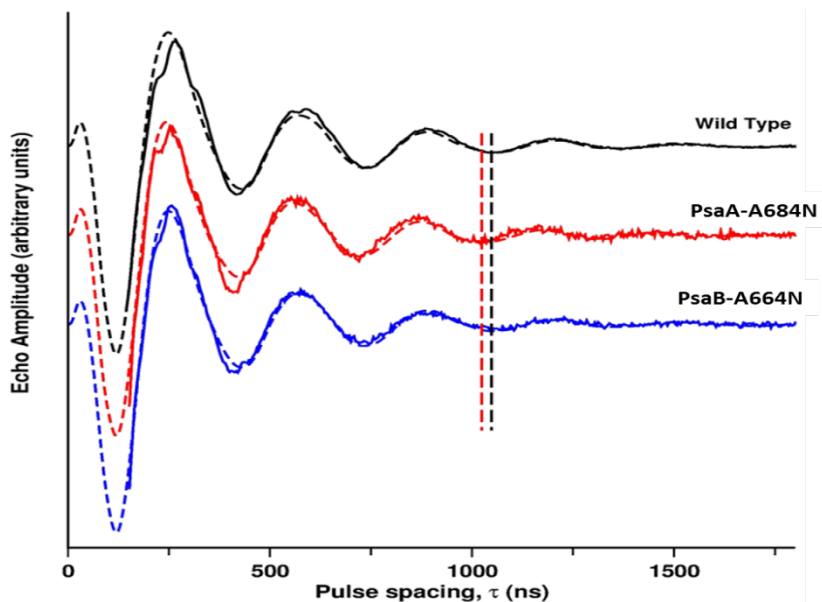
**Figure 2.11.** Simulations of Q-band EPR spectra of  $P_{700}^{+}PhQ_A^{-}$  and  $P_{700}^{+}PhQ_B^{-}$  RPs. The low-field part of the two RP spectra is normalized for better visualization of the difference in the high field part.

### 2.3.8 Out of Phase Echo Envelope Modulation

Pulsed EPR spectroscopy can be used to provide information on the spin-spin interactions between the two radicals of a RP, from which structural information can be extracted. The magnitude of the anisotropic dipolar interaction ( $D$ ) between the unpaired electrons in the RP depends upon the distance ( $1/r^3$ ) and the exchange interaction ( $J$ ) due to electronic coupling between the radicals. This dipolar spin-spin interaction is the origin of the orientation information in time-resolved EPR spectra. In the Hahn two-pulse echo experiment,  $\pi/2$ - $\tau$ - $\pi$ - $\tau$ -echo is applied after the laser flash, where  $\tau$  is the delay time

between the two  $\pi/2$  and  $\pi$  microwave pulses. The echo signal arising from the RP is phase shifted in relation to its spin system at thermal equilibrium and arises in the same phase as that of the applied microwave pulses. The out-of-phase (OOP) echo is due to spin-spin (D) and exchange (J) interactions from the RP. These two parameters change the echo decay as a function of delay time ( $\tau$ ) and this effect is called out-of-phase electron spin echo envelope modulation (OOP-ESEEM). The dipolar interaction energy is approximately two times larger in magnitude than the exchange interaction energy due to large distance between the EPR-detected radicals in RCs. Thus the dipolar interaction energy is the dominant factor in the modulation of ESEEM. Measurement of D, which is very sensitive to the inter-electron distance, allows calculation of the distance between the two radical species in the RP (95-98). The OOP-ESEEM of WT PSI was used to estimate the distance between the  $P_{700}^{\bullet+}$  dimer and PhQ in flash-generated  $P_{700}^{\bullet+}PhQ^{\bullet-}$  (99, 100). These results completely agreed with the later X-ray crystallographic results (21), demonstrating the strength and accuracy of this method. Analyses of ec3 axial ligand mutations (56, 98) showed changes in the modulation frequency of the OOP-ESEEM signal, indicating the presence of the  $P_{700}^{\bullet+}PhQ_B^{\bullet-}$  RP. The rationale for this interpretation hinges on the different spin-spin distances of the  $P_{700}^{\bullet+}PhQ_A^{\bullet-}$  and  $P_{700}^{\bullet+}PhQ_B^{\bullet-}$  RPs. Although the quinones are located at sites related by a C2 symmetry axis running through P700, the spin of  $P_{700}^{\bullet+}$  is not located on the symmetry axis due to its asymmetric localization on  $P_B$  (26). The inter spin distance is  $25.43 \pm 0.01 \text{ \AA}$  for  $P_{700}^{\bullet+}PhQ_A^{\bullet-}$  and  $24.25 \pm 0.01 \text{ \AA}$  for  $P_{700}^{\bullet+}PhQ_B^{\bullet-}$ . Thus, the spin-spin distances are different in the two radical pairs, with that of  $P_{700}^{\bullet+}PhQ_B^{\bullet-}$  being slightly shorter (54).

In order to test the hypothesis that the low-temperature EPR spectrum of the PsaA-A684N mutant contained contributions from the  $P_{700}^{+\bullet}\text{PhQ}_B^{-\bullet}$  RP, we performed OOP-ESEEM experiments. The time-dependent OOP-ESEEM signals (solid lines) are shown along with the calculated traces (dotted lines) in Figure 2.12. The oscillation frequency in PsaA-A680N is higher than that of WT, while it is lower than WT in PsaB-A664N. The increased oscillatory frequency in PsaA-A684N showed increased generation of  $P_{700}^{+\bullet}\text{PhQ}_B^{-\bullet}$ , as the inter spin distance for this radical pair is smaller than that of the A-side RP. The calculated ratios of  $P_{700}^{+\bullet}\text{PhQ}_A^{-\bullet}$  and  $P_{700}^{+\bullet}\text{PhQ}_B^{-\bullet}$  contributions obtained from the fits of the data are 15:85 for PsaA-A684N, 60:40 for WT, and 70:30 for PsaB-A664N.



**Figure 2.12.** OOP-ESEEM traces of the spin-correlated  $P_{700}^{+\bullet}\text{PhQ}^{-\bullet}$  radical pair at 80 K for the PsaA-A680N (red) and PsaB-A660N mutants (blue), compared to WT (black). The vertical black, dashed line indicates the position of the minimum near  $\tau = 1000$  ns for the WT and PsaB-A660N modulation curves. The vertical dashed red line in the position of the minimum for the PsaA-A680N mutant.

indicate the position of the minimum frequency at  $\tau = 750$  ns for the three modulation curves.

### 2.3.9 Measurement of $^3P_{700}$ triplet by transient EPR at low temperature

When forward ET beyond ec3 is blocked, charge recombination (CR) of the  $P_{700}^{++}ec3^{\bullet-}$  RP leads to formation of  $^3P_{700}$  (101). This state later transfers energy to a nearby carotenoid, forming  $^3Car$ , which safely dissipates the absorbed energy by decaying to the ground state with emission of heat. The low-temperature TR-EPR spectrum of  $^3P_{700}$  has unique zero-field splitting parameters and a distinct AEEAAE polarization pattern due to the delocalization of the triplet over the two chlorophylls of  $P_{700}$  (86). It can be observed by scanning a wider magnetic field that used to capture the RP spectra. The transient X-band spectra taken at 80 K over a wider field scan are shown in Figure S2.7. The sharp EAE feature at 345 - 350 mT is due to the  $P_{700}^{++}PhQ_A^{\bullet-}$  RP. This feature is weaker in the PsaA-A680N mutant than that of WT and PsaB-A664N. Thus making mutation on the A-side, decrease the formation of  $P_{700}^{++}PhQ_A^{\bullet-}$  RP. The  $^3P_{700}$  states are of similar amplitude in both the mutants with AEEAAE polarization pattern showing small amount of CR. Thus PsaA-A684N causes only a change in the CS across the two branches and there is no significant charge recombination due to blockage of ET beyond ec3 cofactor.

## 2.4 DISCUSSION

Examination of the crystal structure of PS1 reveals that the ec2 Chl makes few contacts with polypeptide; most of its contacts are with phytyl chains of other chlorophylls, carotenes, etc. Even its axial ligand is a water molecule, rather than an amino acid sidechain. The targeted Ala residue is one of the few places where the polypeptide contacts the ec2 Chl, although just as a van der Waals interaction. Its location afforded us the opportunity to explore the consequences of changing the environment of the ec2 Chl (and ec2/ec3 pair) by appending new functional groups to the  $\alpha$ -carbon of this residue: thiol (Cys), carboxylic acid (Asp), amide (Asn), alkyl chain (Ile), or imidazole (His). Perhaps unsurprisingly, the largest introduced group (His) was tolerated least well, resulting in almost no PSI, while the smallest introduced group (Cys) was tolerated best, as the Cys substitution mutants were the most similar to WT. A beta-branched alkyl chain (Ile) or potentially charged group (Asp) produced changes in the function of PS1 but were not tolerated as well as the Asn substitution, which seemed to represent the best compromise between accumulation of PS1 and effect upon its function. At this point, we do not know how the introduced amide functional group interacts with the ec2/ec3 cofactors. Modeling of the structure seems to preclude the possibility of the amide serving as an alternate axial ligand to ec2 and there are no functional groups of ec3 to which it could H-bond. Therefore, it seems likely that the effects produced by the Asn substitution mutation(s) are due to the increased polar character of the environment and/or subtle structural rearrangements of the cofactors in response to the larger sidechain.



Modifying the region between the ec2 and ec3 chlorophylls on each branch by introducing a new amide group produced a noticeable effect upon the directionality of charge separation in PSI. Time-resolved optical spectroscopy (both *in vivo* and *in vitro*) in the ns-ms timescale indicated that these mutations change the relative use of the two quinones within PS1, although the magnitude of the effect is quite different between the two sides. The PsaA-A684N clearly resulted in a decrease in A-side ET and a corresponding increase in B-side ET. The effect of the PsaB-A664N mutation was much smaller and often nearly impossible to see. The results from time-resolved EPR at room temperature are in agreement with these conclusions. In neither case did we observe evidence indicating that the effect of the mutation was to block forward ET from the ec3 Chl, as was observed in mutants of the ec3 axial ligand (31, 86). There was very little fast decay of  $P_{700}^{+}$  in the 10-50 ns timescale seen in the time-resolved optical measurements, nor did the low-temperature EPR measurements detect elevated  $^3P_{700}$ , which would be produced by charge recombination of  $P_{700}^{+}ec3^{-}$  ( $P_{700}^{+}A_0^{-}$ ). In addition, there was no evidence of a chlorophyll anion persisting beyond 200 ps in the ultrafast optical experiments. Taken together, these results argue for a change in the relative utilization of the two branches for primary CS. This effect is somewhat similar to that seen with mutants in which a hydrogen bond to ec3 is broken (53), although but it is much larger for A-side mutant in this case.

#### 2.4.1 Charge separation at room temperature

The ultrafast optical spectroscopy of the mutants revealed a small effect on the rate of energy trapping. It is important to point out that the observed decay rate of the ~20-ps component is not the rate of initial charge separation; rather, it represents a combination of the primary and secondary electron transfer steps taking place after the energy equilibration between the antenna chlorophylls and RC. Furthermore it must represent a weighted average of events taking place on the two sides. The lifetime of this component increases from 21.5 ps in WT PS1 to 25.6 ps in the PsaA-A684N mutant. Consistent with its much smaller effect, the lifetime is 23 ps in PsaB-A664N, which is quite significant. The fastest fluorescence decay time, associated with trapping of excitation energy, also increases in the PsaA-A684N mutant, from 23.5 to 28.5 ps, while there is no observable difference in the PsaB-A660N mutant. Taken together, this is consistent with the hypothesis that the overall rate of initial charge separation on the A-side (i.e.  $\text{RC}^* \rightarrow \text{P}_{680}^+ \text{P}_{680}^-$ ) is somewhat slowed by the PsaA-A684N mutation, while the corresponding mutant on the B-side has a much smaller effect.

We did not observe a significant decrease in the quantum yield of long-lived charge separation caused by the Ala substitution mutations. When integrated over the range of 620 – 720 nm, the magnitudes of the major bleaching band in the DADS of the long-lived components were comparable between WT and the two mutants. (Normalized on a Chl basis, the bleaching bands in PsaA-A684N and PsaB-A664N were 97% and 99% that of WT PS1, respectively. The peak height is lower in the mutants because of subtle changes in the  $\text{P}_{700}^+ - \text{P}_{700}$  difference spectrum, discussed below.) Thus, if the mutations cause a

decrease in quantum efficiency, it must be very small. In contrast a large drop in quantum efficiency of PS1 CS has been observed in site-directed mutants targeting the PsaA-Asn604 and PsaB-Asn591 residues (Badshah, S.; Sun, J.; Mula, S.; Baker, P.; Lin, S.; Est, A. V.; Golbeck, J.; Redding, K. **manuscript in preparation**), which H-bond with the water molecule serving as the axial ligand of ec2 (21)

Substitution of the methionine axial ligands to the ec3 Chls with histidine in *C. reinhardtii* PS1 resulted in a block of ET from ec3 to PhQ, as seen by persistence of the  $A_0^-$  (ec3<sup>-</sup>) Chl anion radical in the long-lived component of the ultra-fast spectrum (102). This block in forward ET resulted in charge recombination of the  $P_{700}^+A_0^-$  radical pair in ~30 ns, which was seen *in vivo* (87), ruling out biochemical artifacts. We saw no evidence that this was the case in the Ala→Asn substitution mutants described here. There was no additional bleaching band peaking in the 680-684 nm region in the long-lived component of the ultra-fast data, ruling out a long-lived Chl anion species (Figure 6). We also saw no signs of  $P_{700}^+A_0^-$  charge recombination in the ns timescale, either *in vivo* (Figure 5) or *in vitro* (Figure 8). Finally, time-resolved EPR at low temperature did not indicate elevated levels of  $^3P_{700}$ , which would be a major product of this recombination event (Figure S7). Thus, whatever effect the PsaA-A684N and PsaB-A664N mutations have, it must be manifested within the first ~100 ps after excitation.

Given that the mutations have had their influence before formation of the  $P_{700}^+PhQ^-$  radical pair, one would expect that the rates of subsequent electron transfer events would remain the same. Thus, the only effect one would expect to observe is upon directionality of ET (i.e. the relative use of the two cofactor branches). If one expects the introduction

of an amide group near the ec2/ec3 pair to inhibit charge separation within that pair, then the prediction would be a decrease in the use of that branch along with a corresponding increase in the other branch. This is essentially what was seen, although the effect was much larger in the A-side mutant. The effect of the PsaB-A664N mutation was much smaller and difficult to see in most experiments. Therefore, discussion in this section will focus on the PsaA-A684N mutant. Kinetic spectroscopy performed *in vivo* was consistent with an increase in the use of the B-branch and a decrease in the use of the A-branch, as the relative amplitudes of the fast and slow phases of  $\text{PhQ}^-$  reoxidation shifted from 0.9:1 to 1.8:1 (fast to slow). This translates to a change of B-side usage 47% in WT to 64% in the PsaA-A684N mutant. This shift was accompanied by a decrease in the measured lifetime of the fast phase and a small increase in the lifetime of the slow phase. Such changes in lifetime have been seen before in mutants that alter ET directionality (87) and may be due to the fact that these observed lifetimes are actually complicated functions of several rate constants (103). Analysis of the PS1 particles by time-resolved EPR spectroscopy was entirely consistent with the hypothesis of mutation-induced changes in ET directionality within PS1. Although it is not possible to observe the  $\text{P}_{700}^+ \text{PhQ}_\text{B}^- \rightarrow \text{P}_{700}^+ \text{F}_\text{X}^-$  step directly (88) by this technique, due to its limited time resolution, the rapid production of  $\text{P}_{700}^+ \text{F}_\text{X}^-$  does manifest itself in the early spectrum, and this can be used to estimate the relative use of the two branches. The early RP spectrum of the PsaA-A684N mutant is clearly different from the WT spectrum due to a large increase in the contribution of the  $\text{P}_{700}^+ \text{F}_\text{X}^-$  RP spectrum (Figure 9). Although the change was not as visually obvious in the PsaB-A664N mutant, modeling of the data indicated a small

decrease in the amount of  $P_{700}^+F_X^-$  RP contributing to the early transient spectrum. Thus, usage of the B-branch changed from 50% in WT PS1 to ~70% in the PsaA-A684N mutant and to ~30% in the PsaB-A664N mutant. This is more or less in agreement with the optical data, although the effect of the PsaB-A664N mutant was larger.

#### 2.4.2 Change in the spectrum of $P_{700}$ and the RC Chl(s)

The Ala substitution mutant also caused subtle changes in the shape of the  $P_{700}^+ - P_{700}$  difference spectrum. Indications of this effect were initially seen by ms spectroscopy on thylakoid membranes (Figure S3 for normalized spectra), but it is most clear in the long-lived components from the ultrafast transient absorption experiments (Figure 6C). The position of the major bleaching band is not shifted, nor is the zero-crossing point or the broad positive absorption band in the near-infrared. The former is due to the loss of  $P_{700}$  ground-state absorption, while the latter arises from absorption of  $P_{700}^+$  (59, 104). The main difference is on the blue side of the main bleaching band. This region has contributions from the ec2 Chls due to an electrochromic bandshift caused by the positive charge of  $P_{700}^+$ ; the ec2 Chls are the pigments nearest to  $P_{700}$  and their contribution is expected to be strongest (59). Minor shifts of the positive and negative peaks in an electrochromic bandshift spectrum can produce relatively dramatic changes in shape and magnitude of the resulting spectrum. Thus, it is not surprising that these mutations alter this part of the  $P_{700}^+ - P_{700}$  difference spectrum. It is also important to recognize that all 6 of the Chls in the RC are coupled together. Thus, one might expect that a change in any Chl in the RC will produce some changes in the RC spectrum and in the transfer of

excitation energy to the RC from the antenna pigments. This might explain the differences in the fastest component from the ultrafast data (Figure 6A), although this is not clear at this time. Further work will need to be done on the excitonic spectra of these mutants at low temperature to test that idea.

#### 2.4.3 Charge separation at low temperature

Forward ET from  $\text{PhQ}_A$  is very temperature-independent and becomes slower and slower as temperature lowers, eventually becoming completely blocked, forward ET from  $\text{PhQ}_B$  is relatively temperature-independent (105). At very low temperatures below the glass transition temperature ( $\sim 150\text{K}$ ; (106)) ET within PS1 is mainly seen to occur within the A-branch in a reversible fraction, while an “irreversible fraction” is in the  $\text{P}_{700}^+(\text{F}_A/\text{F}_B)^-$  state. It has been argued that the latter fact is explained the former – that is, the irreversible fraction represents a population of PS1 performing B-side ET resulting in transfer of the electron all the way to  $\text{F}_A/\text{F}_B$ , where it remains indefinitely, while the reversible fraction represents a population of PS1 performing A-side ET resulting in the  $\text{P}_{700}^+\text{PhQ}_A^-$  state, which recombines. Thus, any experiment relying on repetitive excitation will quickly produce two populations: one that is effectively dead and one that repetitively performs A-side ET (106). There are several problems with this interpretation. One is that there is no evidence for two populations of PS1, one that performs A-side ET exclusively and one that performs B-side ET exclusively. Presumably interconversion between them would be blocked at low temperature. If this were the case, then mutations that affected directionality would be expected to exert their effect by changing the equilibrium constant of the interconversion reaction. However, it

is much simpler and logical to rationalize the effects of the mutations that effect directionality as an effect upon the CS reactions. It is also difficult to imagine a conformational change that would change directionality in such a drastic way (i.e. 100% A-side to 100% B-side ET); even 0.1% B-side ET would eventually result in complete loss of reversible ET after a few thousand flashes, and this is not seen. Moreover, it was recently shown that incorporation of a high-potential quinone unable to support forward ET to  $F_X$  in both PhQ sites does not result in production of a B-side RP (107). The simplest explanation for the observation of A-side ET at low temperature is that the temperature-dependence of CS is different between the two sides, and that as temperature drops, the A-side becomes more and more dominant. In fact, this prediction was borne out by time-resolved optical studies in the temperature range of 220-295 K, in which it was seen that the relative amplitude of the fast component of  $PhQ^-$  reoxidation dropped with decreasing temperature (105). One can extrapolate from this work that below 80K, almost all CS would occur on the A-side. The reversible and irreversible fractions therefore must be due to another effect of freezing, giving rise to a population that can do forward ET from  $F_X$  to  $F_A/F_B$  and one that cannot.

The EPR spectra of the PsaA-A684N mutant at low temperature are quite distinct from that of WT PS1. As discussed in the Results section, the simplest explanation of the data is that the major RP produced at low temperature in the PsaA-A684N mutant PS1 is  $P_{700}^+PhQ_B^-$ . Firstly, the shape of the Q-band EPR spectrum of the RP in this mutant is almost exactly what was predicted theoretically for the  $P_{700}^+PhQ_B^-$  RP. Secondly, the OOP-ESEEM data can be best explained as an increase in a radical pair with a shorter

inter-spin distance, which is consistent with an increase in the  $P_{700}^{+}PhQ_B^{-}$  RP. This distance is shorter in the  $P_{700}^{+}PhQ_B^{-}$  RP than it is in the  $P_{700}^{+}PhQ_A^{-}$  RP due to the asymmetric localization of the unpaired spin in  $P_{700}^{+}$  on the  $P_B$  (ec1<sub>B</sub>) Chl (54). This would indicate that CS on the B-branch becomes the major process at low temperature in the PsaA-A684N mutant. The simplest way to explain this effect is that the mutation produces a change in the temperature-dependence of CS on the A-branch, such that it no longer becomes the dominant branch. Based on the measurements done at room temperature, the B-branch is already the dominant branch at ~300K in the PsaA-A684N mutant. Evidently, this does not change as the temperature is lowered to ~80K. In fact, the B-branch appears to become even more dominant as the temperature drops, although this is difficult to quantify this rigorously with the set of experiments done here. Clearly, a temperature dependence study must be done to resolve this important question. The effect of the PsaB-A664N mutant is much smaller at cryogenic temperature. This was expected, as the A-branch is already the dominant one in WT at low temperature; it would be difficult to see if a slightly higher amount of the  $P_{700}^{+}PhQ_A^{-}$  RP were produced in the PsaB-A664N mutant. While the OOP-ESEEM data were consistent with a shift to more  $P_{700}^{+}PhQ_B^{-}$  RP in the PsaB-A664N mutant, the change was rather small.

One thing that is abundantly clear is that the reversible and irreversible populations of PS1 at cryogenic temperature have nothing to do with directionality of ET within PS1, nor is blocking of forward ET from  $PhQ_B$  necessary to see the  $P_{700}^{+}PhQ_B^{-}$  RP at cryogenic temperatures. None of the experiment results are consistent with the PsaA-A680N mutation slowing the rate of forward ET from  $PhQ_B$  to  $F_X$ , which would have



been surprising given the distance between the site of the mutation and PhQ<sub>B</sub>. Thus, we would expect that the energetics of ET for this step are unchanged by the PsaA-A684N mutation. Therefore, the observation of P<sub>700</sub><sup>+</sup>PhQ<sub>B</sub><sup>-</sup> RP at cryogenic temperatures in the “reversible population” (since the irreversible is effectively invisible) means that the irreversible population is not due to favorable ET from PhQ<sub>B</sub> to F<sub>X</sub>, leading to creation of the P<sub>700</sub><sup>+</sup>(F<sub>A</sub>/F<sub>B</sub>)<sup>-</sup> state, which does not recombine at cryogenic temperature. This lends support to the claim that the reversible population is due to a block in ET from F<sub>X</sub> to F<sub>A</sub>/F<sub>B</sub> caused by a change locked in during freezing (107).

In the future work on these mutants, it is essential to address the effect of temperature on CS at ec2 cofactor level. This temperature based measurements should be performed at different low-temperature range from 10-150 K and also at variable room temperature range. Further the role of reduced iron-sulfur clusters in the formation of B-side RP of P<sub>700</sub><sup>+</sup>PhQ<sub>B</sub><sup>-</sup> need to be re-evaluated. The reduced iron-sulfur clusters also modulate the back ET through CR and subsequent CS on the two branches. But the way the B-side ET becomes dominant at low temperature with reduced iron-sulfur cluster is still unclear (54, 71). Recent theoretical study of energy transfer from core antenna to the RC showed that this excitation energy transfer to the RC was asymmetric in nature. The low energy exactions are transferred more to the A-branch than to the B-branch, resulting into increased A-branch CS. The origin of asymmetric ET between the two branches begins with the asymmetric excitation energy transfer from the core antenna (45). Thus, analyzing excitation energy in PsaA-A684N and PsaB-A664N is important to monitor any possible rerouting of excitation energy to the non-mutated branch. As currently it is

difficult to say that there is any rerouting of excitation energy or not that causes this increase B-branch ET in PsaA-A684N. Through time-resolved 2D (two dimensional) electronic spectroscopy, we can follow the route of excitation energy till its decay into CS. The 2D electronic spectroscopy is a valuable tool to monitor excitation energy in PSI (108) and it can also be helpful to study both at cryogenic and room temperature based decay at  $P_{700}$  or ec2 cofactor. As currently it is difficult to say that there is any rerouting of excitation energy or not that causes this increase B-branch ET in PsaA-A684N. Through time-resolved 2D electronic spectroscopy, we can follow the route of excitation energy from the antenna till its decay into CS.

## 2.5 CONCLUSIONS

We showed for the first time the  $P_{700}^{*+}PhQ_B^{\bullet-}$  RP formation at ambient and cryogenic temperature through site-directed mutation of the A-branch of the PSI RC. All the EPR spectroscopic methods employed confirmed the competency of bidirectional ET in PSI. By making the A-branch energy trap less favorable for CS results in an increase in B-branch ET. These results support the previously proposed model of CS in which energy trapping occurs at ec2, and ec2 is the primary electron donor. In the future, it is important to study the role of different vibronic modes of the primary electron donor to determine where the electronic transitions convert into vibronic transitions and trap solar excitation energy. This work will be helpful in designing biologically inspired highly efficient artificial solar energy trapping systems.

## 2.6 SUPPLEMENTARY INFORMATION

### 2.6.1 *In vivo* transient absorption spectroscopy

Neither Cys substitution mutant showed any observable effect upon directionality. Their decay kinetics at 395 nm appeared identical to that of the WT strain (data not shown). The PsaA-A684I was intermediate in effect between PsaA-A684N and WT, while the PsaB-A664I mutant was indistinguishable from WT (data not shown).

**Table S2.1.** Lifetimes of energy equilibration in antenna; energy trapping component obtained from global analysis for WT; PsaA-A680N and PsaB-A660N.

<b>Sample</b>	<b>Energy Equilibration Component (ps)</b>	<b>Energy Trapping Component (ps)</b>
WT	1.5	26.5
PsaA-A684N	0.7	25.6
PsaB-A664N	0.5	23

## Helix # 10



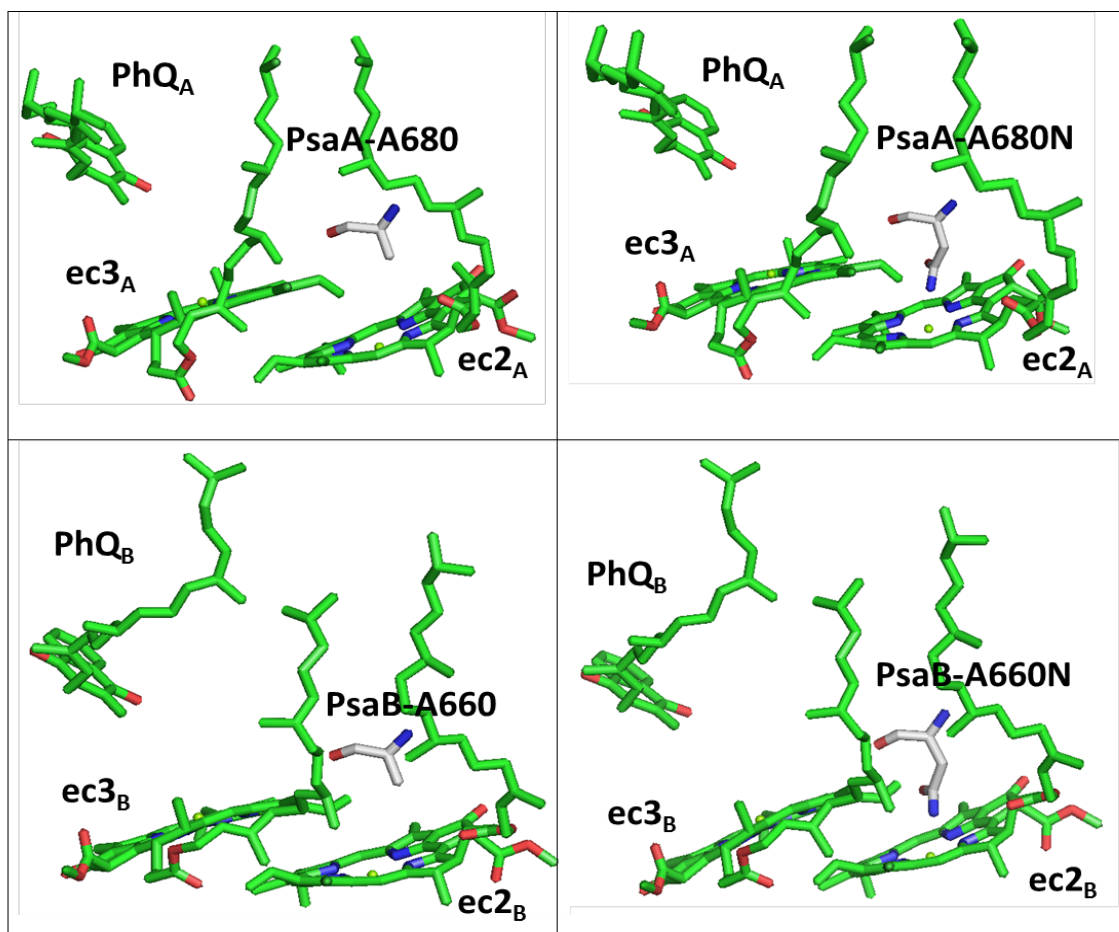
<i>C.reinhardtii</i>	<i>PsaA</i>	666	SAYGLIFLGAHFVWAFSLMFLE
<i>S.elongatus</i>	<i>PsaA</i>	670	SAYGIMFLAGHFVFAFSLMFLE
<i>A.thaliana</i>	<i>PsaA</i>	665	SAYGLEFFLGAHFVWAFSLMFLE
Clustal Consensus			****: **: :****:*****

## Helix # 10

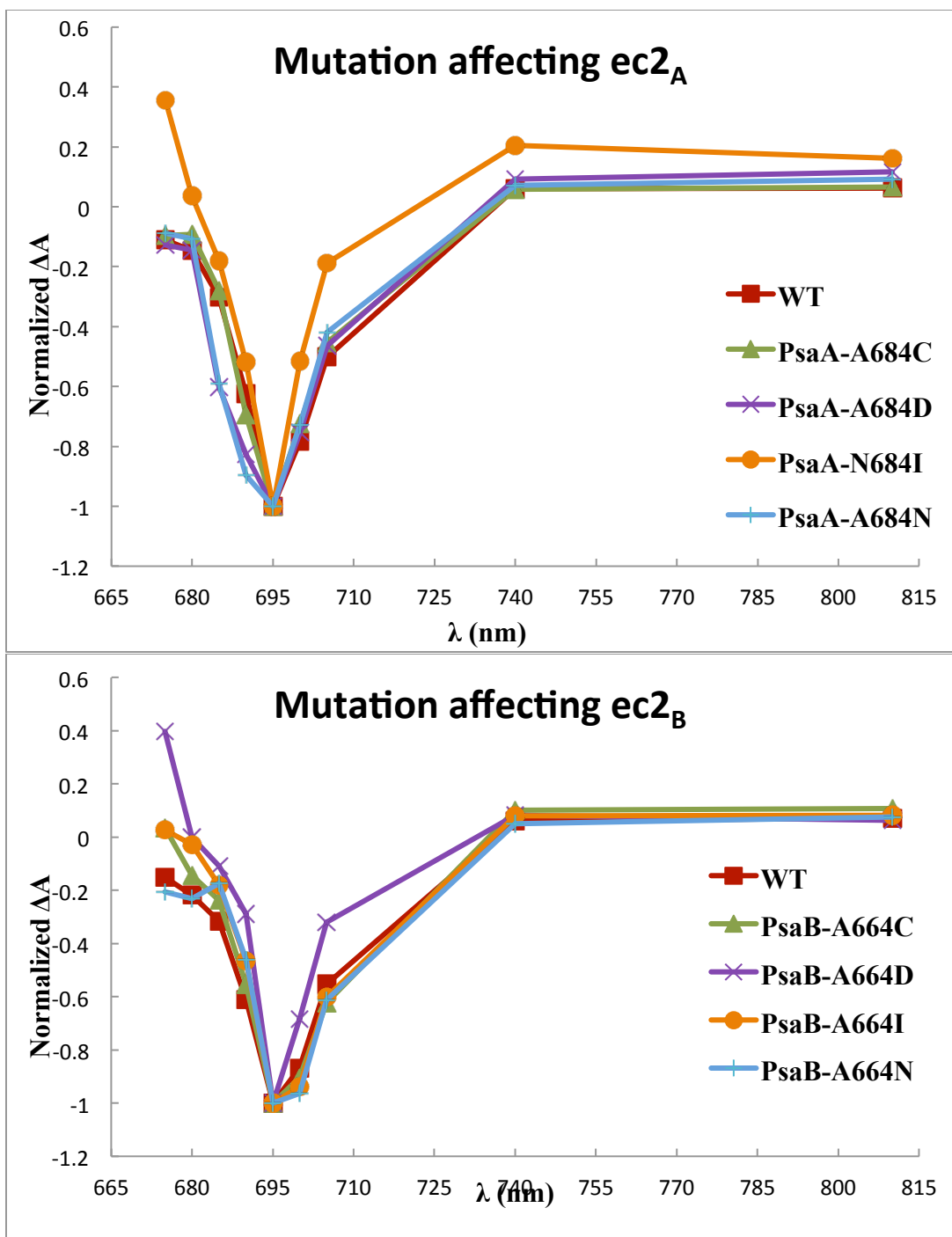


<i>C.reinhardtii</i>	<i>PsaB</i>	646	SVWAWTFLFGHLIYATGFMFLI
<i>S.elongatus</i>	<i>PsaB</i>	651	SVWAWMFLFGHLVWATGFMFLI
<i>A.thaliana</i>	<i>PsaB</i>	644	SVWAWMFLFGHLVWATGFMFLI
Clustal Consensus			***** *****: :*****

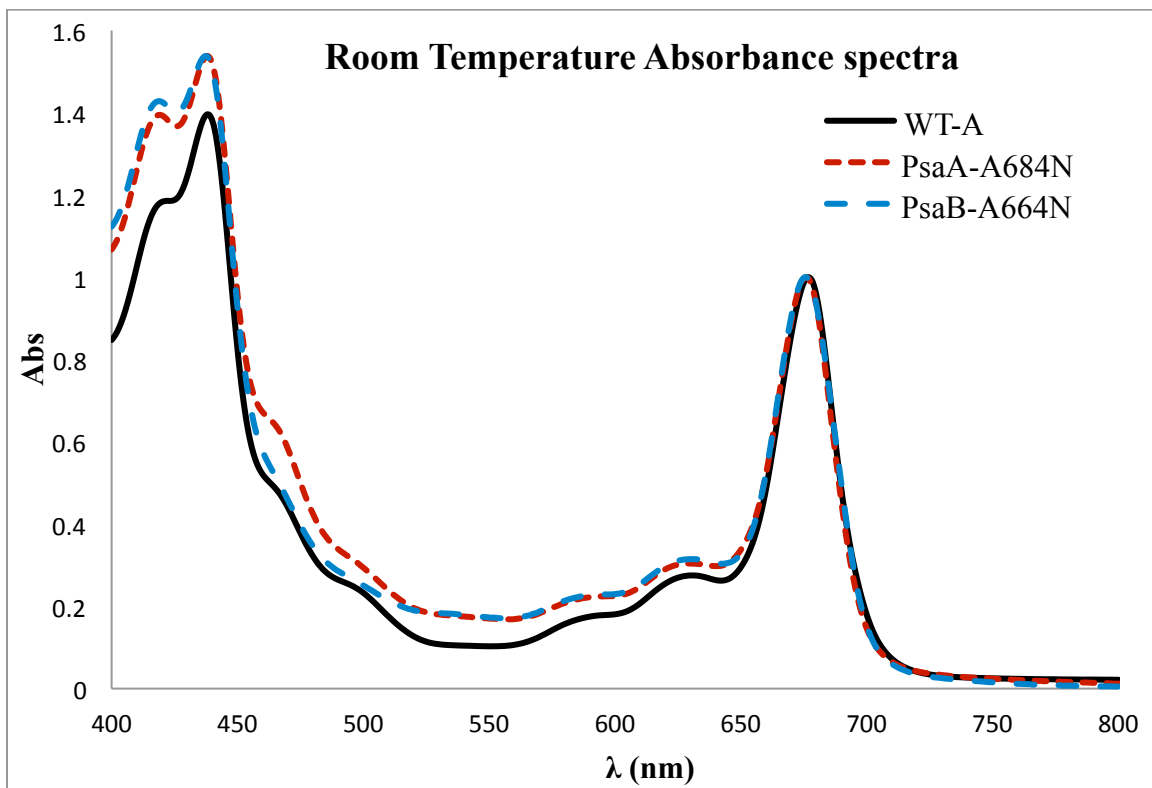
**Figure S2.1.** Sequence alignment of PS1 helix 10 of PsaA and PsaB in *Chlamydomonas reinhardtii*; *Synechococcus elongatus*; and *Arabidopsis thaliana*. Key: "\*": identical. ":" conserved substitutions (same color group). ".": semi-conserved substitution (similar shapes).



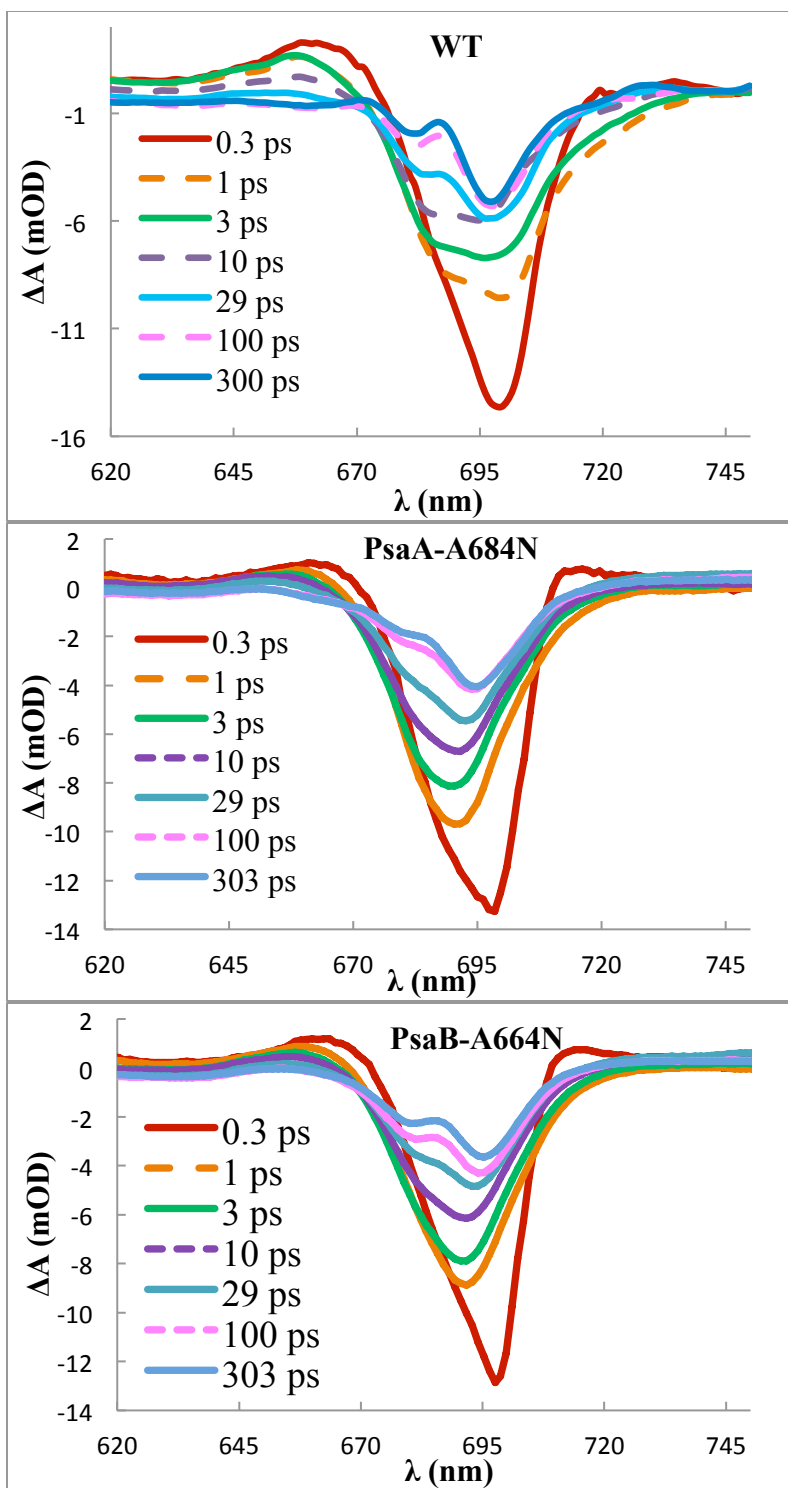
**Figure S2.2.** Position of Alanine residue between ec2 and ec3 chlorophyll. The methyl group of PsaA-A684 and PsaB-A664 is directed towards the ec2 chlorophyll and this alanine is expected to affect the excitation energy coupling and electron transfer between the two chlorophylls.



**Figure S2.3.** Normalized light induced difference spectra of P<sub>700</sub> of different mutants affecting ec2<sub>A</sub> cofactor of A-branch ec2<sub>B</sub> cofactor of B-branch of PSI. The spectra were normalized in order to compare the effect of mutation on the P<sub>700</sub> absorption.

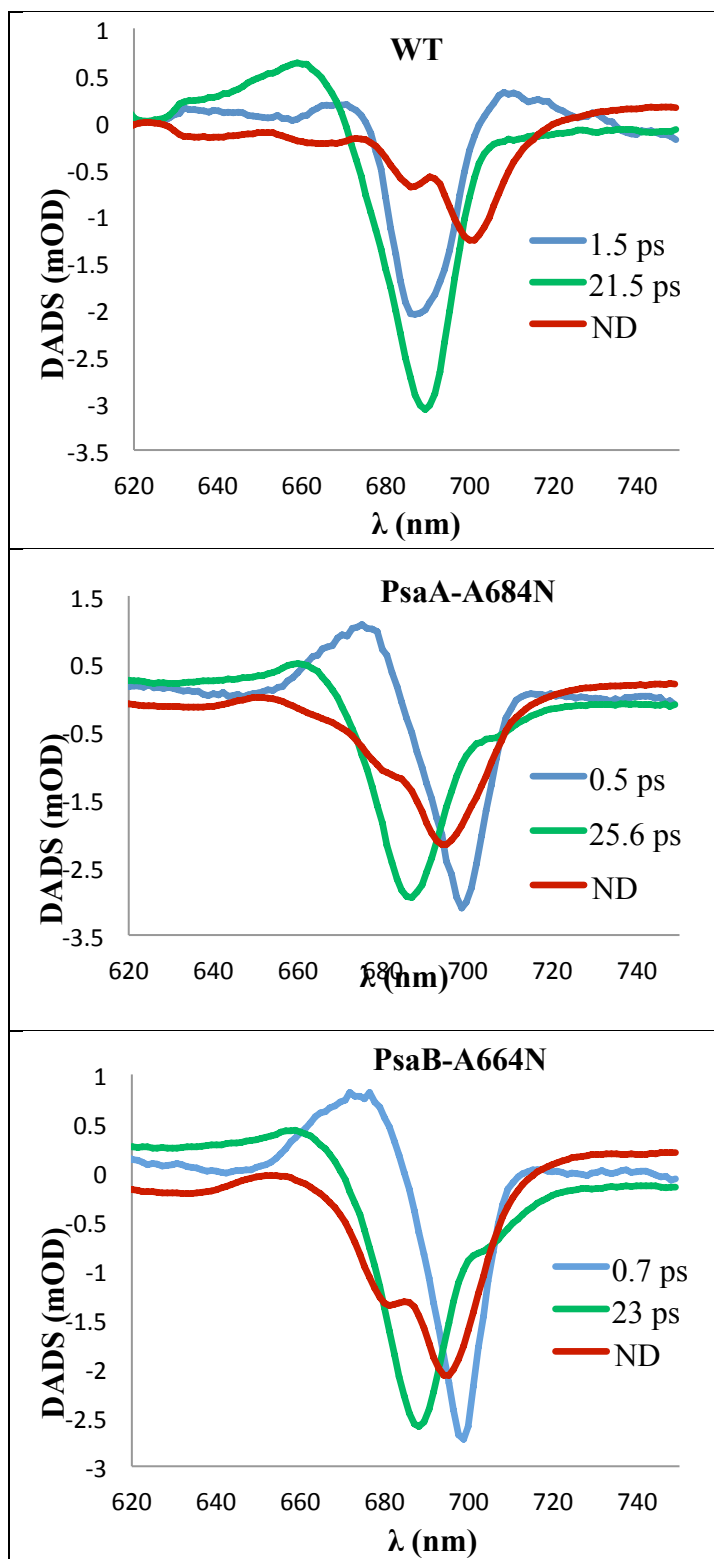


**Figure S2.4.** Absorbance spectra of PSI from WT; PsaA-A684N and PsaB-A664N mutants. All the spectra were normalized to the  $Q_Y$  peak of WT.

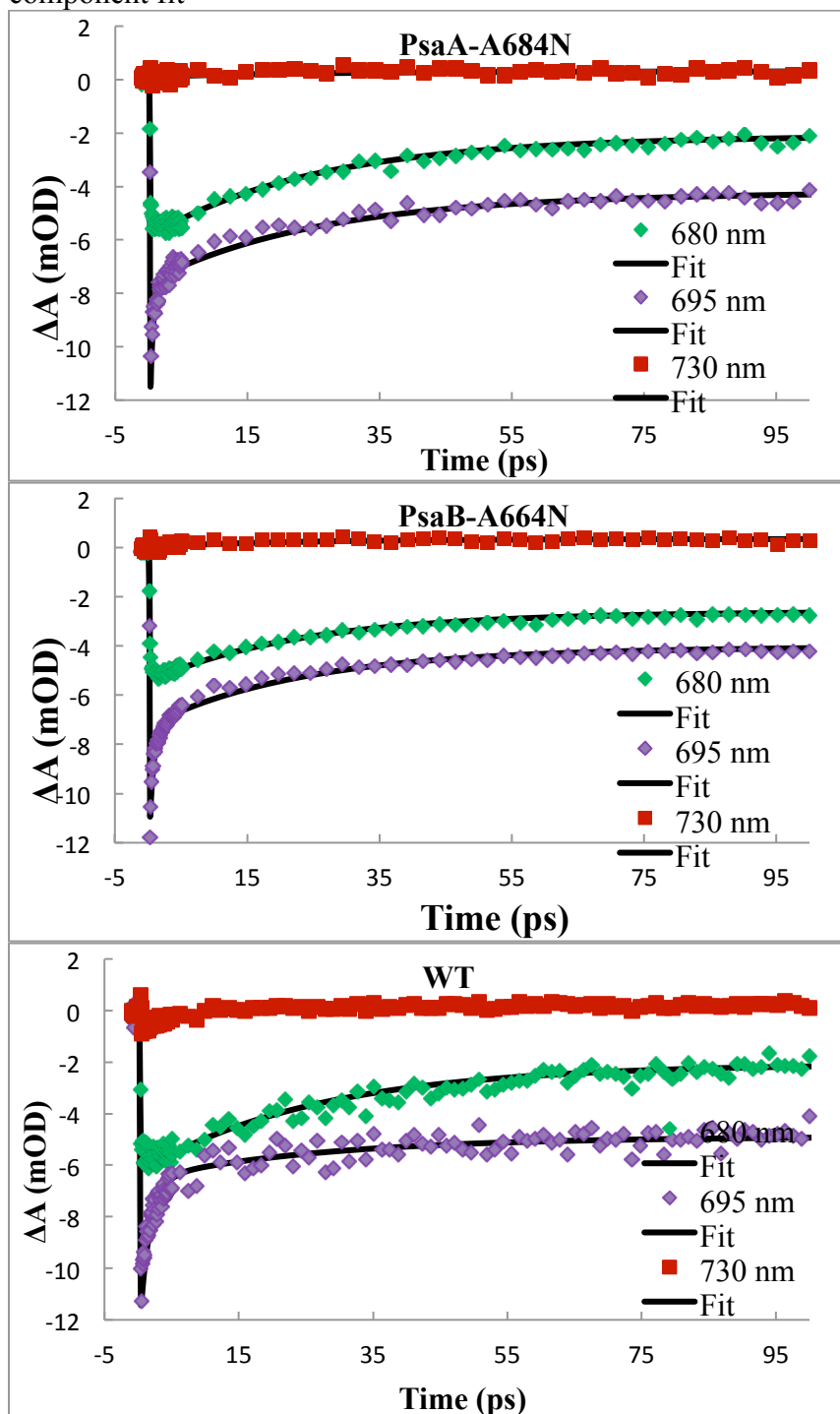


**Figure S2.5.** Transient absorption DS at different delay times after excitation at 700 nm for WT (A), PsaA-A684N (B), and PsaB-A664N (C) PS1.

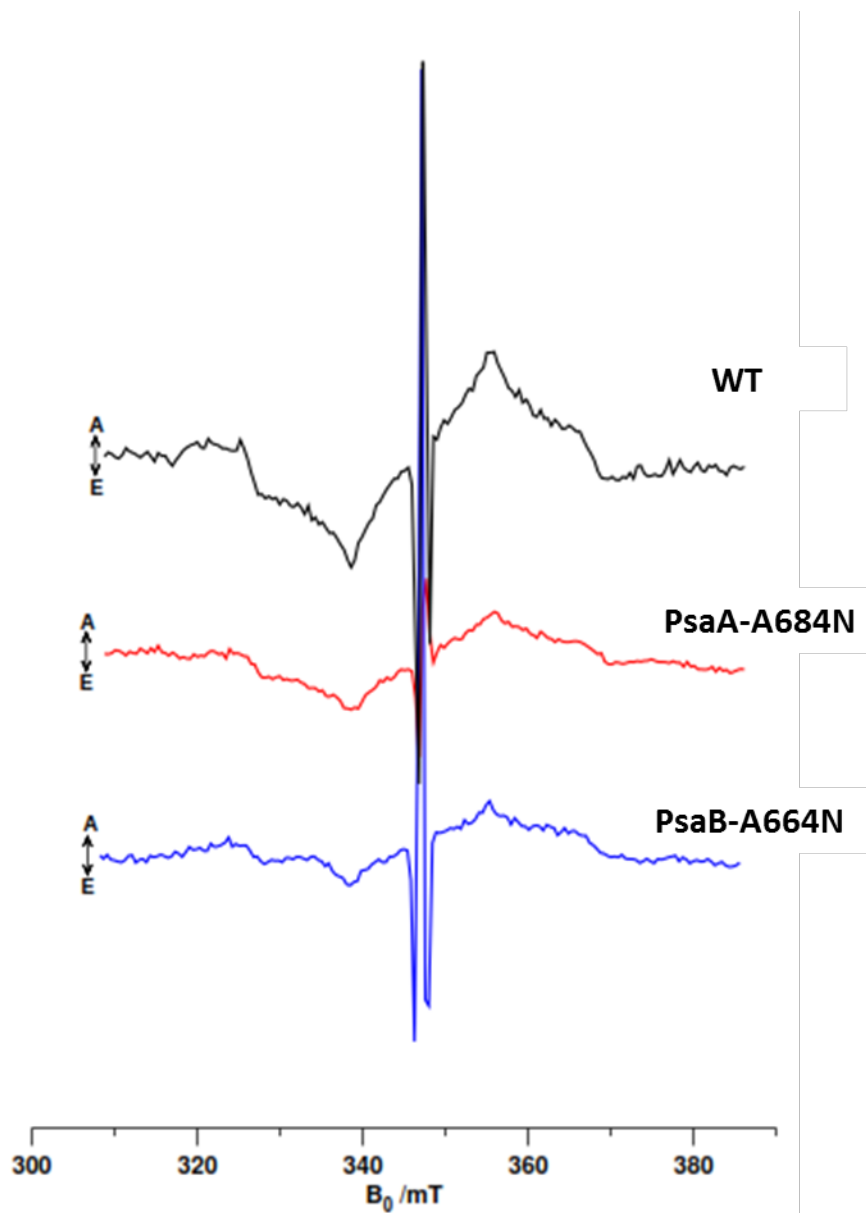




**Figure S2.6.** DADS of WT (A), PsaA-A684N (B) and PsaB-A664N (C) PSI from 3-component fit



**Figure S2.7.** Kinetic traces at 680, 695 and 730 nm obtained from global analysis for WT (A), PsaA-A684N (B), and PsaB-A664N (C) PSI for the first 100 ps after pump flash.



**Figure S2.8.** Transient X-band EPR spectra at 80 K taken at a wider magnetic field scan than in **Figure 2.10A**. The central off scale peaks represent the  $P_{700}^{+}PhQ^{\bullet-}$  RP. Positive amplitude represents absorptive (A) and negative represents emissive EPR signals. PsaB-A664N showed strong changes in polarization patterns while in PsaA-A684N these are absent.

## CHAPTER NO 3

### 3.1 INTRODUCTION

Photosystem I (PSI) is one of the largest pigmented protein complexes, working in collaboration with photosystem II (PSII) in linear electron transfer (ET) mode for the production of reduced nicotinamide adenine dinucleotide phosphate (NADPH) and adenosine triphosphate (ATP) production, which are utilized in the dark reaction of photosynthesis. PSI also works in a cyclic ET mode producing only ATP. The *Thermosynechococcus elongatus* PSI structure at 2.5 Å resolution reveals 100 Chl *a* molecule bound to the PsaA and PsaB subunits of PSI. Beside the six Chl *a* in the reaction center (RC), most of the Chl *a* them make the core antenna, which is used for light harvesting and its conversion into excitation energy, which is transferred to the redox active RC for charge separation. The cofactors of PSI RC are arranged in the form of two functionally active branches that emanates from P700, made of chlorophyll *a* and *a*' (C-13 epimer of Chlorophyll *a*). Then there is a pair of chlorophyll *a* called ec2 and ec3 and phlloquinone (PhQ) on each branch. The two branches recombine at the 4 [Fe-S] clusters called F<sub>X</sub>. Down into PsaC branch there are two additional 4[Fe-S] clusters F<sub>A</sub> and F<sub>B</sub> [1, 2].

Unlike PSII and purple bacterial reaction center, in PSI both branches are used for ET and this phenomenon is called bi-directionality of ET [3-6]. The main difference between the two branches in terms of kinetics is that ET from PhQ<sub>B</sub> towards F<sub>X</sub> is 10 times faster than that of PhQ<sub>A</sub>. In terms of usage, A-branch is

utilized more as compare to B-branch and this utilization of the two branches is specie dependent. For example, in *C. reinhardtii* the ratio of utilization of A: B for ET is 60%: 40% while in *Synechocystis* PCC 6803 it is 70%:30% or 80%:20% [7, 8]. The activity of the two branches in PSI was first reported from spinach PSI particles, where the PhQ- oxidize to FX with two lifetimes [9] but it was challenged that it might be due to the effect of detergent on PhQ- binding pocket. The in vivo analyses of *Chlorella sorokiniana* cells using transient absorption spectroscopy cells provided evidence that the two PhQ- of PSI has different decay lifetimes and a possibility that charge separation occurs on both branches in PSI [10]. Mutagenesis studies of the tryptophan residues that are in pi-stacking with phylloquinone in the two branches of PSI from *C. reinhardtii* proved that electron transfer occur autonomously. Mutation causes an increase in the decay time of semiphylloquinone re-oxidation individually [11]. One of the main factors of 10 fold difference between the rate of electron transfer from PhQA and PhQB towards FX is the strength of an amide hydrogen bond between the respective PhQ and leucine of PsaA-L722 and PsaB-L706. Weakening of the hydrogen bonding by placing a bulky group in place of leucine causes a speed up in rate of ET in both PSI from prokaryotic [12] and eukaryotic species [13].

The upstream cofactors to PhQ in the two branches were also analyzed by mutagenesis studies in cyanobacteria and green algae. The primary electron donor P700 and the primary electron acceptor ec3 in the classical model of CS is investigated both for its role in bi-directionality and origin of primary charge separation. A re-routing or increased CS occurs in the opposite branch due to that of

mutated one and this is observed when a mutation is performed on either branch [7]. Kinetics of ET are also modulated when the ec3 cofactor methionine ligand is changed to other residues in cyanobacteria and green algae but its impact is always high on A-branch [14, 15]. An increase in CS on B-branch due to mutation on A-side is observed but B-branch mutants have no effect on A-branch [16-18]. This difference between the two mutants of ec3 ligand is explained by quantum calculations and molecular dynamic simulations, where a possible inherent asymmetry in the protein environment of the two branches was proposed [19].

The origin and kinetics of primary charge separation in PSI is of great importance due to its 100 % quantum efficiency [20]. The role of ec2 cofactor, which was previously considered as accessory chlorophyll came to lime light in ultrafast transient absorption spectroscopy of PSI of *C. reinhardtii*. Based on three times fast energy trapping process from past studies and a 6-9 ps lifetime of primary CS, it was predicted that ec2 cofactor is a primary electron donor or somehow involved in primary electron transfer step [21]. The  $P_{700}$  as a primary electron donor was also questioned during the observation that breaking the hydrogen bond to the PA has no effect on bi-directionality of ET in PSI of *C. reinhardtii*. It was proposed that it is possible that  $P_{700}$  is a secondary electron donor [22]. Femtosecond transient absorption spectroscopic (TAS) measurements on three different mutants around  $P_{700}$  in *C. reinhardtii* suggested that they have no effect on primary charge separation. The target modeling of ultrafast transient spectroscopy provides the rates of different radical pair (RP) formation, where only the rate constants of secondary radical pairs

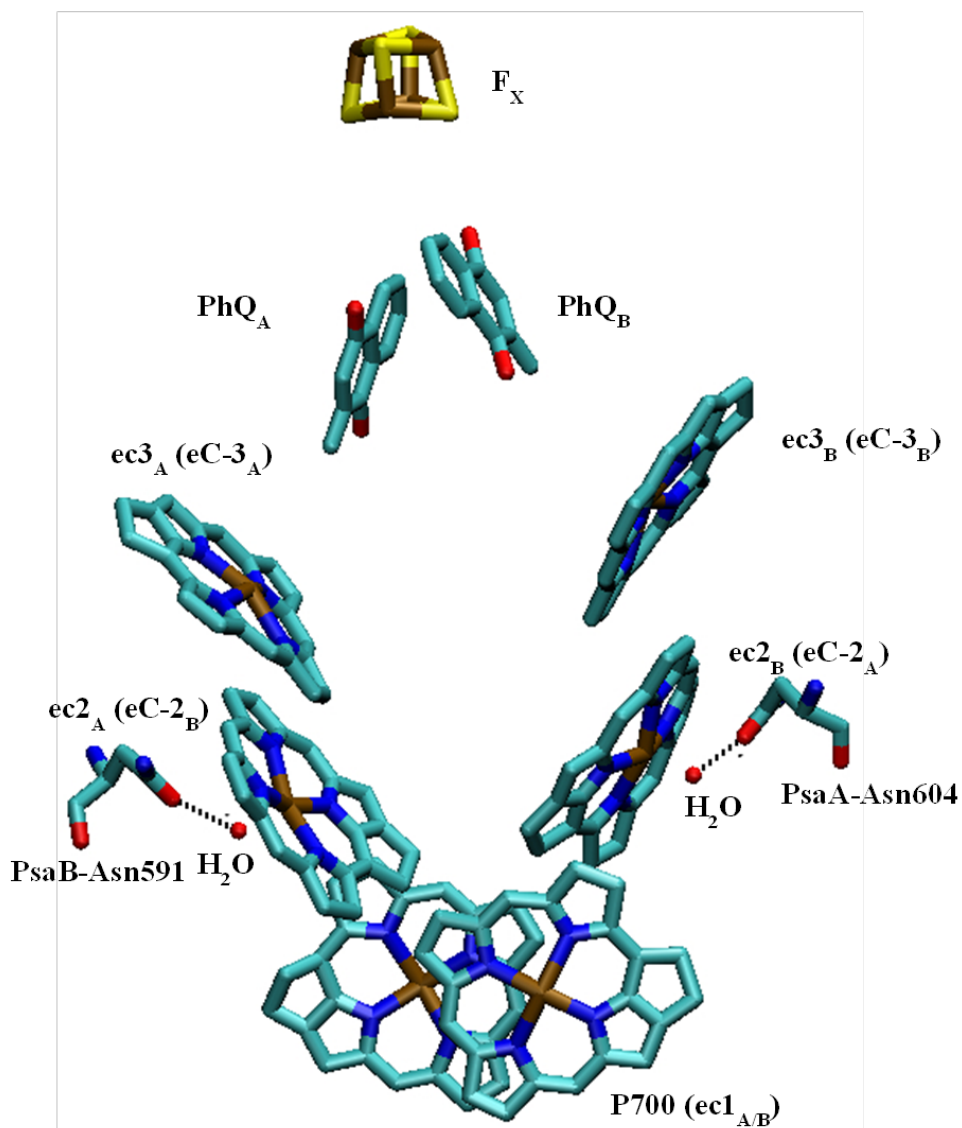
and also their back reactions are modified in these mutants [23]. Disruption of hydrogen bonding between protein and ec3 cofactor in the two branches showed a delay in the chlorophyll cation formation. Target modeling of this spectroscopic data showed that the effect is only on primary RP which is  $ec2+ec3^-$  and in a second step  $ec2^+$  is reduced by P700 [14].

The role of ec2 as primary electron donor is challenged based on theoretical electrostatic measurement and quantum chemical treatment, which showed that ec2 should have a less negative redox potential than ec3 in the excited state and thermodynamically ET from ec2 toward ec3 is not possible [24]. Excitation of *Synechocystis* PCC 6803 PSI with a 20-25 fs duration pulse at 720 nm wavelength initiated ET by giving two bands in 100 fs, in which the 660 nm band was assigned to  $ec3^{\bullet-}$  and 705 nm to  $P_{700}^{\bullet+}$ . The primary charge separation according to this study is  $P_{700}^{\bullet+}+ec3^{\bullet-}$  and this is for the first time that such a fast energy trapping into CS was reported in 60% of the PSI sample. However there are shortfalls in this analysis such as decrease in the bleaching band of 705 nm representing  $P_{700}^{\bullet+}$  from 4 to 50 ps time scale in the difference spectra. However, after the  $P_{700}^{\bullet+}$  cation radical is formed, it should exist for milliseconds and a decrease in its bleaching is not possible unless it is reduced. There is possibility that the red chlorophylls spectrum is considered as the evolution of  $P_{700}^+$  [25, 26].

In order to study the site of primary charge separation and the basic root of directionality in the two branches of PSI, we selected the ec2 chlorophyll site on each branch for mutation. These chlorophylls are the proposed primary donor of

electron transfer but need further investigation to confirm this hypothesis [14, 21, and 23]. If we look into the crystal structure of PSI (Figure 3.1) from *T. elongatus*, there is water molecule that acts as a fifth ligand to the central magnesium atom of ec2 and there is no direct linkage from the protein, however the water molecule makes a hydrogen bonding contact with asparagine from the opposite branch polypeptide. The ec2<sub>A</sub> (alternate nomenclature) or eC2-B (crystal structure nomenclature) central magnesium makes coordinate bond with the oxygen of water by accepting the lone pair of electron from oxygen. Further the side chain carboxyl oxygen of asparagine from opposite polypeptide of helix 9 acts as hydrogen bond acceptor of the water ligand of ec2 (Figure 3.1). We targeted the PsaA-N604 of B-branch and PsaB-N591 of A-branch for mutation. The respective asparagine was mutated to aspartic acid, histidine, lysine, leucine and tyrosine. The effect of these mutations on primary charge separation and directionality of electron transfer was investigated by various spectroscopic methods in this work. **(Note: In some figures the *C. reinhardtii* sequence numbering are used instead of *T. elongatus*. The PsaA-Asn601 = PsaA-Asn604 and PsaB-Asn587= PsaB-N591).**





**Figure 3.1.** Arrangement of electron transfer cofactors in RC of PSI. The figure is constructed from protein data bank file: 1JB0. The  $P_{700}$  is composed of  $ec1A$  and  $ec1B$  chlorophylls. On each branch is a pair of chlorophylls ( $ec2_A ec3_A$  or  $ec2_B ec3_B$ ) and a phylloquinone ( $PhQ_A$  or  $PhQ_B$ ). The  $F_X$  cluster is shared by PsaA and PsaB, while the two terminal iron-sulfur clusters ( $F_A$  and  $F_B$ ) are bound by PsaC subunit. The name used in the parenthesis is from crystallographic database. The position of  $ec2$  and its 5th ligand water (red bead) on each branch of the RC of PSI. PsaA-N604 accepts hydrogen bond from the water molecule on B-branch and PsaB-N591 on A-branch.

## 3.2 MATERIALS AND METHODS

### 3.2.1 Genetic manipulations

The plasmids containing the Asn substitution mutations were prepared via a previously described PCR method and introduced into two background strains of *C. reinhardtii* in which either the *psaA* exon-3 or *psaB* had been deleted (60). These strains also have the FUD7 chloroplast mutation, which is a deletion of the *psbA* gene encoding the D1 core polypeptide of PSII and results in no PSII, and the nuclear *P71* mutation, which causes a decrease in the total amount of LHCII. The respective plasmid for the specific site was mixed with tungsten particles and bombarded on *C. reinhardtii* cells spread on agar plates containing TAP with 75 µg/mL spectinomycin and 100 µg/mL ampicillin, using a home-built gene gun and helium gas at a pressure of approximately 450 psi. The plates were kept in the dark and colonies appeared after 7 days. These colonies were passaged alternately on 300 µg/mL spectinomycin and 100 µg/mL streptomycin every 14 days. The transformants were checked for *psaA* or *psaB* genes and for homoplasmicity by isolating the plasmid DNA and amplification via PCR. These strains were used primarily for *in vivo* analyses.

A second set of background strains had the *P71* nuclear mutation but lacked the FUD7 mutation: PBC12-5 (*psaAA*) and PBC 18-6 (*psaBA*). These backgrounds also have a hexahistidine tag on exon 1 of the *psaA* gene (74). The plasmids were shot in the same way as described above. PSI was isolated from these strains for *in vitro* studies.

### 3.2.2 Crude membrane preparation

One liter of each transformant cells was grown under room light ( $81 \mu\text{Einstein m}^{-2} \text{s}^{-1}$ ) and temperature ( $23^\circ\text{C}$ ) in Tris-acetate phosphate (TAP) media. The cells were harvested by centrifuging at 3500 g for 5 minutes at  $4^\circ\text{C}$ , the supernatant was discarded and the pellet was washed with cell resuspension buffer (0.3 mM sucrose; 25 mM HEPES having pH 7.5 with KOH; 5 mM  $\text{MgCl}_2$ ; 5 mM  $\text{CaCl}_2$ ) and recentrifuged at 3500 g for 5 minutes at  $4^\circ\text{C}$ . The washed cell pellet was suspended in thylakoid resuspension buffer (0.3 mM sucrose; 25 mM HEPES having pH 7.5 with KOH; 10 mM EDTA) and French pressed at 3000 psi. The broken cells or crude thylakoid membrane were washed with thylakoid resuspension buffer and centrifuged at 40000 g for 10 -15 minutes at  $4^\circ\text{C}$  twice. Storing buffer which contains 25 mM HEPES-KOH (pH 7.5); 10 mM EDTA; 1 mM phenylmethylsulfonyl fluoride (PMSF); 10 % Glycerol was added to the pellet. The sample was homogenized with a chilled homogenizer and 1X protease inhibitor buffer (50 mM EDTA; 10 mM Benzamide-HCl; 500  $\mu\text{g/mL}$  Pepstatin A; 200  $\mu\text{g/mL}$  Leupeptin; 100  $\mu\text{M}$  E-64; 100 mM  $\epsilon$ -aminocaproic acid). The crude thylakoid membranes were stored at  $-80^\circ\text{C}$  for later use after flash freezing using liquid nitrogen in aliquots for  $\text{P}_{700}$  estimation through spectroscopy and immunoblot analysis.

### 3.2.3 Growth assays

Cells were grown in 20-25 mL TAP liquid culture overnight and on the next day the cells were counted. About 10  $\mu\text{L}$  of liquid culture of each sample at a density of  $1 \times 10^6$  cells  $\text{mL}^{-1}$  was spotted on TAP and TBP plates. Most plates were left in air, but some were put in microaerobic conditions using anaerobic gas generator pouch system with indicator of

(BD GasPak EZ, Becton, Dickinson and company, USA). The plates were either maintained in the dark or illuminated with white light from fluorescent tubes at low ( $2 \mu\text{Einstein m}^{-2} \text{ s}^{-1}$ ), medium ( $20 \mu\text{Einstein m}^{-2} \text{ s}^{-1}$ ), or high ( $80 \mu\text{Einstein m}^{-2} \text{ s}^{-1}$ ) intensity, which was measured with a LI-COR Photometer (Model LI-250 Light Meter).

#### 3.2.4 Isolation of H<sub>6</sub>-PSI particles

Strains were grown in 6-L flasks using 5 L of medium with constant stirring and bubbling with filtered air under normal room light condition of  $81 \mu\text{Einstein m}^{-2} \text{ s}^{-1}$  and room temperature of approximately  $23^\circ\text{C}$  in TAP medium. The cells were harvested during the early logarithmic phase by centrifugation at  $3500 \text{ g}$  for 5 minutes at  $4^\circ\text{C}$ , washed with cell resuspension buffer (0.3 mM sucrose, 5 mM  $\text{MgCl}_2$ , 5 mM  $\text{CaCl}_2$ , 25 mM HEPES-KOH (4-(2-hydroxyethyl)-1-piperazineethanesulfonic acid), pH 7.5) and centrifuged again. The cells were suspended in thylakoid resuspension buffer (0.3 mM sucrose, 10 mM EDTA, 25 mM HEPES-KOH, pH 7.5) and broken by passage through a French pressure cell at 3000 psi. The broken cells were washed with thylakoid resuspension buffer and centrifuged at  $40000 \text{ g}$  for 10 -15 minutes at  $4^\circ\text{C}$  twice by collecting the green residue and discarded the lower white starch material. Crude thylakoid membranes were homogenized in cold thylakoid resuspension buffer at approximately  $6 \text{ mg Chl mL}^{-1}$  and stored at  $-80^\circ\text{C}$  after flash freezing in liquid nitrogen. Crude thylakoid membranes (CTM) at final concentration of  $0.4 \text{ mg Chl mL}^{-1}$  (PBC12-5 background strains) or  $0.2 \text{ mg Chl mL}^{-1}$  (PBC18-6 background strains) were solubilized by dropwise addition of  $\beta$ -D-dodecylmaltoside ( $\beta$ -DM) to a final concentration of 1/10 volume of 10%  $\beta$ -DM, and the sample was stirred gently for 30 minutes at  $4^\circ\text{C}$  in the

dark. After sample was centrifugation at 64000 g for 25 minutes at 4 °C to remove unsolubilized material, the supernatant was loaded onto a Ni-NTA (Invitrogen) column pre-equilibrated with Solubilization Buffer containing 0.03 %  $\beta$ -DM. The column was washed with Solubilization Buffer containing 0.03 %  $\beta$ -DM and 2 mM imidazole until the efflux was clear. The H<sub>6</sub>-tagged PSI was eluted from the column with elution buffer (300 mM imidazole and 40 mM 2-(*N*-morpholino) ethane sulfonic acid MES-NaOH, pH 6). The eluate were concentrated in Amicon Ultra-15 centrifugal filters with 100 K molecular weight cutoff (Millipore Ltd. Ireland) and washed with Storage Buffer (40 mM CaCl<sub>2</sub>, 40 mM MgCl<sub>2</sub>, 0.03%  $\beta$ -DM, 10% glycerol, 10 mM Tricine, pH 8) to remove imidazole several folds during concentration. The sample was concentrated to a final concentration 2.5-3 mg Chl ml<sup>-1</sup>. Glycerol was added to a final concentration of 20%. Samples were stored in 100  $\mu$ L aliquots by flash freezing in liquid nitrogen at -80 °C.

### 3.2.5 Immunoblot analysis

For immunoblot analysis 20  $\mu$ g/mL of chlorophyll containing crude thylakoid membranes of WT and mutants were taken and equal volume of 2X Lamelli buffer (4% SDS; 20% Glycerol; 125 mM Tris-HCl having pH 6.8; 4 M Urea) was added to it and dissolved by vortexing, then it was diluted by 1X Lamelli buffer, so that it has final concentration of 0.5  $\mu$ g of chlorophyll containing protein. Each sample was heated at 50 °C for 30 minutes in water bath then vortexed briefly and spun at highest speed for 10 minutes. The supernatant was collected for later usage. 10  $\mu$ L of sample containing 0.5  $\mu$ g of protein of each sample was added in wells of 4-10 % Tricine gel. The gel was run at constant voltage of 90 V with 110-125 mA expected current at start and 15 mA at end

for 4 hours in 1X MES-SDS running buffer (pH 7.3). The protein was transferred to the pre-soaked polyvinylidene difluoride (PVDF) membrane [Millipore Corporation, USA] using transferring buffer (1X Tris-glycine SDS; 20 % methanol) in western blot transferring assembly cell at constant voltage of 25 V and 125 mA for 3 hours at 4 °C. The blot membrane was placed in mixture of TBST ( 20 mM Tris-HCl pH 7.5; 500 mM NaCl; 0.05 % Tween 20) along with 5 % non-fat skim milk (NFDM) and 1 mM sodium azide for overnight at 4 °C to block empty protein binding sites on membrane. The blot was placed in a primary  $\alpha$ - PsaA antibody solution (TBST+ 1% NFDM + 1<sup>o</sup> antibodies that is diluted in ratio of 1:2000) and shake gently at room temperature for one and half hour. The blot was washed with TBST three times for fifteen minutes on shaker. The blot was then placed in secondary antibody solution (TBST+ 1% NFDM and 2<sup>o</sup> antibody which is made by 2  $\mu$ L HRP complex [anti rabbit IgG conjugated to horseradish peroxidase and used at 1: 10, 000] and shake gently at room temperature for one hour. The blot was then washed with TBST three times for 15 minutes on shaker. Supersignal West Femto maximum sensitivity substrate (equal volume mixture of stable peroxide solution and luminal/enhancer solution) by Thermo scientific IL, USA was used as chemiluminescent substrate which makes a conjugated complex with the protein-antibodies complex and glow. The blot image was probed with Omega Molecular Imaging System (ULTRA LUM, California, USA) (74).

### 3.2.6 Spectroscopic estimation of PSI ( $P_{700}$ )

Spectroscopically the amount of PSI accumulation in each mutant was measured using Joliot type spectrophotometer called JTS-10 (Bio-logic), which has the capacity to

measure the light induced changes in crude thylakoid membranes with a time resolution of 10  $\mu$ s. For PSI estimation, a sample of 20  $\mu$ g/ml of Chl containing CTM was taken and 40  $\mu$ M of dibromothymoquinone (DBMIB) to inhibit or slow down the cyclic electron flow from cytochrome *b<sub>6</sub>f*, 10  $\mu$ M of Carbonyl cyanide p-[trifluoromethoxy]-phenyl-hydrozone (FCCP) to disrupt the proton gradient if present in the crude thylakoid membranes, 5mM Sodium ascorbate was used as a reducing agent to reduce the oxidized P<sub>700</sub>. For excitation a frequency-doubled Nd:YAG laser (Continuum Electro-Optics, Inc., Santa Clara, CA) emitting 33 mJ pulses at 532 nm (6 ns duration) was used for oxidation of P<sub>700</sub> of PSI. The laser flash has enough energy to saturate the sample. The oxidation of sample was probed with 700 and 810 nm weak actinic flashes from JTS-10 spectrophotometer. The sample was measured in the absorbance mode where a baseline of 20 s was measured initially and then in the illumination period a single laser flash was given to oxidize the P<sub>700</sub>, followed by measuring flashes (10- $\mu$ s red LED passed through a selected interference filter) to monitor oxidation of P<sub>700</sub> by the laser flash in exponential increment way for 1115 ms. These measuring flashes commenced 250  $\mu$ s after the laser flash and after exponential increment increase phase and additional measuring flashes of 18 s, long enough for the bleaching signal to recover entirely. The transients were recorded at wavelength of 675, 680, 685, 690, 695, 700, 705, 740 and 810 nm by using interference filters. The lowest bleaching point was taken for wavelength from 675 to 705 nm while at 740 and 810 nm the positive peak was taken for calculation as at 740 nm and beyond P<sub>700</sub><sup>+</sup> absorb. The transients were taken and a light minus dark difference spectrum was plotted for P<sub>700</sub> of PSI.

### 3.2.7 Time-resolved Optical Spectroscopy of PSI particles

Time-resolved optical spectroscopy with a temporal resolution of ns - ms was performed on PSI particles. A 480-nm probe beam was used to monitor the electrochromic bandshift of pigments in the RC induced by the charge-separated state (primarily due to pigments near  $\text{PhQ}^-$ ) (109). For these measurements, 30  $\mu\text{g}$  of chlorophyll containing PSI sample per 1 mL was diluted into a buffer containing 10 mM Tricine (pH 8), 0.4 M  $\text{CaCl}_2$ , 0.4 M  $\text{MgCl}_2$ , 10% glycerol, 0.03%  $\beta$ -DM, 10 mM sodium ascorbate, and 40  $\mu\text{M}$  phenazine methosulfate (PMS). The sample was excited with a  $\sim 3$ -ns laser pulse generated by a frequency-doubled (532 nm), Q-switched Nd:YAG laser (DCR-11, Spectra Physics, Mountain View, CA) operated in the short-pulse mode. The probe light was provided by a Xe flash tailored with a bank of inductors and capacitors to produce 5- $\mu\text{s}$  pulses. The 480-nm probe and pump beam were filtered through a narrow band (8 nm) interference filter along with colored glass filters (FND 100Q from EG & G) and were paired up in two micrometer multimode fiber optic patch cables (M28L01; Thorlabs, Newton, NJ) through two fixed focus collimation packages (F240FC-543; Thorlabs, Newton, NJ), placed at a distance of 3 m from the sample cuvette to minimize the artifacts due to excitation beam. The two fiber cables were connected to a balanced amplified photodetector (PDB430A; Thorlabs, Newton, NJ) containing DC bandwidth of 350 MHz. Digitizing oscilloscope (DSA 602A with amplifier plug-in 11A52; Tektronix, Beaverton, OR) was used to measure the balance output. The laser flash was detected by a photodiode connected to 11A72 plug-in used to initiate the data acquisition. The rise time of the detection system was measured by using Tris(bipyridine)ruthenium(II) chloride



(Ru (Bipy)<sub>3</sub>Cl<sub>2</sub>) luminescence and was found to be 3 ns(110). The baseline was recorded after every flash by mechanically blocking the pump flash, and this baseline transient was subtracted from that recorded with pump flash on every cycle. Around 1024 to 2048 pairs of flash minus no-flash transients were averaged at a repetition rate of 1 Hz. Software written in LabView controlled the timing sequence and data recording. The PSI sample was contained in 10x10 mm standard quartz cuvette at room temperature. All the kinetic traces were processed by fitting with a multi-exponential function using Marquardt least-squares algorithm that was programmed in IGOR Pro v. 5.2 (Wavemetrics, Lake Oswego, OR). Charge recombination was monitored at 820 nm using a home-built time-resolved spectrophotometer. For these measurements, PS1 particles corresponding to 100 µg were diluted into 400 µL of buffer (same as above except using 0.5 mM sodium ascorbate and 10 µM DCPIP as a reducing agents). The sample was prepared in an anaerobic chamber (Coy Laboratories, Grass Lake, MI) with an atmosphere of 10% H<sub>2</sub> and 90% N<sub>2</sub> to avoid generation of harmful oxygen radicals.

### 3.2.8 Electron Paramagnetic Resonance (EPR) Spectroscopy

Low temperature (80 K) X-band (9 GHz) time/field transient EPR data sets were measure with a modified Bruker ER 200D-SRC spectrometer with an ER 041 X-MR X-band Microwave Bridge. A Flexline ER 4118 X-MD-5WI dielectric resonator was used at low temperature. Light excitation was made using a Continuum Surelite Nd:YAG laser working at 10 Hz, 4.0 mJ/pulse and 532 nm. The temperature of the bath was controlled using an Oxford Instruments CF9335 gas flow cryostate. The transient EPR signal was recorder in direct-detection mode with a home built broadband amplifier (bandwidth 500

MHz) and was digitized through a LeCroy LT322 500 MHz digital oscilloscope. PSI samples were treated with 1mM sodium ascorbate and 50  $\mu$ M phenazine methosulfate (PMS) and the samples were frozen in the dark. Room temperature X-band EPR measurements were performed with a modified Bruker ESP 200 spectrometer equipped with a home built, broadband amplifier (bandwidth >500 MHz). A flat cell and a rectangular resonator were used and the samples were illuminated using a Q-switched, frequency-doubled Continuum Surelite Nd:YAG laser working at 10 Hz, 4.0 mJ/pulse and 532 nm. In order to bring the  $P_{700}$  in the reduced state before the excitation flash, 1 mM sodium ascorbate and 50  $\mu$ M PMS were used as electron donor and mediator.

### 3.2.9 Ultrafast Transient Absorption Spectroscopy

The sample was excited with a laser light of 690nm excitation with a full width at half maximum (FWHM) of 0.15 ps and was probed with white continuum light having central wavelength of 680nm. The pump and probe light was set at magic angle ( $54.7^\circ$ ). Intensity of the excitation light was enough to excite the sample but not to make much annihilation. Measurements were performed in a window from 601 to 750 nm, which is  $Q_Y$  transition of Chlorophyll a of PSI. Data was collected from 0.9 ps before time zero and 2 nanosecond after the excitation pulse. Circular rotating cuvette with a path length of 1.2mm was used so that the laser light didn't excite more than 10% of the measuring PSI particles. Speed of the rotation was set so that the laser shot hit fresh open (reduced  $P_{700}$ ) PSI particles and to avoid the accumulation of long lived intermediates state. The sample concentration was chosen so Optical density of the sample was 0.8 OD at  $Q_Y$

region at 676.14 nm. For stability of PSI and to avoid aggregation issues, the buffer consists of 10 mM Tricine, 0.4 M MgCl<sub>2</sub>, 0.4 M CaCl<sub>2</sub>, 10% glycerol, 0.03%  $\beta$ -DM as a detergent. 40 mM of sodium ascorbate and 50  $\mu$ M of phenazine methosulfate was used as redox agents in order to keep the reaction center in open state during measurements.

### 3.2.10 Time-resolved fluorescence

Time correlated single photon counting (TCSPC) was performed to measure the kinetics of energy trapping in PSI mutant samples. The sample was excited with a Titanium-Sapphire laser (Spectra-Physics, Millennia pumped Tsunami) at 420 nm with a 130 fs pulse duration and 4 MHz repetition rate. Fluorescence emission was collected at a 90° geometry setting and detected using a double-grating monochromator (Jobin-Yvon, Gemini-180) and a microchannel plate photomultiplier tube (Hamamatsu R3809U-50). The polarization of the emission was set at a magical angle of 54.7° relative to that of the excitation. The data acquisition was done using a single photon counting card (Becker-Hickl, SPC-830). The typical IRF had a FWHM of 35 ps, measured from the scattering of sample at 420 nm. The excitation power was 12.1  $\mu$ W at the sample to avoid singlet-singlet annihilation. A time window of 3.3 ns was used and measurements were done from 680 to 740 nm with 10-nm spacing. The PSI particles were diluted to an OD of 0.5 cm<sup>-1</sup> at the Chl *a* Q<sub>y</sub> maximum with a buffer containing 10 mM Tricine (pH 8), 0.4 M MgCl<sub>2</sub>, 0.4 M CaCl<sub>2</sub>, 10 % glycerol, 0.03 %  $\beta$ -DM, 20 mM sodium ascorbate, and 50  $\mu$ M phenazine methosulfate. Global analysis was performed with ASUFIT 6.1 software. The decay-associated spectra (DAS) of fluorescence emission are the wavelength dependent

pre-exponential part,  $A_i(\lambda)$ , from the multiexponential fluorescence decay components, from the equation  $F = \sum A_i(\lambda) \exp(-t/\tau_i)$  and is related to specific exponential lifetime,  $\tau_i$ .

### 3.2.11 Static Fourier Transformed Infrared Difference Spectroscopy

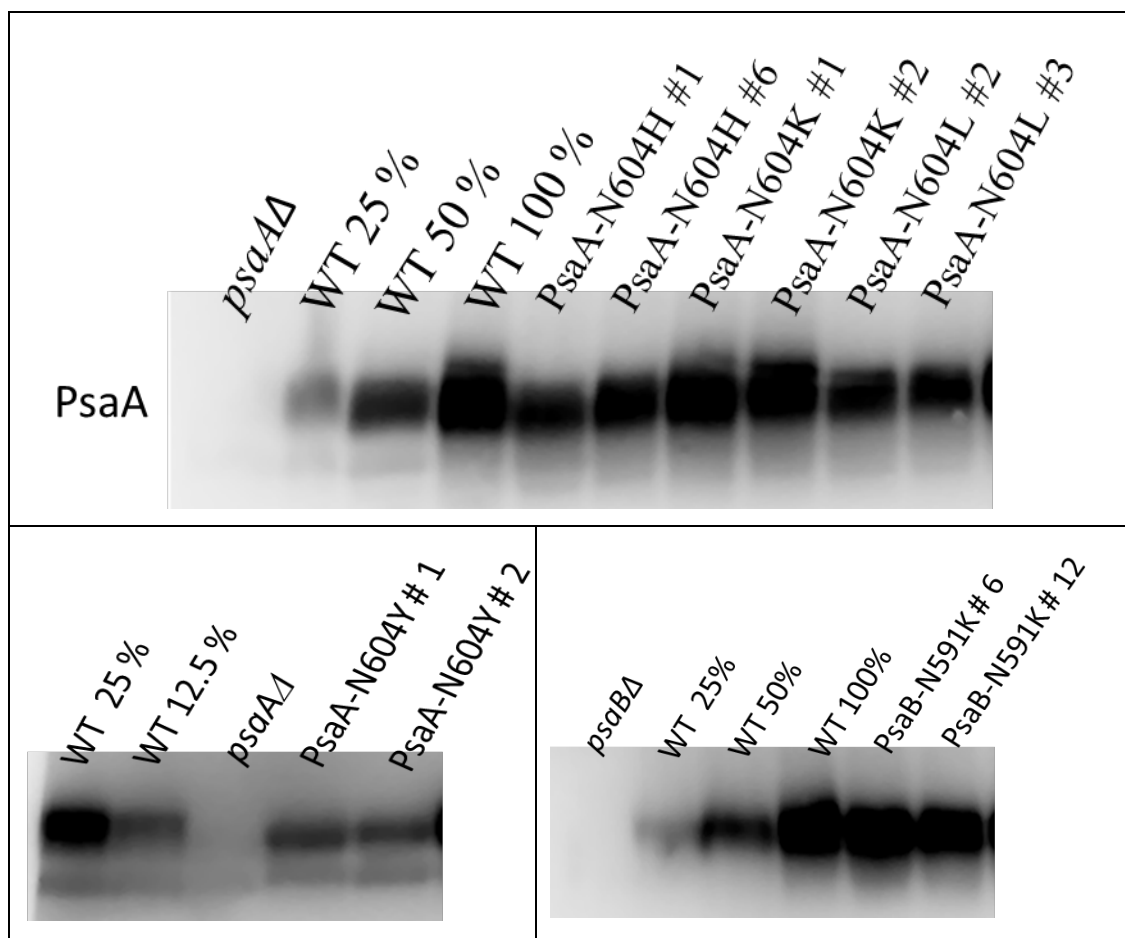
For static Fourier transformed infrared difference spectroscopic measurements, the PS I particles were washed by 50 mM Tris buffer with 0.04%  $\beta$ -DM detergent and spin it down and placed between two rectangular  $\text{CaF}_2$  windows. All the static FTIR difference spectra were recorded on BRUKER VERTEX 80 FTIR spectrometer. For these measurements, a continuous illumination from a 20 mW helium neon laser was used for light excitation. All measurements were performed at room temperature. Spectra in light and dark conditions were recorded and a light-minus-dark and dark-minus-dark spectra were constructed to get the FTIR difference spectra (DS) as described by Wang and colleagues (111, 112).

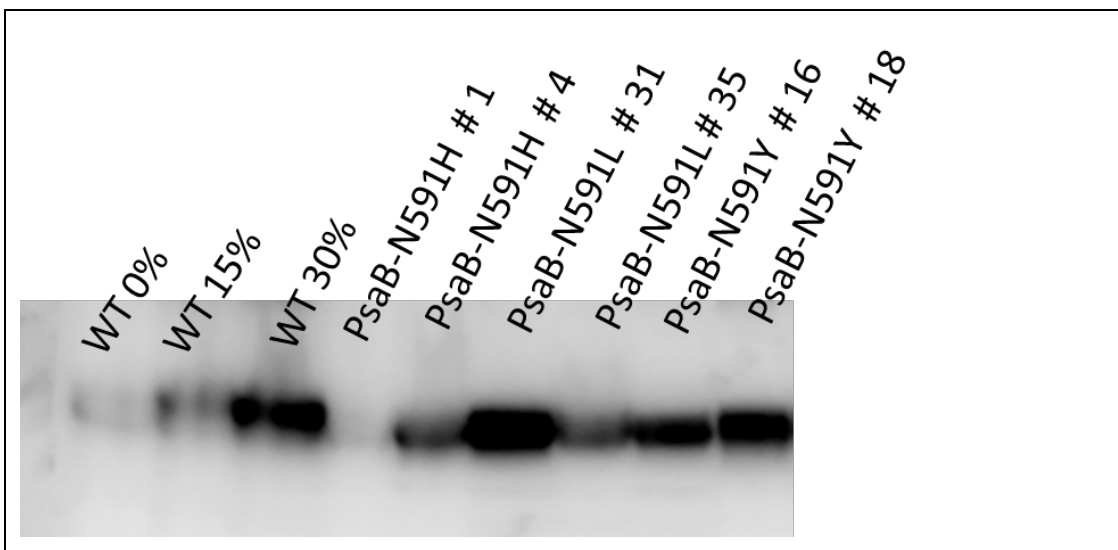
## 3.3 RESULTS

### 3.3.1 Biochemical Characterization

Crude thylakoid membranes of the PSI mutants were used to perform the immunoblots in order to estimate the amount of PSI accumulated in the cells. The level of PSI was estimated using a serial dilution of WT extract into extracts from the *psaA1* or *psaB1* strains; the same amount of total membrane protein was loaded in each lane, leaving the amount of PS1 as the sole variable. The PSI level estimated in this way is roughly in this order for the *ec2<sub>B</sub>* mutants:  $\text{WT} \approx \text{PsaA-N604K} > \text{PsaA-N604L} > \text{PsaA-N604D} \approx \text{PsaA-}$

N604H > PsaA-N604Y (Figure 3.2). For the *ec2<sub>A</sub>* mutants, the order was WT > PsaB-N591K > PsaB-N591D > PsaB-N591L > PsaB-N591Y > PsaB-N591H. Although we observed some variation between transformants, these results largely agreed when two independent transformants were compared. (If this was not the case, additional transformants were analyzed to determine the representative case.) In addition, the PSI levels estimated from immunoblots correlated well with the levels estimated via optical spectroscopy (see next section).





**Figure 3.2.** Western Blot of PsaA-N604 and PsaB-N591 transformants, for the detection of PsaA subunit of PSI. 0.5 $\mu$ g of chlorophyll containing protein of PSI with a volume of 10 $\mu$ L of sample were loaded on 4-10% Tricine gel with a constant voltage of 90V for 4 hour.

### 3.3.2 Spectroscopic estimation of PSI ( $P_{700}$ )

We independently estimated the level of  $P_{700}$  spectroscopically in crude thylakoid membranes. Excitation of PS1 will lead to oxidation of  $P_{700}$  as an electron is transferred to the  $F_A/F_B$  clusters. Charge recombination of  $P_{700}^+ (F_A/F_B)^-$  occurs with a decay time of  $\sim 100$  ms (87). If the electron is lost from  $F_A/F_B$  by donation to an exogenous acceptor (*e.g.*  $O_2$ ), then  $P_{700}^+$  will be reduced by ascorbate in several seconds. Thus, time-resolved measurements in the ms timescale are sufficient to observe  $P_{700}$  bleaching and recovery from a saturating laser flash. We performed this experiment using probe light from 675 nm to 810 nm and the maximum absorption change (seen in the earliest time points) was plotted vs. wavelength to obtain the light-induced ( $P_{700}^+ - P_{700}$ ) difference spectrum (Figure 3.3).

These mutations might affect  $P_{700}$  due to their proximity and also due to the fact that the ec2 and ec3 chlorophylls are excitonically coupled to the  $P_{700}$  dimer. Using the known extinction coefficient of  $P_{700}$  in this species (77), we calculated the level of  $P_{700}$  in each mutant; the results are tabulated in Table 3.1. In general, the PSI level tends to be lower in the PsaB mutants, which affect the A-branch. The lysine mutants in both branches accumulated >80% PSI, as compared to WT, indicating that this substitution was surprisingly well tolerated (Figure 3.3). The tyrosine substitution was in general most poorly tolerated, resulting in a ~25-fold drop in PSI levels for either side. The worst mutant was PsaB-N591H, whose PSI level was ~2-3% of WT; in contrast, the PsaA-N604H mutant accumulated about 10 times more PSI. Similarly, the PsaB-N591L (near ec2<sub>A</sub>) accumulated just under 20% the normal level of PSI, while the PsaA-N604L mutant (near ec2<sub>B</sub>) accumulated just under 90% the WT level of PSI. Conversion of Asn to Asp resulted in a 3-4 fold drop in PSI levels on either side, but the mutation also induced a slight red-shift in the ( $P_{700}^{+} - P_{700}$ ) difference spectra (Figure 3.4). Such shifts were not observed in the other substitution mutants. The possibility of the Asp residues being charged will be discussed below.



**Table 3.1:** Quantification of P<sub>700</sub> bleaching and PsaA polypeptide through immunoblotting in membranes from different mutants. The maximum bleaching at 695 nm was used for estimation of total amount of PSI, using the known extinction coefficient of P<sub>700</sub> in this species (100,000 mM<sup>-1</sup> cm<sup>-1</sup>; (77)).

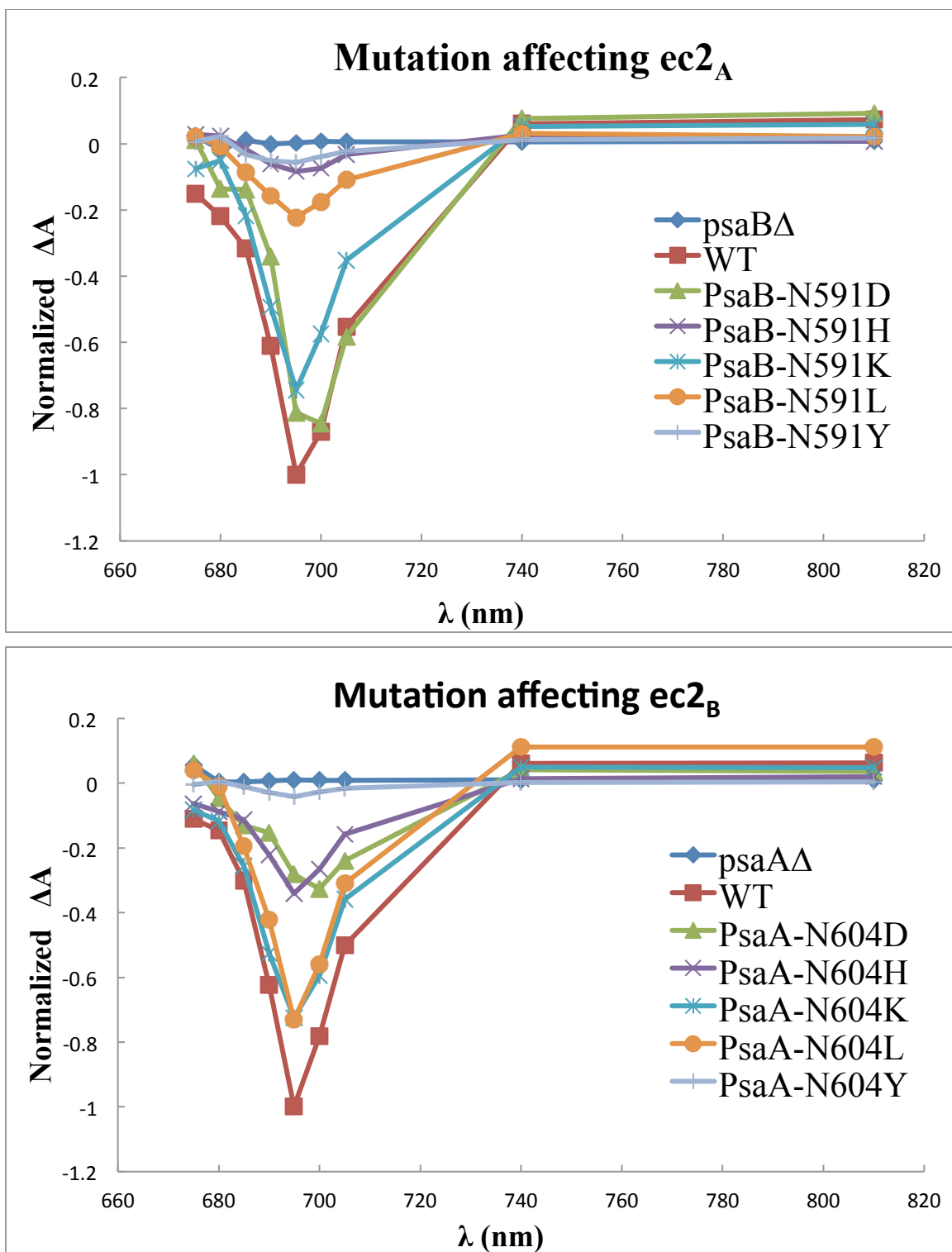
Sample	P <sub>700</sub> level (% WT) <sup>1</sup>	Amount of PSI (% of WT) <sup>3</sup>	Sample	P <sub>700</sub> level (% WT) <sup>2</sup>	Amount of PSI (% of WT) <sup>3</sup>
WT-A	100.00 ± 31	100	WT-B	100.00 ± 9	100
<i>psaAΔ</i>	0	0	<i>psaBΔ</i>	0	0
PsaA-N604D	27.3 ± 9.0 <sup>2</sup>	ND <sup>4</sup>	PsaB-N591D	77 ± 13	ND <sup>4</sup>
PsaA-N604H	37.4 ± 9.0	64 ± 5.7	PsaB-N591H	2.4 ± 3.5	10 ± 5.7
PsaA-N604K	83 ± 14.7	91 ± 0	PsaB-N591K	97.9 ± 34.4	110.5 ± 13.4
PsaA-N604L	88.6 ± 17.0	68 ± 2.8	PsaB-N591L	19 ± 6.6	23 ± 15.6
PsaA-N601Y	4.3 ± 1.4	11.6 ± 1.1	PsaB-N587Y	4.3 ± 2.4	20 ± 2.8

<sup>1</sup>The WT-A level of PSI was 0.040 ± 0.002 μmole of P<sub>700</sub> per mg of Chl.

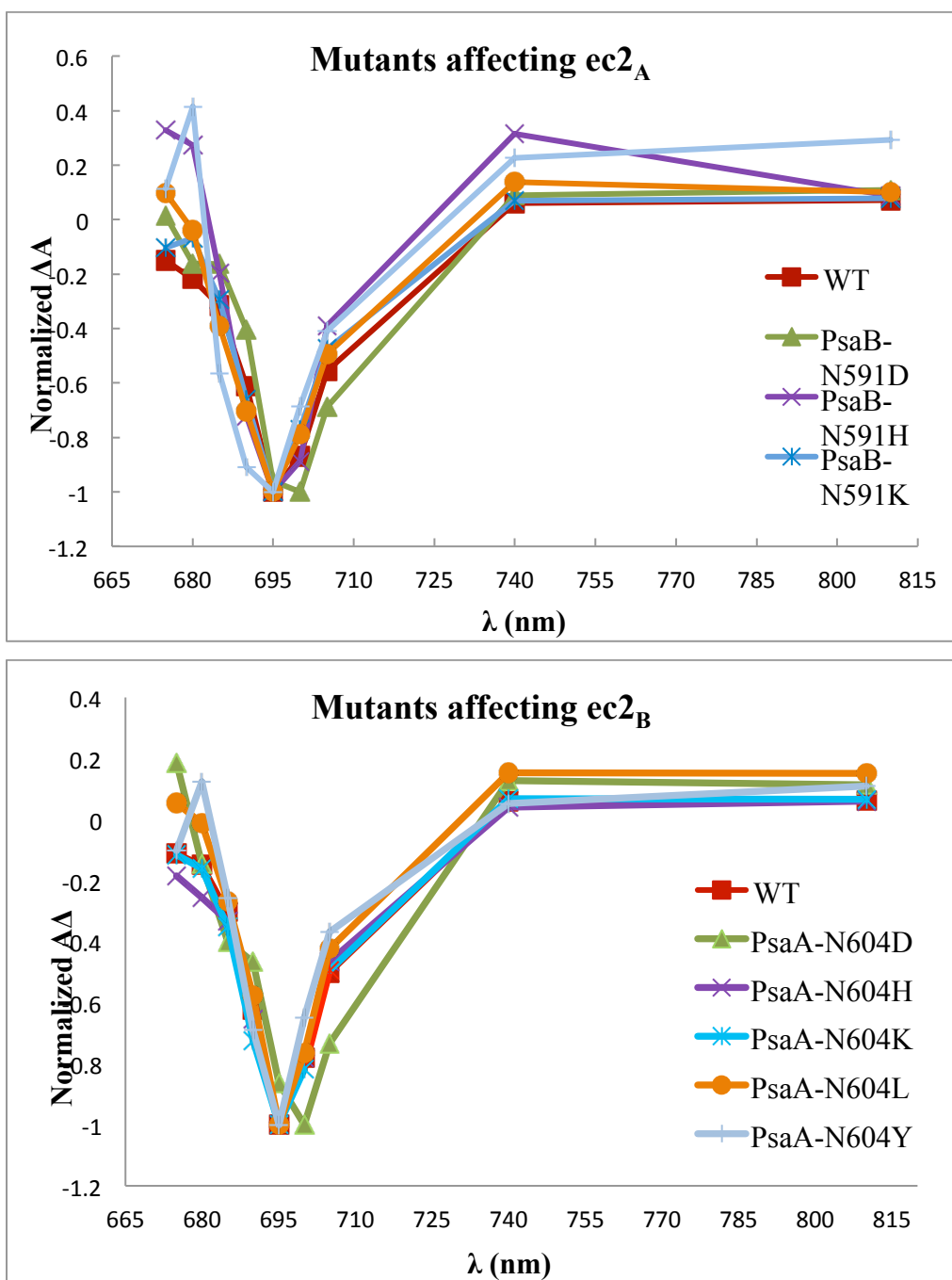
<sup>2</sup>The WT-B level of PSI was 0.054 ± 0.008 μmole of P<sub>700</sub> per mg of Chl.

<sup>3</sup>The quantity of PsaA subunit relative to the chlorophyll in each crude membrane preparation was quantified by densitometry as shown in figure 4.

<sup>4</sup>ND = Not determined



**Figure 3.3.** Normalized light induced difference spectra of  $P_{700}$  of mutants affecting the  $ec2_A$  (A) or  $ec2_B$  (B) Chl of PSI.



**Figure 3.4.** Normalized light induced difference spectra of  $P_{700}$  of different mutants affecting  $ec2_A$  cofactor of A-branch  $ec2_B$  cofactor of B-branch of PSI. The spectra were normalized in order to compare the effect of mutation on the  $P_{700}$  absorption.

### 3.3.3 Growth Characteristics


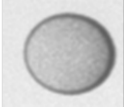
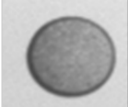
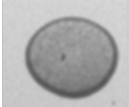


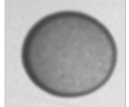



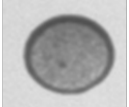


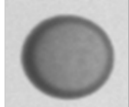

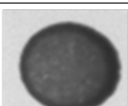
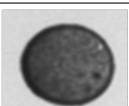
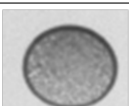
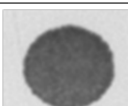
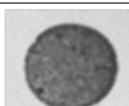
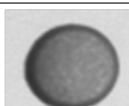
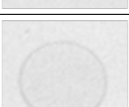


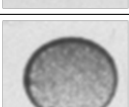
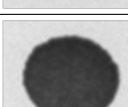

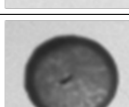

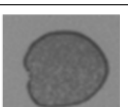


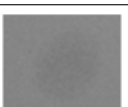




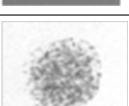



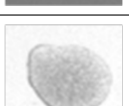
Changes in growth of cells due to mutational effects were determined by performing growth test under different phototrophic and heterotrophic conditions. Under dark conditions on TAP all the mutants grow like WT except PsaA-N60Y, whose growth is scattered. Further *psaAΔ* background strain also grows under dark conditions on TAP. At increasing light conditions (2, 20, 80  $\mu\text{Em}^{-2}$ ), the growth of the sample on TAP media decreasing in the following order WT > PsaA-N604H > PsaA-N604D > PsaA-N604K = PsaA-N604L > PsaA-N604Y (Figure 3.5). The growth of PsaA-N604Y decreases with increase in light and is very poor at 80  $\mu\text{Em}^{-2}$ . On TBP media at early stage, the growth of WT is low and same is the case of mutants while PsaA-N604Y and *psaAΔ* background strain has no autotrophic growth. At later stages, the WT grow fully while in mutants only PsaA-N604H showed growth but other mutants like PsaA-N604D, PsaA-N604K and PsaA-N604L growth is very low. At lower oxygen conditions, the growth of WT and mutants has also low growth.

Mutants that are affecting the A-branch grow in the dark like WT-B and *psaBΔ* background strain (Figure 3.6). In the light conditions on TAP media, the growth of the mutants decreases in the following order with increase in light flux: WT-B > PsaB-N591K > PsaB-N591D > PsaB-N591L > PsaB-N591Y > PsaB-N591H. On TBP plates, for autotrophic growth, the WT-B showed poor growth at early and late stage while the mutants showed no growth at all. Under low oxygen condition on TBP, the WT-B, PsaB-N591Y and PsaB-N591K grow poorly while PsaB-N591D and PsaB-N591L have very poor growth. The PsaB-N591H is completely dead at this condition like the deletion

background strain. At later stages of low oxygen condition on TBP, the growth of the samples decreases in the following order: PsaB-N591K > WT > PsaB-N591Y > PsaB-N591D > PsaB-N591L > PsaB-N591H. Thus the growth test showed that these mutants showed reasonable growth in dark and heterotrophic condition but have very poor autotrophic growth. These results suggest that these mutants accumulate variable levels of PSI heterotrophically and the mutation results in increases in the level of photo-oxidative damage.

	<i>psaAΔ</i>	WT-A	PsaA-N601D	PsaA-N601H	PsaA-N601K	PsaA-N601L	PsaA-N601Y
dark							
2							
20							
80							
TBP -O <sub>2</sub>							
TBP							

**Figure 3.5.** Growth on solid media of WT and PsaA-N604 mutants near *ec2<sub>B</sub>* of PSI. Colonies of *C. reinhardtii* were grown under heterotrophic (acetate, no light), various mixotrophic conditions (acetate with low, medium and high light) and phototrophic (no acetate but high light and anaerobic conditions).

	<i>psaBΔ</i>	WT-B	PsaB-N587D	PsaB-N587H	PsaB-N587K	PsaB-N587L	PsaB-N587Y
dark							
2							
20							
80							
TBP							
TBP -O <sub>2</sub>							

**Figure 3.6** Growth on solid media of WT and PsaA-N591 mutants near *ec2<sub>A</sub>* of PSI. Colonies of *C. reinhardtii* were grown under heterotrophic (acetate, no light), various mixotrophic conditions (acetate with low, medium and high light) and phototrophic (no acetate but high light and anaerobic conditions).

### 3.3.4 Kinetics at 390 nm (phyllosemiquinone decay) in living cells

Based on the estimated amount of PS1 by immunoblot and  $P_{700}$  photobleaching, we selected mutants that accumulated PS1 the best and probed them *in vivo* for the relative use of the two PhQs by pump-probe spectroscopy. We used diagnostic wavelengths at 390 nm (phyllosemiquinone), 430 ( $P_{700}$ ), 440 ( $P_{700}^+ A_0^-$ ), and 480 nm (electrochromic bandshift due to  $PhQ^-$ ) and monitored absorbance from 5 ns to 100 ms after the pump flash. As seen before (51, 113-115), we observed biphasic decay of the absorbance increase at 390 nm, which is primarily due to the phyllosemiquinone ( $PhQ^-$ ). In the WT control strain, the ratio of slow decay (~200-250 ns) to fast decay (~16-25 ns) was about 1.06 (Table 3.2). We can take this ratio as a relative measure of the usage of the A-branch to usage of the B-branch. In the PsaB-N591L mutant (near  $ec2_A$ ), this ratio fell to 0.74, while it rose to 1.81 in the PsaA-N604L mutant (near  $ec2_B$ ). This result is consistent with the hypothesis that the Asn→Leu mutation somehow interfered with charge separation involving the nearby  $ec2$  Chl. The results were not as clear-cut in the rest of the mutants, as the ratio seemed to rise in both substitution mutants, although it was always much greater in the mutants near  $ec2_B$ . The PsaB-N591H mutant displayed very little decay at 390 nm, and showed signs of rapid charge recombination in the tens of ns timescale at 430 nm and 440 nm, which is indicative of recombination of the  $P_{700}^+ A_0^-$  state. This was the only mutant that displayed such behavior. The *in vivo* spectroscopy allowed us to focus our attention on the mutants that appeared to have an effect upon the directionality

of electron transfer within PS1. However, as we have no independent way of assessing the amount of PS1 *in vivo*, we cannot distinguish between a lower yield of charge separation on one branch and a redirection of charge separation from one branch to the other at this level of analysis. Therefore, it was necessary to purify PS1 from the mutants in order to gain a more in-depth view of the consequences of these mutations.

**Table 3.2.** Ratio of slow:fast decay at 390 nm in living cells

Observation	WT	PsaA-Asn604->				PsaB-Asn591->			
		Asp	His	Leu	Lys	Asp	His	Leu	Lys
ratio slow:fast	1.06	2.08	1.25	1.73	2.04	1.44	Nil <sup>1</sup>	0.74	1.18

<sup>1</sup>Very little charge separation was observed in this mutant

### 3.3.5 Nanosecond kinetics at 480 nm (electrochromic bandshift) in purified PS1

We performed time-resolved optical spectroscopy on PS1 particles from the various transformants into a background with low LHCII and a hexahistidine tag at the N-terminus of PsaA. The kinetics of phyllosemiquinone (PhQ<sup>-</sup>) oxidation were monitored at 480 nm, which is due to an electrochromic shift of pigments near PhQ<sup>-</sup> induced by the negative charge. (52, 109). The optical data obtained at 480 nm should thus give similar information as that at 380 nm; however, at 480 nm there is an additional positive component from P700<sup>+</sup>. The time-resolved optical spectra for WT and mutants obtained at room temperature were fitted to two exponential decays. The decay at 480 nm in WT PS1 was biphasic, with lifetimes of 22.3 ns and 216 ns; the amplitudes were 0.94 mOD



and 1.2 mOD, respectively (Figure 3.7; Table 3.3). These values are very similar to what has been observed before (52).

The PsaA-N604L mutant exhibited lifetimes of 20.5 ns (0.45 mOD) and 206 ns (1.2m OD). In contrast, the PsaB-N591L mutant (ec2<sub>A</sub>) had decay components with lifetimes of 20.5 ns (0.92 mOD) and 205 ns (0.34 mOD). Thus, the rates extracted from this analysis did not greatly differ, but the amplitudes were significantly changed. Moreover, the change would be as expected if the affected branch were utilized less as a consequence of the mutation. Thus, the mutation affecting ec2<sub>B</sub> exhibited slower electron transfer, consistent with the hypothesis that less electrons had arrived at PhQ<sub>B</sub> due to an impairment of charge separation in that branch. However, we note that the amplitude of the other component did not increase to compensate; it seemed to be unchanged. Thus, the overall amplitude of decay at 480 nm is lower in both mutants. This would indicate that the quantum yield of charge separation was lower in these mutants.

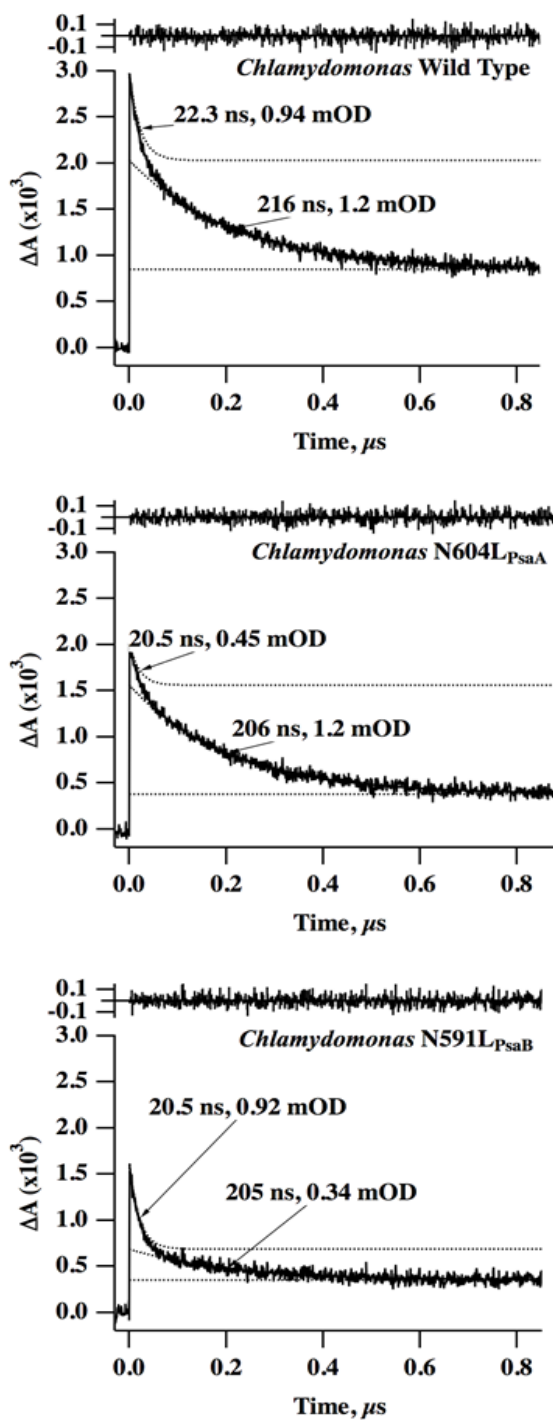
The situation with the other substitution mutants was a bit more complicated. Although the rates determined for the fast and slow decay components were not significantly different from those seen in WT, most of the other mutants caused decreases in the amplitudes of *both* components, although the decreases tended to be larger in the targeted branch. For example, the effect of the PsaA-N604K mutation was to reduce the amplitude of the fast component by more than 2-fold, but it also reduced the amplitude of the fast component by ~12%. In the PsaB-N591K mutant, both branches were strongly affected, with a ~2-fold decrease in the fast component and a 2.7-fold decrease in the slow component. The PsaA-N604H mutant exhibited a decrease in the fast component of about

3-4 fold, while the amplitude of the slow component decreased ~25%. Similar to what was observed *in vivo*, the PsaB-N591H mutant performed very little ET, and displayed large decreases in both the fast (~10-fold) and slow (~6.3-fold) components. (Although this last mutant may seem to be an exception to the rule, the very low signal may have led to an underestimate of the fast component.) Thus, the effect on the “other branch” was always larger in the PsaB substitution mutants, which should primarily affect  $ec2_A$ . Consequently, the PsaB mutants tended to have lower quantum yields of charge separation.

**Table 3.3.** Rates and amplitudes of decay components obtained from transient optical spectroscopy at 480 nm in various purified PS1 preparation from *C. reinhardtii*.

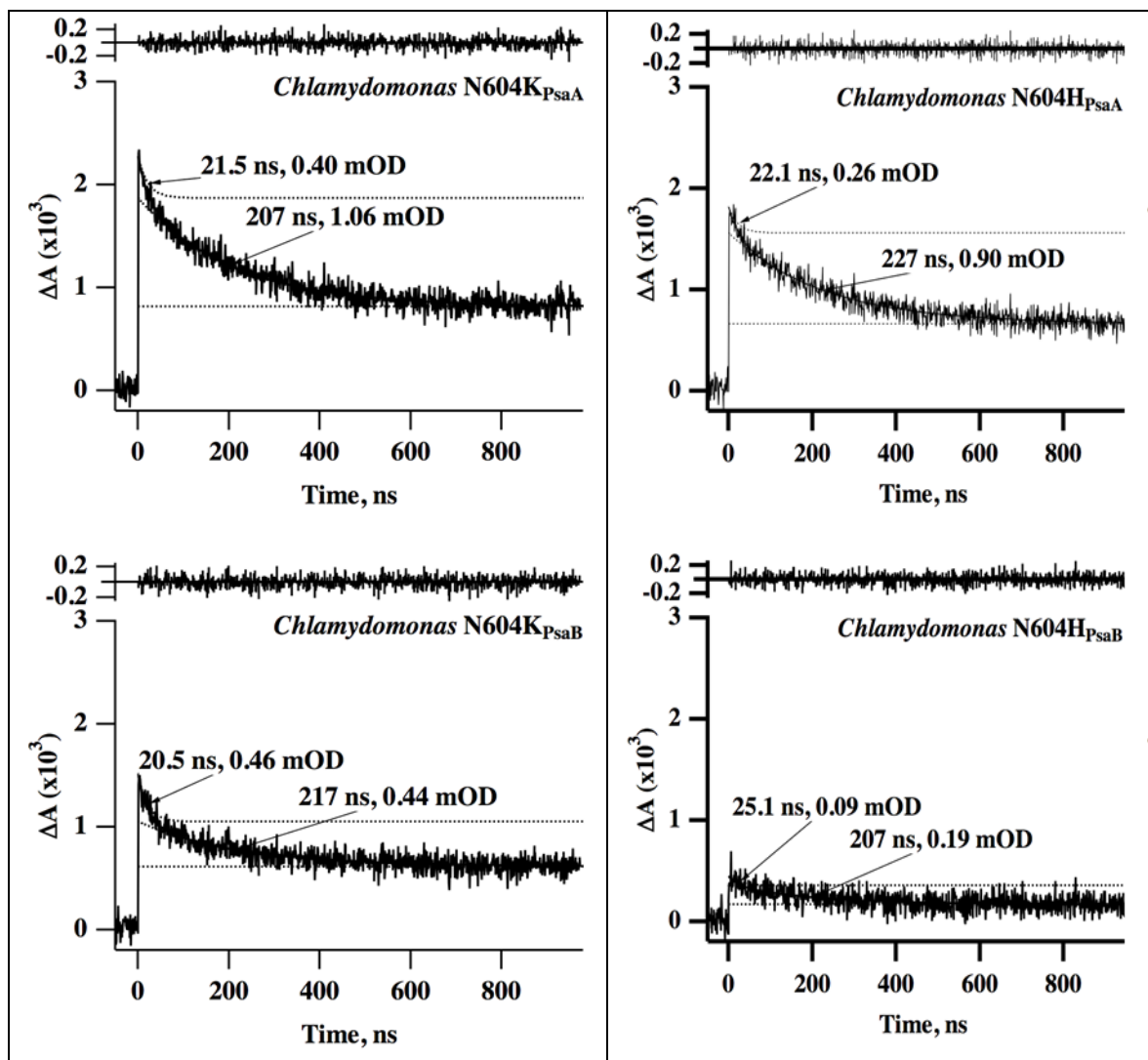
Mutation	amplitude (mOD) of fast decay	rate (ns) of fast decay	amplitude (mOD) of slow decay	rate (ns) of slow decay	$\phi$ at 480 nm [ns components] (%)
WT	0.94	22.3	1.20	216	100 <sup>1</sup>
PsaA-N604H	0.26	22.1	0.90	227	54
PsaB-N591H	0.09	25.1	0.19	207	13
PsaA-N604K	0.40	21.5	1.06	207	68
PsaB-N591K	0.46	20.5	0.44	217	42
PsaA-N604L	0.45	20.5	1.20	206	77
PsaB-N591L	0.92	20.5	0.34	205	59

<sup>1</sup> Assumed to be 100%. Quantum yields in the mutants are expressed as relative to WT.



**Figure 3.7** Time-resolved optical spectroscopic kinetics at 480 nm for the WT, PsaA-N604L and PsaB-N591L. The data is presented in a linear time axis, so that the lifetime

and contributions of the two phases can be easily differentiated. The residuals from the fits are shown above the main trace.



**Figure 3.8.** Time-resolved optical spectroscopic kinetics at 480 nm for the PsaA-N604K, PsaB-N591K, PsaA-N604H and PsaB-N591H. The data is presented in a linear time axis, so that the lifetime and contributions of the two phases can be easily differentiated. The residuals from the fits are shown above the main trace.

### 3.3.6 Charge recombination between $P_{700}^+ F_{A/B}^-$ radical pair and its intermediate states

Oxidized  $P_{700}$  ( $P_{700}^+$ ) was followed directly by monitoring absorption of chlorophyll cation radical at 820 nm in two time windows: a few ms and  $\sim 2$  s. The data from these two windows were united and a global fit was obtained. In the case of *C. reinhardtii* PSI, three decay components were necessary to fit the data (Figure 3.10 and Figure 3.11). Charge recombination of  $P_{700}^+(F_A/F_B)^-$  has a lifetime of 50 - 100 ms and accounts for much of the decay. A variable amount of slow decay (hundreds of ms to  $\sim 1$ s) was observed, and is assigned to electron donation from PMS to  $P_{700}^+$  in those PSI RCs from which the electron had “escaped” (via reduction of exogenous acceptors). The additional decay seen in algal PSI was in the  $\mu$ s timescale. In the control PSI, it exhibited a decay time of  $\sim 70$   $\mu$ s and accounted for about one third of the decay. The origin of this is not known. We did not observe any decay in the nanosecond timescale, demonstrating that none of the mutations caused charge recombination from ( $P_{700}^+ ec3^-$  (Table 3.4) (87).

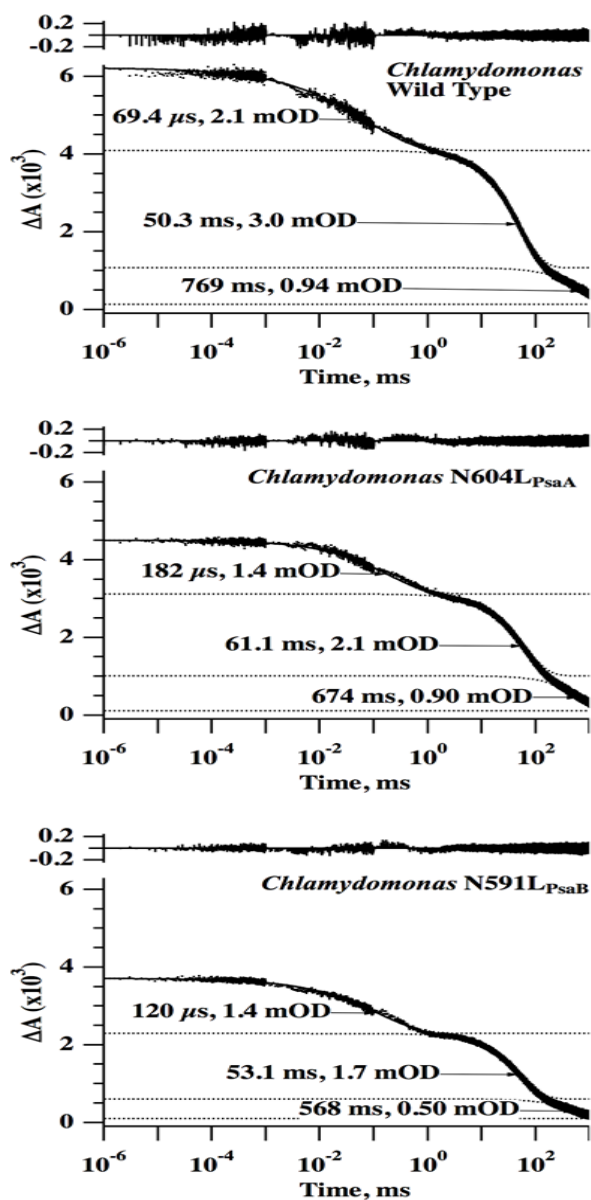
These measurements allowed an independent test of the hypothesis that the quantum yield of stable charge separation has been decreased in these mutants. By summing the total amount of decay at 820 nm (or the total amount of decay at 820 nm in the ms-sec timescale), we can estimate the amount of  $P_{700}^+$  generated (normalized to total Chl) in each PS1 preparation. We can do the same for the 480-nm decay in the ns timescale. Note that the electrochromic bandshift produced by  $PhQ^-$  on the two sides will not necessarily be of equal magnitude. However, working with the assumption that they are equal, one

arrives at a similar number for the amount of electrons arriving at the quinones in PS1. Taken together, this analysis demonstrates that the lost charge separation must stem from early event(s), before production of the  $P_{700}^+PhQ^-$  state. Moreover, the lack of charge recombination in the nanosecond timescale also suggests that it is a very early event, before production of the  $P_{700}^+A_0^-$  ( $P_{700}^+ec3^-$ ) state.

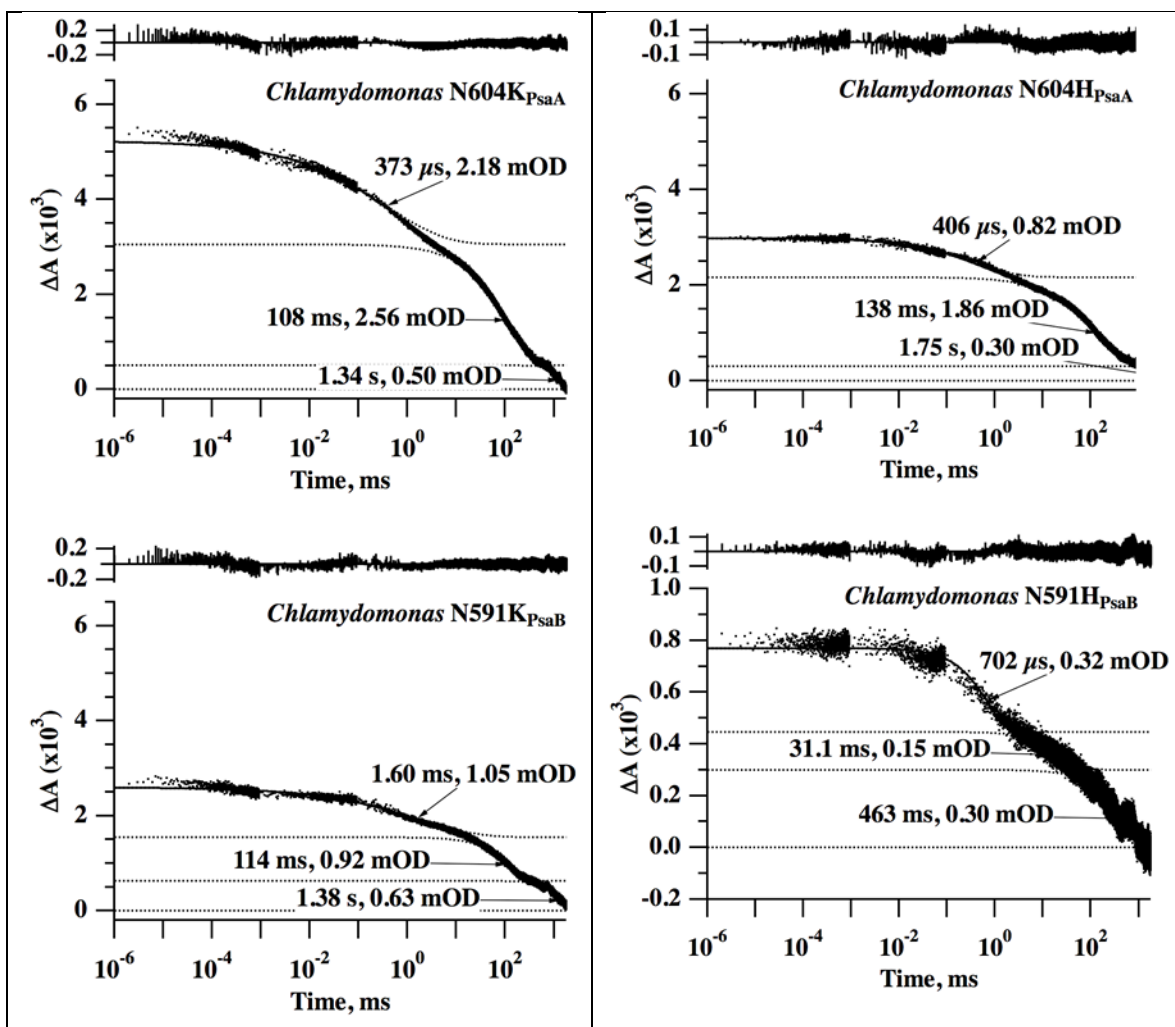
**Table 3.4.** Rates and amplitudes of decay components in the ns-s at 820 nm in various purified PS1 preparation (*C. reinhardtii* and *Synechocystis sp.* PCC 6803).

Mutation	P <sub>700</sub> <sup>+</sup> decay components	Assignment	Φ at 820 nm [ms component] (%)
WT	2.1 mOD, 70 μs	( <sup>3</sup> Chl)	100 <sup>1</sup>
	3.0 mOD, 50 ms	[F <sub>A</sub> /F <sub>B</sub> ] <sup>-</sup> → P <sub>700</sub> <sup>+</sup>	
	0.94 mOD, 770 ms	DCPIP → P <sub>700</sub> <sup>+</sup>	
PsaA-N604H	0.82 mOD, 410 μs	( <sup>3</sup> Chl)	55
	1.86 mOD, 140 ms	[F <sub>A</sub> /F <sub>B</sub> ] <sup>-</sup> → P <sub>700</sub> <sup>+</sup>	
	0.30 mOD, 1.75 s	DCPIP → P <sub>700</sub> <sup>+</sup>	
PsaB-N591H	0.32 mOD, 700 μs	( <sup>3</sup> Chl)	11
	0.15 mOD, 31 ms	[F <sub>A</sub> /F <sub>B</sub> ] <sup>-</sup> → P <sub>700</sub> <sup>+</sup>	
	0.30 mOD, 460 ms	DCPIP → P <sub>700</sub> <sup>+</sup>	
PsaA-N604K	2.18 mOD, 370 μs	( <sup>3</sup> Chl)	78
	2.56 mOD, 108 ms	[F <sub>A</sub> /F <sub>B</sub> ] <sup>-</sup> → P <sub>700</sub> <sup>+</sup>	
	0.50 mOD, 1.34 s	DCPIP → P <sub>700</sub> <sup>+</sup>	
PsaB-N591K	1.05 mOD, 1.6 ms	F <sub>X</sub> <sup>-</sup> → P <sub>700</sub> <sup>+</sup>	39
	0.92 mOD, 114 ms	[F <sub>A</sub> /F <sub>B</sub> ] <sup>-</sup> → P <sub>700</sub> <sup>+</sup>	
	0.63 mOD, 1.38 s	DCPIP → P <sub>700</sub> <sup>+</sup>	
PsaA-N604L	1.4 mOD, 182 μs	( <sup>3</sup> Chl)	76
	2.1 mOD, 61 ms	[F <sub>A</sub> /F <sub>B</sub> ] <sup>-</sup> → P <sub>700</sub> <sup>+</sup>	
	0.90 mOD, 674 ms	DCPIP → P <sub>700</sub> <sup>+</sup>	
PsaB-N587L	1.4 mOD, 120 μs	( <sup>3</sup> Chl)	56
	1.7 mOD, 53 ms	[F <sub>A</sub> /F <sub>B</sub> ] <sup>-</sup> → P <sub>700</sub> <sup>+</sup>	
	0.50 mOD, 570 ms	DCPIP → P <sub>700</sub> <sup>+</sup>	





**Figure. 3.9**  $P_{700}^+$  reduction kinetics monitored at 810 nm in WT, PsaA-N604L and PsaB-N591 PS1 particles. The time axis is plotted in logarithmic scale, with a computer generated fit in solid line with three lifetime components.



**Figure. 3.10**  $P_{700}^{+}$  reduction kinetics monitored at 810 nm in PsaA-N604K, PsaB-N591K, PsaA-N604H and PsaB-N591H PS1 particles. The time axis is plotted in logarithmic scale, with a computer generated fit in solid line with three lifetime components.

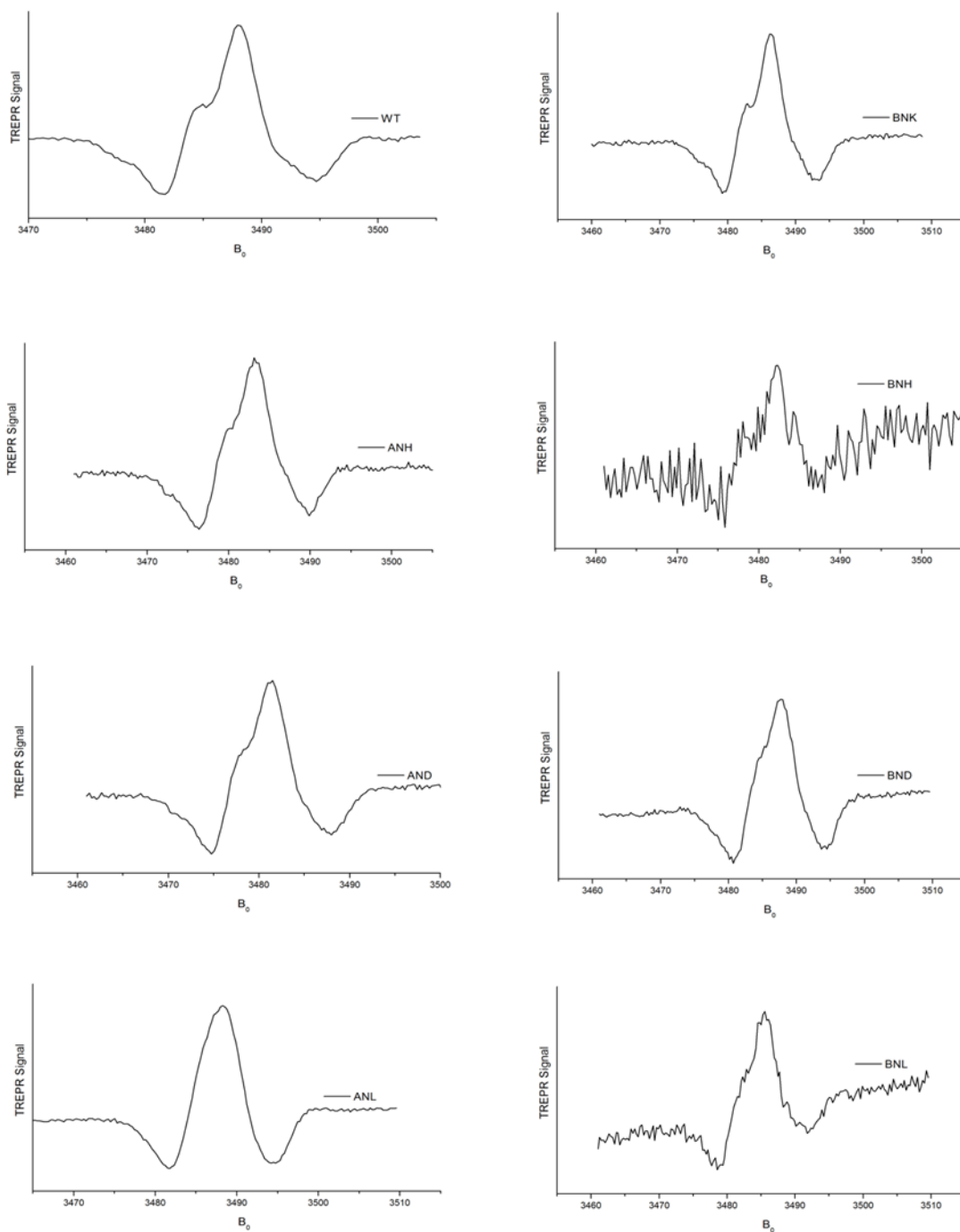
### 3.3.7 Low Temperature Transient EPR Spectra of $P_{700}^{+}PhQ^{-}$

Time-resolved electron paramagnetic resonance (TR-EPR) spectroscopy is a very useful method to analyze electron transfer events in photosynthetic complexes. In this technique, the sample is excited with a short laser flash and the EPR signal is monitored using continuous microwave irradiation at a fixed frequency and magnetic field. After obtaining transients at multiple field positions, one can construct transient EPR spectra at specific time delays after the flash. These experiments can provide information about ET events within photosynthetic RCs in terms of the different radical pairs formed, their magnetic characteristics, and the rates of their formation and decay. It also gives information about the triplet states formed by charge recombination ( $^3P_{700}$ ) or by intersystem crossing in the antenna chlorophylls. Another advantage of this instrument is that it provides information about the geometric and kinetic characteristics of the radical pairs. Thus the influence of changes in the protein environment of the cofactor due to mutation can be obtained from the changes observed in magnetic properties, and that can be correlated with the obtained kinetics. The main limitation of the technique is its low sensitivity and time resolution, which is on the order of tens of ns, precluding direct observation of ET from  $PhQ_B$  to the  $F_X$  cluster. The light-induced paramagnetic states are detected using continuous wave (CW) microwave irradiation. The field modulation and lock-in detection methods used commonly to detect the steady state signal with a Boltzmann population distribution of spin states are not used here, as the time resolution of the lock-in detection is limited by the modulation frequency and the bandwidth of the lock-in amplifier. Electron spin polarization (ESP) occurs when the radical pairs are

formed quickly from the excited singlet state of the donor, in which the electrons are strongly correlated. This phenomenon ends when they are separated, however it lives long enough to be detected as a non-Boltzmann distribution of the electron spin states and coherent oscillations of the spin system. ESP displays absorptive (A) and emissive (E) signals that enhance the amount of information and the signal strength three fold. This increase in signal strength is useful in the direct detection and enhance the bandwidth of the spectrometer to improve the response time (88). For example, excitation of PS1 produces the  $P_{700}^{+\bullet}PhQ^{-\bullet}$  state, in which the spins of the two radicals are correlated, having originated from the initial charge separation event. This gives rise to strong EPR signal from the spin-correlated radical pair. Previous work has shown that at low temperature, the signal is from  $P_{700}^{+\bullet}PhQ_A^{-\bullet}$ , with almost no contribution from the other radical pair ( $P_{700}^{+\bullet}PhQ_B^{-\bullet}$ ), and that electron transfer from the quinone to  $F_X$  is blocked. Thus, at low temperature, this technique should report upon the efficiency of charge separation in the A-branch (85).

Figure (Low Temp EPR) displays the X-band transient EPR spectrum of WT and four pairs of mutants taken at 80K. The WT spectrum shows a spin polarization pattern of E/A/E and looks very similar to spectra reported in the literature for *C. reinhardtii* PSI (50, 92). On the low-field side, the absorptive peak has a shoulder representing the partially resolved methyl hyperfine coupling (hfc) from PhQ, which also plays a big part in determining the width of the central peak in the spectrum. The effect of the methyl hfc is more along the C-CH<sub>3</sub> bond, as the methyl group is electron withdrawing, so electron density is more concentrated at the C-CH<sub>3</sub> bonding position. Furthermore, this coupling is

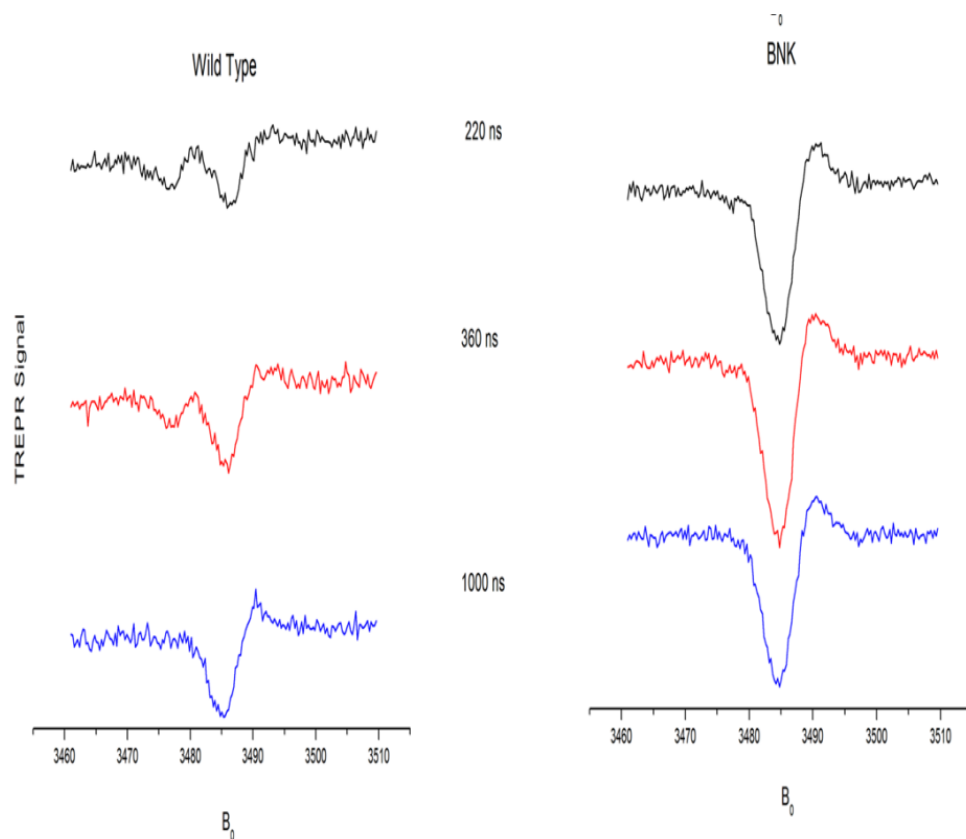
close to the Y-axis of the  $\text{PhQ}^{\bullet-}$  g-tensor. It is generally considered that when the magnetic field is along this axis during measurement, then the methyl hfc is partially resolved in the middle absorptive peak of the  $\text{P}_{700}^{++}\text{PhQ}_A^{\bullet-}$  TR-EPR spectrum. The hfcs are sensitive to the local environment and provide insight into the asymmetry of the spin density distribution over the  $\text{PhQ}^{\bullet-}$  radical (91, 116). This shoulder is smaller in *C. reinhardtii* PSI as compared to cyanobacterial PSI (89, 117). In WT and PsaB-N591K mutant the signature of the hfc can be clearly observed. It is smaller in PsaA-N604D, PsaB-N591D, PsaA-N604H, PsaB-N591H, PsaB-N591L mutants, but it is completely absent in PsaA-N604L. Secondly, the spectral width of WT can be used for comparison here, which has the low field emissive bleaching peak near 3482 T while the upper field emissive bleaching peak is near 3495 T. The spectral width and positions of the emissive bleaching peaks of  $\text{P}_{700}^{++}\text{PhQ}^{\bullet-}$  in the WT and mutants are the same; however there is a small shift in the spectra towards the lower magnetic field in some of the mutant PSI centers. This shift is observed in PsaA-N604D, PsaA-N604H and PsaB-N591H mutants. The third important character is the Signal/Noise (S/N) ratio of the  $\text{P}_{700}^{++}\text{PhQ}^{\bullet-}$  RP signal as an indicator of the CS activity of ET in each mutant. The decrease in the S/N ratio seen in the PsaB-N591H and PsaB-N591L mutants shows that these mutants have lower CS on the A-branch, consistent with optical spectroscopic results shown earlier (Figure 3.8-3.11).



**Figure 3. 11.** Low temperature spin polarized X-band transient EPR spectra recorded at 80 K for WT, PsaB-N591K, PsaA-N604H, PsaB-N591H, PsaA-N604D, PsaB-N591D, PsaA-N604L and PsaB-N591L.

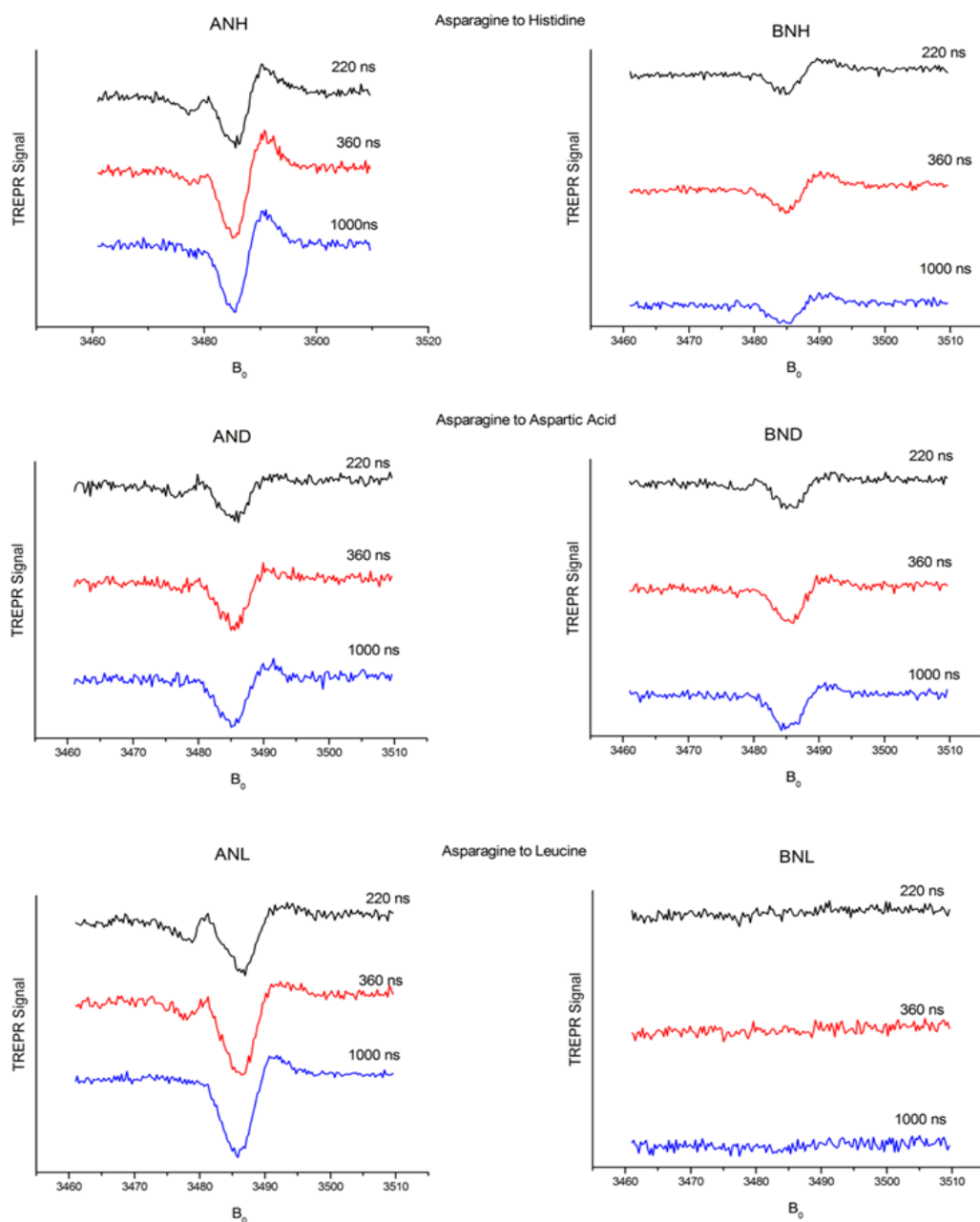
### 3.3.8 Room Temperature Transient EPR Spectroscopy

We performed room temperature transient X-band EPR spectroscopy for *ec2* mutants to monitor the activity of ET in both branches of PSI. The advantage of doing transient EPR at room temperature over low temperature is that we can measure the kinetics and ratio of ET between the two branches and down the iron sulfur clusters. In this method, the PSI sample is irradiated continuously with weak power microwaves and the time-resolved EPR response is measured after a laser flash. The transients are measured at a range of magnetic field positions, making a time/field data set from which the EPR spectrum at a given time can be calculated (118). Figure 3.13 shows the transient EPR signal at 220 ns, 360 ns and 1000 ns after the laser flash. In case of WT and the four B-branch mutants (PsaA-N604D, PsaA-N604H, PsaA-N604K and PsaA-N604L), there are two emissive (negative) signals observed at 220 ns. The one at lower magnetic field is a contribution from  $P_{700}^{+\bullet}PhQ^{-\bullet}$ , while the signal at the upper field mainly originates from the  $P_{700}^{+\bullet}FeS^{-\bullet}$  radical pair. As electron transfer from  $PhQ_A^{-\bullet}$  towards  $F_X$  occurs, the  $P_{700}^{+\bullet}PhQ^{-\bullet}RP$  signal decays and  $P_{700}^{+\bullet}FeS^{-\bullet}$  signal evolves. Thus these mutants inhibit most of the B-branch CS and ET on A-branch is utilized. In most of the A-branch mutants (PsaB-N591D, PsaB-N591H, PsaB-N591K), only the emissive spectrum of  $P_{700}^{+\bullet}FeS^{-\bullet}$  is seen at 220 ns and it is constant throughout the time course. This demonstrates that most of the CS occurs in the B-branch in these mutants, thus leading to more ET via  $PhQ_B$ . Almost no RP signal was observed in the PsaB-N591L mutant PS1, consistent with it performing very little stable CS.



**Figure 3.12.** Spin polarized X-band room temperature transient EPR spectroscopy of PSI particles from WT and PsbB-N591K.



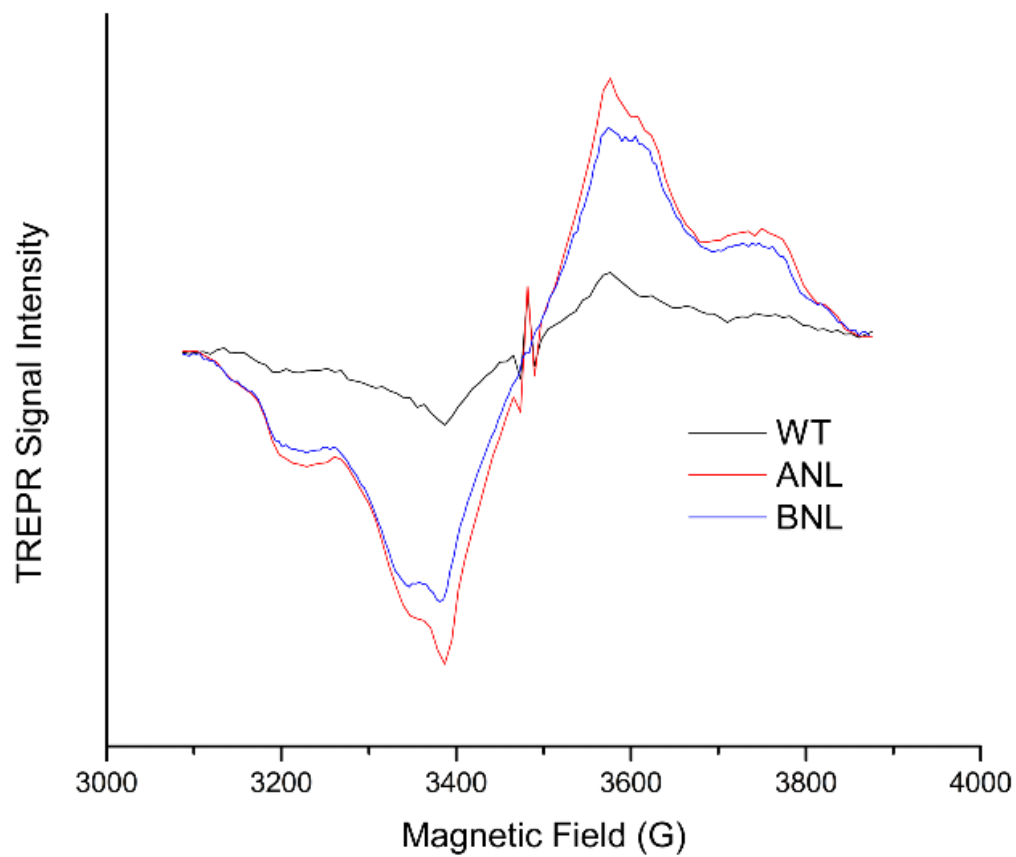


**Figure 3.13.** Spin polarized X-band room temperature transient EPR spectroscopy of PSI particles from PsaA-N604D, PsaA-N604H, PsaA-N604L mutants which are affecting  $ec2_B$  of B-branch and PsaB-N591D, PsaB-N591H, PsaB-N591L which are affecting  $ec2_A$  of A-branch.

### 3.3.9 Observation of P<sub>700</sub> Triplet (<sup>3</sup>P<sub>700</sub>) due to charge recombination by Transient EPR spectroscopy

When ET from the A<sub>0</sub> cofactor (ec3) downward is blocked, charge combination from the P<sub>700</sub><sup>•+</sup>A<sub>0</sub><sup>•-</sup> state results in production of the <sup>3</sup>P<sub>700</sub> triplet state. The triplet state is easily observable by EPR spectroscopy, as its lifetime is on the order of μs. Moreover, the low temperature TR-EPR spectrum of <sup>3</sup>P<sub>700</sub> has unique zero field splitting (ZFS) features and a specific AEEAAE polarization pattern, due to the delocalization of the triplet over the two chlorophylls of P<sub>700</sub>, which is quite distinctive from that of <sup>3</sup>Chl *a* formed via inter system crossing (ISC) from the single excited state. The single excited states are formed on the antenna chlorophylls due to high excitation energy and it is used for dissipation via carotenoids that has shorter lifetime. If these <sup>3</sup>Chl *a* transfer its energy to oxygen molecule then it creates harmful oxygen radical species that are destructive for the protein (119). Figure 3.14 shows the <sup>3</sup>P<sub>700</sub> and <sup>3</sup>Chl *a* state formation at a time window of 0.25 - 1.4 μs. The WT and mutants all display a polarization pattern typical of ISC, thus demonstrating that the loss of stable CS is not due to CR from the P<sub>700</sub><sup>•+</sup>A<sub>0</sub><sup>•-</sup> state, consistent with the ultra-fast optical data. This level of <sup>3</sup>Chl *a* state formed in the two mutant PS1 preparations is higher than seen in WT PS1. This may be due to a slightly higher amount of disconnected Chl pigments in the mutant preps, due to the lower level of mutant PS1 accumulated in the cells. The amount of contaminating LHC is low but constant, thus the ratio of unconnected LHC to PS1 rises in preparations from mutants

that accumulate low levels of the PS1 complex, which agreed with the time resolved fluorescence.



**Figure 3.14.** Comparison of the triplet spectra of PSI samples from WT, PsA-N604L and PsB-N591L mutants at early time after the laser flash.

### 3.3.10 Ultrafast Transient Absorption Spectroscopy

Figure 3.15 and figure 3.16 represents the transient absorption difference spectra of WTs and mutants at different delay times after excitation with a laser pulse of 690 nm. The data is taken by considering 10 single value decomposition (SVD) components of the original data. It is based on weighted factor of the components so that real components are considered. At 690 nm wavelength, the laser light will excite the chlorophyll pigments of antenna as well as reaction center (RC)  $Q_Y$  band region. In WT's, the prompt decrease in bleaching between 1 to 10 ps showed that the excitation energy of antenna is transferred to the RC and the equilibrated excited state of reaction center ( $RC^*$ ) is ready to trap the excitation energy. This trapping of excitation energy into charge separation (CS) is completed in the form of charge separation (CS) with in the 10 ps time scale [figure 3.15]. In this time resolved spectra (TRS), the 29 ps gives a clear formation of  $P_{700}^+$ , that is the secondary electron transfer step by formation of stable secondary radical pair (RP2) with two bands. The 695 nm to the red edge of the spectrum representing the cationic state of  $P_{700}$ , and 680 to 682 nm band of the  $ec3^-$  anion formation or simply the  $ec3$  chlorophyll absorption. At 29 ps time delay after excitation, the 681 and 696 nm bands have the same amplitude but with the passage of time, a decrease in the amplitude of 681 nm band occurs and the final results is a small 681 nm band and a larger 696 nm band is established at 303 ps and this does not change until 2 ns, which is the time window of our instrument measurement. Both the A and B-side WT behaved the same

way in energy transfer and electron transfer processes quantitatively and qualitatively in terms of amplitude.

The transient absorption difference spectra at different delay times of mutants affecting the A-branch CS includes PsaB-N591D, PsaB-N591H, PsaB-N591K, PsaB-N591L and PsaB-N591Y are presented in figure 3.15 and figure 3.16. The PsaB-N591D shows two bands at 10 ps while these become dominant at later times. The 682 nm band bleaches more than that of the WT; this showed the presence of long lived antenna chlorophylls that absorb in this region. The PsaB-N591K transients and band shapes are also similar to WT-B. In PsaB-N591H, the initial transients are similar but at later timescale it is difficult to see the formation of the  $P_{700}$  difference spectrum. The reason is that in the 29-303 ps transients, the 682 nm band is missing, while the 696 nm band has smaller amplitude showing decrease CS in this mutant. The PsaB-N591L mutant has two clear bands at 3 ps, but at later delay times the one on the red edge of the spectrum is present while the blue one is absent. The later spectra of PsaB-N591L have full fluctuation by going up and down; this might be due to the scattering process in the cuvette during measurement as this mutant is more unstable than that of PsaA-N604L and PSI particles aggregates after an hour during measurement. The main information from the amplitude of 29 to 303 ps time resolved difference spectra showed that mutation affecting the A-branch has lower quantum yield in terms of charge separation, as they are affecting the efficiency of the trap and the excitation energy is wasted.

In the B-branch mutants that include PsaA-N604D, PsaA-N604H, PsaA-N604K and PsaA-N604L the transients are presented from 1-303 ps timescale in figure 3.15 and

3.16. The PsaA-N604D has no effect on CS and the difference spectra at 29-303 ps are even higher in amplitude than WT. This increase in amplitude is due to the fewer outer antennas attached to the PSI, as the sample used is based on equal amount of chlorophyll. The PsaA-N604H and PsaA-N604L have similar transients but the amplitude of the transient absorption difference spectra at 100 and 303 ps have smaller amplitude and has two bands one around 682 nm and the other at 696 nm. In PsaA-N604K the decay of excitation energy is quite fast. In the 100 and 303 ps transient difference spectra, the 680 nm band is also missing. These time resolved difference spectra of the mutants give information about the decay of excited antenna into a  $P_{700}$  difference spectrum showing energy trapping and electron transfer. They hint that making mutation close to ec2 chlorophyll on each branch causes a decrease in CS depending on the branch.

Global analysis of the transient spectroscopic data was performed with ASUfit software to get information about the kinetics of overall excitation energy transfer; energy trapping in the independent trap on each branch and to see how much mutation affect the efficiency of the trap. Each transient absorption data set was fitted with four exponential decay components over the wavelength region between a 620 nm to 740 nm range. The four lifetime components are in the range of 0.05-0.09 ps, 1.0-2.9 ps, 14-29.7 ps, and 4.45-42.75 ns, for all samples studied. The fitting results of energy equilibration and energy trapping are given in Table 3.5. The first component obtained from the fitting with a femtosecond lifetime represents the coherence spike from chlorophylls excited state annihilation or the artifacts of excited state laser pulse, judging from its spectral shape. The second component with a lifetime of 2 to 3 ps is the EET within the antenna

system and/or decay of excited state of antenna due to singlet-singlet excitation annihilations. Those two components are not the focus of this study. Here, only the 18-30 ps component, which represents energy trapping component and the long-lived component, showing the stable  $P_{700}^{+}$  and  $PhQ^{-}$  are compared. The 20 ps lifetime of energy trapping is a combination of several processes, which includes energy equilibration between internal antenna and the excited reaction center and its decay to the primary and secondary radical pair formation in sequential series inside the RC. Though the energy trapping lifetime is not affected by the mutation, the amplitude is almost a 40 % decrease in PsaA-N604H, PsaA-N604K and PsaA-N604L as compared to the WT (Figure 3.17). These three mutations are affecting the B-branch, which is used in *C. reinhardtii* around 40 % while the A-branch is used 60%. The mutation of PsaA-N604H, PsaA-N604K and PsaA-N604L has no effect on the lifetime of energy trapping and it is around 22 ps like WT. The spectra of these mutants were also normalized for overall changes in the long lived difference spectra and there were minor changes observed in the 680 nm band area. Thus, these mutations affect the trapping efficiency of the respective branch trap and showed that it is  $ec2_B$ , which is the primary electron donor involved in charge separation on the B-branch. The non-decaying component lifetime in WT is nanosecond and same is the case in mutants.

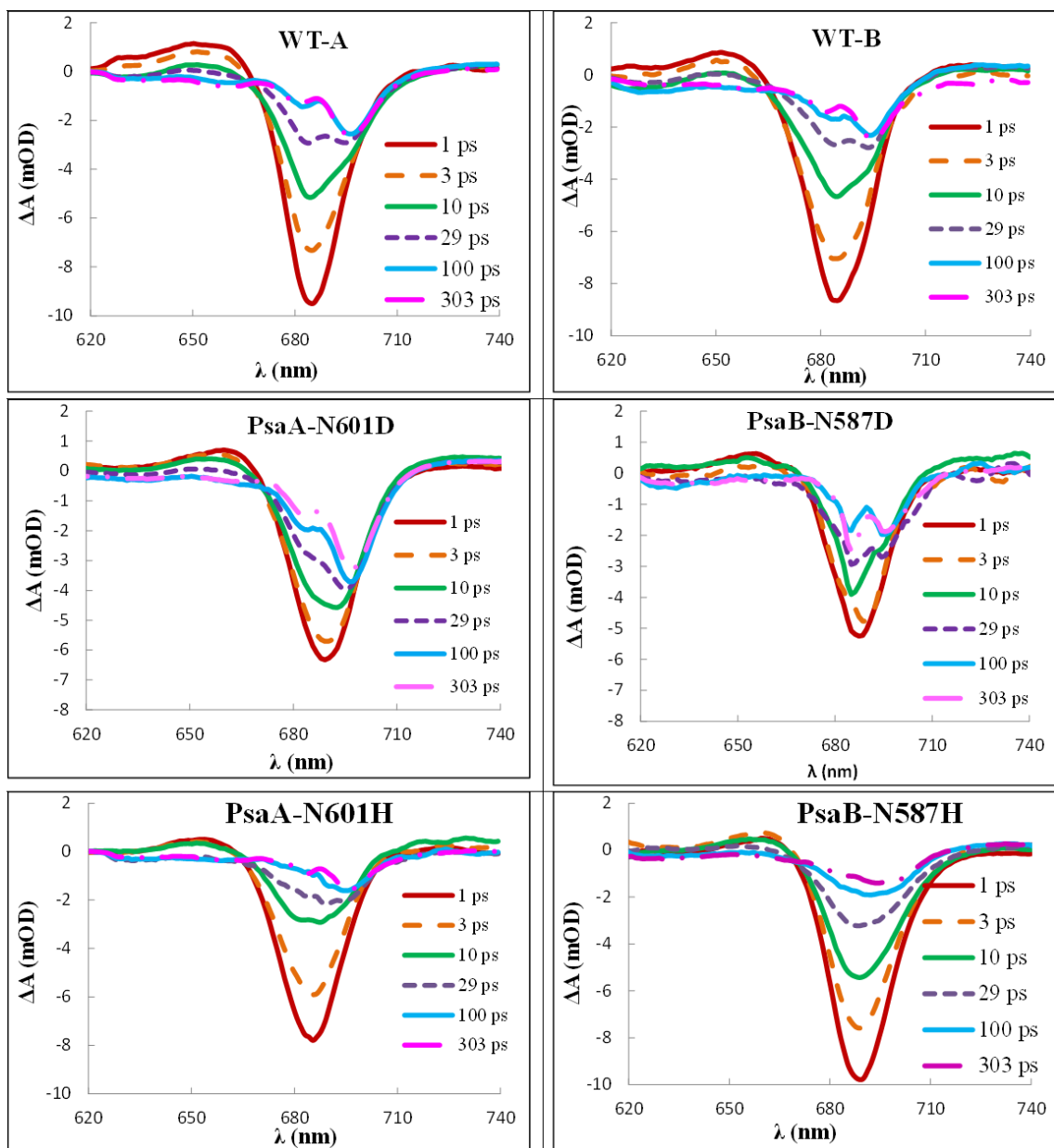
The transient absorption difference spectra of WT-B, PsaB-N591D, PsaB-N591H, PsaB-N591K and PsaB-N591L, which are affecting the A-branch of PSI, were also fitted to four components for global analyses to get the lifetimes and amplitudes. The two fast components are representing energy equilibration and antenna decay while the other two

represent the energy trapping and non-decaying component as shown in Table 3.5. The energy trapping component in the DADS of PsaB-N591H and PsaB-N591L has a lifetime of 27 ps as compared to the WT-B 18 ps. The amplitude of this component is of the same size as WT-B, which showed that it is combination of other components and needs further evaluation. However, the long lived components of these mutants have share from long lived antenna and free chlorophylls which makes the DADS complicated. During the fitting process different methods were used to remove this component as much as possible to get the DS of P<sub>700</sub>. The DADS of these mutants are a bit longer in lifetime due to the presence of this long lived free antenna component. The DADS of the PsaA-N604D and PsaB-N591D is shifted towards the red. This red shift effect was also observed in crude membrane measurements for PSI estimation and it is further studied through FTIR spectroscopy. Thus, ultrafast transient absorption spectroscopy also revealed that mutation near ec2 on the respective branch in PSI causes a decrease in the stable CS. These mutations thus provide the idea that both branches are active for electron transfer in PSI and ec2 is the cofactor from where charge separation occurs by trapping the excitation energy harvested by the antenna of PSI.

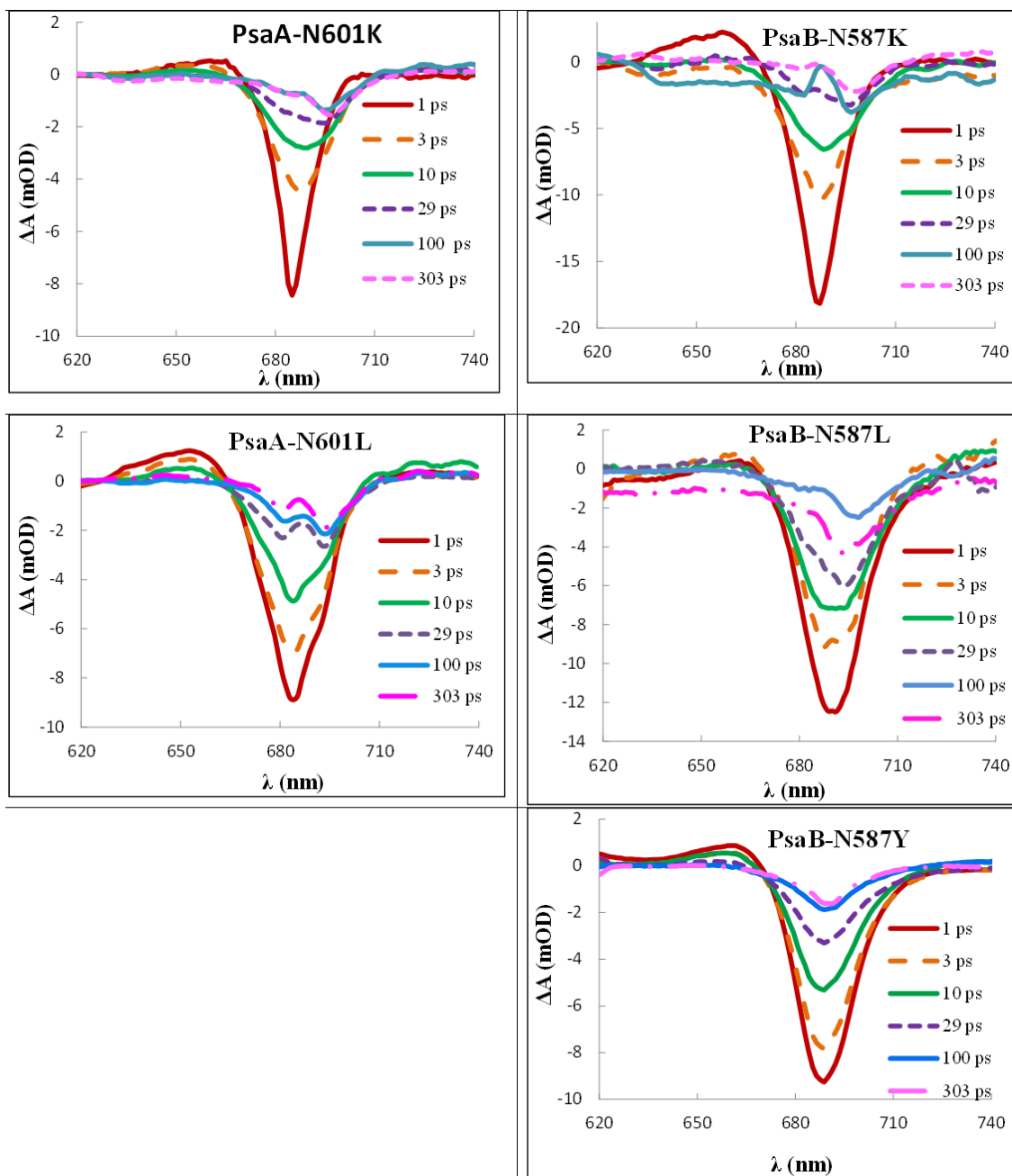


**Table 3.5.** Lifetimes of the energy equilibration and trapping components obtained from DADS of PSI mutants near ec2 chlorophyll from *C. reinhardtii*. The quantum yield of stable CS is also calculated by considering it 100% in WT.

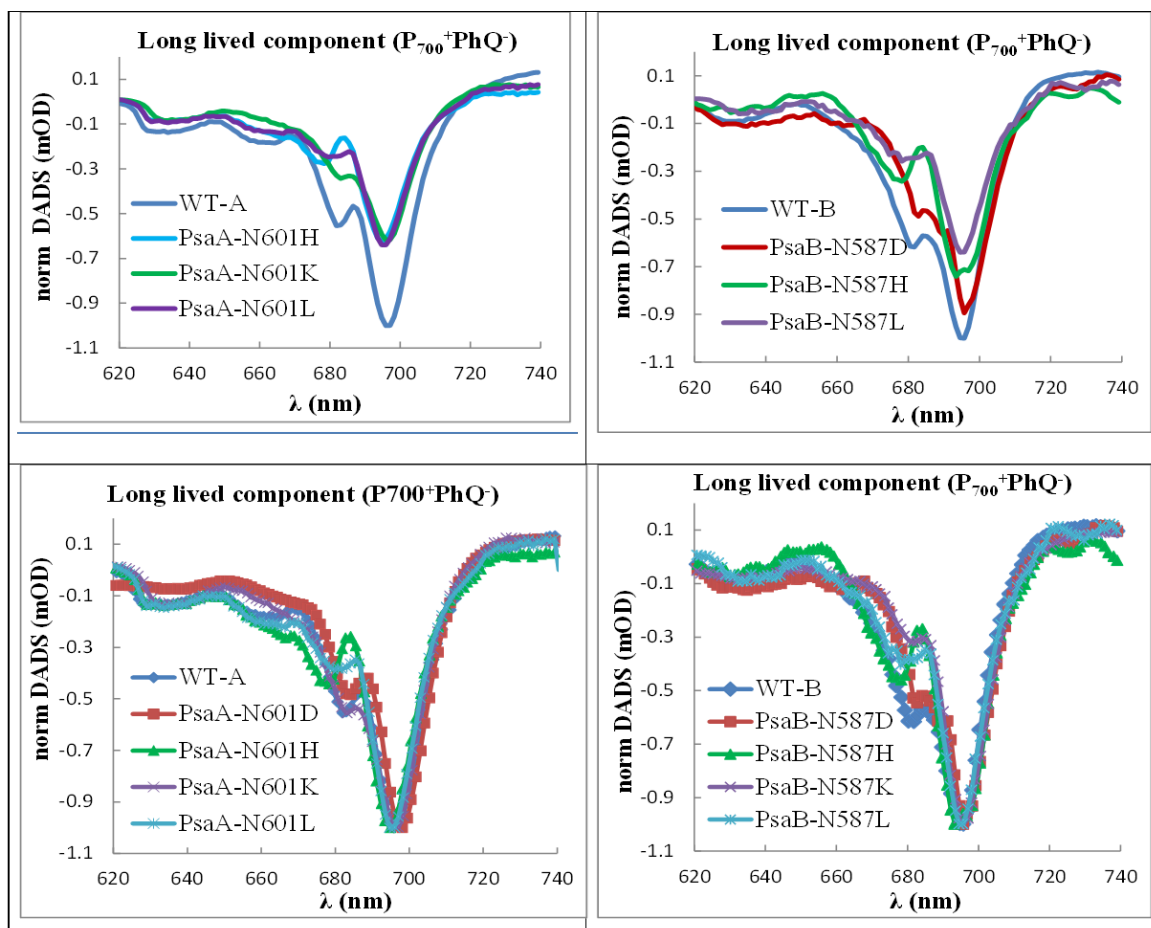
Sample	Equilibration component life time ( $\tau_2$ ) ps	Energy trapping component life time ( $\tau_3$ )	Quantum yield of stable CS (%).
WT-A	1.5	21.8	100
PsaA-N604D	1.0	29.7	Similar to WT
PsaA-N604H	2.9	22.5	60
PsaA-N604K	1.7	22.0	60
PsaA-N604L	2.7	21.5	61
WT-B	1.2	18	100
PsaB-N591D	3.7	24	90
PsaB-N591H	1.6	23.5	70
PsaB-N591K	1.1	29.7	Similar to WT
PsaB-N591L	1.0	26.7	61



**Figure 3.15.** Transient absorption difference spectra of WT-A, WT-B, PsaA-N604D, PsaB-N591D, PsaA-N604H and PsaB-N591H at different delay times after 690 nm excitation wavelength.



**Figure 3.16.** Transient absorption difference spectra of PsaA-N604K, PsaB-N591K, PsaA-N604L, PsaB-N591L and PsaB-N591Y at different delay times after 690 nm excitation wavelength.



**Figure 3.17.** Normalized Decay associated difference spectra (DADS) of WT and mutants near  $ec2_{A/B}$  cofactor in the RC of PSI. The top panel shows normalization for amplitude of the long lived component representing  $P_{700}^{+}PhQ^{-}$  as 100 %. The decrease in amplitude (maximum bleaching at 695 nm) due to mutation is compared with WT. The lower panel shows normalization of the same  $P_{700}$  bleaching band of WT and mutants for overall comparison of the spectra in all the PSI samples.

### 3.3.11 Time-Resolved Fluorescence

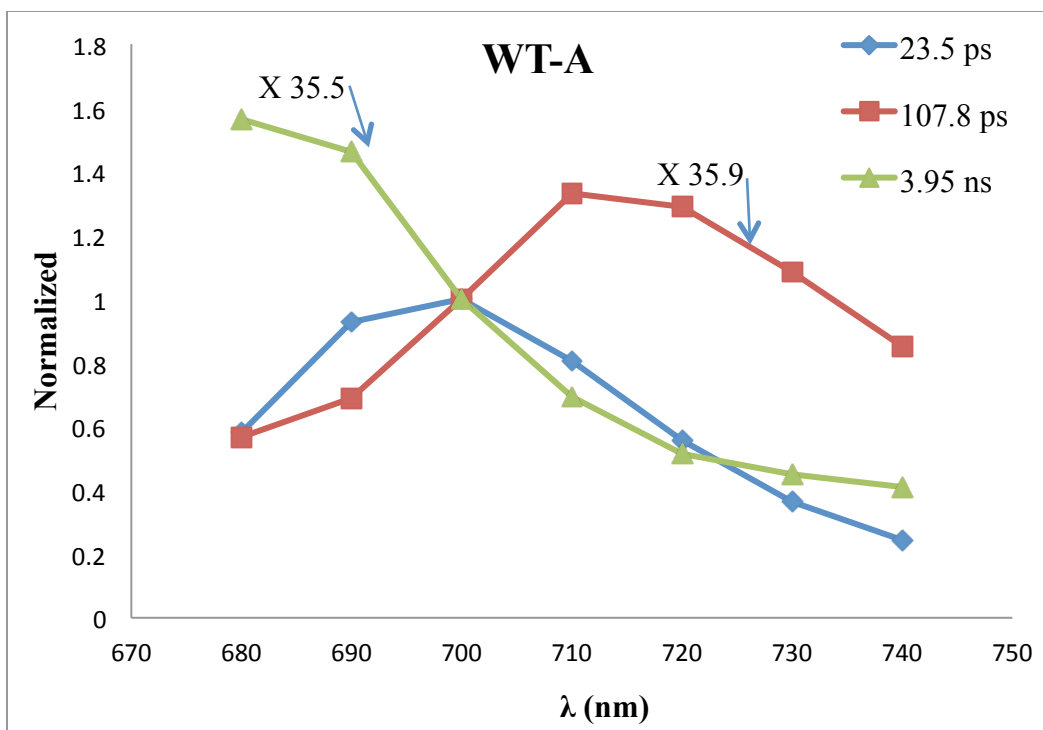
Time-resolved fluorescence studies of PSI particles were performed at room temperature in a spectral window of 680 - 740 nm with 10-nm spacing. The PSI sample was excited with excitation pulses at 420 nm and a time window of 3.3 ns. Figure 3.18 and figure 3.19 shows the decay-associated fluorescence spectra observed in WT PSI. The data obtained at different wavelengths were fitted with three components simultaneously using a global analysis method (see Materials and Methods for details). DAS of time-resolved fluorescence of the WT showed a lifetime of around 20 ps, 100-200 ps and  $\geq 3$  ns (Table 3.6). For the WT-A, the 23.5-ps component is completely positive in amplitude and its maximum peak is at 700 nm; it is assigned to energy trapping in the RC. For WT-B, the fast component is similar in characteristic but the DAS has a maximum 690 nm wavelength measurement and a lifetime of 24.6 ps. The second component has a lifetime of 108 ps for WT-A and 154 ps for WT-B. It has very small amplitude and has a maximum peak near 710 nm for both. The amplitude of this component is 36 times lower than the energy trapping component. This component can be assigned to slow excitation transfer to the trap from red chlorophylls in the peripheral antenna that absorb at longer wavelengths. An uphill transfer of excitation energy is required from the red chlorophylls to the RC before it can be trapped (34). The final component has a lifetime of 3-4 ns and positive amplitude near 680 - 690 nm. This component can be assigned to the free LHCI and perhaps free chlorophyll in the sample. The amplitude of this component is 35.5 times lower than the energy trapping component (Figure 3.18). The

lifetime of this component was essentially the same in all the preparations, although its amplitude was increased in mutants that accumulate PSI poorly, as expected. Thus, this component will not be discussed further, as it is not relevant to excitation energy transfer within PSI.

We can envision two possible effects of the mutations upon decay of the excited state. If the mutations simply make the targeted trap less efficient, then they would slow the overall rate of trapping, and this would be manifested as an increase in the trapping lifetime. On the other hand, if the mutations open a new pathway for excited state decay, this would most likely be manifested as a *decrease* in the lifetime of decay of the pre-existing component(s) that overlapped temporally with the new process. The decay time of the middle component was always in the range of 100 - 250 ps and did not vary in a systematic way. However, the fastest component was faster in almost every mutant. The mutations at the PsaA-Asn604 site, which should affect primarily  $ec2_B$  had a modest affect, reducing the trapping time from ~24 ps to ~20-22 ps depending upon the mutation. The mutations at PsaB-Asn591 site ( $ec2_A$ ), however, had a much more drastic effect. While the acceleration of the fastest component was nonexistent in PsaB-N591K (25 ps) and modest in PsaB-N591D (19 ps) and PsaB-N591D (18 ps), it was extreme in PsaB-N591Y (10 ps) and PsaB-N591L (4 ps). Thus, these results seem most consistent with the creation of a new channel for dissipation of excitation energy, which is fast enough to compete with charge separation.

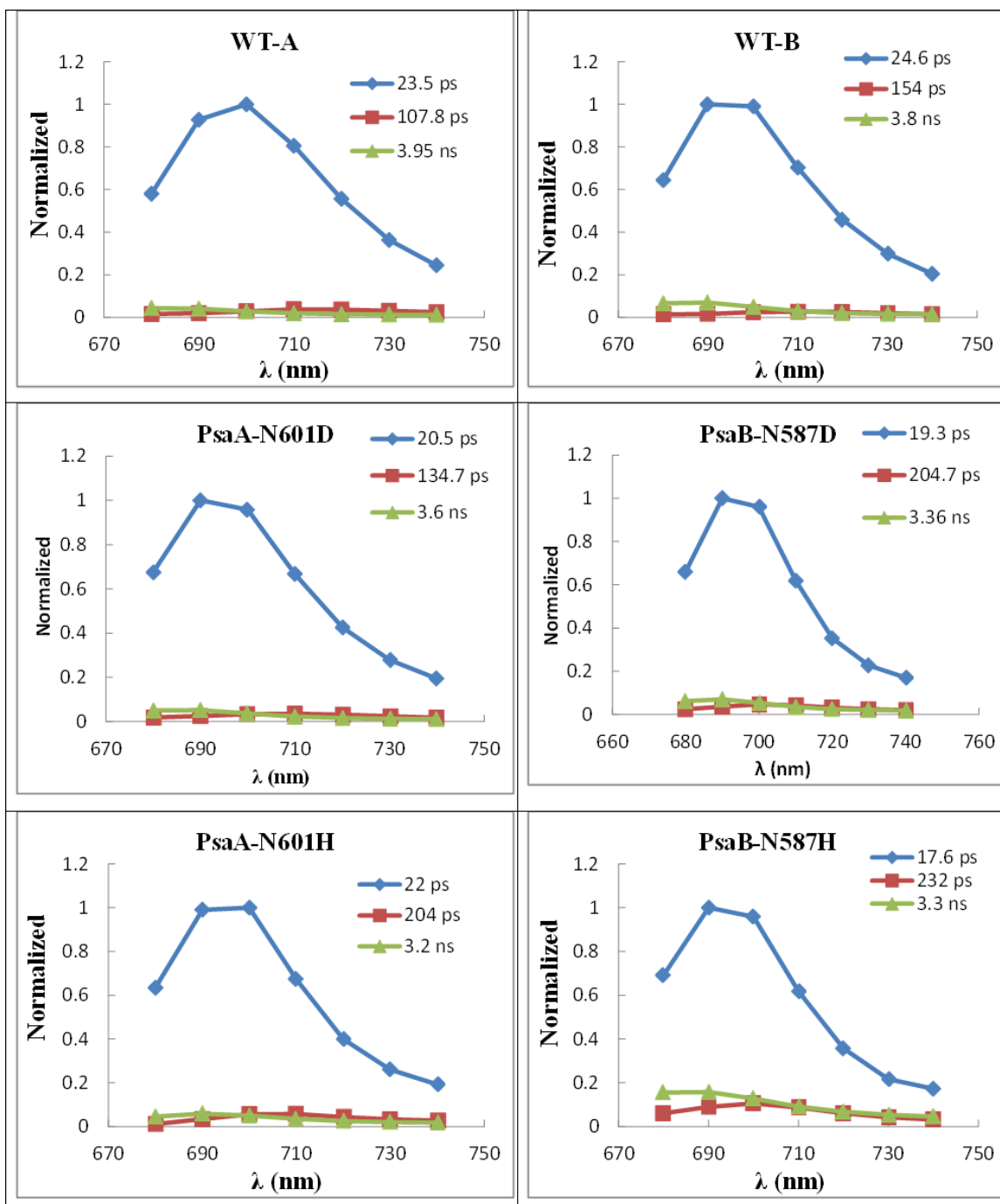
**Table 3.6** Difference of fast and slow excitation energy lifetime components of WT and mutants obtained from DAS using TCSPC.

<b>Sample</b>	<b>fast energy trapping component (ps)</b>	<b>slow energy trapping component (ps)</b>	<b>Long lived uncoupled antenna/Chlorophylls component (ns)</b>	<b><math>\chi^2</math></b>
WT-A	23.5	107.8	3.9	1.2
WT-B	24.6	154	3.8	1.1
PsaA-N604D	20.5	134.7	3.6	1.1
PsaA-N604H	22	204	3.2	1.2
PsaA-N604K	21.4	242.7	3.7	1.4
PsaA-N604L	22.5	242	3.3	1.1
PsaB-N591D	19.3	204.7	3.4	1.2
PsaB-N591H	17.6	232	3.3	1.2
PsaB-N591K	25	198.5	3.4	1.2
PsaB-N591L	4	152	3	1.2
PsaB-N591Y	9.8	104.3	3.4	1.3

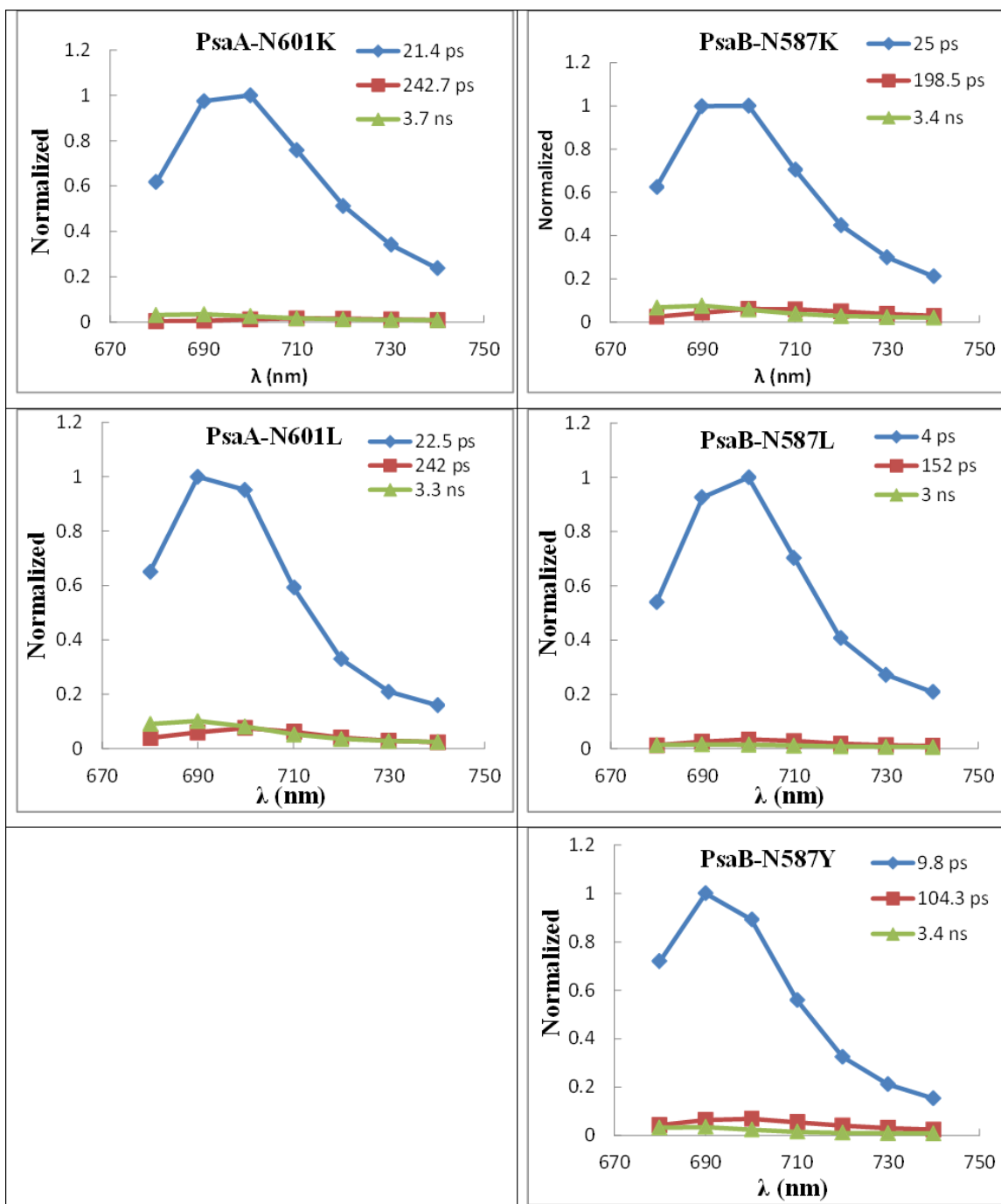


**Figure 3.18.** Decay associated spectra (DAS) of PSI particle obtained from global analyses using three components fit of WT. The slow component was multiplied with 35.5 while the long lived component was multiplied with 35.9 to normalize it with the energy trapping component at 700 nm wavelength.





**Figure 3.19.** Decay associated spectra (DAS) of PSI particles obtained from global analyses using three components fit of WT and ec2 mutants of reaction center.



**Figure 3.20.** Decay-associated spectra (DAS) of PSI particles obtained from global analyses using three components fit of WT and ec2 mutants of reaction center.

### 3.3.12 FTIR Spectroscopy

#### 3.3.12.1 $P_{700}^+/P_{700}$ FTIR Difference Spectra of WT PS1

Figure 3.21 shows normalized difference spectra of two WT PS1 from 1300  $\text{cm}^{-1}$  to 1900  $\text{cm}^{-1}$  frequency range. This difference spectrum is obtained by recording the ground state absorption of PSI by taking dark minus dark spectra, and light minus dark spectra in which continuous illumination was used for excitation that causes formation of  $P_{700}^+F_{A/B}^-$ . In this static FTIR difference spectrum, the positive bands represent the oxidized form of  $P_{700}$  after bleaching while the negative bands represent the ground state absorption of the  $P_{700}$ . WT PS1 exhibits positive bands at 1653, 1668, 1687, 1717, 1742, 1754  $\text{cm}^{-1}$  and negative bands at 1681, 1700, 1733 and 1748  $\text{cm}^{-1}$ . In the chlorophyll molecule, the  $13^1$ -keto group and the  $13^3$ -ester carbonyl group give specific FTIR bands that have been previously assigned (*111*, *112*, *120*). The 1733(-)/1742(+) and 1748(-)/1754(+)  $\text{cm}^{-1}$  pairs have been assigned to the  $13^3$  ester C=O's of  $P_A$  and  $P_B$  of  $P_{700}$  respectively; both modes are upshifted upon oxidation of  $P_{700}$  (Table 3.7). The higher frequency ester C=O mode is considered free from hydrogen bonding, which is why it is assigned to  $P_B$ . The 1733(-)/1742(+)  $\text{cm}^{-1}$  represents the  $13^3$  ester C=O's of  $P_A$ , which makes a hydrogen bond to a water molecule. The large (and somewhat wide) negative band at  $\sim 1700 \text{ cm}^{-1}$  is thought to result from the overlap of the FTIR absorption bands from the  $13^1$ -keto groups of  $P_A$  and  $P_B$ , the former at  $\sim 1694 \text{ cm}^{-1}$  and the latter at  $\sim 1703 \text{ cm}^{-1}$ ; the lower frequency of the  $13^1$ -keto group of  $P_A$  is explained by H-bonding from PsaA-Thr739 (*60*, *111*). Upon cation formation, these bands upshift by 19  $\text{cm}^{-1}$  in case of  $P_A^+$  and by 20  $\text{cm}^{-1}$  in the case

of  $P_B^+$ . Thus, the positive bands at  $1656(+)$   $\text{cm}^{-1}$  and  $1718(+)$   $\text{cm}^{-1}$  are assigned to the  $13^1$ -keto groups of  $P_A^+$  and  $P_B^+$ , respectively. Breton *et al.* (121) used the peak to peak amplitude of  $1717(+)/1697(-)$  and  $1656(+)/1637(-)$   $\text{cm}^{-1}$  FTIR vibrational differential signal for calculation of charge distribution on the two  $13^1$  keto C=O groups (Table 3.7). The differential region between  $1600$  to  $1608$   $\text{cm}^{-1}$  is usually assigned to the macrocycle C=C marker of penta-coordinated chlorophyll of  $P_{700}/P_{700}^+$ . Similarly  $1555$   $\text{cm}^{-1}$  is also assigned to the macrocycle C=C marker of penta-coordinated chlorophyll ring. During the excited state, as the bond order is reduced so these bands downshift and positive features can be seen at  $1543$  and  $1511$   $\text{cm}^{-1}$ . The bands from  $1550$  to  $1660$   $\text{cm}^{-1}$  in the difference spectra are usually assigned to signatures from the protein backbone [3, 4].

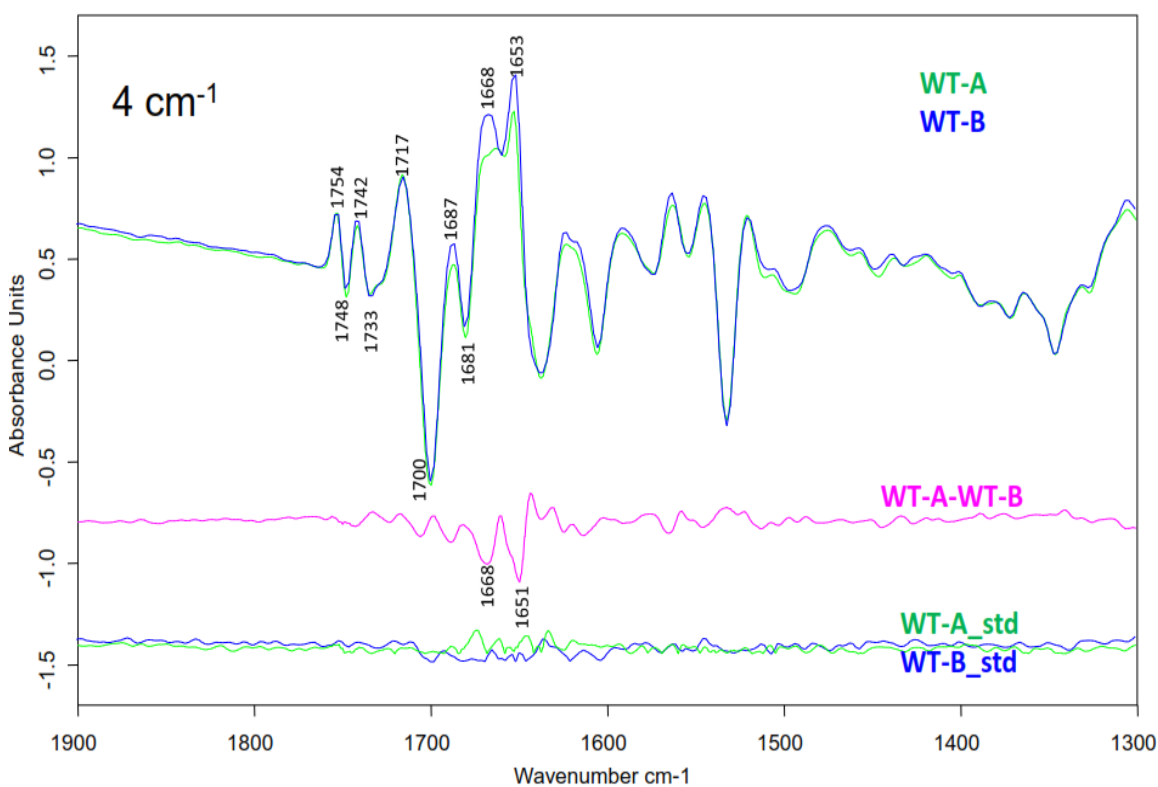
**Table 3.7.** Stretching frequencies ( $\text{cm}^{-1}$ ) of  $P_{700}$  of WT PSI from *C. reinhardtii* and *Synechocystis* from this work and from literature (60, 111, 122-124).

Groups	$P_{700}$	Groups	$P_{700}^+$
$13^3$ ester C=O's of $P_A$	<b>1733(-)</b>	$13^3$ ester C=O's of $P_A^+$	<b>1742(+)</b>
$13^3$ ester C=O's of $P_B$	<b>1748(-)</b>	$13^3$ ester C=O's of $P_B^+$	<b>1754(+)</b>
$13^1$ keto C=O of $P_A$	<b>1637(-)</b>	$13^1$ keto C=O of $P_{A+}$	<b>1656(+)/ 1687(+)</b>
$13^1$ keto C=O of $P_B$	<b>1698/ 1700(-)</b>	$13^1$ keto C=O of $P_{B+}$	<b>1717/ 1718 (+)</b>

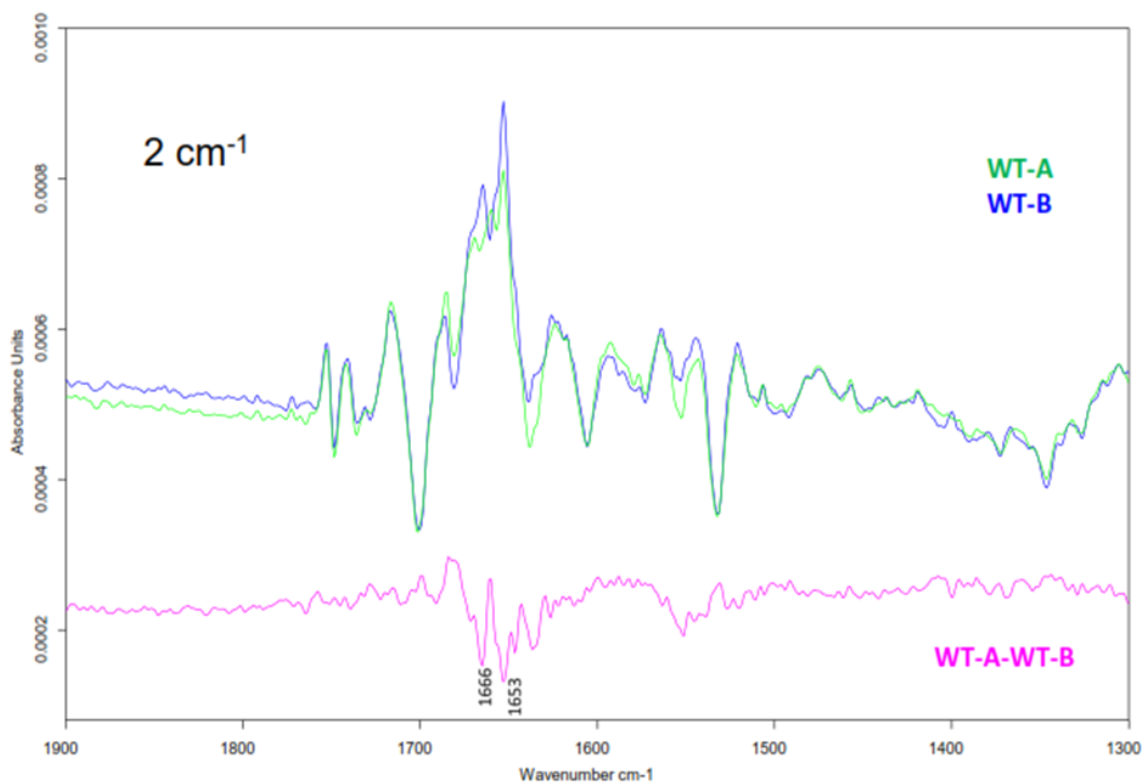
### 3.3.12.2 Double difference spectrum of two WT

The WT-A minus WT-B double difference spectrum (DDS) has small differences in the ground state at  $1653$  and  $1668$   $\text{cm}^{-1}$  in terms of amplitude; the residual of the standard deviation is shown at the bottom (Figure 3.22). When the difference spectrum of WT-A is subtracted from WT-B, then there are two band regions, where the two WT have difference in terms of intensity, one is at  $1653$  and the other is  $1666$  to  $1668$   $\text{cm}^{-1}$ . The reason for this difference might be that relaxation of protein after charge separation is a

bit different in the two WT. The ratio of protein to chlorophyll is slightly different in the two PSI preparations and this might be due to solubilization or growth conditions of *C. reinhardtii* cells. However, there are no significant differences in the 1690 to 1760  $\text{cm}^{-1}$  region, which is our focus of interest where the ester and keto carbonyl bands absorb, while at 1666 or 1668  $\text{cm}^{-1}$  region and 1655 (+)  $\text{cm}^{-1}$  are assigned to protein backbone.



**Figure 3.21.**  $P_{700}^{+}/P_{700}$  FTIR Difference Spectra of WT-A and WT-B overlapped for differences. The WT-A minus WT-B spectrum is presented in pink color, while the lower label shows the standard deviation in both WT's.



**Figure 3.22.**  $P_{700}^+/P_{700}$  FTIR Difference Spectra of WT-A and WT-B overlapped for differences. The WT-A minus WT-B spectrum is presented in pink color.

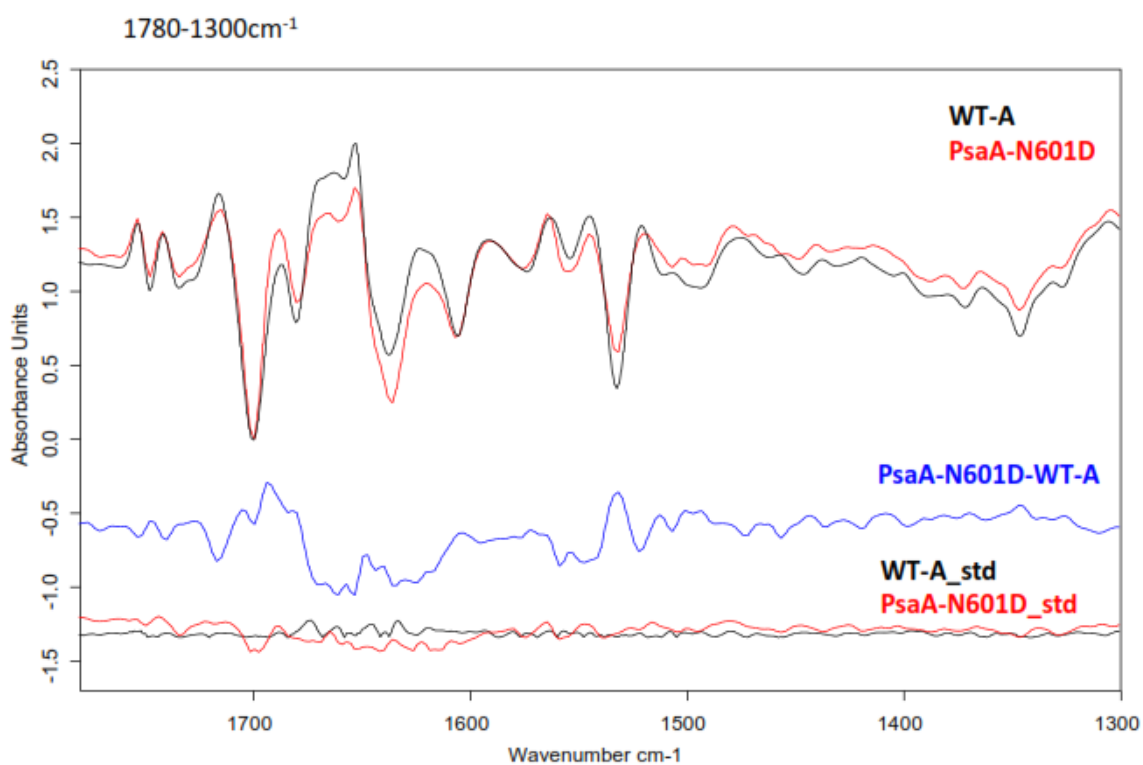
### 3.3.12.3 $P_{700}^+/P_{700}$ FTIR Difference Spectra of Asp substitution mutants

For introducing a negative charged residue near the predicted primary cation  $ec2^+$ , we used Asn to Asp mutations. We expect that a negative charge near the cation will prolong the life of this primary donor and we can see its features spectroscopically and have different kinetics. Secondly, we also expect that this negatively charged residue will affect the electron density and cationic state of the  $P_{700}$ . Infrared spectroscopic studies of catalytic proteins with aspartic acid residues at the catalytic site showed special vibrational spectral markers for protonated and non-protonated states. The C=O

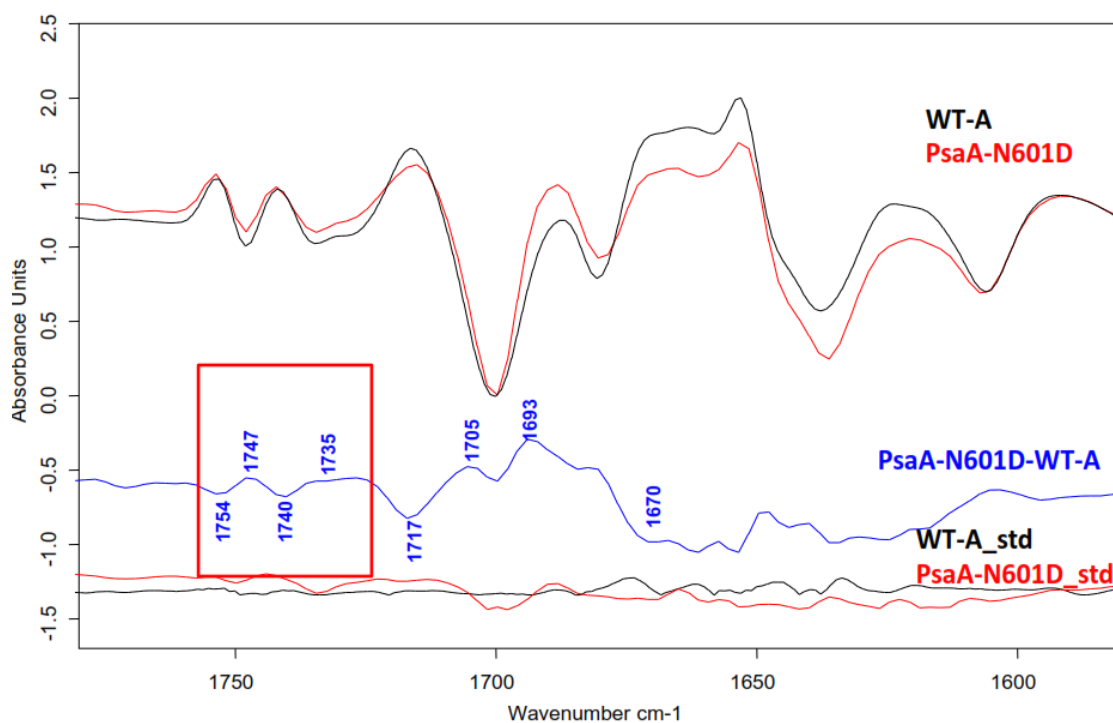
stretching frequency of protonated carboxylic group occurs in the region of 1700 to 1775  $\text{cm}^{-1}$  while the asymmetric and symmetric stretching frequencies of a  $\text{COO}^-$  group range in the region of 1555 to 1410  $\text{cm}^{-1}$  range (125). The  $\text{C=O}$  stretching frequency is a delicate infrared structural sensor for observational and measurement of hydrogen bonds of the buried  $\text{COOH}$  groups. Based on computational calculation, a single hydrogen bond with either a carbonyl oxygen ( $\text{HO-C=O}$ ) or with the hydroxyl hydrogen ( $\text{HO-C=O}$ ), there is downshift of 30-35  $\text{cm}^{-1}$  in the stretching frequency of  $\text{C=O}$ , while two H-bonds at a time will result into a shift from 1776.4 to 1705.5  $\text{cm}^{-1}$ . The H-bonding for  $\text{COOH}$  groups are sometimes more specific, for example if the  $\text{COOH}$  group is from Asparagine/Glutamine two H-bonds result into 1709.9  $\text{cm}^{-1}$  vibration band; Aspartic/Glutamic acid with two H-bonds have 1702.9  $\text{cm}^{-1}$  band (126). The effect of changing PsaA-Asn604 to Asp near ec2<sub>B</sub> can be seen in the FTIR double difference spectrum (DDS) in Figure 3.23 and 3.24. The main changes in the spectrum can be seen in 13<sup>3</sup>-ester carbonyl groups of PsaA-N604D, where  $\text{P}_\text{B}^+$  mode (1754  $\text{cm}^{-1}$ ) is not affected but the ground state  $\text{P}_\text{B}$  vibration mode downshifts by 1-2  $\text{cm}^{-1}$  due to the mutation. In the case of  $\text{P}_\text{A}$ , both the ground states as well as the cationic state  $\text{P}_\text{A}^+$  are affected. There is a 2  $\text{cm}^{-1}$  downshift from 1742  $\text{cm}^{-1}$  to 1740  $\text{cm}^{-1}$  in vibration mode of  $\text{P}_\text{A}^+$  and upshift of 2  $\text{cm}^{-1}$  from 1733  $\text{cm}^{-1}$  to 1735  $\text{cm}^{-1}$ . The 13<sup>1</sup>-keto carbonyl vibration mode of  $\text{P}_\text{B}^+$  is at 1717  $\text{cm}^{-1}$  and there is gain in its amplitude as compared to the WT; The  $\text{P}_\text{B}$  in ground state absorbs at 1700  $\text{cm}^{-1}$  but near this region, in the double difference spectrum, a new 1705  $\text{cm}^{-1}$  small peak appeared. The 1693  $\text{cm}^{-1}$  and 1670  $\text{cm}^{-1}$  vibrations band in the double difference can be assigned to the 13<sup>1</sup>-Keto-carbonyl of  $\text{P}_\text{A}^+$  and  $\text{P}_\text{A}$ . So here the PsaA-

N604D indirectly affects the  $13^1$ -Keto-carbonyl of  $P_A^+$  and  $P_A$  vibration bands by inhibiting the charge separation (CS) on B-side and the more favorable CS pathway is A-side, and due to the negative charge near the vicinity of  $P_B^+$  the charge density will be pushed towards  $P_A^+$ . The amplitude of  $P_A$  and  $P_A^+$  are lower for PsaA-N604D than in the WT, further, the  $P_B^+$  amplitude is also a bit decreased. Thus, the vibration band of the  $13^1$ -keto-carbonyl of  $P_A^+$  and  $P_A$  are affected. The differences in the peak at  $1660\text{ cm}^{-1}$  can be assigned to the changes brought by the asparagine to aspartic acid side chain. These can be assigned to the C=O stretching band frequency as they have higher molar absorptivity (125, 127). PsaB-N591D mutation is affecting the A-branch by lowering the CS on this branch. As the contribution of the B-branch is unchanged and if PsaB-N591D is un-protonated then the negative charge will influence the  $P_{700^+}/P_{700}$  difference spectrum. The FTIR DS and DDS of PsaB-N591D is shown in figure 3.25 and 3.26, there is an increase in the amplitude of DS of PsaB-N591D as compared to the WT from  $1687$  to  $1623\text{ cm}^{-1}$  region. In the DDS the main differences are observed in the region from  $1702$ - $1661\text{ cm}^{-1}$ . The  $13^1$ -Keto carbonyl of  $P_B$  has vibrational mode in the  $1700\text{ cm}^{-1}$  in the WT and it is upshifted by  $2\text{ cm}^{-1}$  in the PsaB-N591D mutant. There are also some changes from  $1682$  to  $1650\text{ cm}^{-1}$  vibration modes in the DDS of PsaB-N591D mutation as shown by the peaks in figure 3.26. These peaks can be assigned to the mutation of asparagine to aspartic acid, where  $1661$  and  $1668$  gives the largest peaks in the DDS. Thus, these are C=O (CONH<sub>2</sub>) stretching bands of aspartic acid. Although, we cannot predict the protonation of Aspartic acid side chain here in this DDS (125, 127).

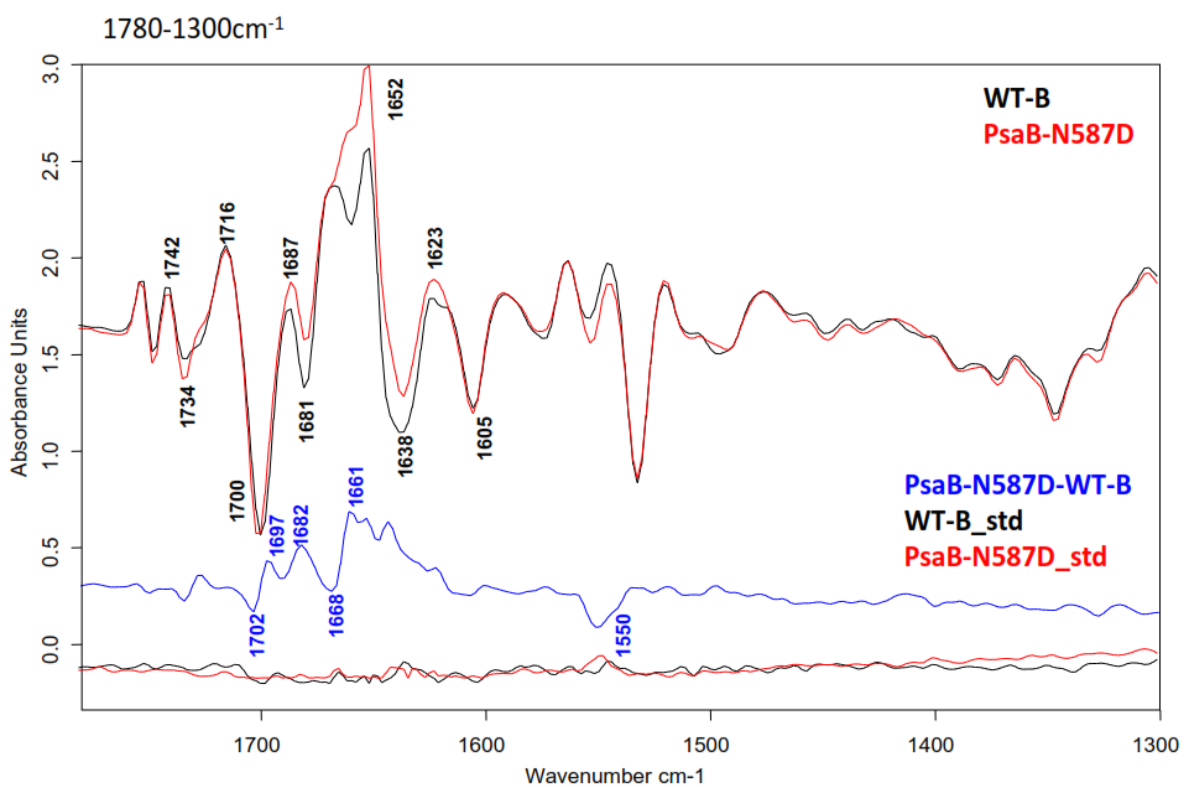




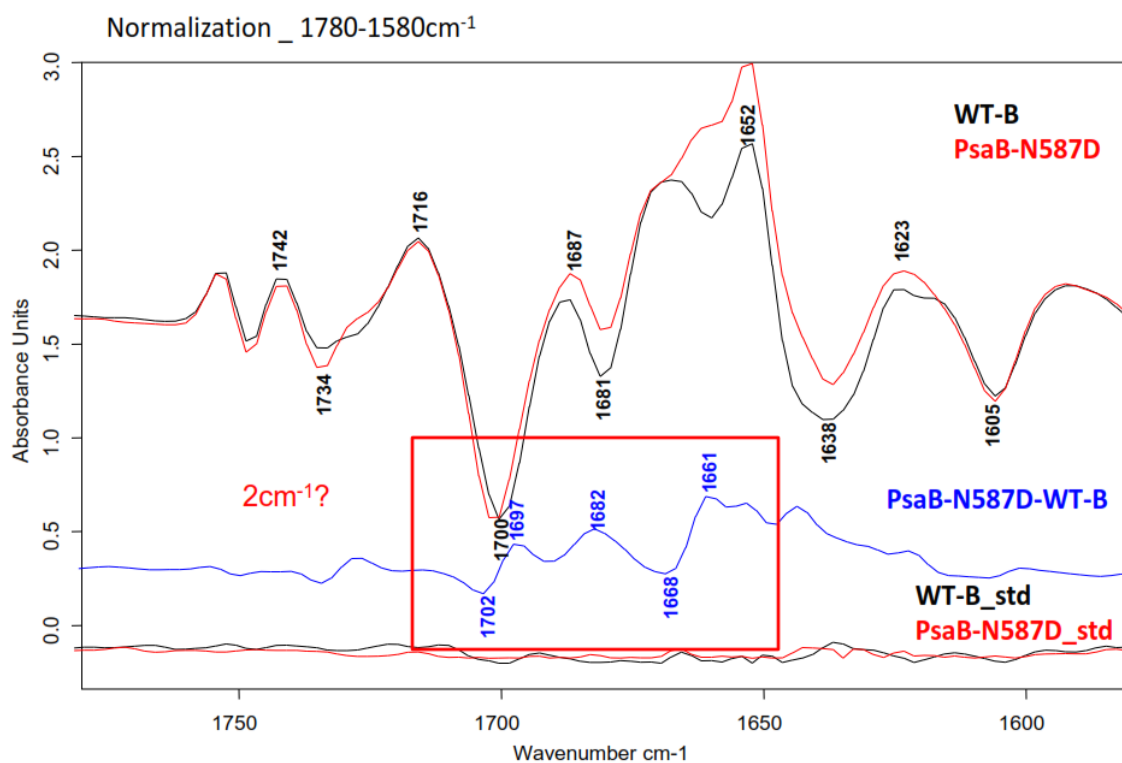
**Figure 3.23.**  $P_{700}^+/P_{700}$  FTIR Difference Spectra of PsaA-N604D superimposed on WT-A for comparison. The PsaA-N604D minus WT-A double difference spectrum is presented in blue color, while at lower panel shows the standard deviation of WT-A and PsaA-N604D.



**Figure 3.24.**  $P_{700}^+/P_{700}$  FTIR Difference Spectra of PsaA-N604D superimposed on WT-A for comparison from 1800 to 1600  $\text{cm}^{-1}$ . The PsaA-N604D minus WT-A double difference spectrum is presented in blue color, while at lower panel shows the standard deviation of WT-A and PsaA-N604D.



**Figure 3.25.**  $P_{700}^+/P_{700}$  FTIR Difference Spectra of PsaB-N591D superimposed on WT-B for comparison from 1800 to 1300 cm<sup>-1</sup>. The PsaB-N591D minus WT-B double difference spectrum is presented in blue color, while at lower panel shows the standard deviation of WT-B and PsaB-N591D.



**Figure 3.26.**  $P_{700}^+/P_{700}$  FTIR Difference Spectra of PsaB-N591D superimposed on WT-B for comparison from 1800 to 1650 cm<sup>-1</sup>. The PsaB-N591D minus WT-B double

difference spectrum is presented in blue color, while at lower panel shows the standard deviation of WT-B and PsaB-N591D.

#### 3.3.12.4 $P_{700}^+/P_{700}$ FTIR Difference Spectra of Lysine mutants

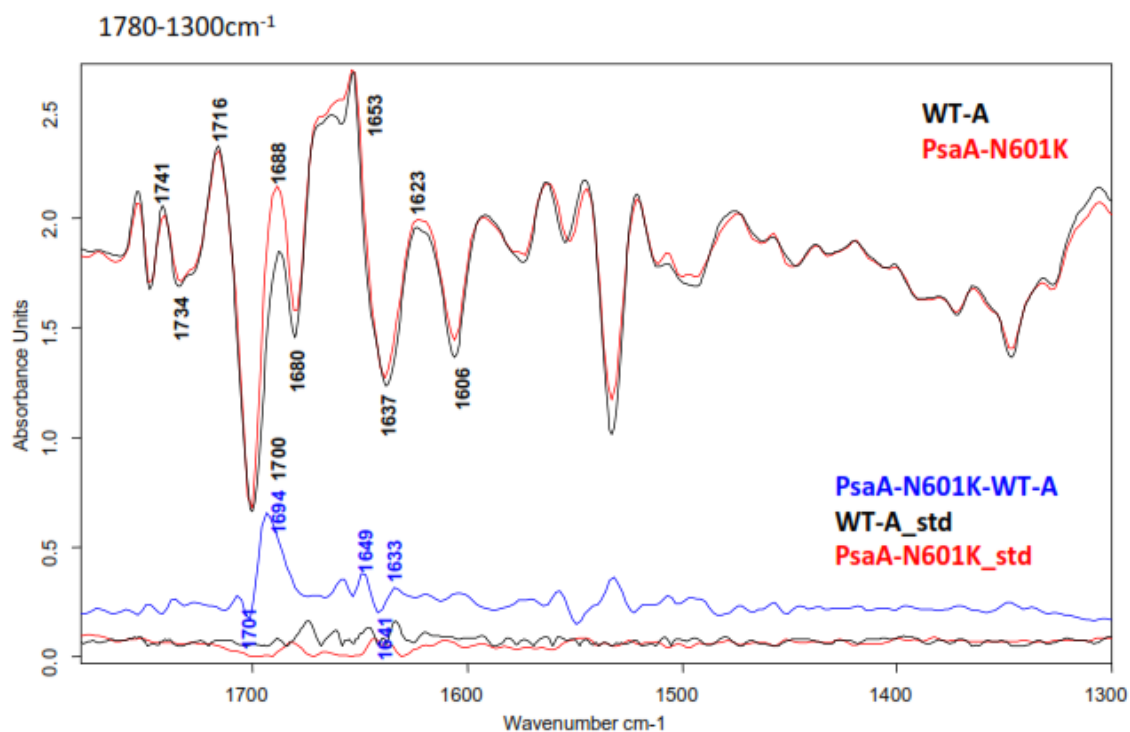
Introduction of lysine in place of asparagine at position PsaA-N604, which is affecting the B-branch, could possibly act like a new ligand for  $ec2_B$ , where the nitrogen atom of  $\epsilon$ -amino group of lysine would be the fifth ligand for the central Mg atom of  $ec2_B$ . This kind of ligand is typically not present in photosynthetic complexes, as the amine group is protonated under physiological conditions in aqueous solution. But if the lysine side chain is buried deep inside the hydrophobic membrane protein then the protein environment lowers the  $pK_a$  of lysine and the lone pair of electron present on nitrogen atom of  $\epsilon$ -amino group can make a coordinated bond with Mg of chlorophyll molecule (30, 128). In terms of accumulation of PSI, they behave like WT. The FTIR difference spectra are shown in figure 5a-b. In contrast to the Asp mutations, the Lys substitution mutations do not cause any shifts of the ester carbonyl bands in the 1730-1760  $cm^{-1}$  region. The primary effects are seen on the bands assigned to the  $13^1$ -keto group and to other bands in the 1630-1670  $cm^{-1}$  region, which will be discussed below for each mutant.

For the PsaA-N604K mutant, a pronounced effect is seen from 1701  $cm^{-1}$  to 1634  $cm^{-1}$ . In the double difference spectra the main bands are 1701  $cm^{-1}$  which can be assigned to  $13^1$  keto C=O of  $P_B$  and it is upshifted by one  $cm^{-1}$ . The 1694  $cm^{-1}$  is a new band in the double difference spectra of PsaA-N601K and it is due to mutation, when its amplitude is more at 1688  $cm^{-1}$  than the WT. The 1694  $cm^{-1}$  band can be assigned to the  $13^1$  keto C=O

of  $P_A^+$ , which is 1687  $\text{cm}^{-1}$  in WT and shifts by 6  $\text{cm}^{-1}$  in PsaB-N591K upon cation formation. The perturbed vibration bands from 1657 to 1634  $\text{cm}^{-1}$  are the main effects of lysine mutation on the protein. These bands are 1657, 1653, 1648, 1641 and 1634  $\text{cm}^{-1}$  and are clearly prominent in the double difference spectrum of WT minus PsaA-N604K mutation. Generally the free or unligated lysine  $\epsilon$ -amino group absorbs in the 1626 to 1629  $\text{cm}^{-1}$  regime and these bands originate from an asymmetric plane bending vibrations while the bands at 1526 and 1527  $\text{cm}^{-1}$  arise from symmetric vibrations (129). But here in this double difference spectrum we propose that the amine group of lysine is acting like a perfect ligand for the central Mg atom of ec2<sub>B</sub> chlorophyll and water is displaced from its ligated position. This is a totally new ligand which is not usually present in photosynthetic complexes. Thus, we can assign the 1623  $\text{cm}^{-1}$  region to the asymmetric bending frequency to the lysine ( $\text{NH}^+$ ) group which is ligated to the central magnesium of ec2 chlorophyll of the reaction center. In the literature of FTIR spectroscopy of protein, a positively charged side chain of a lysine COOH group has C=O frequency of 1689.2  $\text{cm}^{-1}$ , thus the band around 1688  $\text{cm}^{-1}$  can also be assigned to the side chain of lysine of PsaA-N604K (126). In the DDS of WT minus PsaA-N604K the 1657 and 1653  $\text{cm}^{-1}$  bands arise due to an increase in amplitude of DS of PsaA-N604K, and can be assigned to the  $13^1$  keto C=O  $P_A^+$ , which in the WT are normally at 1656  $\text{cm}^{-1}$ . The 1638  $\text{cm}^{-1}$  can be assigned to the ground state of  $13^1$  keto C=O  $P_A$  as in WT it is at 1637  $\text{cm}^{-1}$  that gets upshifted to 1653 and 1657  $\text{cm}^{-1}$  in  $P_A^+$  state.

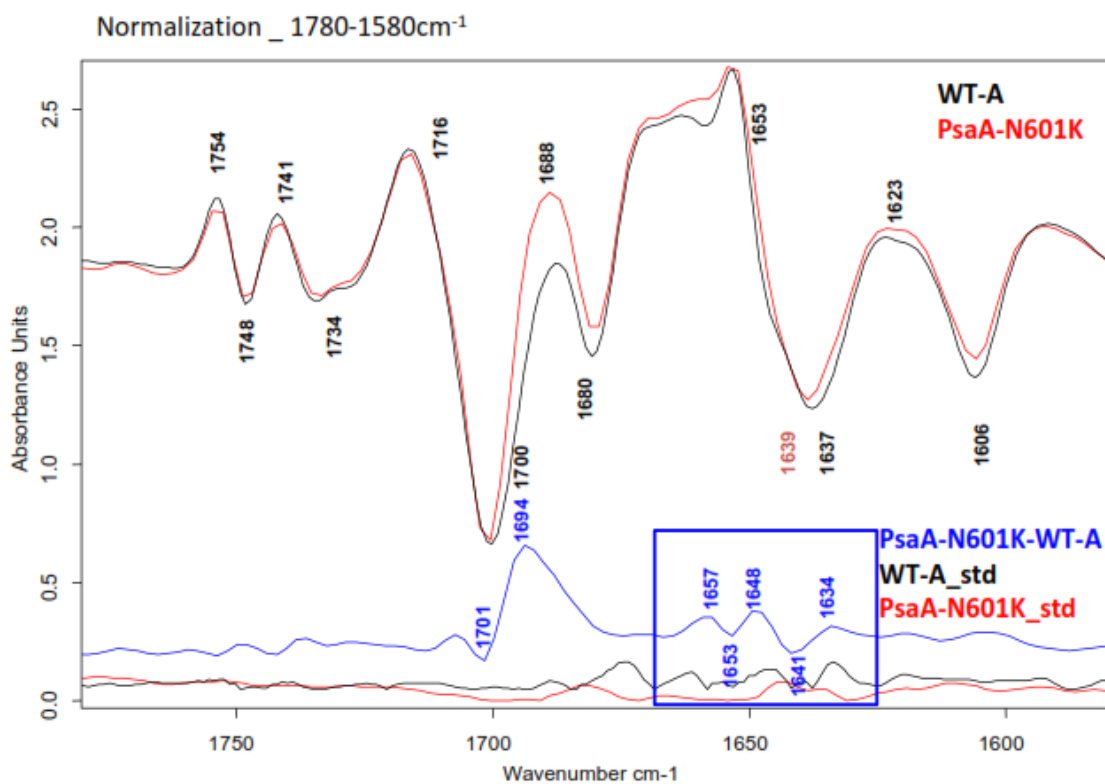
Figure 3.29 and 3.30 shows the FTIR difference spectra of PsaB-N591K mutant which is the expected ligand of ec2<sub>A</sub> on A-branch. In the double difference spectrum the

perturbed bands are 1705, 1698, 1690, 1667, 1658, 1647, 1643, 1638, 1630  $\text{cm}^{-1}$ . In the double difference spectra shown in Figure 3.29 and 3.30, the 1705 and 1698  $\text{cm}^{-1}$  vibrations can be assigned to the ground state  $13^1$  keto C=O of  $P_B$ , which normally in the WT is either at 1700 or 1698  $\text{cm}^{-1}$ , but here in the mutant DS they are shifted by 3  $\text{cm}^{-1}$ , and in DDS it is at 1705  $\text{cm}^{-1}$  so the shift is 5  $\text{cm}^{-1}$  for  $13^1$  keto C=O of  $P_B$ . Thus, the PsaB-N591K has some effect on the B side chlorophyll of  $P_{700}$  in ground state but has no effect on  $P_B^+$  which usually gives bands at 1717  $\text{cm}^{-1}$  in WT. In case of  $P_A$ , the  $13^1$  keto C=O band is upshifted by 1  $\text{cm}^{-1}$  and it is at 1638  $\text{cm}^{-1}$  in DS of PsaB-N591K, which is 1637  $\text{cm}^{-1}$  for WT. The  $13^1$  keto C=O band of  $P_A^+$  are also perturbed and it is upshifted by 2  $\text{cm}^{-1}$  as compared to the WT which is normally at 1656  $\text{cm}^{-1}$ . The 1647 and 1630  $\text{cm}^{-1}$  bands in the DDS can be assigned to the effect of lysine  $\epsilon$ -amine group of PsaB-N591K, which acts as new ligand for  $ec2_A$  chlorophyll. The 1690 and 1667  $\text{cm}^{-1}$  vibration bands in the DDS can be assigned to the changes in the  $13^1$  keto C=O of  $P_A$  and its hydrogen bonding environment which is affected by the PsaB-N591K mutation along the  $ec2_A$  chlorophyll.

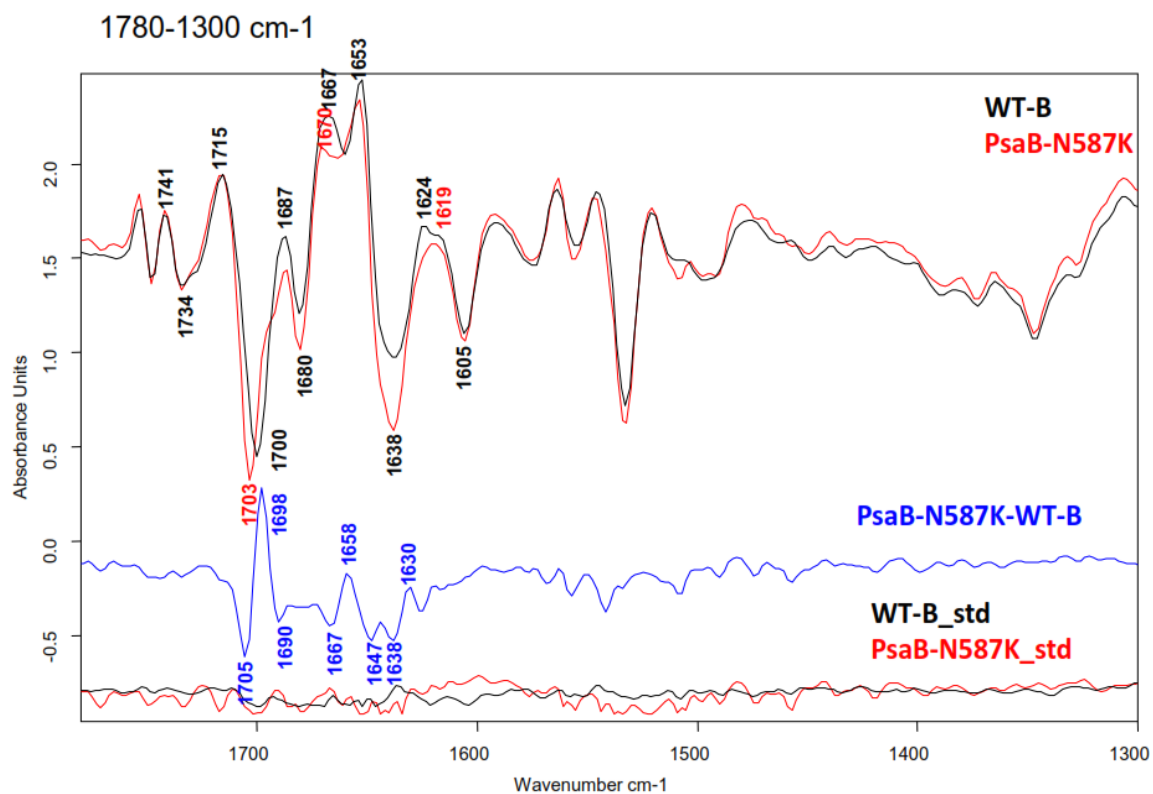


**Figure 3.27.**  $P_{700}^+/P_{700}$  FTIR Difference Spectra of PsaA-N604K superimposed on WT-A for comparison from 1800 to 1300  $\text{cm}^{-1}$ . The PsaA-N604K minus WT-A double difference spectrum is presented in blue color, while at lower panel shows the standard deviation of WT-A and PsaA-N604K.

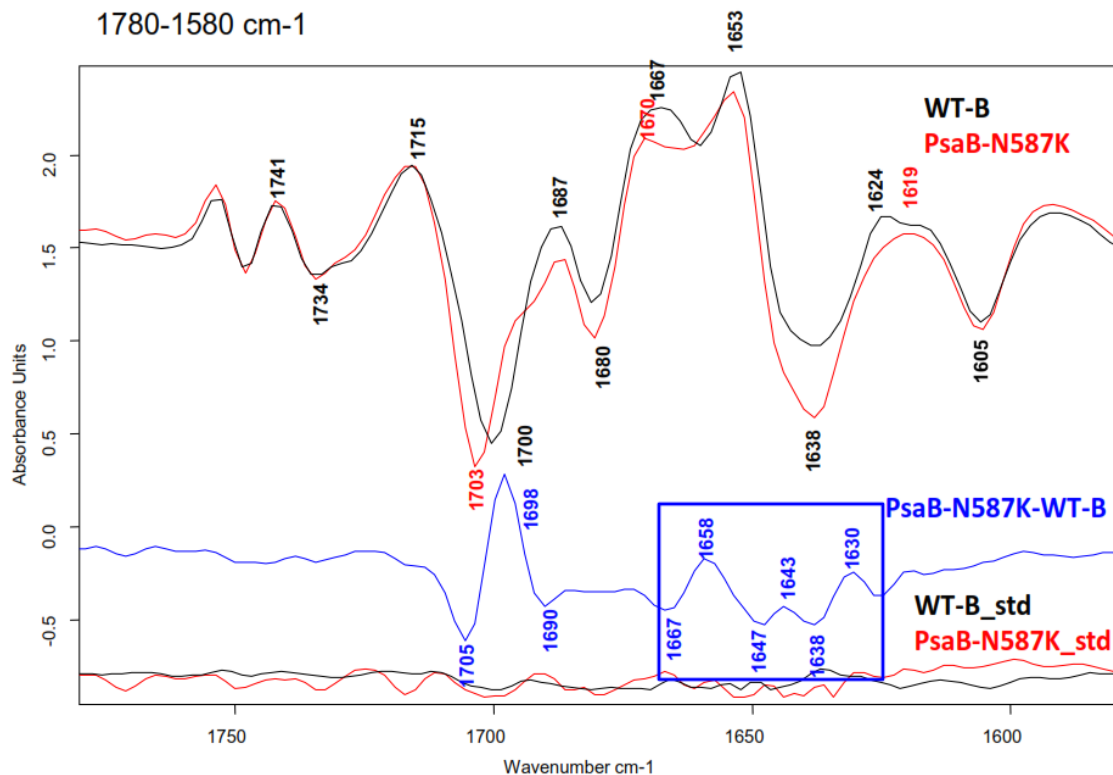




**Figure 3.28.**  $P_{700}^+/P_{700}$  FTIR Difference Spectra of PsaA-N604K superimposed on WT-A for comparison from 1800 to 1650 cm<sup>-1</sup>. The PsaA-N604K minus WT-A double difference spectrum is presented in blue color, while at lower panel shows the standard deviation of WT-A and PsaA-N604K.



**Figure 3.29.**  $P_{700}^+/P_{700}$  FTIR Difference Spectra of PsaB-N591K superimposed on WT-B for comparison from 1800 to 1300 cm<sup>-1</sup>. The PsaB-N591K minus WT-B double difference spectrum is presented in blue color, while at lower panel shows the standard deviation of WT-B and PsaB-N591K.

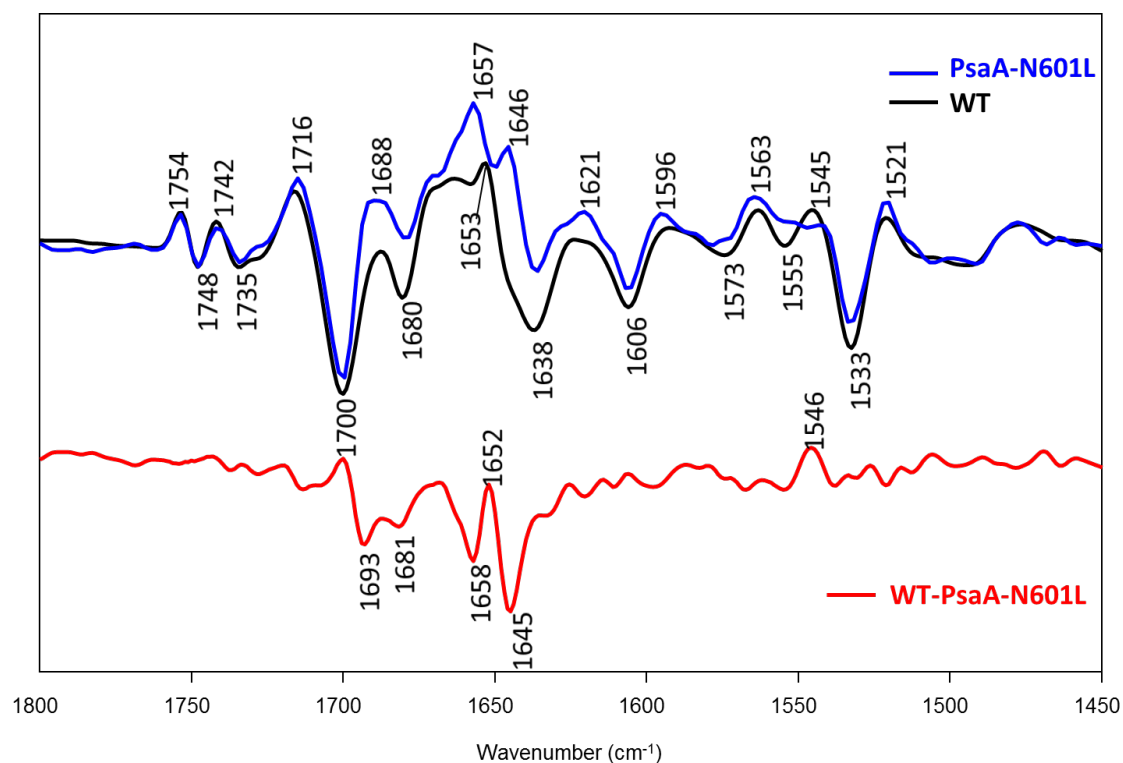


**Figure 3.30.**  $P_{700}^+/P_{700}$  FTIR Difference Spectra of PsaB-N587K superimposed on WT-B for comparison from 1800 to 1650  $\text{cm}^{-1}$ . The PsaB-N587K minus WT-B double difference spectrum is presented in blue color, while at lower panel shows the standard deviation of WT-B and PsaB-N587K.

### 3.3.12.5 $P_{700}^+/P_{700}$ FTIR Difference Spectra of Leucine mutants

From static FTIR difference spectroscopy of aspartic acid and lysine mutants introduced near ec2, we observed that making mutation at ec2 can induce effects upstream on the  $P_{700}$ . These effects are changes in the amplitude of both  $P_A$  and  $P_B$  in ground and in their cationic form after CS. In order to investigate the nature of interactions that cause upstream changes in  $P_{700}$ , we also performed the FTIR difference spectroscopy of asparagine to leucine mutant on the respective branch. Thus, in leucine mutant we are

expecting that if there is an effect on  $P_{700}$ , then it will only be hydrophobic. Figure 3.31 shows the FTIR difference spectroscopy of PsaA-N604L mutant, WT PSI and the DDS of these two in the range of 1800 to 1500  $\text{cm}^{-1}$ . As the PsaA-N601L is affecting the  $\text{ec2}_B$  ( $\text{eC-2A}$ ) of B-branch ET by inhibition of the energy trapping at this cofactor, the A-branch ET is unaffected as observed from transient optical spectroscopy. The bands that show decreases in amplitude includes  $13^1$  keto C=O of  $P_B$  at 1700  $\text{cm}^{-1}$  and  $13^1$  keto C=O of  $P_A$  at 1638  $\text{cm}^{-1}$  in the ground state, while those bands which showed increase in amplitude are 1688 and 1657  $\text{cm}^{-1}$  for  $13^1$  keto C=O of  $P_A^+$  and 1716  $\text{cm}^{-1}$  of  $13^1$  keto C=O of  $P_B^+$ . The bands of the  $13^1$  keto C=O of  $P_A^+$  gets broader too and there is a new band at 1646  $\text{cm}^{-1}$ . In the DDS of WT minus PsaA-N604L, the positive bands at 1700  $\text{cm}^{-1}$  and 1652  $\text{cm}^{-1}$  thus showed that leucine has effect on keto carbonyl in ground state for  $P_B$  and in oxidized form of  $P_A$ . The negative peaks in the DDS are 1693, 1681, 1658 and 1645  $\text{cm}^{-1}$  and all showed the impact of mutation on the  $13^1$  keto C=O of  $P_A^+$ . There are also amplitude changes in the bands between 1600 and 1500  $\text{cm}^{-1}$  with a prominent 1546  $\text{cm}^{-1}$  band in the DDS. These bands originate mostly from the protein backbone due to the size of leucine and also from macrocycle C=C marker of penta-coordinated chlorophyll ring.



**Figure 3.31.** FTIR D.S. of PsaA-N604L overlaid with that of WT in 1800 to 1450  $\text{cm}^{-1}$  range. The WT minus PsaA-N604L double difference spectrum is presented in red color.

### 3.4 DISCUSSION

In this work, we presented the role of ec2 cofactors in energy trapping and primary CS in the two branches of PSI RC from *C. reinhardtii*. The six chlorophylls of the RC are so compact that it is difficult to see any specific band of ec2 cofactor in the P700 DS. Secondly, the presence of red chlorophylls dampens the exact time formation of early chlorophyll cation in the ultrafast transient absorption spectroscopy. We used a combined strategy of generating point mutants near the ec2 cofactor in the two branches of PSI and investigated the ET activity through different time resolved spectroscopic methods to unravel the role of this cofactor. The PsaA-N604 and PsaB-N591 mutants ceased their growth when spotted on TBP for autotrophic growth like methionine ligand of ec3 from

*C. reinhardtii* (68). Mutation near ec3 in PSI of *C. reinhardtii* cell has some growth in lower oxygen conditions but making mutations close to ec2 have negligible growth, which means they are more sensitive to oxygen radicals produced during energy trapping and electron transfer events. Introduction of larger amino acids have a more debilitating effect on the accumulation of PSI as compared to smaller amino acid residue. The A-branch mutants are accumulated less as compared to the B-branch mutants. These results are opposite to the previous mutagenesis studies, in which it was observed that the B-branch is more sensitive to mutation (68, 130). Besides depending upon the size of the substituted amino acid introduced, it is the A-branch that is more sensitive to mutation. We can also predict that the energy dissipated as a heat instead of CS on the two branches might also generate increased amount of reactive oxygen species that are harmful for not only PSI but other membrane bound proteins.

The bi-directionality of ET at the nanosecond time range (reoxidation of  $\text{PhQ}_{A/B}^{\bullet-}$ ), which is the result of primary charge separation, is important to measure. The *in vivo* spectroscopic measurements provided the initial indication about how mutation near ec2 can affect the CS and rate of ET on the two branches. The observable decrease in the ET amplitude on the modified branches in PsaA-N604 and PsaB-N591 mutants confirm that the energy trap is modulated and the excitation energy is cast off. This dissipation of energy near ec2 cofactor is different than the way mutation changes electron transfer at ec3 or  $\text{P}_{700}$  and even in the case of PsaA-A684 and PsaB-A664 mutants near ec2. Thus, the effect of mutation near ec2 is quite different in its action from ec3(53, 87, 114) and  $\text{P}_{700}$  (60). This modification of the energy trap varies in the mutants.

Mutation of asparagine to aspartic acid on both the branches have similar amplitudes of  $\text{PhQ}_{A/B}^{\bullet-}$  and decay kinetics like WT. In PsaA-N604K and PsaB-N591K mutants PSI have some decrease in amplitude and also redistribution of ET between the two branches. In PsaA-N604H and PsaA-N604L, a decrease in the amplitude is observed. The case of PsaB-N591H and PsaA-N591L is very distinct from the rest of the mutants and the WT. As the lifetime of the two phases in the WT and mutants are 26 ns ( $\pm 3$  ns depending on the strain) and 240 ns ( $\pm 6$  ns depending on the strain). The fast 5 ns phase present in PsaB-N591H and PsaB-N587L is interesting and complex to explain. This fast phase of around 5 ns is probably due to either charge recombination (CR) or some excited state process. The CR can be ruled out as 5 ns are very fast and cannot be CR. This back reaction or recovery is like a spike and is present in both 430 and 440 nm wavelengths. This fast decay is associated with chlorophyll species. It needs further confirmation if we measure it in the whole spectral region from 400-480 nm. The fast recovery of chlorophyll bleaching can be assigned from the recombination of the proposed  $[\text{ec}2^+\text{ec}3^-]$  or  $\text{P}_{700}^+\text{ec}3^-]$  to their ground state of  $[\text{ec}2\text{ec}3]$  or  $\text{P}_{700}\text{ec}3]$ , and the other possibility is its decay to the excited state of the RP  $[(\text{ec}2\text{ec}3)^*]$  or  $(\text{P}_{700}\text{ec}3)^*]$ . The other possibility is decay of some excited chlorophyll state or the whole excited state reaction center ( $\text{RC}^*$ ) in the absence of photochemistry of a CS state that recovers in 2 ns. This fast recovery phase masks the 15-25 ns fast phase of PhQ re-oxidation and this fast decay is explained in our proposed model of a new channel of excitation energy decay.

The nanosecond-millisecond transient spectroscopic measurements of isolated PSI particles support the view that the mutation near the ec2 cofactor inhibits CS

as measured at 480 and 820 nm. Secondly, there is no nanosecond and tens of microsecond component in 820 nm measurements which can show intermediate state species like  $P_{700}^{+}ec3^{-}$ ;  $P_{700}^{+}PhQ^{-}$  and  $P_{700}^{+}F_X^{-}$  etc. Further, the CR to form the  $^3P_{700}$  state is also not present. Thus, the un-trapped or trapped energy at the level of primary CS is lost without forming any  $^3P_{700}$  state. These mutants near ec2 are completely different from that of ec3 ligand mutants. These mutants are modulating the thermodynamics parameters of the actual primary electron donor that is ec2 on each branch. This refutes the classical model of CS, where ET initiates from  $P_{700}$ . In ec3 ligand mutants, where a methionine is replaced with a histidine, causes inhibition of CS but this amount of charge separation inhibition is equal to the CR from different RP (31). The PsaA-N604L; PsaB-N591L and PsaA-N604K mutations inhibit CS on their specific branch. But the PsaA-N604H; PsaB-N591H and PsaB-N591K have influence on both of the branches. The size and spatial arrangement of the mutated residue on the two branches also matters. The effect of a single mutant on the two branches can be explained based on the excitonic coupling model, where the six chlorophylls of the RC are acting as a single molecule when RC is equilibrated in excitation energy with the core antenna. However, single point mutation affecting only the mutated branch cannot be explained by the excitonic coupling model. The PsaA-N604L and PsaB-N591L mutants from *C. reinhardtii* have similar results to that of *Synechocystis* PCC 6803 asparagine to leucine and histidine mutants near ec2 cofactor. The only difference was in the 820 nm measurement where there was an additional component in the microsecond time range that we can assign to the chlorophyll *a* triplet decay originating from the LHCI, as it is absent in case of cyanobacteria. Thus,



making mutation near ec2 affects only the efficiency of the trap but not the electron transfer kinetics. This effect confirms that ec2 is the sink for excitation energy to form the primary electron donor.

The ultrafast transient absorption spectroscopic investigation of energy transfer and trapping process in the WT and mutants supported the view that mutation inhibits stable charge separation, while the rates of ET are unaffected. The effect of mutation on the overall charge separation is evident from the decrease in the size of bleaching in the non-decaying spectrum of  $P_{700}^{+}PhQ^{-}$  in the mutants. The change in efficiency of energy trap is more obvious in the mutants of A-branch as compared to B-branch. The PsaB-N591H; PsaB-N591L and PsaB-N591Y are a good example of decrease in amplitude of the non-decaying spectrum. EPR spectroscopy at cryogenic and room temperature showed the ET process in these mutants. Most of the spectral shapes are similar as reported in the literature of PSI particles (89). The mutation near ec2 has no modification down the two branches in terms of ET rates. The decrease in the absorption polarization patterns representing  $P_{700}^{+}FeS^{-}$  RP in both low temperature and room temperature points towards a decrease in charge separation. Although the X-band EPR spectroscopy results are of qualitative nature but the EPR spectra at cryogenic temperature of PsaB-N591H and PsaB-N591L has weak signals of  $P_{700}^{+}PhQ^{-}$  RP, presenting inhibition of CS at the ec2 level.

The decrease in the efficiency of charge separation in the mutants came in a new form in time resolved fluorescence. We interpret the decrease in the lifetime of energy trapping component in the DAS from fluorescence study of the mutants as a new

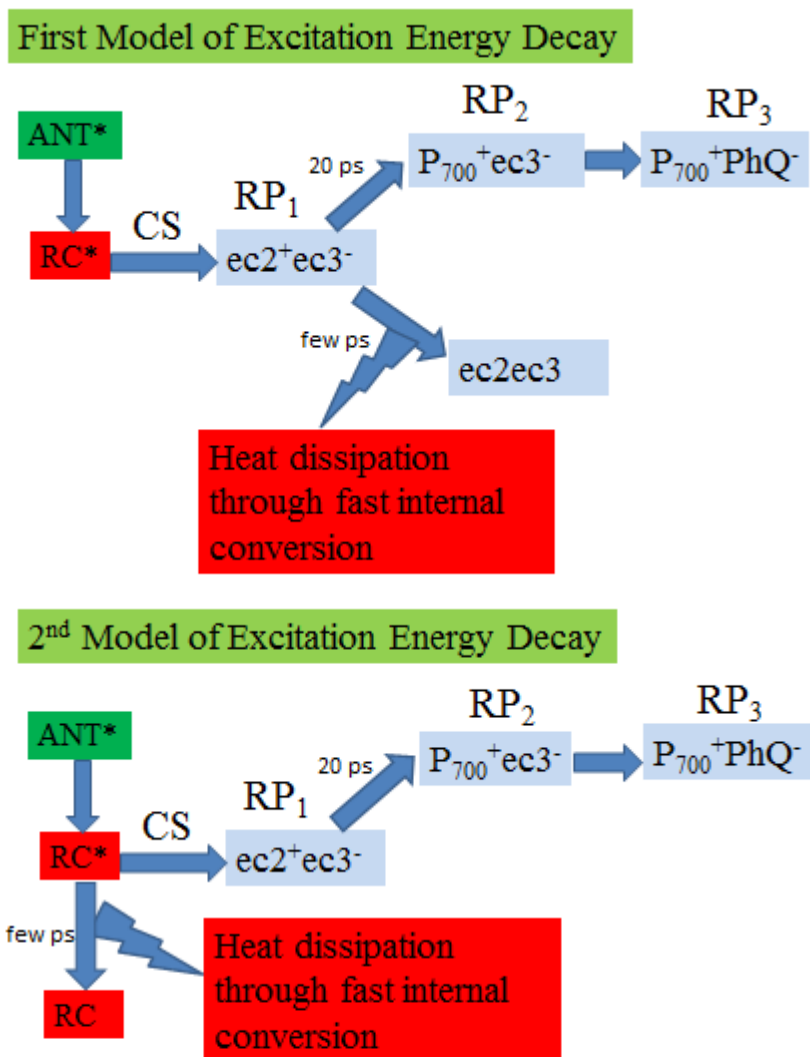
channel for energy transfer into heat. This fast new channel is in competition with charge separation process and its contribution is high in the mutants where CS is inhibited more. For example, the decrease in the lifetime of energy trapping component in PsaB-N591H; PsaB-N591L and PsaB-N591Y is more obvious. The time resolved fluorescence observations are completely different from that of other point mutation studies, where mutants were made close to the P700 in the RC of PSI. For example in the PsaB-H656N mutant, which converts the axial ligand of  $P_B$  from His to Asn, showed an increase in the lifetime of energy trapping from 30 ps to 65 ps. Thus, there is an increase in the energy trapping component lifetime, demonstrating a slow trapping process (131).

We can explain the energy trapping process in the mutants close to ec2, which is based on the proposed model. When excited state energy is equilibrated between the antenna and RC, there are two possibilities for PSI that has trapping efficiency of 100%, that either it is trapped on A-branch or B-branch depending upon the protein dynamics in the location of RC. The mutations make the ec2 site less efficient for trapping, as a result this energy should be disposed somewhere if it is not trapped. We proposed here a new channel or a new functional pathway through which this energy is released to the protein environment. This occurs either at excited RC or the energy is trapped in the primary RP of  $ec2^+ec3^-$ , but due to instability of this RP and its protein bath from mutation it recombines and the energy is dissipated into the protein, presented in the schematic diagram of figure 3.32. The possible fast decay of excitation energy occurs at the interface of electronic to vibronic transition at ec2 cofactor or the energy is trapped in the form of unstable primary CS that recombine very fast and loss to the protein

environment. Thus, time resolved fluorescence measurements in *C. reinhardtii* provide a better clue about how the excitation energy is cast off if it is not used for CS. Based on these results, we can now confidently view the role of ec2 as a primary and the P<sub>700</sub> as a secondary electron donor that reduced the oxidized ec2<sup>+</sup>. Secondly, in both branches the CS is independently initiated at ec2, showing bi-directionality of ET in PSI.

The other unusual observations from these mutagenic studies of PSI are: 1) the red shift in the light induced P<sub>700</sub> DS of PsaA-A604D and PsaB-N591D (Figure 3.4 and Figure 3.17). These P<sub>700</sub> DS showed that asparagine to aspartate substitution influence the P700 dimer absorbance properties. 2) High level of accumulation of PsaA-N604K and PsaB-N591K PSI. The red shift in the P700 DS can be explained on the basis that mutants near ec2 can cause changes upstream on P<sub>700</sub> in both its ground and oxidized form of P<sub>700</sub>. Theoretical studies also predicted that ec2 cofactor can influence the P<sub>700</sub> properties (25). The changes near ec2 cofactor can thus also influence the P<sub>700</sub> environment, which in turn modifies the spectral properties of P<sub>700</sub>. FTIR spectroscopy revealed that both the ground and cationic state vibratory properties of P<sub>700</sub> are influenced by PsaA-N604D and PsaB-N591D. Although it is difficult to establish the protonation state of aspartic acid at this point but it is clear that a mutation near ec2 cofactor modulates the electronic properties of P<sub>700</sub> dimer. The lysine mutants also have 5-6 cm<sup>-1</sup> shifts in the keto carbonyl bands and a new band at 1623 cm<sup>-1</sup> in FTIR P<sub>700</sub> DS. From these observed modifications, it is clear that ec2 cofactor has contribution in the FTIR P<sub>700</sub> DS. Secondly mutations near ec2 cofactor influence the P<sub>700</sub> dimer by various types of interactions that also includes hydrophobic as observed in the case of PsaA-N604L.

For establishing the role of lysine  $\epsilon$ -amino group to acts as a ligand of chlorophyll, some theoretical spectral calculations are required to identify specific vibrational bands of ec2 chlorophyll Mg-lysine interaction.



**Figure 3.32.** Proposed models of excitation energy decay from the excited state of reaction center. Due to mutation near ec2, the excitation energy is released to the ground state after energy equilibration between antenna and reaction center. Where ANT\* = excited state of antenna; RC\* = excited reaction center; CS = charge separated state; RP = radical pair.

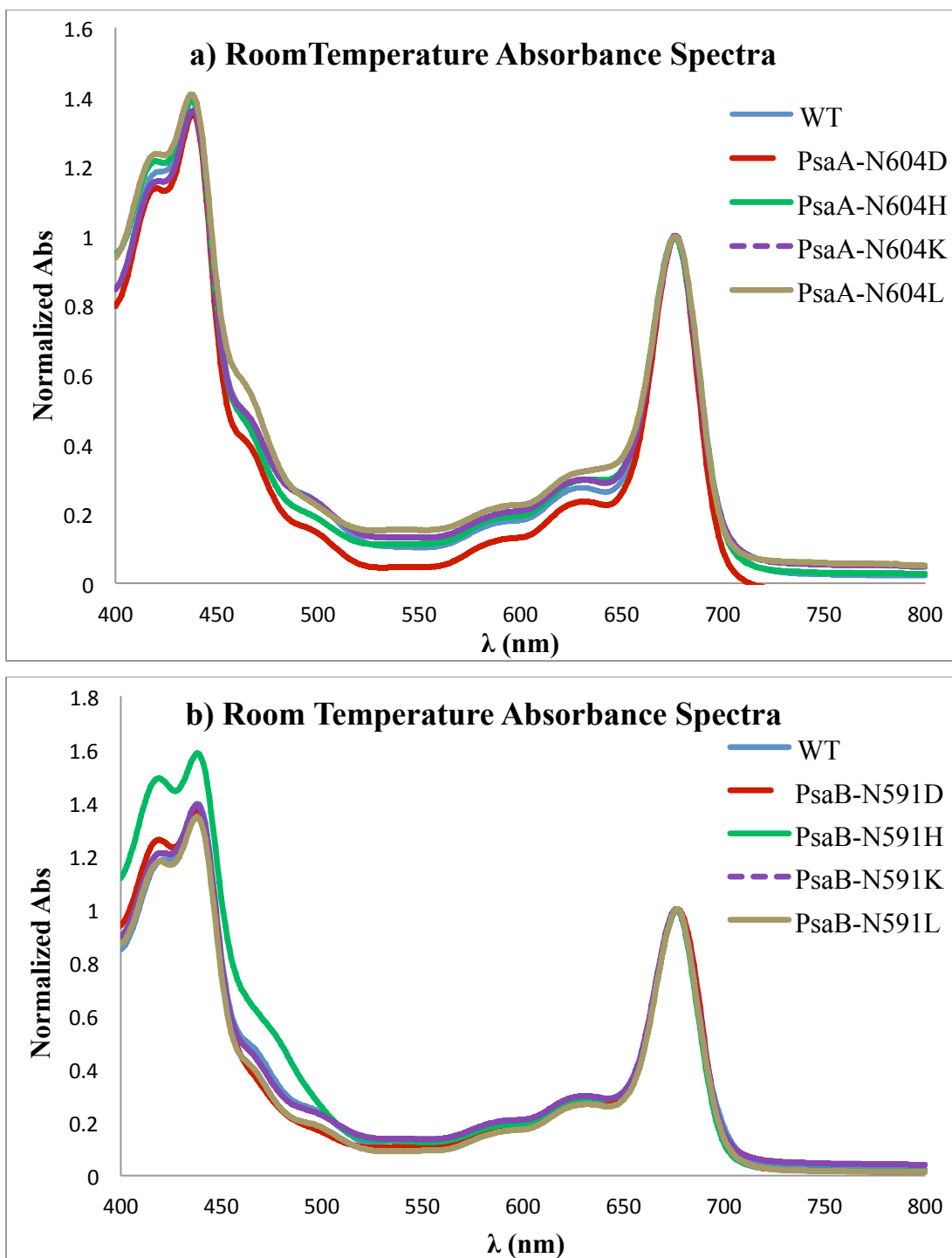
### 3.5 CONCLUSIONS

Transient absorption spectroscopic methods of point mutants near ec2 cofactors provide the evidence that a decrease in stable CS is due to inefficiency of the excitation energy trap. Due to modulation in the protein environment of ec2 cofactor, it is possible that the biophysical properties of ec2 cofactor are modified and it became less efficient trap for excitation energy. Thus, the photon absorbed is not utilized for CS but instead it is wasted as a heat through a new channel. Time resolved fluorescence of the mutants with a decreased level of stable CS showed a faster decay of fluorescence. This gives the idea that there are two processes in competition with one another, one is ET and the other is a faster decay of excitation energy to the ground state. Thus, our experimental analysis showed that ec2 is the primary electron donor on each side from where CS is initiated in photosystem I.

### 3.6 SUPPLEMENTARY INFORMATION

#### 3.6.1 Room temperature absorbance spectroscopy

Room temperature absorbance spectroscopy was performed for the WT and mutants of ec2<sub>A/B</sub> cofactors. As these mutations are in the RC so there is no modification present in the overall absorbance spectra of the mutants as compare to the WT. All the spectra were normalized to the main peak at Q<sub>Y</sub> region and these spectra are superimposable on one another. Thus showing that the spectral distribution area of the LHCI antenna chlorophyll absorption wavelengths in the mutants is similar to that of the WT.



**Figure S3.1.** Normalized Room temperature absorbance spectra of a) WT, PsaA-N604D, PsaA-N604H, PsaA-N604K and PsaA-N604L. b) WT, PsaB-N591D, PsaB-N591H, PsaB-N591K, PsaB-N591L mutants of *C. reinhardtii* PSI particles. There are no major differences in the absorbance spectra of the WT and mutants.

## CHAPTER NO 4

### 4.1 INTRODUCTION

Photosystem I (PSI) is a large pigmented protein complex of the photosynthetic machinery inside the cell. It functions as a light-induced oxidoreductase enzyme that oxidizes cytochrome c or plastocyanin and reduces ferredoxin (132). A 2.5 Å crystallographic structure of PSI from thermophilic cyanobacterium *Thermosynechococcus elongatus* is available in trimeric form. Each monomer has 12 subunits and bound 128 cofactors, which have 96 chlorophylls, 22 carotenoids, four lipids, two phylloquinone and three 4Fe-4S clusters. Out of the 96 chlorophyll *a* molecules, 90 of them make the core antenna. This core antenna harvest solar energy and converts it into excitation energy, which is transferred to the redox active reaction center (RC) for charge separation. The cofactors of PSI RC are present inside the protein in the form of two functionally active branches that stems from P<sub>700</sub>, made of chlorophyll *a* and *a*' (C-13 epimer of Chlorophyll *a*). There is a pair of chlorophyll *a* called ec2 and ec3 and phylloquinone (PhQ) on each branch. The two branches recombine at the 4 [Fe-S] clusters called F<sub>X</sub>. In the PsaC subunit there are two additional 4[Fe-S] clusters names as F<sub>A</sub> and F<sub>B</sub> (21, 24).

Functionally both branches of PSI are active for electron transfer (ET) utilization, termed as bi-directionality of ET (132-135). The main difference between the two branches in terms of kinetics is that ET from PhQ<sub>B</sub> towards F<sub>X</sub> is ten times faster than that of PhQ<sub>A</sub>. In terms of usage, the A-branch is used more as compared to the B-

branch, and it is species dependent. For example, in *C. reinhardtii* the ratio of utilization of A-branch to B-branch for ET is close to one another but in *Synechocystis PCC 6803* the A side is more dominant (53, 118). The 100 % quantum efficiency of PSI is attributed due to the fast excitation energy transfer from the core, and it's trapping in the RC without any loss of energy. The antenna absorbs a photon and converted it into excitation energy. Later the RC traps this excitation energy in the form of stable CS. This trapping of energy occurs in both branches as presented from the decay of reduced two phylloquinone with two lifetimes (136).

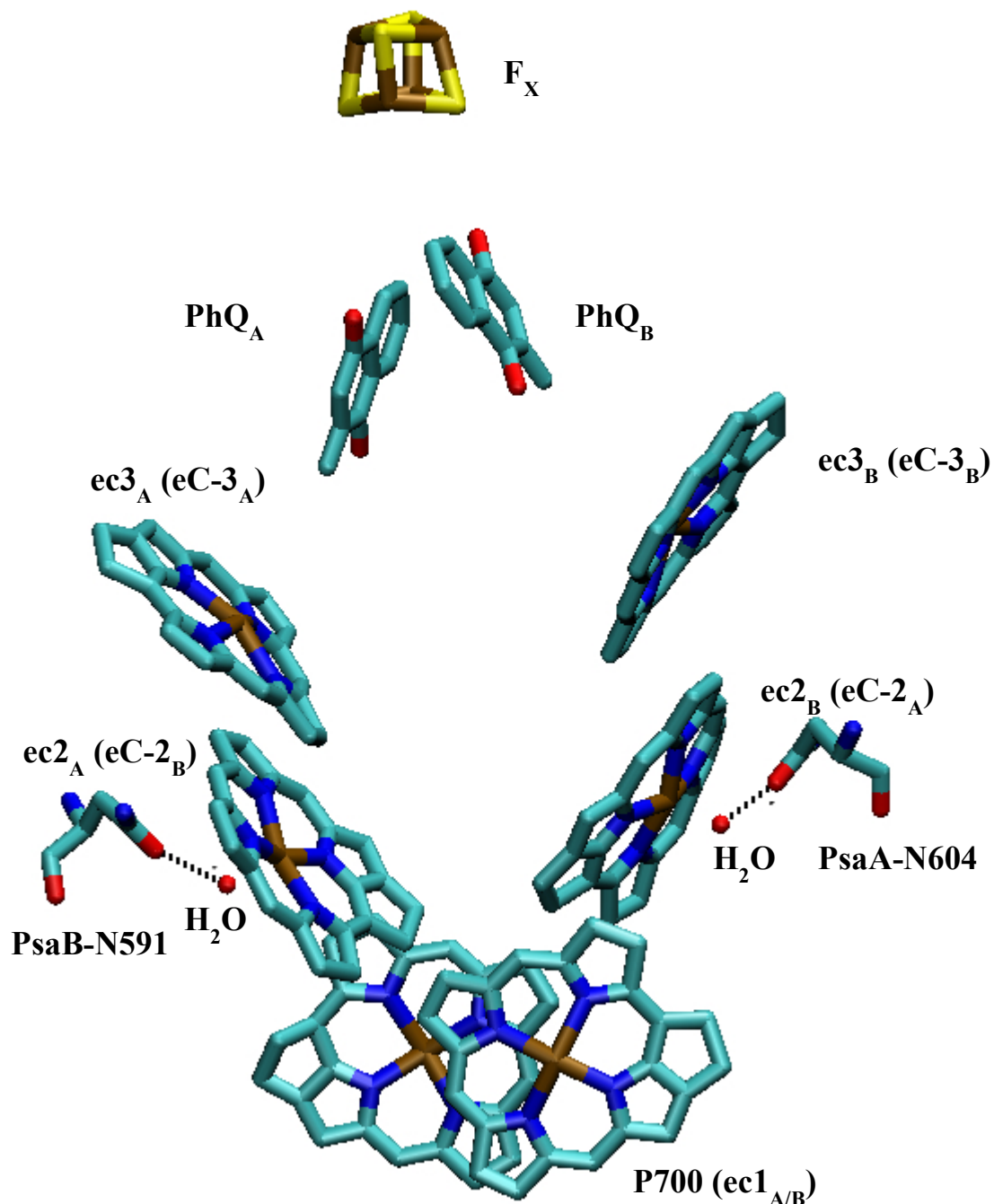
There are two models of CS and ET in PSI. According to the well-accepted classical model, the CS starts from  $P_{700}$  by donating an electron to ec3 chlorophylls, which is the primary electron acceptor. The first radical pair (RP) formed is  $P_{700}^{++}ec3^{\bullet-}$  and in the next step electron moves towards PhQ. In this model, ec2 chlorophylls are not considered in ET events. Mutagenic studies of amino residues closed to  $P_{700}$  revealed that it has no control over the primary CS in the two branches (29, 60). The second proposed model considered ec2 chlorophyll as a primary electron donor. In this new model the excited reaction center ( $RC^*$ ) leads to the formation of  $ec2^{++}ec3^{\bullet-}$ . In the second step,  $P_{700}$  reduces  $ec2^{++}$  and becomes oxidized forming  $P_{700}^{++}ec3^{\bullet-}$  as a  $RP_2$  (11, 29, 43, 62, 84, 137). Theoretical electrostatic measurement and quantum chemical calculations predicted a less negative redox potential for ec2 cofactor than ec3 in the excited state and thermodynamically ET from ec2 toward ec3 is unfavorable (63). Exciting PSI sample from *Synechocystis sp.* PCC 6803 with a 20 fs duration pulse at 720 nm wavelength initiated ET by giving two bands in 100 fs. In this time-resolved spectrum, the 660 nm



band is from  $ec3^+$  and 705 nm from  $P_{700}^{++}$ . There are shortfalls in this analysis such as loss of bleaching band of 705 nm representing  $P_{700}^{++}$  from 4 to 50 ps time scale in the difference spectra. However, after the generation of  $P_{700}^{++}$  cation radical, it should exist for milliseconds, and a decrease in its bleaching is not possible unless it is reduced (64, 65). The long wavelength absorbing chlorophylls in the core antenna of PSI from cyanobacteria absorb in the sub-picosecond time scale during energy equilibration process in the antenna, and these red chlorophylls have charge transfer character. These red chlorophylls dampen the early cationic absorption of primary electron donor, and it is very difficult to interpret the early kinetics (66, 138). The dynamics and energy equilibration role in PSI with and without red chlorophylls need to be established explicitly in terms of their competition with the RC for excitation energy (37, 139, 140).

We consider both cyanobacteria and green algae species to examine the role of  $ec2$  cofactors in the respective branches of PSI RC. These two different species will rule out the effects of any structural differences and the variations due to long wavelength chlorophylls on the rates of excitation energy and electron transfer. Mutagenesis is a method of choice that reveals the activity of particular amino acid in the functional site of protein. In this pigmented protein complex, the pigment cofactor plays a role in excitation energy transfer and charge separation supported by the surrounding protein. Therefore, we can indirectly modulate the properties of the pigment cofactor by modulating the protein residue that is closely interacting with it. The RC of PSI (Figure 4.1) from *T. elongatus* reveals that a water molecule acts as a fifth ligand to the central magnesium atom of  $ec2$ , and there is no direct linkage from the protein. The ligated water

molecule makes a hydrogen bonding contact with the nearby asparagine from the opposite branch polypeptide. The central magnesium atom of ec2 chlorophyll makes a coordinate bond with the oxygen of water by accepting the lone pair of electron from the oxygen atom. While the side chain carboxyl oxygen of asparagine from opposite polypeptide of helix 9 serves as hydrogen bond acceptor. The PsaA-N604 of B-branch and PsaB-N591 of A-branch are substituted by a number of residues. Here we present the results of Asn to Leu from both *C. reinhardtii* and *Synechocystis sp.* PCC 6803, while some further supporting results from cyanobacterium with Asn to His and Asn to Met mutants are presented in supplementary information. We study the effect of these mutations on primary charge separation and directionality of electron transfer using various transient spectroscopic methods in this section.



**Figure 4.1.** Arrangement of electron transfer cofactors in RC of PSI. The figure is constructed from protein data bank file: 1JB0. The P<sub>700</sub> is a dimer and a combination of ec1<sub>A</sub> and ec1<sub>B</sub> chlorophylls. On each branch is a pair of chlorophylls (ec2<sub>A</sub>ec3<sub>A</sub> or ec2<sub>B</sub>ec3<sub>B</sub>) and a phylloquinone (PhQ<sub>A</sub> or PhQ<sub>B</sub>). The F<sub>X</sub> cluster is shared by PsaA and PsaB while PsaC subunit binds the two terminal iron-sulfur clusters (F<sub>A</sub> and F<sub>B</sub>). The water molecule is a 5<sup>th</sup> ligand of the central Mg atom of ec2 on each branch. PsaA-N604

accepts a hydrogen bond from the water molecule on B-branch and PsaB-N591 on A-branch.

## 4.2 MATERIALS AND METHODS

### 4.2.1 Genetic manipulations

The plasmids containing the Asn substitution mutations were prepared via a previously described PCR method and introduced into two background strains of *C. reinhardtii* in which either the *psaA* exon-3 or *psaB* had been deleted (60). These strains also have the nuclear *P71* mutation, which causes a decrease in the total amount of LHCII. The respective plasmid for the particular site was mixed with tungsten particles. These plasmids were bombarded on *C. reinhardtii* cells spread on agar plates containing TAP with 75 µg/mL spectinomycin and 100 µg/mL ampicillin, using a home-built gene gun and helium gas at a pressure of approximately 450 psi. The plates were kept in the dark and colonies appeared after seven days. These colonies were passaged alternately on 300 µg/mL spectinomycin and 100 µg/mL streptomycin every 14 days. The transformants were checked for *psaA* or *psaB* genes and homoplasticity by isolating the plasmid DNA and amplification via PCR. These strains were used primarily for *in vivo* analyses.

A second set of background strains had the *P71* nuclear mutation but lacked the FUD7 mutation: PBC12-5 (*psaAΔ*) and PBC 18-6 (*psaBΔ*). These backgrounds also have a hexahistidine tag on exon 1 of the *psaA* gene (74). The mutants from *Synechocystis sp. PCC 6803* were made according to the previously established methods (141), and pure PSI particles were isolated using n-dodecyl-β-D- maltoside detergent (31).

#### 4.2.2 Isolation of H<sub>6</sub>-PSI particles

*C. reinhardtii* strains were grown in 6-L flasks using 5 L of medium with constant stirring and bubbling with filtered air under normal room light condition of 81  $\mu\text{Einstein m}^{-2} \text{ s}^{-1}$  and room temperature of approximately 23 °C in TAP medium. The cells were harvested during the early logarithmic phase by centrifugation at 3500 g for 5 minutes at 4 °C. The cells were washed with cell resuspension buffer (0.3 mM sucrose, 5 mM MgCl<sub>2</sub>, 5 mM CaCl<sub>2</sub>, 25 mM HEPES-KOH (4-(2-hydroxyethyl)-1-piperazineethanesulfonic acid), pH 7.5) and centrifuged again. The cells were suspended in thylakoid resuspension buffer (0.3 mM sucrose, 10 mM EDTA, 25 mM HEPES-KOH, pH 7.5) and broken by passage through a French pressure cell at 3000 psi. The broken cells were washed with thylakoid resuspension buffer and centrifuged at 40000 g for 10 - 15 minutes at 4 °C twice by collecting the green residue and discarded the lower white starch material. Crude thylakoid membranes were homogenized in cold thylakoid resuspension buffer at approximately 6 mg Chl mL<sup>-1</sup> and stored at -80 °C after flash freezing in liquid nitrogen. Crude thylakoid membranes (CTM) at final concentration of 0.4 mg Chl mL<sup>-1</sup> (PBC12-5 background strains) or 0.2 mg Chl mL<sup>-1</sup> (PBC18-6 background strains) were solubilized by dropwise addition of  $\beta$ -D-dodecylmaltoside ( $\beta$ -DM) to a final concentration of 1/10 volume of 10%  $\beta$ -DM. During solubilization, the sample was stirred gently for 30 minutes at 4 °C in the dark. After sample was centrifugation at 64000 g for 25 minutes at 4 °C to remove nonsolubilized material, the supernatant was loaded onto a Ni-NTA (Invitrogen) column pre-equilibrated with Solubilization Buffer containing 0.03 %  $\beta$ -DM. The column was washed with

Solubilization Buffer containing 0.03 %  $\beta$ -DM and 2 mM imidazole until the efflux was clear. The H<sub>6</sub>-tagged PSI was eluted from the column with elution buffer (300 mM imidazole and 40 mM 2-(*N*-morpholino) ethane sulfonic acid MES-NaOH, pH 6). The eluate were concentrated in Amicon Ultra-15 centrifugal filters with 100 K molecular weight cutoff (Millipore Ltd. Ireland). The concentrated PSI was washed with Storage Buffer (40 mM CaCl<sub>2</sub>, 40 mM MgCl<sub>2</sub>, 0.03%  $\beta$ -DM, 10% glycerol, 10 mM Tricine, pH 8) to remove imidazole several folds during concentration. The sample was concentrated to a final concentration 2.5-3 mg Chl ml<sup>-1</sup>. Glycerol was added to a final concentration of 20%. Samples were stored in 100  $\mu$ L aliquots by flash freezing in liquid nitrogen at -80 °C.

#### 4.2.3 Time-resolved Optical Spectroscopy of PSI particles

Time-resolved optical spectroscopy with a temporal resolution of ns - ms was performed on PSI particles. A 480-nm probe beam was used to monitor the electrochromic bandshift of pigments in the RC induced by the charge-separated state (primarily due to pigments near PhQ<sup>-</sup>) (109). For these measurements, 100  $\mu$ g of chlorophyll-containing PSI sample per 1 mL was diluted into a buffer containing 10 mM Tricine (pH 8), 0.4 M CaCl<sub>2</sub>, 0.4 M MgCl<sub>2</sub>, 10% glycerol, 0.03%  $\beta$ -DM, 10 mM sodium ascorbate, and 40  $\mu$ M phenazine methosulfate (PMS). The sample was excited with a  $\sim$ 3-ns laser pulse generated by a frequency-doubled (532 nm), Q-switched Nd: YAG laser (DCR-11, Spectra-Physics, Mountain View, CA). It was operated in the short-pulse mode. The probe light was provided by a Xe flash tailored with a bank of inductors and capacitors to produce 5- $\mu$ s pulses. The 480-nm probe and pump beam were filtered through a narrow band (8 nm)

interference filter along with colored glass filters (FND 100Q from EG & G). The two beams were paired up in two micrometer multimode fiber optic patch cables (M28L01; Thorlabs, Newton, NJ) through two fixed focus collimation packages (F240FC-543; Thorlabs, Newton, NJ). The two packages were placed at a distance of 3 m from the sample cuvette to minimize the artifacts due to the excitation beam. The two fiber cables were connected to a balanced amplified photo-detector (PDB430A; Thorlabs, Newton, NJ) containing DC bandwidth of 350 MHz. Digitizing oscilloscope (DSA 602A with amplifier plug-in 11A52; Tektronix, Beaverton, OR) was used to measure the balance output. The laser flash was detected by a photodiode connected to 11A72 plug-in used to initiate the data acquisition. The rise time of the detection system was measured by using Tris(bipyridine)ruthenium(II) chloride ( $\text{Ru}(\text{Bipy})_3\text{Cl}_2$ ) luminescence and was found to be three ns (110). The baseline was recorded after every flash by mechanically blocking the pump flash, and this baseline transient was subtracted from that recorded with pump flash on every cycle. Around 1024 to 2048 pairs of flash minus no-flash number of transient were averaged at a repetition rate of 1 Hz. Software written in LabView controlled the timing sequence and data recording. The PSI sample was contained in 10 X 10 mm standard quartz cuvette at room temperature. All the kinetic traces were processed by fitting with a multi-exponential function using Marquardt least-squares algorithm that was programmed in IGOR Pro v. 5.2 (Wavemetrics, Lake Oswego, OR). Charge recombination was monitored at 820 nm using a home-built time-resolved spectrophotometer. For these measurements, PS1 particles corresponding to 100  $\mu\text{g}$  were diluted into 400  $\mu\text{L}$  of buffer (same as above except using 0.5 mM sodium ascorbate and

10  $\mu$ M dichlorophenolindophenol (DCPIP) as reducing agents). The sample was prepared in an anaerobic chamber (Coy Laboratories, Grass Lake, MI) with an atmosphere of 10 %  $H_2$  and 90 %  $N_2$  to avoid generation of harmful oxygen radicals.

#### 4.2.4 Quantum Yield of Charge Separation

The total amount of stable charge separation in PSI from *C. reinhardtii* WT and Asn to Leu mutant pair was measured using a Joliot type spectrophotometer (JTS-10). The  $P_{700}$  bleaching was measured at wavelength of 810 nm. The 810 nm was chosen because the  $P_{700}^+$  cation has a very broad and unstructured absorption band in the near infrared from 730-850 (142, 143). For each sample measurement, 10  $\mu$ g/mL of chlorophyll-containing PSI was used in triplicate. The Nd:YAG laser (Continuum Electro-Optics, Inc., Santa Clara, CA) emitting 33-mJ pulses at 532 nm (6 ns duration) was used for oxidation of  $P_{700}$  of PSI. The laser flash has enough energy to saturate the sample. The oxidation of the sample was probed with 810 nm weak actinic flashes from JTS-10 spectrophotometer. The sample was measured in the absorbance mode where a baseline of 20 s was measured initially and then in the illumination period a single laser flash was given to oxidize the  $P_{700}$ , followed by measuring flashes (10- $\mu$ s red LED passed through a selected interference filter) to monitor oxidation of  $P_{700}$  by the laser flash in exponential increment way for 1115 ms. These measuring flashes commenced 250  $\mu$ s after the laser flash and after exponential increment increase phase and additional measuring flashes of 18 s, long enough for the bleaching signal to recover entirely. At 810 nm the positive peak was taken for calculation as at 810 nm;  $P_{700}^+$  absorb (144).



#### 4.2.5 Electron Paramagnetic Resonance (EPR) Spectroscopy

Low temperature (80 K) X-band (9 GHz) and Q-band (35 GHz) time/field transient EPR data sets were measured with a modified Bruker ER 200D-SRC spectrometer. The ER 041 X-MR X-band or ER 051QR Q-band microwaves Bridge were used in this spectrometer for the respective X and Q-band measurements. A Flexline ER 4118 X-MD-5WI dielectric resonator was used at low temperature. Light excitation was made using a Continuum Surelite Nd:YAG laser operating at 10 Hz, 4.0 mJ/pulse and 532 nm. The temperature of the bath was controlled using an Oxford Instruments CF9335 gas flow cryostat. The transient EPR signal was recorded in direct-detection mode with a home built broadband amplifier (bandwidth 500 MHz) and was digitized through a LeCroy LT322 500 MHz digital oscilloscope (145). PSI samples were treated with 1mM sodium ascorbate and 50  $\mu$ M phenazine methosulfate (PMS) and the samples were frozen in the dark. Room temperature X-band EPR measurements were performed with a modified Bruker ESP 200 spectrometer equipped with a homemade, broadband amplifier (bandwidth >500 MHz). A flat cell and a rectangular resonator were used, and the samples were illuminated using a Q-switched, frequency-doubled Continuum Surelite Nd:YAG laser working at 10 Hz, 4.0 mJ/pulse and 532 nm. In order to bring the  $P_{700}$  in the reduced state before the excitation flash, 1 mM sodium ascorbate and 50  $\mu$ M PMS were used as electron donor and mediator.

#### 4.2.6 Ultrafast Transient Absorption Spectroscopy

The sample was excited with a laser light of 690nm excitation with a full width at half maximum (FWHM) of 0.15 ps and was probed with white continuum light having central wavelength of 680 nm. The pump and probe light was set at magic angle (54.7°). Intensity of the excitation light was enough to excite the sample, but not to make much annihilation. Measurements were performed in a window from 601 to 750 nm, which is  $Q_Y$  transition of Chlorophyll a of PSI. Data was collected from 0.9 ps before time zero and 2 nanosecond after the excitation pulse. Circular rotating cuvette with a path length of 1.2 mm was used so that the laser light didn't excite more than 10% of the measuring PSI particles. Speed of the rotation was set so that the laser shot hit fresh open (reduced  $P_{700}$ ) PSI particles and to avoid the accumulation of long-lived intermediates state. The PSI sample concentration in units of optical density from *C. reinhardtii* was always 0.8 OD at 676 nm and for *Synechocystis* sp. PCC 6803 it was also 0.8OD at 679 nm of  $Q_Y$  region. For stability of PSI and to avoid aggregation issues, the buffer consists of 10mM Tricine, 0.4 M  $MgCl_2$ , 0.4 M  $CaCl_2$ , 10% glycerol, 0.03%  $\beta$ -DM as a detergent. 40 mM of sodium ascorbate and 50  $\mu$ M of phenazine methosulfate were used as redox agents in order to keep the reaction center in the open state during measurements.

#### 4.2.7 Time-resolved fluorescence

Time correlated single photon counting (TCSPC) was performed to measure the kinetics of energy trapping in PSI mutant samples. The sample was excited with a Titanium-Sapphire laser (Spectra-Physics, Millennia pumped Tsunami) at 420 nm with a 130 fs

pulse duration and 4 MHz repetition rate. Fluorescence emission was collected at a 90° geometry setting and detected using a double-grating monochromator (Jobin-Yvon, Gemini-180) and a microchannel plate photomultiplier tube (Hamamatsu R3809U-50). The polarization of the emission was set at a magical angle of 54.7° relative to that of the excitation. The data acquisition was done using a single photon counting card (Becker-Hickl, SPC-830). The typical IRF had a FWHM of 35 ps, measured from the scattering of sample at 420 nm. The excitation power was 12.1  $\mu$ W at the sample to avoid singlet-singlet annihilation. A time window of 3.3 ns was used, and measurements were done from 680 to 740 nm with 10-nm spacing. The PSI particles were diluted to an OD of 0.5  $\text{cm}^{-1}$  at the Chl *a*  $Q_y$  maximum with a tricine buffer [10 mM Tricine (pH 8), 0.4 M  $\text{MgCl}_2$ , 0.4 M  $\text{CaCl}_2$ , 10 % glycerol, 0.03 %  $\beta$ -DM] along with 20 mM sodium ascorbate, and 50  $\mu$ M phenazine methosulfate. Global analysis was performed with ASUFIT 6.1 software. The decay-associated spectra (DAS) of fluorescence emission are the wavelength dependent pre-exponential part ( $A_i(\lambda)$ ), from the multi-exponential fluorescence decay components. These decay components were obtained by applying the equation  $F = \sum A_i(\lambda) \exp(-t/\tau_i)$  and is related to specific exponential lifetime,  $\tau_i$ .

## 4.3 RESULTS

### 4.3.1 Nanosecond kinetics at 480 nm (electrochromic bandshift) in PS1

We performed time-resolved optical spectroscopy on PS1 particles of WT and the mutations generated near the *ec2* site on each branch respectively in *Synechocystis sp.* PCC 6803 and *C. reinhardtii* from the various transformants into a background with a hexahistidine tag. The kinetics of phyllosemiquinone ( $\text{PhQ}^\bullet$ ) oxidation were monitored at

480 nm, which is due to an electrochromic band shift of pigments near  $\text{PhQ}^-$  induced by the negative charge. (52, 109). The optical data obtained at 480 nm give information about the amount of CS occur on individual branch in terms of semiphylloquinone formed that induced the ECS on the nearby cofactors and the decay rates of two ECS. At 480 nm, there is an additional long lived positive component that arises from  $\text{P}_{700}^+$  formation. The time-resolved optical spectra of WT and mutants from both species obtained at room temperature were fitted to two exponential decays. The decay at 480 nm in WT PS1 from both organisms was biphasic. In *C. reinhardtii*, PSI has lifetimes of 22.3 ns and 216 ns; the amplitudes were 0.94 mOD and 1.2 mOD, respectively. While in *Synechocystis* sp. PCC 6803 WT PSI the fast phase has a lifetime of 17.2 ns with amplitude of 0.65 mOD. The slow phase from A-branch has a lifetime of 207 ns with amplitude of 1.2 mOD. The increased in amplitude on B-branch in *C. reinhardtii* as compare to *Synechocystis* sp. PCC 6803 is also evident here. The other difference is that the rate of both phases in *Synechocystis* sp. PCC 6803 are a bit faster than *C. reinhardtii* PSI as shown in figure 4.2 and table 4.1. These results are very similar to the previous observations (52). In *C. reinhardtii*, the usage of the two branches is approximately equal but in *Synechocystis* sp. PCC 6803, it is 70-80 % of ET on A-branch and 30-20% on B-branch (53, 54).

In *C. reinhardtii* the PsaA-N604L mutant exhibited lifetimes of 20.5 ns (0.45 mOD) and 206 ns (1.2m OD), as presented in figure 4.2. While in *Synechocystis* sp. PCC 6803 PsaA-N604L has lifetime of 18.3 ns (0.30 mOD) and 212 ns (1.1 mOD). Thus in both the specie the effect of asparagine to the leucine mutation is on the amplitude of

ET on B-side (Table 4.1). This 50 % inhibition of CS shows a decrease in the energy trapping efficiency of the B-branch only while the A-branch is unaffected and works normally in terms of magnitude of CS and rate of ET. In contrast, the PsaB-N591L mutant affecting  $ec2_A$  had decay components with lifetimes of 20.5 ns (0.92 mOD) and 205 ns (0.34 mOD) in *C. reinhardtii*. Thus, the rates extracted from this analysis did not greatly differ, but the amplitudes are significantly changed. Moreover, the change would be as expected if the affected branch is utilized less as a consequence of the mutation. The PsaB-N591L mutant of cyanobacteria has fast phase of 17.8 ns (0.67 mOD) and slow phase of 203 ns (0.31 mOD). Thus, the effect is four-fold on the inhibition of CS in A-branch in both cyanobacteria and green algae.

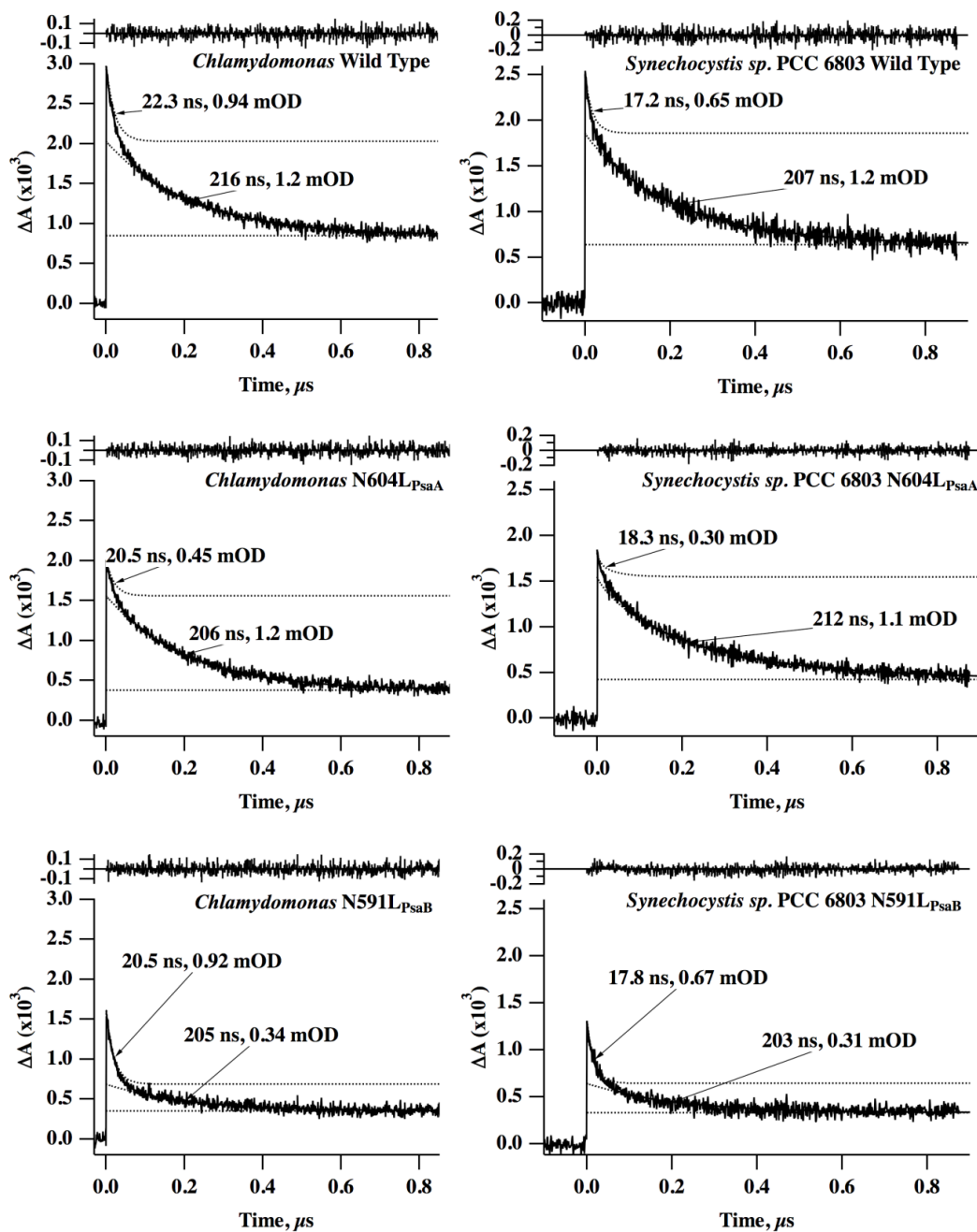
In *Synechocystis* sp. PCC 6803, we also analyzed two additional set of mutants, where the PsaA-N604 and PsaB-N591 were mutated to histidine and methionine. The PsaA-N604H acting on the B-branch has a fast phase amplitude modulation only, with the lifetimes of 17.8 (0.30 mOD) and slow phase of 210 ns (1.20 mOD) as shown in Figure S4.2. The total reduction in the quantum yield of CS is 81 % (Table S4.1). In PsaB-N591H, the charge separation on the A-branch is inhibited by 45 % as compared to WT. Conversion of asparagine to methionine in PsaA-N604M results into no effect on the B-branch CS. While the PsaB-N591M has very minor effect on the A-branch, with a 10% decrease in CS, as shown in Figure S4.2 and Table S 4.1. Thus, the mutation affecting  $ec2_B$  exhibited less fast electron transfer, consistent with the hypothesis that fewer electrons had arrived at  $PhQ_B$  due to an impairment of charge separation in that branch. However, we note that the amplitude of the other component

did not increase to compensate; it is unchanged. Thus, the overall amplitude of decay at 480 nm is lower in both mutants. This decrease in amplitude indicates that the quantum yield of charge separation is lower in these mutants.

**Table 4.1.** Rates and amplitudes of decay components obtained from transient optical spectroscopy at 480 nm in various purified PS1 preparation (*C. reinhardtii* and *Synechocystis sp.* PCC 6803).

Mutation	amplitude (mOD) of fast decay	rate (ns) of fast decay	amplitude (mOD) of slow decay	rate (ns) of slow decay	$\phi$ at 480 nm [ns components] (%)
WT ( <i>C. reinhardtii</i> )	0.94	22.3	1.20	216	100
WT ( <i>Synechocystis sp.</i> PCC 6803)	0.65	17.2	1.20	207	100
PsaA-N604L ( <i>C. reinhardtii</i> )	0.45	20.5	1.20	206	77
PsaA-N604L ( <i>Synechocystis sp.</i> PCC 6803)	0.30	18.3	1.12	212	76
PsaB-N591L ( <i>C. reinhardtii</i> )	0.92	20.5	0.34	205	59
PsaB-N591L ( <i>Synechocystis sp.</i> PCC 6803)	0.67	17.8	0.31	203	53

<sup>1</sup> Assumed to be 100%. Quantum yields in the mutants are expressed as relative to WT.



**Figure 4.2.** Transient absorbance difference traces at 480 nm for PS I complexes from *C. reinhardtii* (left) and *Synechocystis sp. PCC 6803* (right). The two WT, PsaA-N604L,

PsaA-N604L, PsaB-N591L and PsaB-N591L mutant are shown side by side for comparison. The Chl concentration is 100  $\mu\text{g ml}^{-1}$  for all the measurements. The points depict the experimental data, and the fit is in the form of a solid line. The differences between experimental and fit data are in the form of residual. The data sets were from 64 averages.

#### 4.3.2 Charge recombination between $\text{P}_{700}^{+} \text{F}_{\text{A/B}}^{-}$ radical pair and its intermediate states

Oxidized  $\text{P}_{700}$  ( $\text{P}_{700}^{+}$ ) was followed directly by monitoring absorption of chlorophyll cation radical at 820 nm in two time windows: a few ms and  $\sim 2$  s. The data from these two windows were united and a global fit was obtained (Figure 4.3). In the case of *C. reinhardtii* WT PSI, three decay components were necessary to fit the data; in contrast, only two components were required for WT PSI from *Synechocystis sp.* PCC 6803. Charge recombination of  $\text{P}_{700}^{+}(\text{F}_{\text{A}}/\text{F}_{\text{B}})^{-}$  has a lifetime of 50 - 100 ms and accounts for much of the decay. A variable amount of slow decay (hundreds of ms to  $\sim 1$ s) was observed, and is assigned to electron donation from DCPIP to  $\text{P}_{700}^{+}$ . In these PSI RCs, the electrons had “escaped” (via reduction of exogenous acceptors). The additional decay seen in algal PSI was in the  $\mu\text{s}$  timescale. In the control PSI, it exhibited a decay time of  $\sim 70$   $\mu\text{s}$  (2.1 mOD) and accounted for about one-third of the decay. The origin of this is unclear, but we can assign it to the triplet state of chlorophyll in the antenna through intersystem crossing. We did not observe any decay in the nanosecond timescale, demonstrating that none of the mutations caused charge recombination from  $\text{P}_{700}^{+}\text{A}_0^{-}$  ( $\text{P}_{700}^{+}\text{ec3}^{-}$ ) (87). In WT PSI from *Synechocystis sp.* PCC 6803, the 49.9 ms with 5.0 mOD is the back reaction from reduced  $\text{F}_{\text{A}}/\text{F}_{\text{B}}$  to oxidized  $\text{P}_{700}$ . The second component with a 1.31 s lifetime and 2.3 mOD is the ET from DCPIP to  $\text{P}_{700}^{+}$ , as shown in Table 2. All the



WT components are added and considered as 100 % of quantum yield for CS in order to calculate this value in the mutants.

The 820 nm measurement data fitting of PsaA-N604L from *C. reinhardtii* is resolved into three components with lifetime and amplitudes of 182  $\mu$ s (1.4 mOD); 61 ms (2.1 mOD) and 674 ms (0.9 mOD). The 182  $\mu$ s (1.4 mOD) component can be assigned to the  $^3\text{Chl}$  state from LHC1 like WT, shown in figure 4.3. The 61 ms lifetime component with 2.1 mOD amplitude is the charge recombination between  $\text{P}_{700}^+$  and  $[\text{F}_\text{A}/\text{F}_\text{B}]^-$ . While the 674 ms (0.9 mOD) lifetime component is ET from DCPIP to the long-lived  $\text{P}_{700}^+$ . The quantum yield of CS in PsaA-N601L at 820 nm from *C. reinhardtii* is 75 %, which showed excitation energy loss of 24% at  $\text{ec2}_\text{B}$ , almost similar result at 480 nm. The asparagine to leucine counterpart in *Synechocystis sp.* PCC 6803 exhibits four parts. The 453 ns (0.57 mOD) lifetime component is the back reaction between  $\text{ec3}_\text{B}^-$  and  $\text{P}_{700}^+$ . There are two millisecond components; one with a lifetime and amplitude of 1.86 ms (0.43 mOD) that can be assigned to CR between  $\text{P}_{700}^+$  and  $\text{F}_\text{X}^-$ . The second component with a 58.54 ms lifetime and amplitude of 2.5 mOD is a major one, and it is the CR between  $\text{P}_{700}^+$  and  $[\text{F}_\text{A}/\text{F}_\text{B}]^-$ . The final component is 1.33 s (1.7 mOD) that arise from DCPIP to  $\text{P}_{700}^+$ . The quantum yield of this PsaA-N604L is 71 % that is quite close to its 480 nm measurement and to that of its *C. reinhardtii* counterpart, as presented in table 4.2.

The back ET in PsaB-N591L from *C. reinhardtii* affecting the A-branch  $\text{ec2}_\text{A}$  has three components. The 120  $\mu$ s with a 1.4 mOD of amplitude originates from  $^3\text{Chl}$  in LHC1 through intersystem crossing of excitation energy. The major 53 ms (1.7 mOD) is

obviously CR between  $P_{700}^{+}$  and  $[F_A/F_B]^{-}$ . Some of the  $P_{700}^{+}$  is still left unreduced for a long time, which is reduced by DCPIP, this component has lifetime of 570 ms (0.5 mOD). The PsaB-N591L complement in *Synechocystis* sp. PCC 6803 is PsaB-N591L, which also shows three components. The fastest component with lifetimes of 27.7  $\mu$ s (1.0 mOD) is the back ET from  $PhQ_A^{-}$  to  $P_{700}^{+}$ . This component differs from that of PsaB-N587L of *C. reinhardtii*. Charge recombination between  $P_{700}^{+}$  and  $[F_A/F_B]^{-}$  in PsaB-N591L has a lifetime of 68.5 ms and an amplitude of 1.5 mOD. The 1.26 s (1.1 mOD) component lifetime is the usual reduction of  $P_{700}^{+}$  by DCPIP. The quantum yield of CS in these two counterpart mutants in algae and cyanobacteria is 56 % and 49 %, as presented in table 4.2. These measurements are close to that of 480 nm forward ET on the A-branch.

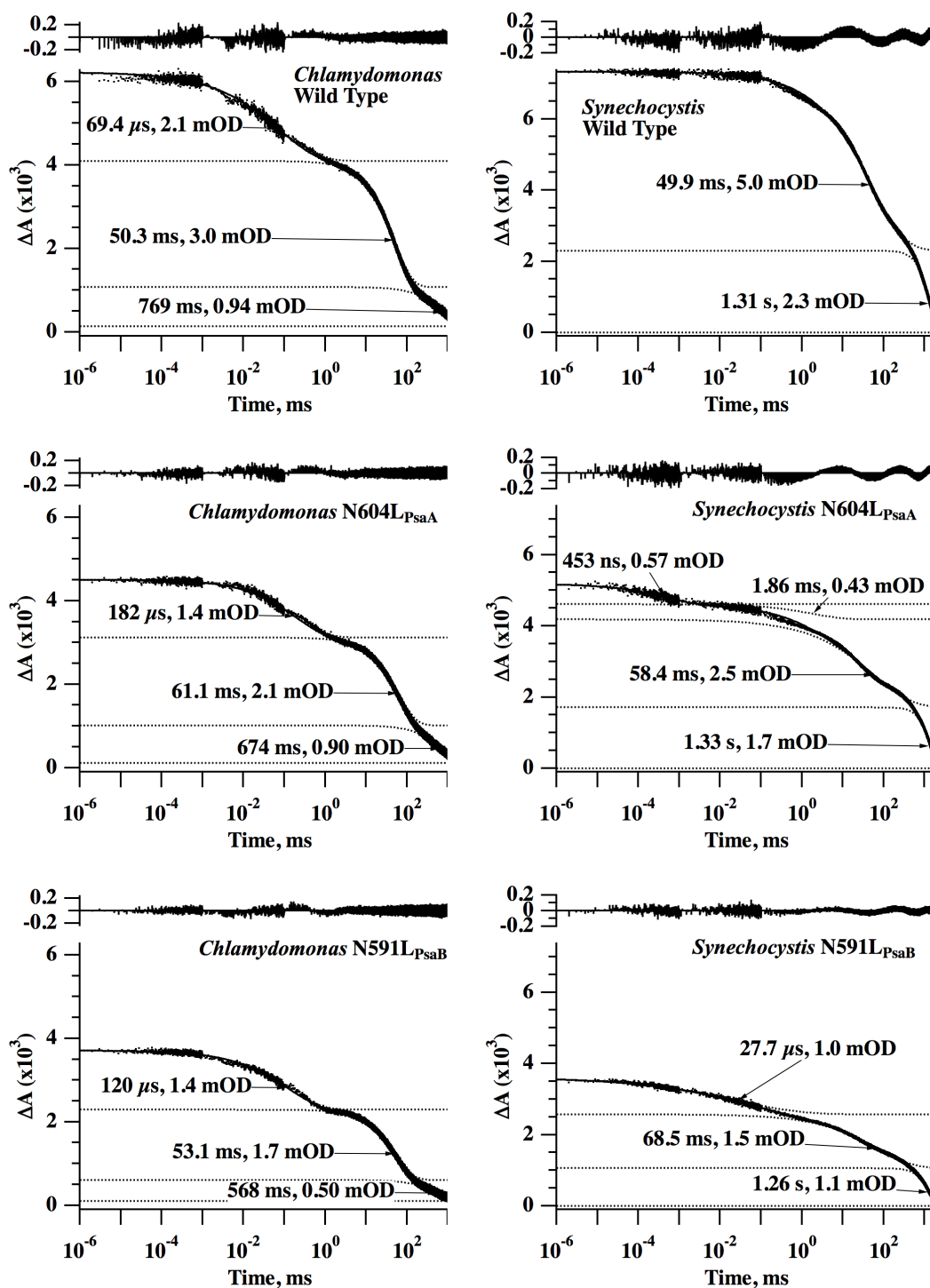
The PsaA-N604H mutation from *Synechocystis* sp. PCC 6803 at 820 nm has four lifetime components and quantum yield of 71 %. The fastest lifetime is 29.4 ns (0.47 mOD) is the CR between  $PhQ_B^{-}$  to  $P_{700}^{+}$ , figure S4.3. The ms lifetime components fragmented into 1.42 ms (0.96 mOD) and 47.6 ms (1.8 mOD), which we assigned to CR between  $P_{700}^{+}$  and  $[F_A/F_B]^{-}$ . PsaB-N591H on the A-branch has similar charge inhibition like PsaB-N591L, and its quantum yield is 49 % as calculated in table S4.2. The back ET measurement in PsaA-N604M at 820 nm fits four different kinetic components. The fastest component with a lifetime of 292 ns (0.32 mOD) is CR between  $PhQ_A^{-}$  to  $P_{700}^{+}$ . The 832  $\mu$ s (1.1 mOD) is CR between  $P_{700}^{+}$  and  $F_X^{-}$ . The third kinetic component of 68 ms (3.0 mOD) which is the usual back ET from  $[F_A/F_B]^{-}$  to  $P_{700}^{+}$ . The long-lived lifetime component of 1.32 s (2.0 mOD) is the reduction of  $P_{700}^{+}$  by DCPIP. There is a 9 %

reduction in quantum yield of CS in this mutant as compared to WT. In PsaB-N591M, which is on the dominant A-branch has a CS quantum yield of 84 %. Its 820 nm decay of  $P_{700}^{+}$  has three kinetic phases, as depicted in figure 4.3. The 27.7  $\mu$ s (1.0 mOD) is the back ET from  $PhQ_A^{-}$  to  $P_{700}^{+}$ . Charge recombination between  $P_{700}^{+}$  and  $[F_A/F_B]^{-}$  has a lifetime of 68.5 ms with an amplitude of 1.5 mOD. The long-lived phase of 1.26 s (1.1 mOD) is a reduction of  $P_{700}^{+}$  by DCPIP as presented in table S4.2.

The ns-ms transient absorption spectroscopy at both 480 and 820 nm shows a decrease in quantum yield of CS in PSI from both cyanobacteria and algae. This change is due to modulation of the energy trap at the site of ec2 cofactor on the mutated branch. The effect of mutation is more noticeable on A-branch than on B-branch. The difference in the ns- $\mu$ s kinetic phases between the two species is present only at 820 nm. These differences are due to the presence of outer antenna (LHC1) in *C. reinhardtii*, which is absent in *Synechocystis sp.* PCC 6803. There are also some minor back ET from PhQs and ec3 cofactor of the RC in *Synechocystis sp.* PCC 6803 but absent in *C. reinhardtii* PSI mutants. The untrapped energy in the RC is lost to the ground state by a new mechanism as there is no formation of  $^3P_{700}$  state in these mutants from both species. Thus, we measure the different radical pair formation and any possible  $^3P_{700}$  state generation through EPR spectroscopy at room and cryogenic temperatures.

**Table 4.2.** Rates and amplitudes of decay components in the ns-s at 820 nm in various purified PS1 preparation (*C. reinhardtii* and *Synechocystis sp.* PCC 6803). <sup>1</sup>Assumed to be 100 %. Quantum yields in the mutants are expressed as relative to WT.

Mutation	P <sub>700</sub> <sup>+</sup> decay components	Assignment	Φ at 820 nm [ms component] (%)
WT ( <i>C. reinhardtii</i> )	2.1 mOD, 70 μs	( <sup>3</sup> Chl)	100 <sup>1</sup>
	3.0 mOD, 50 ms	[F <sub>A</sub> /F <sub>B</sub> ] <sup>-</sup> → P <sub>700</sub> <sup>+</sup>	
	0.94 mOD, 770 ms	DCPIP → P <sub>700</sub> <sup>+</sup>	
WT ( <i>Synechocystis sp.</i> PCC 6803)	5.0 mOD, 49.9 ms	[F <sub>A</sub> /F <sub>B</sub> ] <sup>-</sup> → P <sub>700</sub> <sup>+</sup>	100 <sup>1</sup>
	2.3 mOD, 1.31 s	DCPIP → P <sub>700</sub> <sup>+</sup>	
PsaA-N604L ( <i>C. reinhardtii</i> )	1.4 mOD, 182 μs	( <sup>3</sup> Chl)	76
	2.1 mOD, 61 ms	[F <sub>A</sub> /F <sub>B</sub> ] <sup>-</sup> → P <sub>700</sub> <sup>+</sup>	
	0.90 mOD, 674 ms	DCPIP → P <sub>700</sub> <sup>+</sup>	
PsaA-N604L ( <i>Synechocystis sp.</i> PCC 6803)	0.57 mOD, 453 ns	A <sub>0B</sub> <sup>-</sup> → P <sub>700</sub> <sup>+</sup>	71
	0.43 mOD, 1.86 ms	F <sub>X</sub> <sup>-</sup> → P <sub>700</sub> <sup>+</sup>	
	2.5 mOD, 58.4 ms	[F <sub>A</sub> /F <sub>B</sub> ] <sup>-</sup> → P <sub>700</sub> <sup>+</sup>	
	1.7 mOD, 1.33 s	DCPIP → P <sub>700</sub> <sup>+</sup>	
PsaB-N591L ( <i>C. reinhardtii</i> )	1.4 mOD, 120 μs	( <sup>3</sup> Chl)	56
	1.7 mOD, 53 ms	[F <sub>A</sub> /F <sub>B</sub> ] <sup>-</sup> → P <sub>700</sub> <sup>+</sup>	
	0.50 mOD, 570 ms	DCPIP → P <sub>700</sub> <sup>+</sup>	
PsaB-N591L ( <i>Synechocystis sp.</i> PCC 6803)	1.0 mOD, 27.7 μs	A <sub>1A</sub> <sup>-</sup> → P <sub>700</sub> <sup>+</sup>	49
	1.5 mOD, 68.5 ms	[F <sub>A</sub> /F <sub>B</sub> ] <sup>-</sup> → P <sub>700</sub> <sup>+</sup>	
	1.1 mOD, 1.26 s	DCPIP → P <sub>700</sub> <sup>+</sup>	

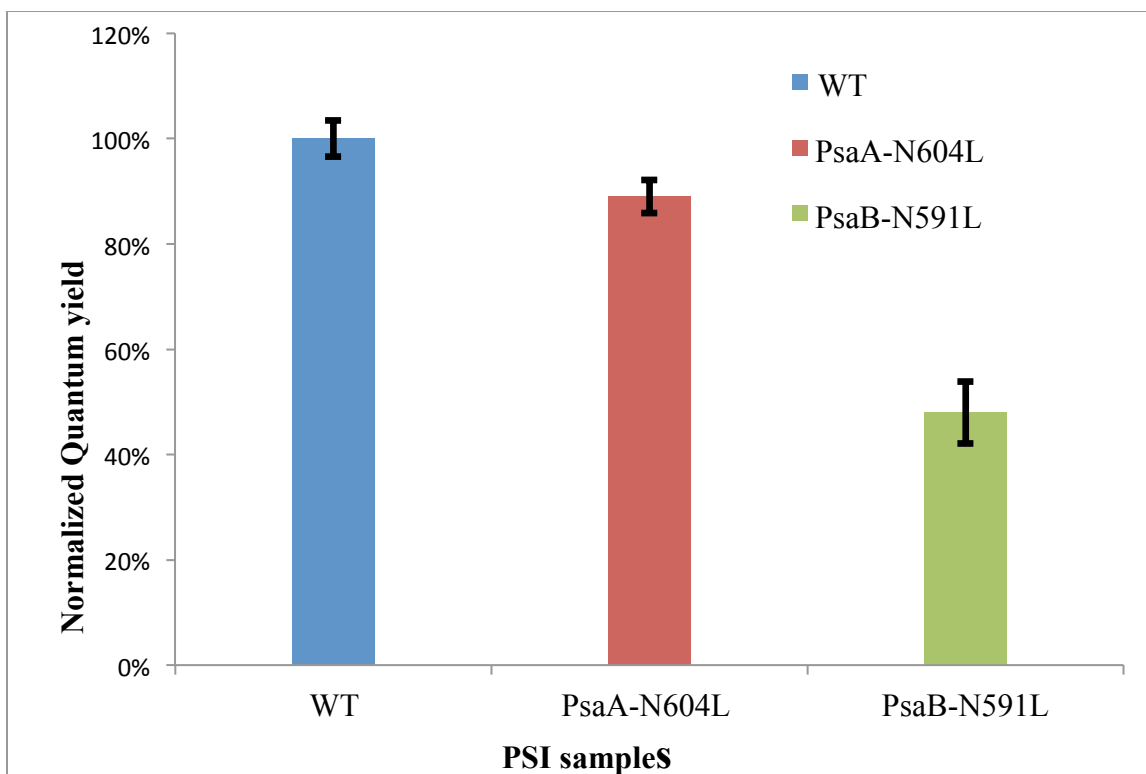


**Figure 4.3.** Transient absorbance difference traces at 820 nm for PS I complexes from *C. reinhardtii* (left column) of WT; PsaA-N604L and PsaB-N591L mutants. The 820 nm

decay kinetic of PSI from *Synechocystis sp.* PCC 6803 (right column) WT; PsaA-N604L and PsaB-N591L mutants. The wild-type, PsaA-N604L, and PsaB-N591L mutants are shown in the top, middle, and bottom row, respectively. The Chl concentration is 100  $\mu\text{g ml}$  for both species. The data sets, which were collected at time windows of 1 ns to 1  $\mu\text{s}$ , and from 1  $\mu\text{s}$  to 100  $\mu\text{s}$ , and from 100  $\mu\text{s}$  to 100 ms too were stitched together to portray multiple kinetic phases on one plot. The absorbance values are plotted on a log scale, and were fitted using a multi-exponential decay. The experimental data are shown as points and the fit is shown as the solid line. The differences between experimental and fit data are plotted as a residual. The data sets were from 64 averages.

#### 4.3.3 Quantum Yield of Charge Separation

We also measure the amount of stable charge separation in *C. reinhardtii* WT PSI particles and the two mutants PsaA-N604L and PsaB-N591L at 810 nm using transient absorption spectrophotometer of JTS-10. At 810 nm, we monitored the formation and decay of  $\text{P}_{700}^{+}$ . The amount of positive absorption in the transient of WT is calculated and considered as 100% ( $\pm 3.4$ ), as presented in figure 4.4. In PsaA-N604L, the level of quantum yield of CS decreased to 89% ( $\pm 3.1$ ) as compared to WT on the basis of the same amount of chlorophyll. The PsaB-N591L had a more profound effect on the energy trap and reduced the quantum yield of CS to 48 % ( $\pm 5.9$ ). These results agreed with other transient spectroscopic results and showed that excitation energy is lost at the ec2 cofactor site due to mutation.



**Figure 4.4.** The amount of stable charge separation in WT; PsaA-N604L and PsaB-N591L PSI particles. For each sample 10  $\mu\text{g/mL}$  of PSI was taken and a saturating laser flash of 532 nm was used for excitation of the sample. Light induced changes were monitored through 810 nm weak probe LED pulses.

#### 4.3.4 Room Temperature Transient EPR Spectroscopy

We performed room temperature transient X-band EPR spectroscopy for ec2 mutants to monitor the activity of ET in both branches of PSI. The advantage of doing transient EPR at room temperature over low temperature is that we can measure the kinetics and ratio of ET between the two branches and down the iron-sulfur clusters. In this method, the PSI sample is irradiated continuously with weak power microwaves and the time-resolved EPR response is measured after a laser flash. The transients are measured at a range of magnetic field positions, making a time/field data set from which the EPR spectrum at a

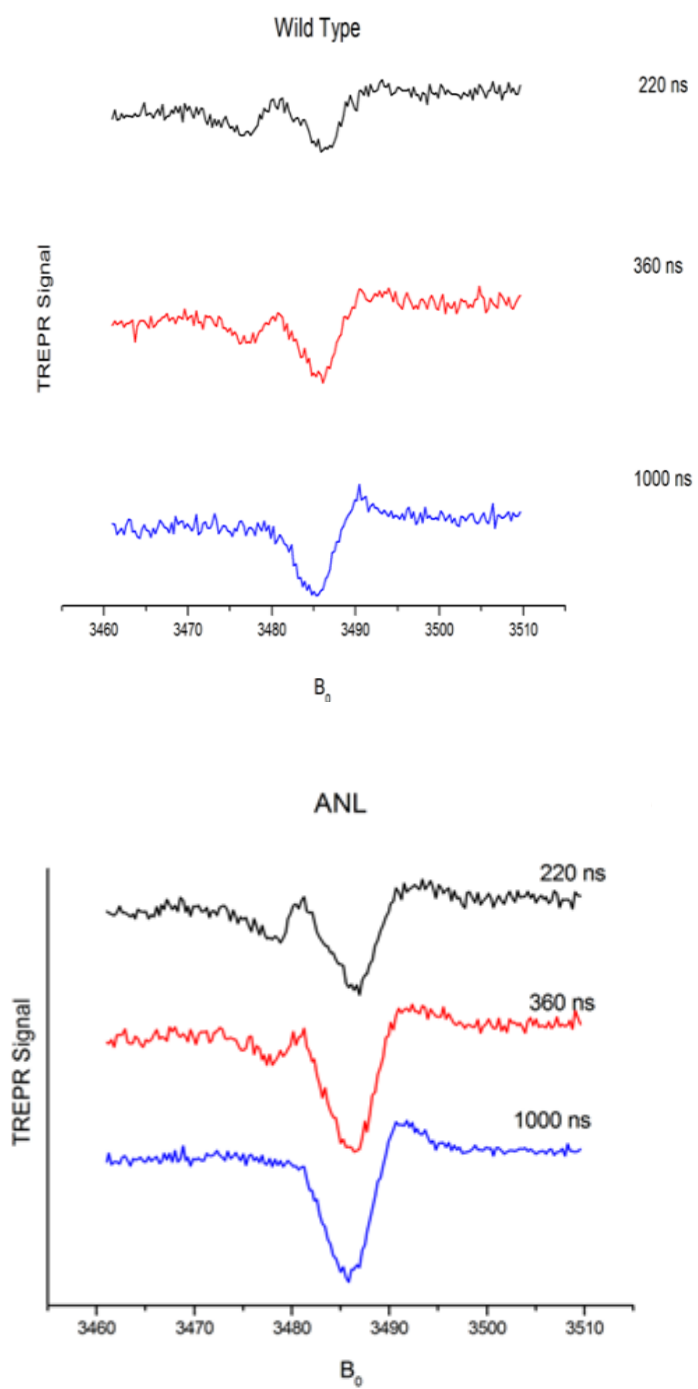
given time can be calculated (118). Figure 4.5 shows the transient EPR signal at 220 ns, 360 ns and 1000 ns after the laser flash from *C. reinhardtii* PSI samples of WT and Asn to Leu mutants. In the case of WT and PsaA-N604L there are two emissive (negative) signals observed at 220 ns. The one at lower magnetic field is a contribution from  $P_{700}^{+}\text{PhQ}^{-}$ , while the signal at the upper field mainly originates from the  $P_{700}^{+}\text{FeS}^{-}$  radical pair. As electron transfer from  $\text{PhQ}_A^{-}$  towards  $F_X$  occurs, the  $P_{700}^{+}\text{PhQ}^{-}$  RP signal decays and  $P_{700}^{+}\text{FeS}^{-}$  signal evolves. In PsaA-N604L, at 220 ns the  $P_{700}^{+}\text{PhQ}^{-}$  RP should be larger than that of WT but here it is not the case due to low S/N ratio of EPR instrument. For PsaB-N591L mutant, there was no signal of RP.

The room temperature X-band EPR spectroscopic results of *Synechocystis sp.* PCC 6803 were very encouraging, as shown in figure 4.6 and figure S4.4. The transient EPR signal at 240 and 1000 ns are shown in the upper panel, and the kinetics signal extracted at two magnetic field positions “a” and “ b” are in the lower panel. The WT sample at 240 ns gives the usual EAE spin polarization pattern, where E = emission and A = absorption. This signal arise from the  $P_{700}^{+}\text{PhQ}_A^{-}$  RP. At later times, as the electrons moves pass PhQ towards the FeS cluster, the emissive signal is mainly from  $P_{700}^{+}$  part of the  $P_{700}^{+}\text{FeS}^{-}$  RP. The special spectral marker at the left side in the form of a shoulder in the absorptive polarization pattern of  $P_{700}^{+}\text{PhQ}_A^{-}$  RP represents the y-axis hyperfine splitting of the C-3 protons of the methyl group. It arises due to the asymmetric distribution of the electronic density on the phylloquinone ring. This electronic density is high at the quinone carbon near to the methyl group. By comparing the PsaA-N604L to the WT EPR spectrum, the first thing that is distinctive is the 240 ns transient signal of

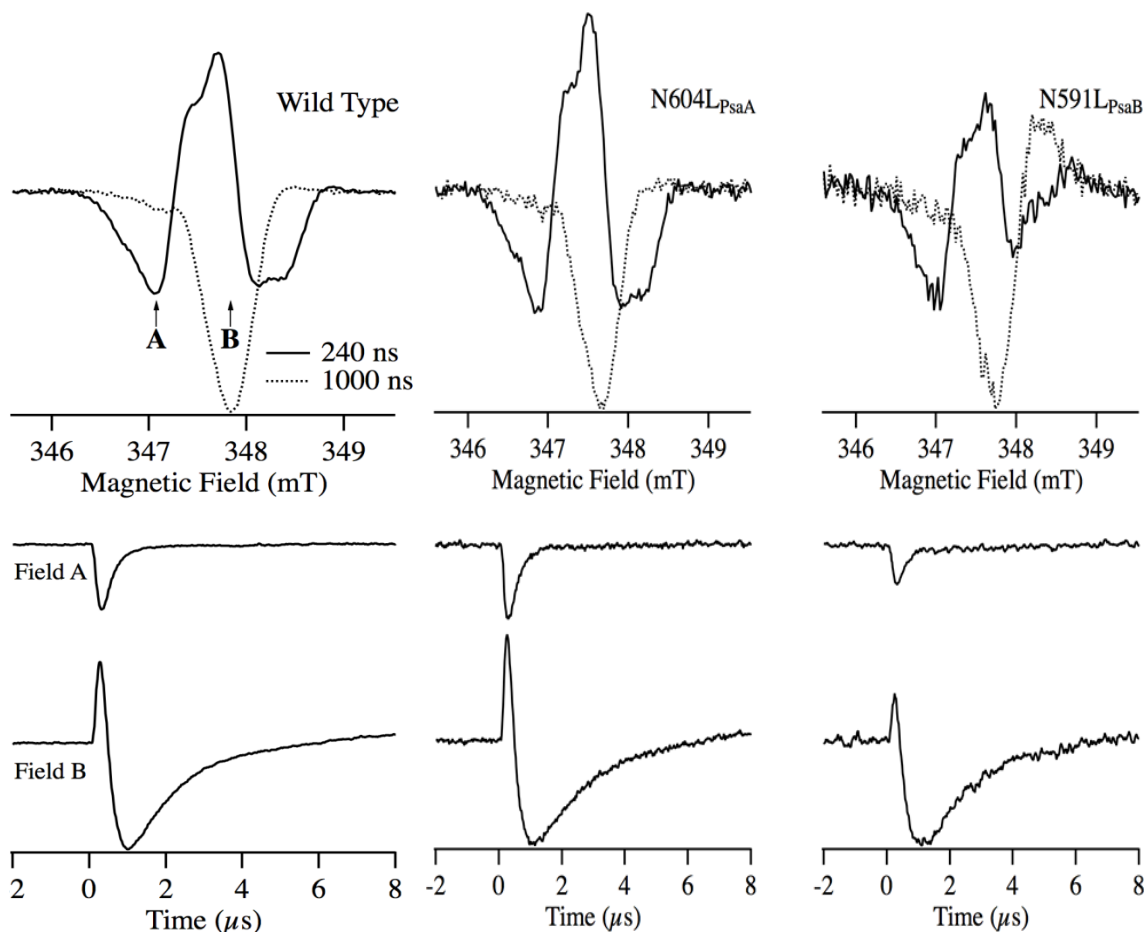


$P_{700}^{*+}PhQ_A^{-}$ RP, which is larger in amplitude. This increase arises when the B-side ET is blocked or inhibited, and ET occurs mostly on A-branch (53). Thus, electrons escape on the B-branch PhQ is beyond the detection limit due to the low time resolution of EPR and creates the negative emissive signal of  $P_{700}^{*+}FeS^{-}$  RP. In the 1000 ns transient, the  $P_{700}^{*+}FeS^{-}$  RP signal is of same the magnitude like WT but at the side the low S/N ratio is evident. The transient collected at the two field positions also revealed that the level of  $PhQ_A^{*+}$  is more than that of WT at the earlier time. The room temperature transient EPR spectrum of PsaB-N591L exhibited a decrease in the  $P_{700}^{*+}PhQ_A^{-}$  signal representing the blockage of A-side ET. Further, the later 1000 ns spectrum representing  $P_{700}^{*+}FeS^{-}$  RP is lower and has low S/N ratio as compared to WT. This decrease in RP formation is also evident from the two transient taken at position “a” and “b”. The influence of PsaB-N591L is large on the A-branch that results into decrease in the CS process.

We also monitor the room temperature EPR for Psa-N604M and PsaB-N591M pair and PsaA-N604H; PsaB-N591 pair, where the PsaB-N591M reveals a bit noisy spectra showing a decrease in the quantum yield. The PsaA-N604H spectra and the transients at two field positions are similar to WT, as presented in figure S4.4. While PsaB-N591H has similar spectra like PsaB-N591L revealing a decrease in A-side ET as the 240 ns  $P_{700}^{*+}PhQ_A^{-}$ RP and the 1 $\mu$ s  $P_{700}^{*+}FeS^{-}$ RP is lower in amplitude and has low S/N ratio. These results supported the optical transient spectroscopic data and revealed that the mutation only affect the quantum yield while they have no effect on the redistribution of ET between the two branches nor on their rate.



**Figure 4.5.** Spin polarized X-band room temperature transient EPR spectroscopy of PSI particles from WT and PsaA-N604L mutant affecting  $ec2_B$  of B-branch.



**Figure 4.6.** Spin polarized X-band room temperature transient EPR spectroscopy of PSI particles from *Synechocystis sp.* PCC 6803 WT and PsaA-N604L mutant affecting ec2<sub>B</sub> of B-branch and PsaB-N591L which is affecting ec2<sub>A</sub> of A-branch.

#### 4.3.5 Low-temperature TREPR Spectra of $P_{700}^{+\bullet}\text{PhQ}^-$

Excitation of PS1 produces the  $P_{700}^{+\bullet}\text{PhQ}^-$  state, in which the spins of the two radicals are correlated, having originated from the initial charge separation event. This gives rise to strong EPR signal from the spin-correlated radical pair. Previous work has shown that at low temperature, the signal is from  $P_{700}^{+\bullet}\text{PhQ}_A^-$ , with almost no contribution from the other radical pair ( $P_{700}^{+\bullet}\text{PhQ}_B^-$ ). Further, the electron transfer from the quinone to  $F_X$  is blocked at low temperature. Thus, at low temperature, this technique should report upon the efficiency of charge separation in the A-branch (85). Figure 4.7 displays the X-band transient EPR spectrum of WT and PsaA-N604L and PsaB-N591L pair of mutants from *C. reinhardtii* at 80 K. The WT spectrum shows a spin polarization pattern of E/A/E and looks very similar to spectra reported in the literature for *C. reinhardtii* PSI (50, 92). On the low-field side, the absorptive peak has a shoulder representing the partially resolved methyl hyperfine coupling (hfc) from PhQ. This shoulder also plays a big part in determining the width of the central peak in the spectrum. The effect of the methyl hfc is more along the C-CH<sub>3</sub> bond, as the methyl group is electron withdrawing, so electron density is more concentrated at the C-CH<sub>3</sub> bonding position. Furthermore, this coupling is close to the Y-axis of the  $\text{PhQ}^-$  g-tensor. When the magnetic field is along this axis during measurement, then the methyl hfc is partially resolved in the middle absorptive peak of the  $P_{700}^{+\bullet}\text{PhQ}_A^-$  TR-EPR spectrum. The methyl hfc is sensitive to the local environment and provide insight into the asymmetry of the spin density distribution over the  $\text{PhQ}^-$  radical (91, 116). This shoulder is smaller in *C. reinhardtii* PSI as compared to cyanobacterial PSI (89, 117). In WT PSI, the signature of the methyl hfc can be clearly

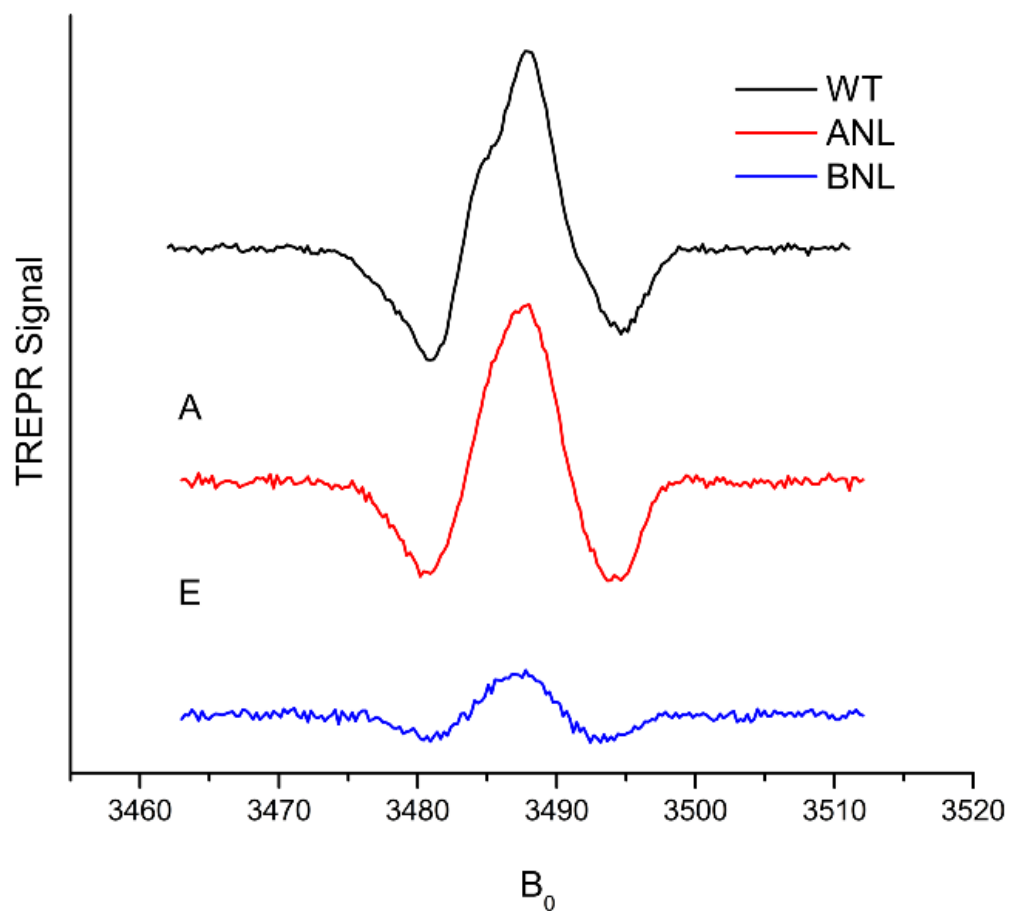
observed. It is smaller in PsaB-N591L mutants, but entirely absent in PsaA-N604L. Secondly the spectral width of WT can be used for comparison here, which has the low field emissive bleaching peak near 3482 T while the upper field emissive bleaching peak is near 3495 T. The spectral width and positions of the emissive bleaching peaks of  $P_{700}^{+}\text{PhQ}^{-}$  in the WT and mutants are the same. The third important character is the Signal/Noise (S/N) ratio of the  $P_{700}^{+}\text{PhQ}^{-}$  RP signal as an indicator of the CS activity of ET in each mutant. The decrease in the S/N ratio seen in the PsaB-N591L shows that these mutants have lower CS on the A-branch, consistent with optical spectroscopic results shown earlier.

We also performed X-band and Q-band EPR spectroscopy at low temperature of 80 K on the *Synechocystis sp.* PCC 6803 WT; PsaA-N604L and PsaB-N591L samples to analyze ET activity (Figure 4.8, and 4.9). The WT PSI in X-band spectrum reveals the usual spectral characteristics of  $P_{700}^{+}\text{PhQ}_A^{-}$  with EAE polarization pattern and a partially resolved methyl hyperfine coupling in the absorptive peak of phylloquinone as shown in figure 4.8. In the Q-band, the WT has E/A/A/E/A polarization pattern at low-temperature. Here E=emissive and A=absorptive spin-polarized patterns, indicating the  $P_{700}^{+}\text{PhQ}_A^{-}$  RP (figure 4.9). In the case of PsaA-N604L, the spectrum at X-band is similar to the WT but the Q-band is different in terms of the absorptive peak and shoulder of methyl hfc of  $\text{PhQ}_A$ . This better resolution points towards the inhibition of CS on B-branch due to mutation. This spectrum reveals that at cryogenic temperature, there is further decrease in ET towards  $F_X$  that results in the evolution of a fine  $P_{700}^{+}\text{PhQ}_A^{-}$  spectrum. The same observation also holds correct for PsaA-N604M and PsaA-N604H

(Data not shown). PsaB-N591L of cyanobacteria also showed electron transfer activity at low temperature but as can be seen in both X and Q-band spectra the level of S/N ratio is low. This lower S/N ratio of the spectrum depicts the lower quantum yield of CS, and the signal of  $P_{700}^{*+}PhQ_A^{\bullet-}$  is smaller but better than that of *C. reinhardtii* PsaB-N587L sample. This low S/N ratio is also observed in the PsaB-N591M and PsaB-N591H sample (Data not shown). The low-temperature EPR analyses also showed that the mutation near ec2 blocks the formation of RP and it is more on evident on the A-branch mutants as compared to the B-branch in both green algae and cyanobacteria.

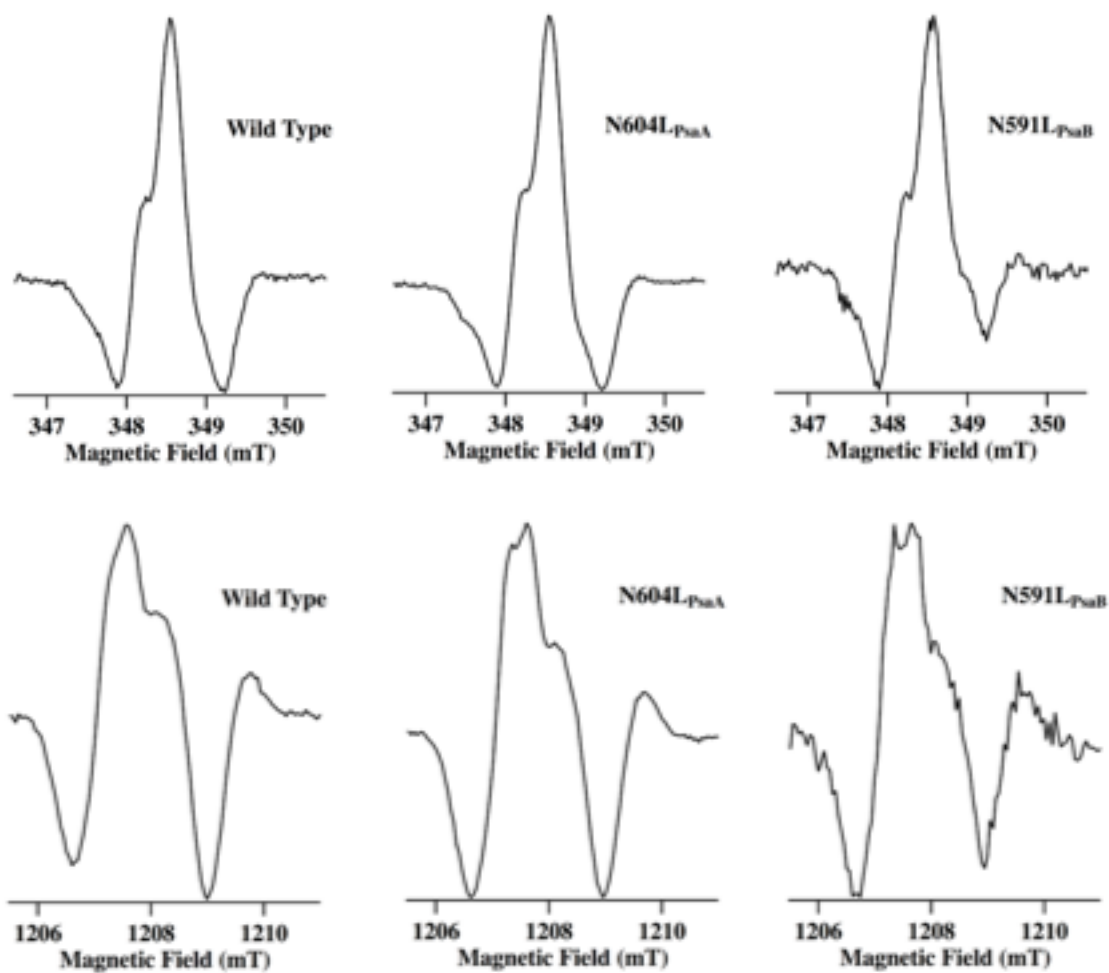
From the transient optical spectroscopy and room temperature EPR spectroscopy it was found that the mutation near ec2 on both branches results into decrease in quantum yield of stable charge separation. Although the transient optical spectroscopy at 820 nm exhibited very low charge recombination (CR) between  $P_{700}^{*+}ec3^{\bullet-}$  but to investigate the loss of excitation energy further we are also analyzing the low-temperature EPR spectra of these mutants for the formation of triplet state of  $P_{700}$  ( $^3P_{700}$ ) and antenna chlorophylls ( $^3Chl$ ). The formation of  $^3P_{700}$  states occurs from back ET in  $P_{700}^{*+}ec3^{\bullet-}$ . The  $^3Chl$  are generated either due high excitation or when the RC is closed due to CS. The  $^3Chl$  is very harmful as it generates singlet oxygen ( $^1O_2$ ) species that damage the protein. The carotenoids present in the antenna quenches the energy from  $^3Chl$  by forming the carotenoid triplet state ( $^3Car$ ) that disposes off its energy to the protein environment instead of building  $^1O_2$  state. In low temperature X-band spin-polarized transient EPR spectra of *C. reinhardtii* WT; PsaA-N604L and PsaB-N591L there is a good number of  $^3Chl$  states populated (Figure S4.4). The amount of  $^3Chl$  is

three-fold higher in PsaA-N604L and PsaB-N591L than that of WT; however there is the absence of the  $^3P_{700}$  in all the samples. These results agree with that of the transient absorption spectroscopy with nanosecond-millisecond time resolution of the same PSI samples. The  $^3Chl$  are generated due to the presence of free chlorophylls and unattached LHCI, and its amount is more in the mutants as compared to the WT. We also found this free LHCI in the TCSPC fluorescence measurements of these PSI particles. Figure S4.5 shows the spin-polarized transient EPR spectra of WT; Asn to Leu and Asn to His pairs of mutants near ec2 at 80 K from *Synechocystis sp.* PCC 6803. The central peak represents the  $P_{700}^{*+}PhQ^{\bullet-}$  RP. As can be seen in the WT and all the mutants, there is the absence of  $^3P_{700}$  state and  $^3Chl$  state. These results provide the evidence that the unused excitation energy is lost to the protein bath through some new process due to mutation.



**Figure 4.7.** Low temperature spin polarized X-band transient EPR spectra of WT, PsA-N604L and PsB-N591L mutants PSI particles of *C. reinhardtii* recorded at 80 K.





**Figure 4.8.** Low temperature spin polarized X-band (upper row) and Q-band (lower row) transient EPR spectra recorded at 80 K for WT, PsaA-N604L; PsaB-N591L PSI particles from *Synechocystis sp.* PCC6803.

#### 4.3.6 Ultrafast Transient Absorption Spectroscopy

Figure 4.9 shows the transient absorption difference spectra (DS) of WT and mutant PSI from *C. reinhardtii* (Left column) from 1 ps to 303 ps and *Synechocystis sp.* PCC6803 (right column) from 0.5 ps to 291 ps after the pump pulse. In *C. reinhardtii* WT, the prompt decrease in bleaching between 1 and 10 ps showed that the excitation energy of antenna is transferred to the RC. During the early few picoseconds, energy transfer and equilibration process is complete and the equilibrated excited state of reaction center (RC\*) is ready to trap the excitation energy. The initial trapping of excitation energy into charge separation (CS) starts within the 10 ps time scale [figure 4.9]. The time resolved spectra (TRS) at the 29 ps gives a clear indication of  $P_{700}^{+}$ , which is the secondary electron transfer step is initiated by forming a stable secondary radical pair (RP2). It has two bands one around 695nm to the red edge of the spectrum representing the cationic state of  $P_{700}$  and 680 to 682 nm band of the  $ec3^{-}$  anion formation or simply the  $ec3$  chlorophyll absorption. At 29 ps time delay after excitation, the 681 and 696 nm bands have the same amplitude but with the passage of time the 681 nm band decreases in amplitude and the 696 nm band becomes dominant. This difference spectrum with 696 nm bleaching band is fully established at 303 ps, and this doesn't change until 2 ns, which is the time window of our instrumentation measurement. The forward electron transfer from PhQ occurs in the timescale of tens to hundreds of ns, most of the long-lived spectra at later timescale will represent  $P_{700}^{+}PhQ^{-}$ .

In *Synechocystis sp.* PCC6803 WT, the transient absorption spectra at 0.5 ps shows a broad bleaching between 675 and beyond with a maximum at 702 nm,

representing a loss of the ground state upon excitation of the core antenna. There is positive absorption between 620 nm (and below) to 675 nm, most likely due to excited state absorption(64, 65). The bleaching of antenna decreases as the excitation energy moves from the core to the RC. In the 3 ps transient DS there is development of a shoulder at 691-692 nm, representing the formation of the radical pair. The 10 ps transient DS shows two bleaching bands at 687 nm and 703 nm separated by a peak at 692. As the electron is transferred further down the branch and stable  $P_{700}^{+}PhQ^{-}$  is formed, we see the characteristic light-induced ( $P_{700}^{+} - P_{700}$ ) DS like WT PSI of *C. reinhardtii*.

In *C. reinhardtii*, the PsaA-N601L transient difference spectra mostly look like WT but the bleaching bands are thinner in width and become smaller in amplitude at later time as compared to WT. In the 29 ps spectrum, we can see the formation of stable  $P_{700}^{+}$  state and a smaller band of ec3 chlorophyll for PsaA-N604. The decrease in amplitude in the later transient DS showed inhibition of charge separation due to mutation. The transient DS in the PsaA-N604L mutant of *Synechocystis sp.* PCC6803 also appear somewhat similar to its WT, but with a drop in stable CS, as presented in figure 9. This increase blockage of CS is evident in the A-branch Asn to Leu mutation in both the species. The PsaB-N591L mutant has two clear bands at three ps but at later delay times the one on the red edge of the spectrum is present while the blue one is absent. The later spectra of PsaB-N591L have fluctuation by going up and down. This fluctuation is due to the scattering process in the during measurement as this mutant is more unstable than that of PsaA-N604L and PSI particles aggregates after an hour. The main information from

the amplitude of 29 to 303 ps time-resolved spectra showed that the mutation affecting the A-branch has lower quantum yield in terms of charge separation. Similarly, the shapes of the transient DS in PsaB-N591L mutant of cyanobacteria are similar to WT, but the inhibition of CS is similar to that in the PsaA-N591H mutant (Figure S4.4). Although a prominent shoulder in the red region is not obvious in these two mutants, there is the hint of a shoulder in the early DS of both Asn to Leu mutants from *Synechocystis sp.* PCC6803.

In the case of the PsaA-N604H and PsaB-N591H mutants (Figure S4.7), there are two peaks at the beginning after sample excitation. For PsaA-N604H, the maximum bleach is also at 702 nm, but there is a prominent shoulder centered at ~716 nm, which is absent in the WT. It persists for ~three ps and then disappears. While the rest of the spectral changes are similar to those in WT, the amplitude is lower. We interpret this as an inhibition of charge separation due to mutation at the site of ec2 Chl. A similar red shoulder also appears in the PsaB-N591H mutant, but in this case the inhibition of CS is so extreme that the long-lived  $P_{700}^{+}PhQ^{-}$  DS are difficult to observe. These observations showed that a mutation near ec2 cofactor is affecting the efficiency of the trap. The exciton absorbed by the PSI particles are not fully used and wasted as compared to the WT, which trapped it in the form of stable charge-separated state. These time-resolved difference spectra of the mutants give information about the branch usage for energy trapping and electron transfer. These results hint that ec2 chlorophyll on each branch works independently, and both branches are active in terms of energy trapping and electron transfer.

We performed global analyses of the femtosecond transient absorption data to extract the kinetics of different spectral components (e.g. antenna excitation, energy equilibration/transfer, trapping and formation of different transient radical pair). The global analyses here represent a fitting of the whole data by 3 or 4 components, where each component has a possible contribution from the previous process or the next one. For example, the energy-trapping component may have a contribution from energy transfer and energy equilibration processes due to the presence of red chlorophylls too. From the DADS, we here only present the energy trapping and non-decaying component for comparison in the *C. reinhardtii* and *Synechocystis sp.* PCC 6803 WT and its mutants (Figure 4.10-4.13). Figure S4.12 and S4.13 shows quality of the fit and kinetics. The lifetime of energy trapping component is 22 ps in WT of *C. reinhardtii* and 25 ps in WT of *Synechocystis sp.* PCC 6803. The energy trapping component mainly represents energy trapping, but it also contains contributions from excited  $RC^*$ , where charge separation can occur on each branch, resulting in the  $ec2_A^+ec3_A^-$  or  $ec2_B^+ec3_B^-$  radical pair. The non-decaying section of the nanosecond lifetime in WT of *C. reinhardtii* and *Synechocystis sp.* PCC 6803 represents the  $P_{700}^+PhQ^-$  difference spectrum. This non-decaying part of the DADS is similar to the P700 difference spectrum of the respective specie as reported in the literature (77, 143). In *C. reinhardtii* WT, the main bleaching band is around 695-696 nm in the non-decaying spectrum and it is at 703 nm in *Synechocystis sp.* PCC 6803. For the normalization purpose both the WT sample amplitude are considered as 100 % of quantum yield of CS (34, 136). For the estimation

of quantum yield of CS, we compared the amplitude of the long-lived component of the mutants with that of the WT, which is 100 % (Table 4.3).

In *C. reinhardtii*, PsaA-N604L has energy trapping lifetime of 21.5 ps and is similar to WT. Though the energy trapping lifetime is not affected by the mutation, the amplitude is almost 40 % decrease in PsaA-N604L as compared to the WT. This mutation is affecting the B-branch, in which ET is around 40-50 % in *C. reinhardtii*. Thus, these mutations affect the trapping efficiency of the respective branch. These results showed that  $ec2_B$  is the primary electron donor and the first cofactor involved in primary charge separation on B-branch (Table 4.1). The counterpart of PsaA-N604L in *Synechocystis sp.* PCC 6803 is PsaA-N604, and it has energy trapping lifetime of 24 ps, which is one ps faster than that of WT. The non-decaying component of PsaA-N604L is smaller in amplitude by around 14 % but due to a baseline shift in the 675 to 720 nm region, we left it unchanged.

The energy trapping component in the DADS of PsaB-N591L from *C. reinhardtii* has lifetime of 27 ps. We remove the unwanted bleaching band at 686 nm in PsaB-N591L, which arise due to scattering from aggregation of particles. The amplitude of the non-decaying component is also 40 % less than that of WT. In *Synechocystis sp.* PCC 6803, the energy trapping component of PsaB-N591L mutation has two broad peaks of similar amplitude centered at 689 nm and 704 nm. We also note that the decay times of the trapping component are significantly longer in the PsaB-N591L mutants, increasing from 25 ps in WT to 42 ps, respectively. The non-decaying component of PsaB-N591L showed a decrease in amplitude due to mutation at  $ec2A$ . The quantum yield of CS in

PsaB-N591L is 36 %, showing most of energy trapping on the A-branch is blocked (Table 4.3). We also analyzed the ultrafast electron transfer in PsaA-N604H and PsaB-N591H pair of mutants from *Synechocystis* sp. PCC 6803. The energy trapping component in PsaA-N604H decreases from 25 ps in WT to 22 ps while, in PsaB-N591H, it is 31 ps. The energy trapping component in the DADS of PsaA-N604H is noticeably different. PsaA-N604H has a main bleaching peak at 692 nm (somewhat red-shifted compared to WT), a shoulder at 702 nm, and a distinct peak at 716 nm (Figure S4. 8). Similarly, the energy trapping spectrum of PsaB-N591H mutant has major bleaching peaks at 688, 704 nm, and 616 nm (Figure S4. 8). The non-decaying component of PsaA-N604H shows 82% CS, and it falls to 44 % in PsaB-N591H (Figure S4.9).

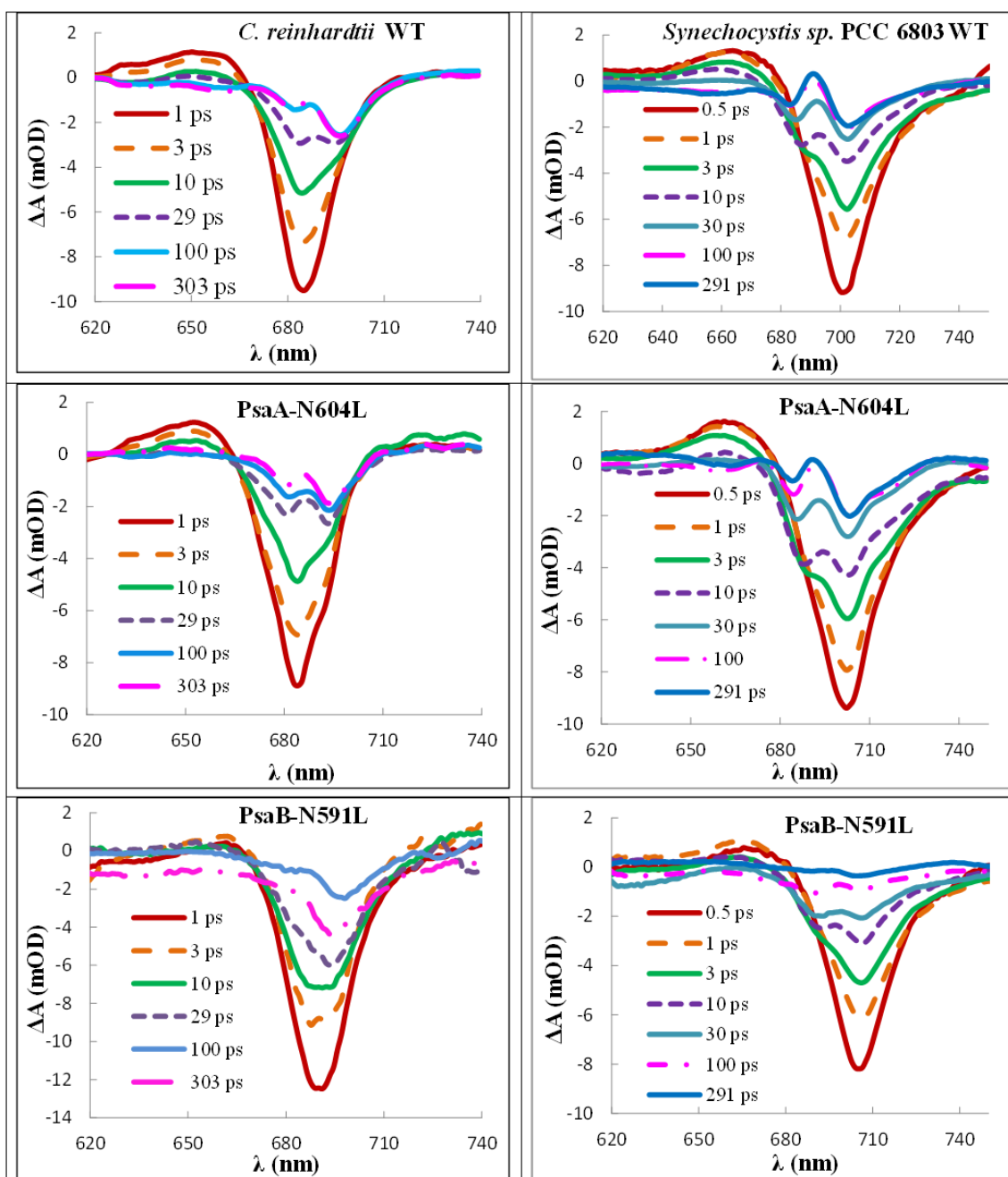
Taken together, these data would indicate that the mutations targeting the ec2 Chls have a profound effect upon energy trapping and initial CS, especially those affecting ec2<sub>A</sub>. If the two ec2-ec3 pairs are competitive traps, then the overall rate of CS reflects CS on the two branches. Furthermore, it would expect that the rate for initial CS within ec2<sub>A</sub>ec3<sub>A</sub> is faster than within ec2<sub>B</sub>ec3<sub>B</sub> since a majority of CS occurs on this side (11, 29). Thus, one would expect that a large loss of the faster CS on the A-branch results in a decrease in overall CS rate. In contrast, a small decrease of the slower CS on the B-branch would result in a slight increase in overall CS rate. This increase in the rate is exactly what we see and is in agreement with the loss of long-lived charge-separated state in the mutants. Furthermore, the substitution of Asn for His on either side results in a marked alteration in the shape of the DADS associated with trapping, most notably a new peak in the 715-720 nm region. The Leu substitution has a somewhat smaller effect.

Consistent with their smaller effects upon trapping rate and quantum yield, the B-side mutations provoke smaller changes in the DADS of the trapping component.

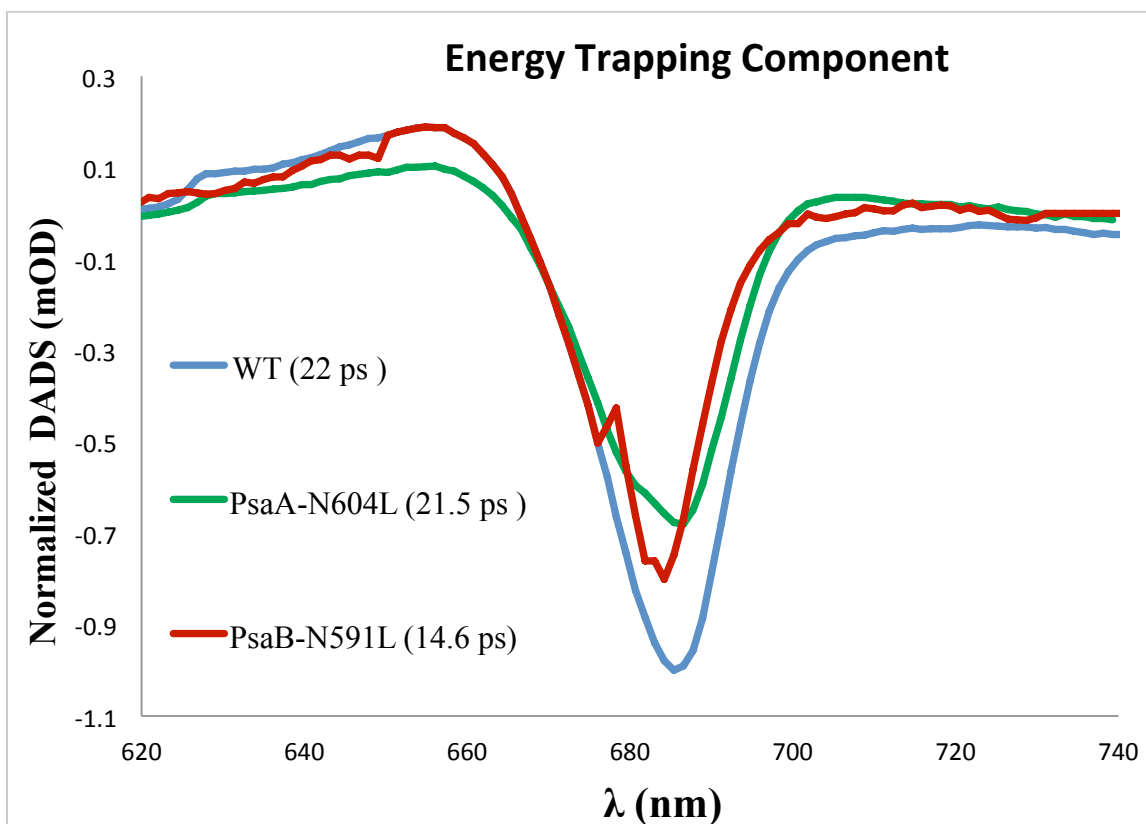
**Table 4.3:** Quantum yield of Charge separation calculated from non-decaying spectra of PSI particles of *C. reinhardtii* at 696 nm and *Synechocystis PCC 6803* at 703 WT and mutants. The maximum bleaching corresponds to  $P_{700}^{+} \text{PhQ}^{-}$  formation after excitation of laser pump. This spectrum looks like the spectrum of  $P_{700}^{+} F_{A/B}^{-}$  but as our time window is 1ns and after 50 ps the RP formed is  $P_{700}^{+} \text{PhQ}^{-}$  so we considered it as the spectrum of  $P_{700}^{+} \text{PhQ}^{-}$ .

Sample	Lifetime of the energy trapping component	Quantum Yield
WT ( <i>C. reinhardtii</i> )	22	100 %
WT ( <i>Synechocystis sp.</i> PCC 6803)	25	100 %
PsaA-N604L ( <i>C. reinhardtii</i> )	21.6	61 %
PsaA-N604L ( <i>Synechocystis sp.</i> PCC 6803)	24	87 %
PsaB-N591L ( <i>C. reinhardtii</i> )	14	61 %
PsaB-N591L ( <i>Synechocystis sp.</i> PCC 6803)	42	36 %

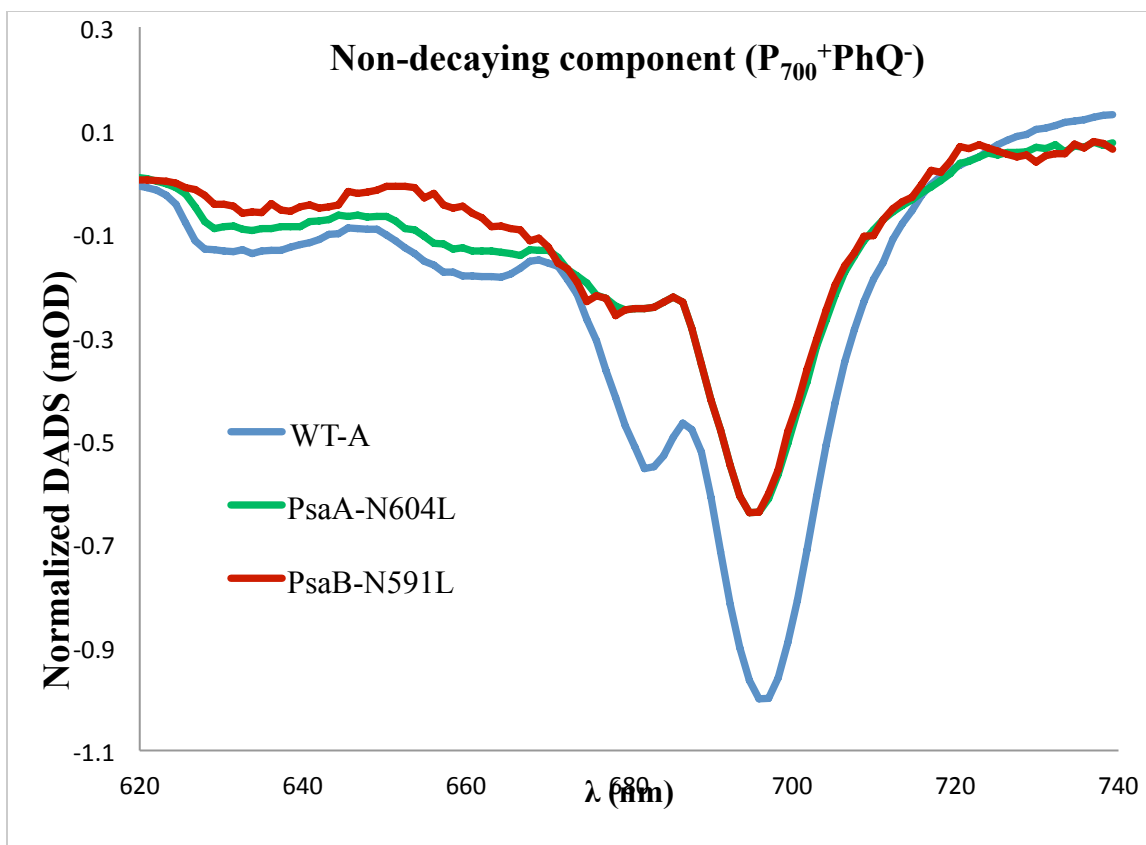




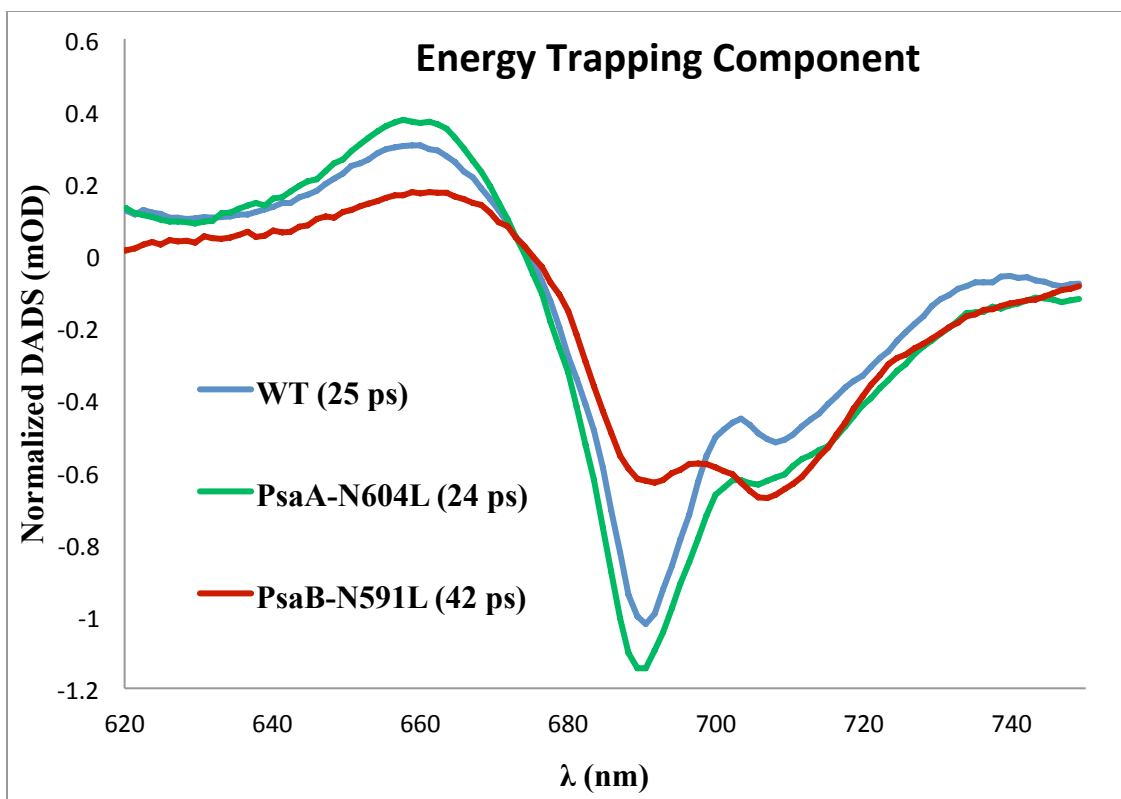
**Figure 4.9.** Transient absorption difference spectra of PSI at different delay times. Left column: shows WT; PsaA-N604L and PsaB-N591L mutants from *C. reinhardtii* obtained by using excitation at 690 nm. The right column presents WT; PsaA-N604L and PsaB-N591L mutants from *Synechocystis sp.* PCC 6803 acquired by using excitation at 700 nm.



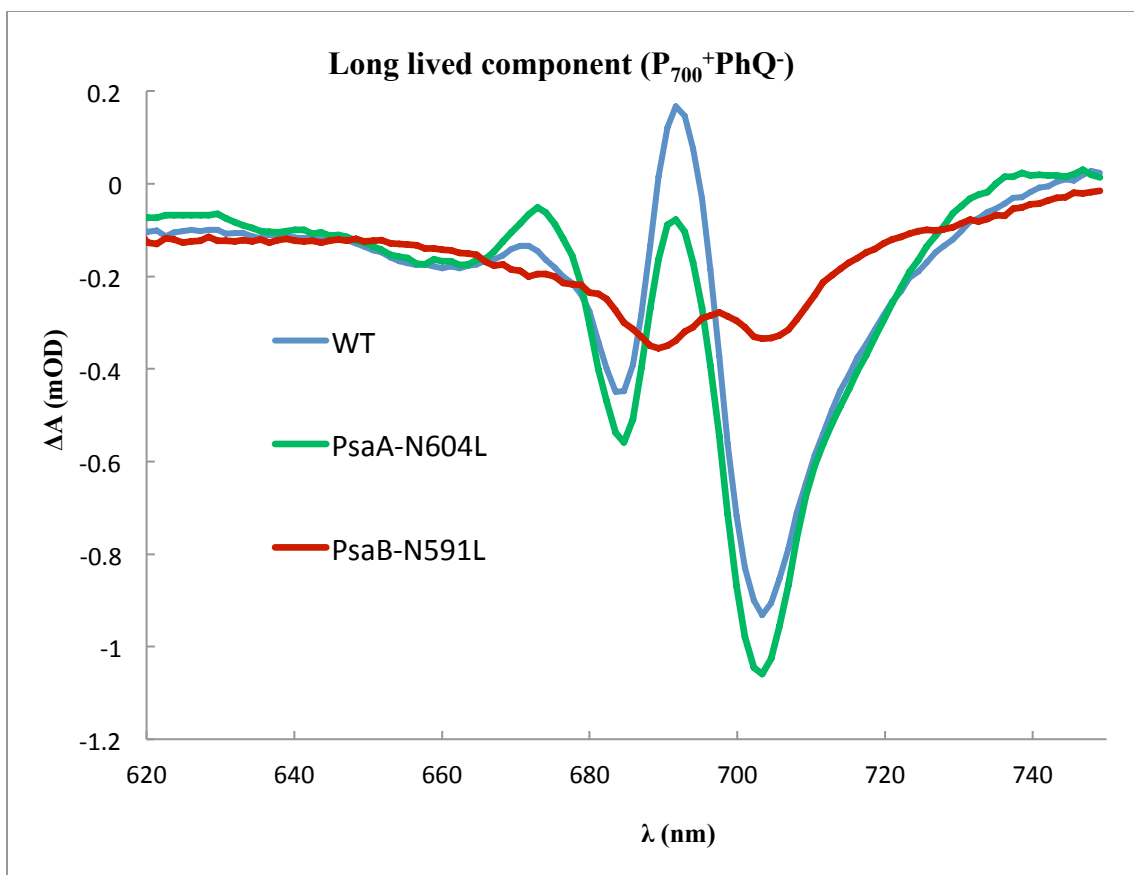
**Figure 4.10.** Energy trapping component of DADS from WT; PsaA-N604L and PsaB-N591L mutant PSI of *C. reinhardtii*. The spectra are normalized to the maximum amount of bleaching in WT.



**Figure 4.11.** Non-decaying component of normalized decay associated difference spectra (DADS) from WT; PsaA-N604L and PsaB-N591L mutant PSI of *C. reinhardtii*. The spectra are normalized to the maximum amount of bleaching in WT.



**Figure 4.12.** Energy trapping component of DADS from WT; PsaA-N604L and PsaB-N591L mutant PSI of *Synechocystis sp.* PCC 6803. The spectra are normalized to the maximum amount of bleaching in WT.



**Figure 4.13.** Long lived component of DADS from WT; PsaA-N604L and PsaB-N591L mutant PSI o *Synechocystis sp.* PCC 6803. The spectra are normalized to the maximum amount of bleaching in WT.

#### 4.3.7 Time-Resolved Fluorescence

Room temperature time-resolved fluorescence was performed using the time-correlated single photon counting (TCSPC) method. This method allows measurement of the energy trapping process along with the lifetime of other components, such as free chlorophylls and uncoupled antenna. An excitation wavelength of 420 nm was used to excite the Soret region of Chl *a*. Figure 4.13 shows three component fit of the time-resolved fluorescence from both *C. reinhardtii* and *Synechocystis sp.* PCC 6803 PSI samples. Decay associated spectra (DAS) of time-resolved fluorescence of the *C. reinhardtii* WT showed a lifetime of around 23.5 ps, 108 ps and  $\geq 3$  ns. The 23.5-ps component is completely positive in amplitude, and its maximum peak is at 700 nm; it is assigned to energy trapping in the RC. The second component has a lifetime of 108 ps. It has very small amplitude and has a maximum peak near 710 nm for both. The amplitude of this component is 36 times lower than the energy trapping component. This component can be assigned to slow excitation transfer to the trap from red chlorophylls. These chlorophylls absorb at longer wavelengths and an uphill transfer of energy from the red chlorophylls occurs before RC trap it (34, 146). The final component has a lifetime of 3-4 ns and positive amplitude near 680 - 690 nm. This component can be assigned to the free LHCI and perhaps free chlorophyll in the sample. The amplitude of this component is 35.5 times lower than the energy trapping component (Figure 4.13). The lifetime of this component was essentially the same in all the preparations, although its amplitude varies in mutants that accumulate PSI poorly, as expected. Thus, this component will not be discussed further in the

mutants. In PSI particles from *Synechocystis sp.* PCC 6803 WT, the dominant component has a 19 ps lifetime and a peak at 700 nm; it represents the energy-trapping process. The DAS of the 63 ps component likely represents slow excitation energy transfer from core antenna red chlorophylls to the RC, as it peaks around 710 - 720 nm. The expected slower decay is due to the uphill energy transfer required to move energy to the trap. The last component has negligible amplitude peaking at ~680 nm and a lifetime of 3.6 ns, and is assigned to decay of excited free Chl. The decay of excitation energy into the energy trapping components are faster in *Synechocystis sp.* PCC 6803 WT than that of the *C. reinhardtii*.

We can predict two possible effects of the mutations upon decay of the excited state. If the mutations simply make the targeted trap less efficient, then they would slow the overall rate of trapping, and this would result as an increase in the trapping lifetime. On the other hand, if the mutations open a new pathway for excited state decay. This new pathway would most likely result into a decrease in the lifetime of decay of the pre-existing component(s) that overlapped temporally with the new process. However, the structure of the *C. reinhardtii* PSI-LHCI super complex and *Synechocystis sp.* PCC 6803 trimeric form are different so other mechanistic possibilities cannot be ruled out. In PsaA-N604L of *C. reinhardtii* the energy trapping component has a lifetime of 22.5 ps, which is 1ps faster than the WT. While the minor slow trapping component has increase in lifetime from 108 to 252 ps. The same point mutation in *Synechocystis sp.* PCC 6803 is PsaA-N604L has increase in the lifetime of both energy trapping components, a fast one has a lifetime of 23.4 ps and the slower one increases to 143.5 ps.

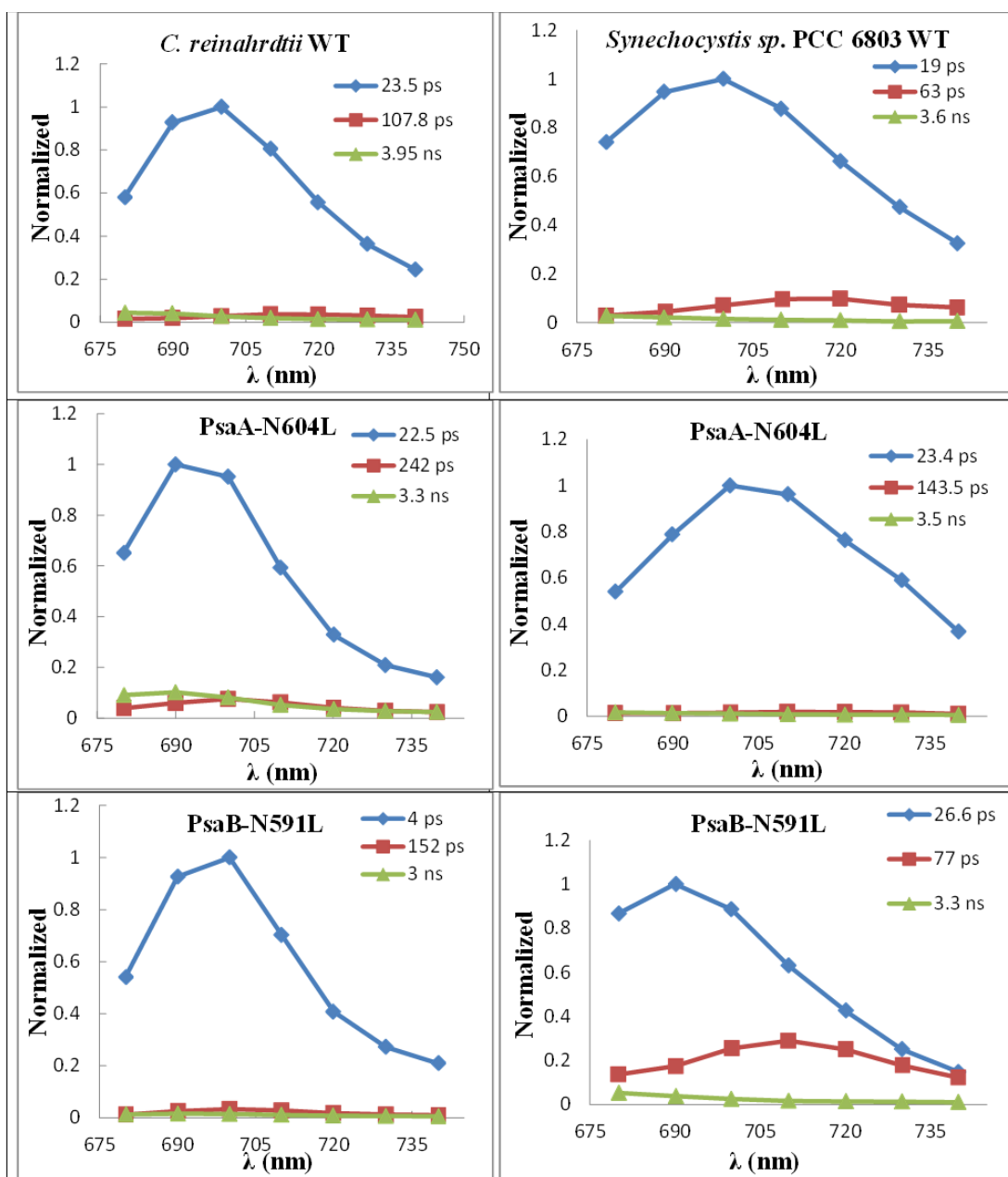
The PsaB-N591L mutation near the  $ec2_A$  of *C. reinhardtii* has a very fast major energy trapping component of four ps, and a minor one is 152 ps. This decrease in excitation energy trapping lifetime points to some other process instead of energy trapping into charge separation process. From the transient absorption spectroscopic results, it was observed that the mutation causes inefficiency of the energy trap in PsaB-N591L and other mutants. The counterpart of PsaB-N591L in *Synechocystis sp.* PCC 6803 is PsaB-N591L, and its fluorescence decay spectrum showed increase in the energy trapping lifetimes. The major fast energy trapping process has a lifetime of 26.6 ps, and a minor one has a lifetime of 77 ps, as presented in figure 13. Thus, PsaB-N591L has a slower decay of excitation energy.

We also examine the Asn to His mutation in cyanobacteria. PsaA-N604H has major energy trapping component with a lifetime of 19.7 ps and the minor one has 54 ps lifetime and looks like WT as shown in figure S 4.10 and table 4.4. The PsaB-N591H also slows down the excitation energy trapping, and the dominant component has lifetime of 31.6 ps, and a minor one is 97.5 ps. We also analyzed monomeric PSI samples, to check the differences between PSI trimer and monomer forms of PSI particles (Figure S 4.12). For WT, the dominant 22 ps component represents trapping in the form of CS. This component was significantly slower in the PsaB-N591L mutant, which also contained a large amount of free Chl. The largest difference between the trimeric and monomeric samples was the increased lifetime of the intermediate component; e.g. in WT, the lifetime increased by a factor of  $\sim 3$ . This behavior has been observed previously (34).



**Table 4.4.** Difference of fast and slow excitation energy lifetime components and the long lived non-decaying component of WT and mutants from *C. reinhardtii* and *Synechocystis* sp. PCC 6803 obtained from DAS using TCSPC.

<b>Sample</b>	<b>fast energy trapping component (ps)</b>	<b>slow energy trapping component (ps)</b>	<b>Long lived uncoupled antenna/Chlorophylls component (ns)</b>
<b>WT-A</b> ( <i>C. reinhardtii</i> )	23.5	107.8	3.9
<b>WT</b> ( <i>Synechocystis</i> sp. PCC 6803)	19	63	3.6
PsaA-N604L ( <i>C. reinhardtii</i> )	22.5	242	3.3
PsaA-N604L ( <i>Synechocystis</i> sp. PCC 6803)	23.4	143.5	3.5
PsaB-N591L ( <i>C. reinhardtii</i> )	4	152	3
PsaB-N591L ( <i>Synechocystis</i> sp. PCC 6803)	26.6	77	3.3



**Figure 4.14.** Decay associated fluorescence spectra (DAS) of PSI particles obtained from global analyses of WT; PsaA-N604L and PsaB-N591L mutants from *C. reinhardtii* in left column. While DAS of WT; PsaA-N604L and PsaB-N591L mutants of PSI trimers from *Synechocystis* sp. PCC 6803. The maximum peak of the fast energy trapping component was considered as 1 and the data was normalized to it.

## 4.4 DISCUSSION

### 4.4.1 The ec2 cofactor as a primary electron donor

Previous mutagenesis studies of the essential electron transfer cofactors of PSI RC exhibits either an increase or decrease in rates of ET on the two branches. The data presented here revealed for the first time that the mutation near ec2 affects the quantum yield of CS on the mutated branch. This experimental confirmation of the ec2 cofactor site involvement in energy trapping on the two branches further strengthens the bi-directionality of ET in PSI. Depending on the branch and type of mutation, mutation near ec2 on the A-branch results into around 40-50 % decrease in ET downstream while it is 20-30 % on the B-branch. This inhibition of CS is evident from a decrease in the electrochromic shift (ECS) or decay of the amplitude of reduced phylloquinone. There were no drastic changes observed in the lifetimes and rates of ET on the ns-ms timescale. While the non-mutated branch is unaffected without causing any change in the amplitude and lifetime of ET on the other branch. The results of Asn to Leu pair of mutants from both cyanobacteria and green algae agrees very well and further supported by Asn to His pair and Asn to Met pair of mutants from *Synechocystis sp.* PCC 6803. Contrary to the previous view that ec2 cofactor cannot be the primary electron donor but might be involved somehow in a primary electron acceptor in combination with ec3 cofactor in the form of a dimer. But here the mutational analysis revealed that ec2 chlorophylls are the redox active cofactors and a change in its electron-phonon coupling results into diminish energy trapping. This decrease in trapping efficiency revealed the modification of the

electronic and vibrational transitions of ec2 cofactor, and it cannot perform its natural efficient trapping function. The decay of untrapped excitation energy due to inefficiency of the trap is also important in terms of its decay route. This new route explains the modification in the ultrafast lifetimes and spectral characteristics of energy trapping component in both transient absorption and time-resolved fluorescence results.

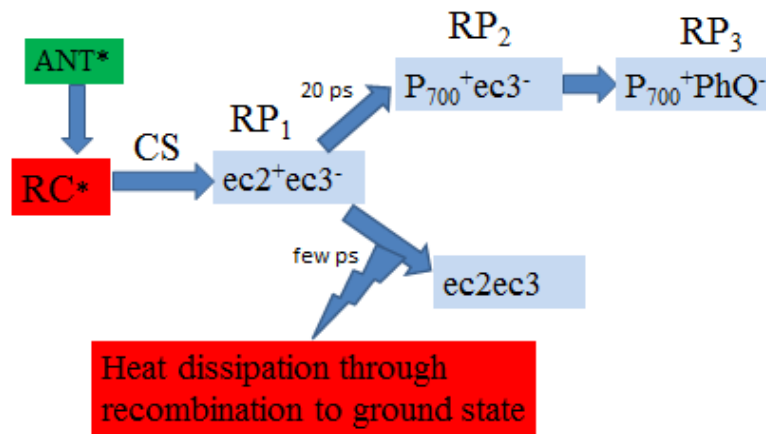
#### 4.4.2 Absence of $^3P_{700}$

The absence of  $^3P_{700}$  in these mutants PSI samples revealed that if there is any unstable CS occurs that the trapped energy for few ps timescale is between ec2ec3 chlorophylls pair on the respective branch. The consequence of this is  $ec2^+ec3^-$  RP formation, which recombine and energy is released to the ground state through the fast proposed channel. This new RP also shows that the  $^3P_{700}$  formation only occurs from charge recombination between  $P_{700}^+ec3^-$  RP, when inhibition of ET occurs beyond ec3. Furthermore, it can also be inferred that these mutations have no direct effect on ec3 cofactor in terms of excitation energy and ET activity. The absence of  $^3P_{700}$  is also evident in these mutants at room temperature as observed from ns-ms transient absorption spectroscopy at 820 nm measurements. In low-temperature transient EPR, where the level of  $^3P_{700}$  state increases due to inactivity of B-branch but this is also negligible in our measurements. This lack of  $^3P_{700}$  showed that opening the fast channel for untrapped excitation energy becomes dominant over that of the  $^3P_{700}$  state route in mutation close to ec2 in PSI.

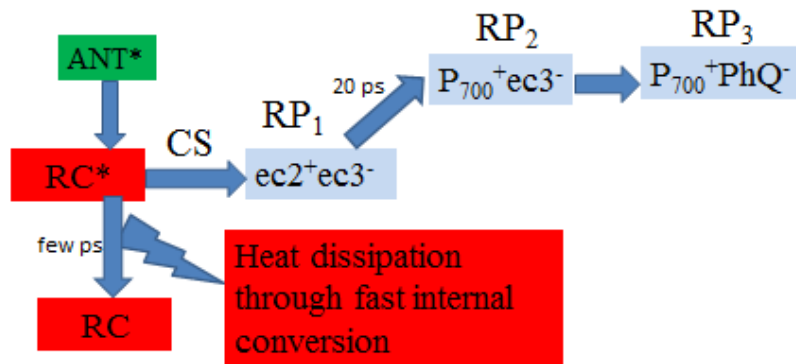
#### 4.4.3 Models of Excitation Energy Decay

The first proposed model of excitation energy decay is through a fast charge recombination (CR) process from  $ec2^+ec3^-$  RP. Initially the transfer of excitation energy from the antenna to the RC results in energy equilibration between the two physical compartments. The six chlorophylls share the excitation energy equally, and the next forward step is the formation of the fast  $ec2^+ec3^-$  RP. However, introducing mutation near  $ec2$  causes unfavorable secondary ET step and results into charge recombination in the fast  $ec2^+ec3^-$  RP. And the energy is cast off to the ground state via a new channel by a fast internal conversion process as presented in figure 4.14. In the second model, we proposed that the excitation energy is transferred to the RC to form the excited RC ( $RC^*$ ). By introducing mutation near  $ec2$ , the  $RC^*$  cannot convert this excitation energy into CS by trapping. This results into loss of this excitation energy to the ground state through a new channel by a fast internal conversion process. The third similar model is that the excitation energy from the  $ec2ec3^*$  pair on the mutated branch is lost to the ground state through fast internal conversion process.

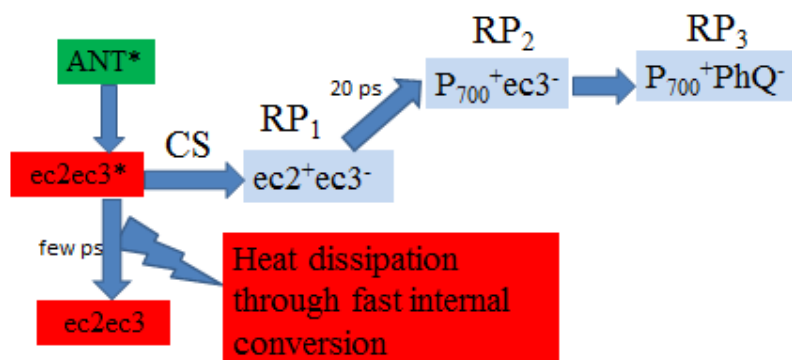
A) Model of Excitation Energy Decay: Effect after CS



B) Model of Excitation Energy Decay: Effect before CS



### C) Model of Excitation Energy Decay: Effect before CS



**Figure 4.15.** Proposed models of excitation energy decay from the excited state of reaction center. Due to mutation near ec2, the excitation energy is released to the ground state after energy equilibration between antenna and reaction center. Where ANT\* = excited state of antenna; RC\* = excited reaction center; CS = charge separated state; RP = radical pair.

#### 4.4.4 Difference in the lifetimes of energy trapping between *C. reinhardtii* and *Synechocystis* sp. PCC 6803

The *C. reinhardtii* mutants have a decrease in lifetime of their energy trapping component, and this is very profound when mutation is on A-branch near ec2, where Asn is changed to Leu. This modification in energy trapping is observed from both ultrafast transient absorption spectroscopy as well as time-resolved fluorescence. We proposed that such a decrease in the lifetime is only possible when there are a ps or sub-picosecond process that contributes to the decay of excitation energy. This energy decay channel is in competition with the normal energy trapping into CS process. From global analyses, we

could not determine any spectral marker of this new decay channel but it is possible that by using target analysis we can unravel this new channel.

In *Synechocystis sp.* PCC 6803, where the A-side mutations showed around 50% inhibition of CS along with an increase in the lifetime of energy trapping process. In the excitation energy trapping component of A-side mutants of PsaB-N591L and PsaB-N591H, we observed a two to three fold increase in the lifetime. This increase in the lifetime of energy trapping process can be explained based on the presence of red chlorophylls. The red chlorophylls are present in the core antenna of *Synechocystis sp.* PCC 6803, although the exact locations of these chlorophylls are not clear. It is also predicted that they are present near the RC (146) or between monomer-monomer interfaces, where trimerization occurs (21). The observed bleaching bands at 707-710 nm and 714-717 nm regions of the energy trapping components from the DADS of ultrafast transient absorption spectroscopy of *Synechocystis sp.* PCC 6803 points towards the red chlorophylls contribution as previously observed (64, 146). The contribution of red chlorophylls is also evident in the slow phase of energy trapping from TCSPC of PsaB-N591H and PsaB-N591L. This increase in lifetime due to red chlorophylls as a competitor of ec2 cofactors of RC is also evident in TCSPC measurement of monomer PSI form too, which is greater than that of trimeric PSI. These red chlorophylls hindered the new channel that is suitable for disposing of the untrapped excitation energy. The long wavelength chlorophylls are always in equilibrium with the RC\* for excitation energy. So instead of disposing of it through a new channel, either it stays on the red chlorophylls for a longer time as the first choice is to trap this energy instead of disposing



of as a heat. The other reason for increase lifetime might be that the excitation energy travel between the red chlorophylls and RC\* several times so that either it is trapped or wasted through the new channel. Further, the difference between the monomer and trimeric PSI mutants can be explained based on the same first choice of energy trapping instead of wasting. In PSI trimer, when the excitation energy is transferred to the modified ec2 on a specific branch, then it is returned to either the red chlorophyll or it is transfer to the other two monomers in line. But if they are also unable to utilize it for CS then the new channel will be used to release the excitation energy through the fast internal conversion process. To a large extent these results also explain the two different mechanism of energy trapping, where trap limited model holds true for energy trapping in green algae. While transfer to the trap limited model explains most of the transient absorption and fluorescence data best in cyanobacteria.

#### 4.4.5 New channel of excitation energy decay and primary CS

The new channel of excitation energy decay is always functional, as there is a continuous supply of photon during daylight that is absorbed by the antenna. From the antenna, it is transferred to the RC in the form of an exciton. The PSI cannot utilize all the absorbed photons for CS due to time limitation, as in increased light condition the rate of absorption is high and ET from ec2 down to  $F_{A/B}$  takes time. Therefore, there must be some fast way of this excitation energy decay. The new channel of excitation energy can be explored further through target analysis of ultrafast transient absorption spectroscopic and time-resolved fluorescence data. Where the specie associated decay spectra (SADS) and evolution associated decay spectra (EADS) will represent the formation and decay of

different components in time. If the fast channel has some distinctive spectral characteristics then, it will also be observed as it is a separate compartment.

In PSI, the excitation energy transfer, equilibration, and its decay into the two pathways can be further studied through ultrafast two-dimensional (2D) electronic spectroscopy. As from the electronic spectroscopy we can get a further idea of the site energies of each cofactor in the RC or a closer view of RC with excited state properties (108). The 2D electronic spectroscopy of mutants PSI will possibly explain how the ec2 cofactors on the two branches are handling the excitation energy and why this difference in trapping energy lifetime is present between *C. reinhardtii* and *Synechocystis sp.* PCC 6803.

The time evolution of primary cation formation in PSI during energy trapping can be studied better with ultrafast time-resolved visible pump infra-red probe spectroscopy (66, 138). The infra-red spectroscopy has the power to differentiate between the two side ec2 cofactors in the PsaA-Asn604 and PsaB-Asn591 mutants. The mutation near ec2 can change the vibrational signature of the modulated side chlorophyll, and it will be possible to monitor the evolution of primary cation. Observation of primary CS through Ultrafast IR spectroscopy will be more helpful in mutated PSI particles from *C. reinhardtii* free of red chlorophylls (139).

This new channel can also be further evaluated using fluorescent amino acid substitution at the site of ec2 cofactor or by attaching fluorophores near the RC (147). As the PSI has 100 % quantum efficiency, with every photon absorb is utilized for CS if the RC is open. While the oxidized P<sub>700</sub> can still absorb the excitation energy but the utilization or path of

this energy was not determined earlier (38, 40, 148, 149). Thus, we can propose the dissipation of the same excitation energy absorbed by the  $P_{700}^{+}$  or closed RC through this new channel for excitation energy decay.

#### 4.5 CONCLUSIONS

We investigated the role of the ec2 cofactor in the RC of PSI, which was the proposed primary electron donor. Making mutation near ec2 on their respective branch causes a decrease in quantum yield of CS. This decrease is obvious from both transient absorption spectroscopic measurements performed in the time resolution of femtosecond to picosecond and nanosecond to millisecond timescale. The transient EPR spectroscopy at cryogenic and room temperature also supported the decrease in quantum yield in the mutants. Time-resolved fluorescence strengthens the proposed new route of untrapped excitation energy decay. We can now confidently assign ec2 cofactor on each branch of the RC as the primary electron donor in PSI.

#### 4.6 SUPPLEMENTARY INFORMATION

**Table S4.1.** Rates and amplitudes of decay components in the ns at 480 nm in various purified PS1 preparation from *Synechocystis sp.* PCC 6803.

Mutation	amplitude (mOD) of fast decay	rate (ns) of fast decay	amplitude (mOD) of slow decay	rate (ns) of slow decay	$\phi$ at 480 nm [ns components] (%)
WT	0.65	17.2	1.20	207	100
PsaA-N604H	0.30	17.8	1.20	210	81
PsaB-N591H	0.65	17.1	0.37	204	55
PsaA-N604M	0.69	17.0	1.20	211	102
PsaB-N591M	0.68	17.7	1.0	210	91

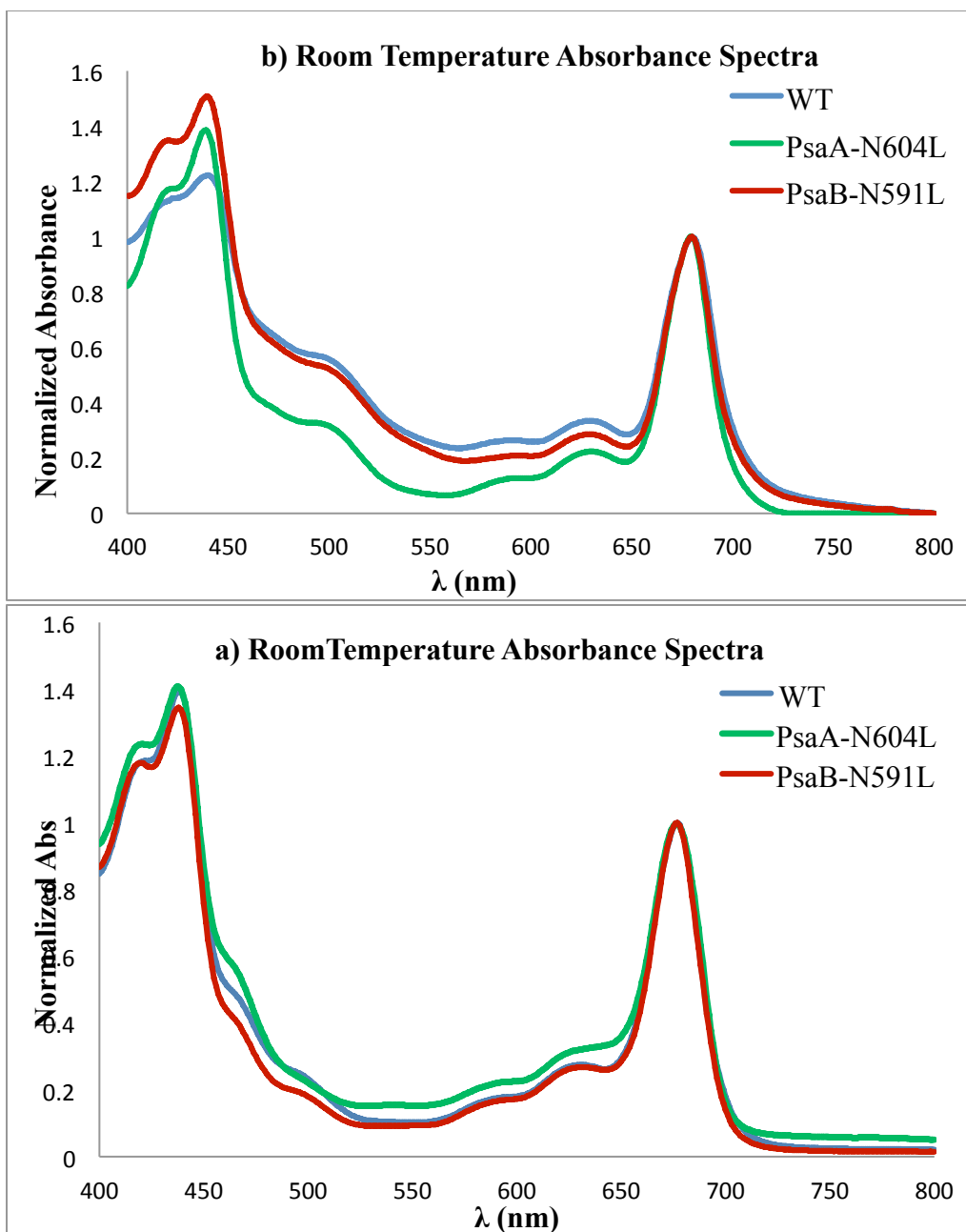
<sup>1</sup>Assumed to be 100%. Quantum yields in the mutants are expressed as relative to WT.

**Table S4.2.** Rates and amplitudes of decay components in the ns-s at 820 nm in various purified PS1 preparation from *Synechocystis* sp. PCC 6803. <sup>1</sup>Assumed to be 100 %. Quantum yields in the mutants are expressed as relative to WT.

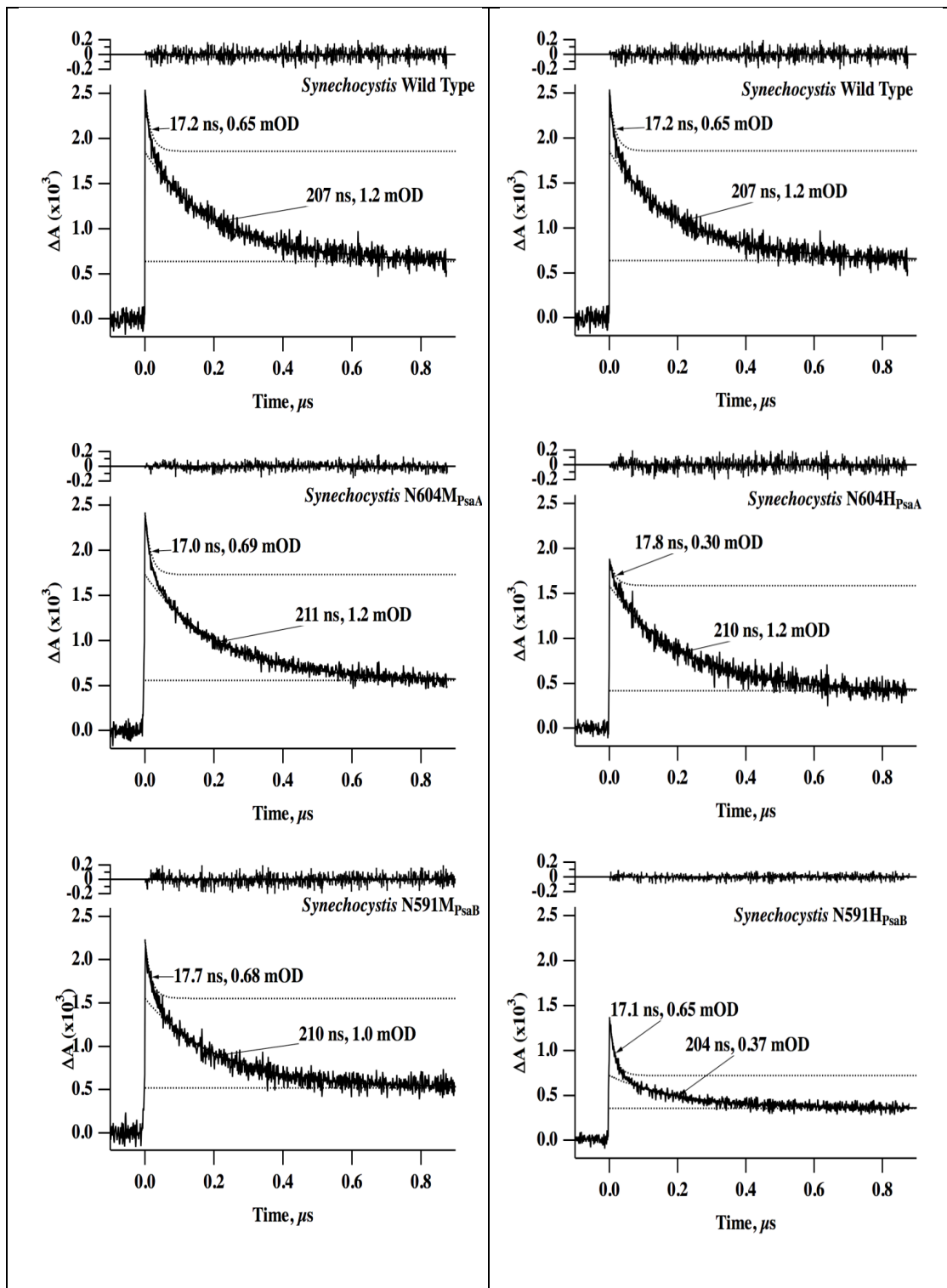
Mutation	P <sub>700</sub> <sup>+</sup> decay components	Assignment	φ at 820 nm [ms component] (%)
WT	5.0 mOD, 49.9 ms	[F <sub>A</sub> /F <sub>B</sub> ] <sup>-</sup> → P <sub>700</sub> <sup>+</sup>	100 <sup>1</sup>
	2.3 mOD, 1.31 s	DCPIP → P <sub>700</sub> <sup>+</sup>	
PsaA-N604H	0.47 mOD, 29.4 ns	A <sub>0B</sub> <sup>-</sup> → P <sub>700</sub> <sup>+</sup>	71
	0.96 mOD, 1.42 ms	[F <sub>A</sub> /F <sub>B</sub> ] <sup>-</sup> → P <sub>700</sub> <sup>+</sup>	
	1.8 mOD, 47.6 ms	[F <sub>A</sub> /F <sub>B</sub> ] <sup>-</sup> → P <sub>700</sub> <sup>+</sup>	
	1.5 mOD, 1.36 s	DCPIP → P <sub>700</sub> <sup>+</sup>	
PsaB-N591H	1.5 mOD, 9.99 μs	A <sub>1</sub> <sup>-</sup> → P <sub>700</sub> <sup>+</sup>	49
	1.3 mOD, 44.1 ms	[F <sub>A</sub> /F <sub>B</sub> ] <sup>-</sup> → P <sub>700</sub> <sup>+</sup>	
	1.3 mOD, 1.33 s	DCPIP → P <sub>700</sub> <sup>+</sup>	
PsaA-N604M	0.38 mOD, 292 ns	A <sub>0B</sub> <sup>-</sup> → P <sub>700</sub> <sup>+</sup>	89
	1.1 mOD, 832 μs	[F <sub>X</sub> ] <sup>-</sup> → P <sub>700</sub> <sup>+</sup>	
	3.0 mOD, 65.8 ms	[F <sub>A</sub> /F <sub>B</sub> ] <sup>-</sup> → P <sub>700</sub> <sup>+</sup>	
	2.0 mOD, 1.32 s	DCPIP → P <sub>700</sub> <sup>+</sup>	
PsaB-N591M	2.0 mOD, 27.7 μs	A <sub>1A</sub> <sup>-</sup> → P <sub>700</sub> <sup>+</sup>	84
	1.5 mOD, 68.5 ms	[F <sub>A</sub> /F <sub>B</sub> ] <sup>-</sup> → P <sub>700</sub> <sup>+</sup>	
	1.1 mOD, 1.26 s	DCPIP → P <sub>700</sub> <sup>+</sup>	

**Table S4.3.** Quantum yield of charge separation calculated at 703 nm in WT; PsaA-N604H and PsaB-N591H from *Synechocystis* sp. PCC 6803 from ultrafast transient absorption spectroscopy.

Sample	Quantum Yield of Charge Separation at 703 nm
WT	100%
PsaA-N604H	82%
PsaB-N591H	44%

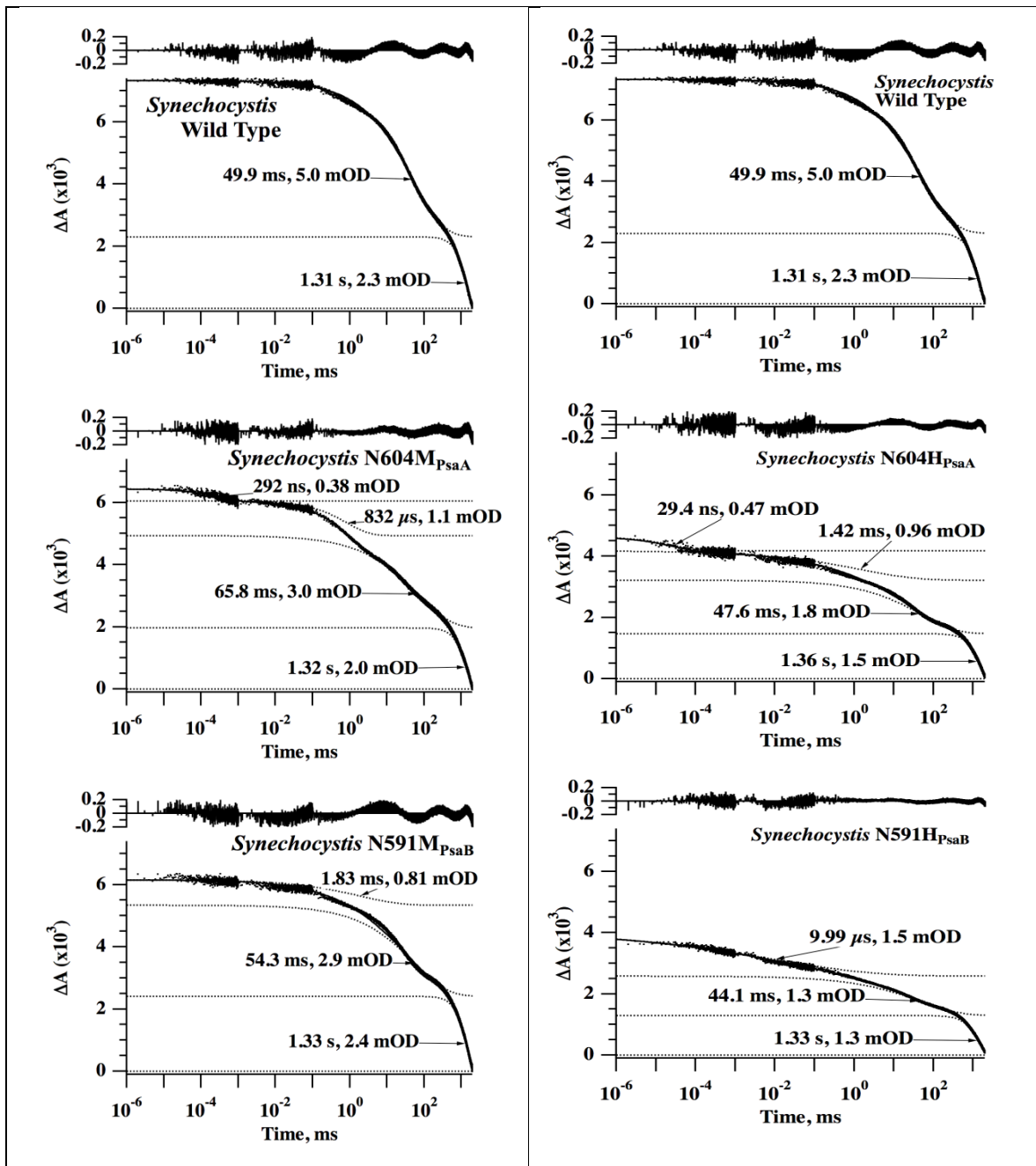


**Figure S4.1.** a) Room temperature absorbance spectra of P WT; PsaA-N604L and PsaB-N591L mutants PSI from *C. reinhardtii*. b) Room temperature absorbance spectra of P WT; PsaA-N604L and PsaB-N591L mutants PSI from *Synechocystis* sp. PCC 6803.

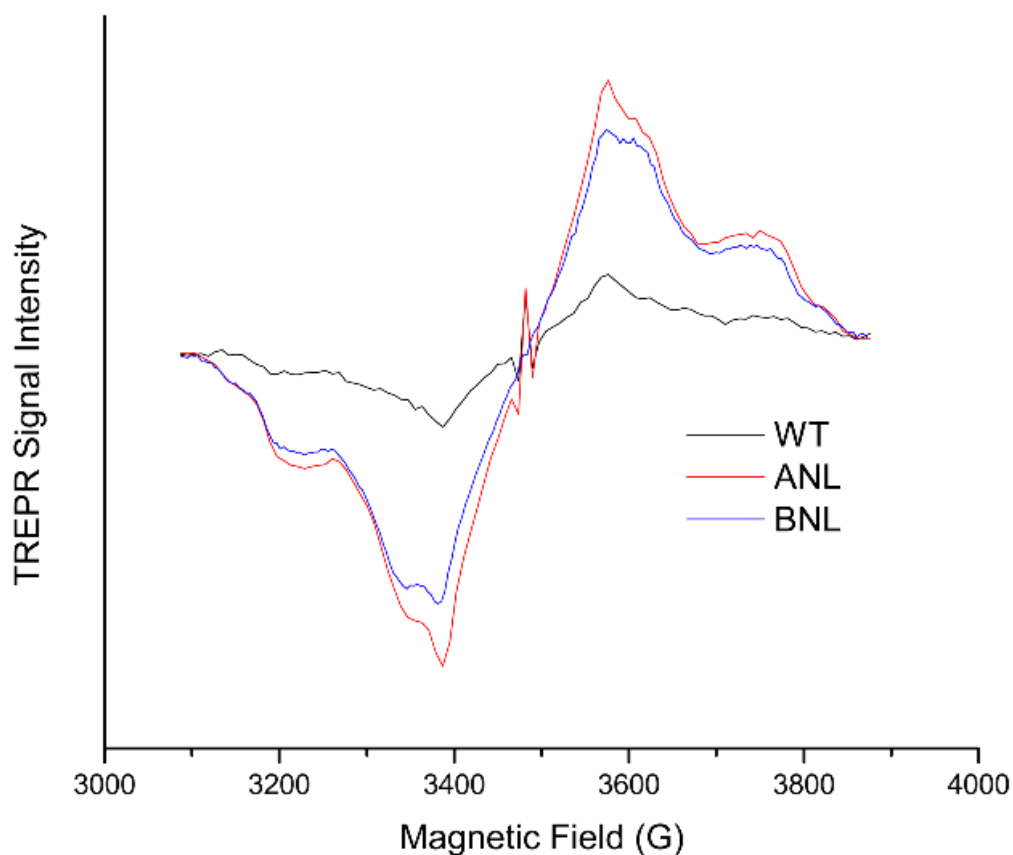




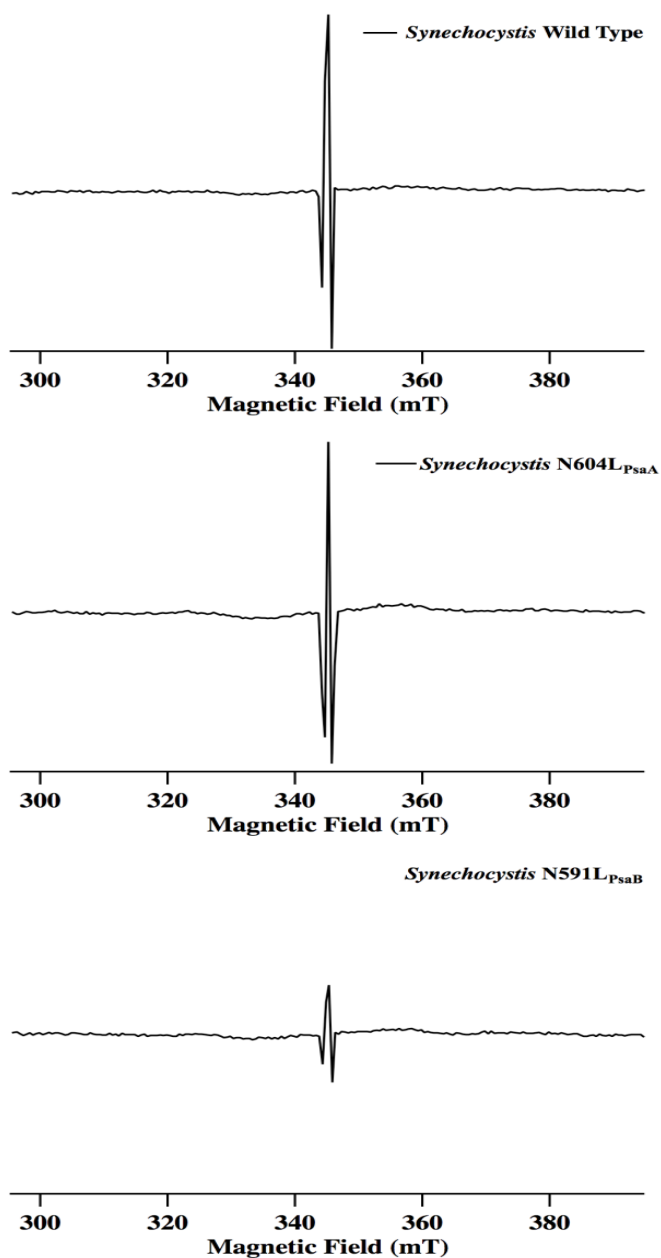
**Figure S4.2.** Transient absorbance difference traces at 480 nm for PS I complexes from *Synechocystis sp.* PCC 6803. The WT; PsaA-N604M; PsaB-N591M in left column. In the right column WT; PsaA-N604H and PsaB-N591H. The Chl concentration is 100  $\mu\text{g ml}^{-1}$ . The experimental data are shown as points and the fit is shown as the solid line. The differences between experimental and fit data are plotted as a residual. The data sets were from 64 averages.



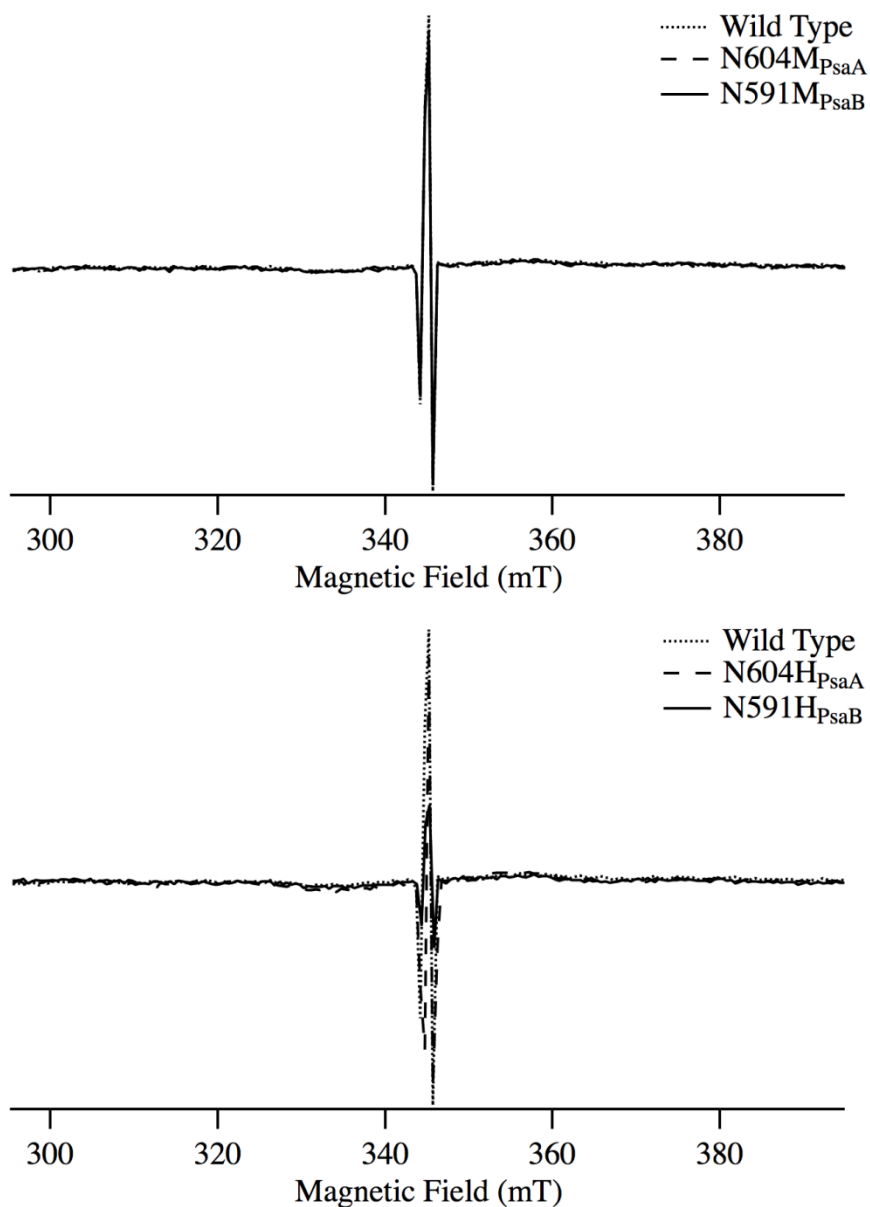
**Figure S4.3.** Transient absorbance difference traces at 820 nm for PS I complexes from *Synechocystis* sp. PCC 6803. The WT; PsaA-N604M; PsaB-M591M are shown in the left column. In the right column are WT; PsaA-N604H; PsaB-N591H mutants respectively. The Chl concentration is 100  $\mu\text{g ml}$ . The data sets, which were collected at time windows of 1 ns to 1  $\mu\text{s}$ , and from 1  $\mu\text{s}$  to 100  $\mu\text{s}$ , and from 100  $\mu\text{s}$  to 100 ms to were stitched together to portray multiple kinetic phases on one plot. The absorbance values are plotted on a log scale, and were fitted using a multi-exponential decay. The experimental data are shown as points and the fit is shown as the solid line. The differences between experimental and fit data are plotted as a residual. The data sets were from 64 averages.



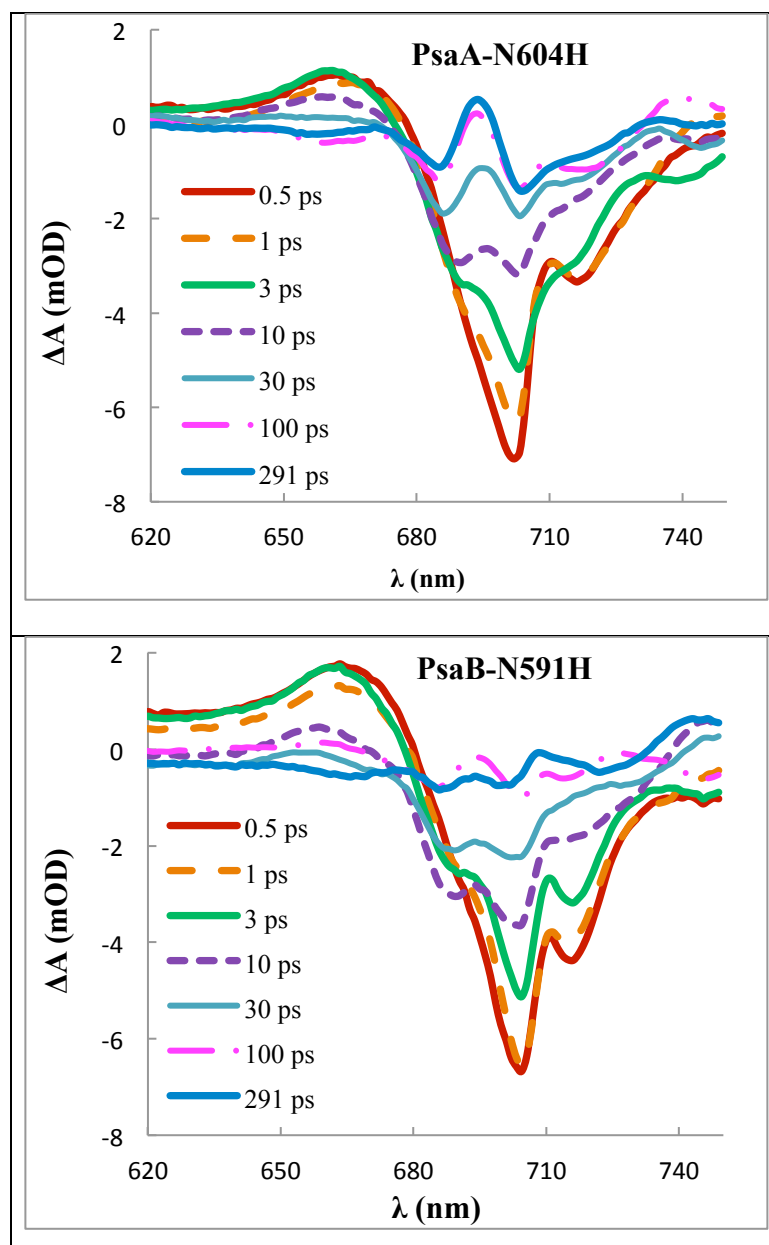
**Figure S4.4.** Comparison of the spin polarized transient X-band EPR spectra of PSI samples from WT, PsaA-N604L and PsaB-N591L mutants for the  $^3\text{P}_{700}$  and  $^3\text{Chl}$  at 1  $\mu\text{s}$  time after the laser flash. The  $^3\text{P}_{700}$  are absent, while the  $^3\text{Chl}$  are present almost 3 fold in the two mutants as compare to WT.



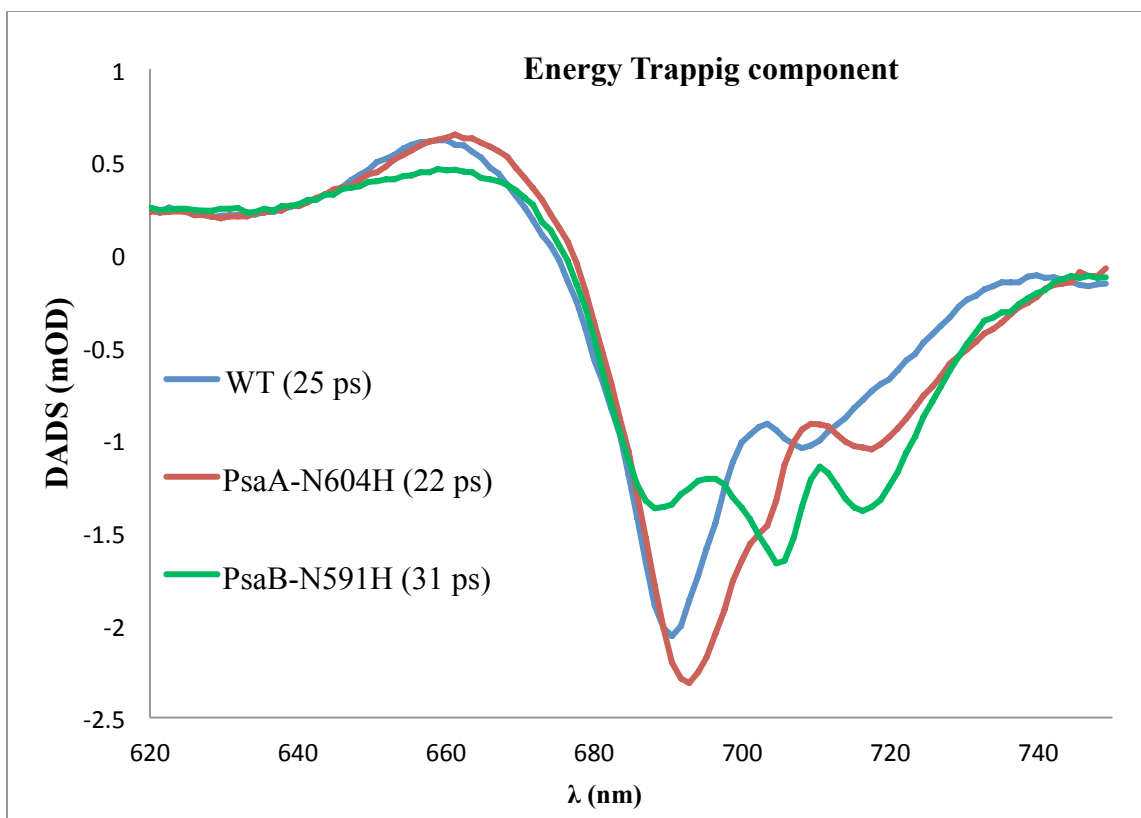
**Figure S4.5.** Spin polarized transient EPR spectra of Chl triplet states in the WT; PsaA-N604L, and PsaB-N591L mutants of *Synechocystis* *sp.* PCC 6803. The EAE polarization pattern is characteristic of the  $P_{700}^+A_1^-$  radical pair. Note the absence of both a spin polarized  $P_{700}$  triplet and an antenna Chl intersystem crossing triplet. The spectra were recorded at 80 K and extracted from the time/field datasets in a time window centered at 1  $\mu$ s after the laser flash.



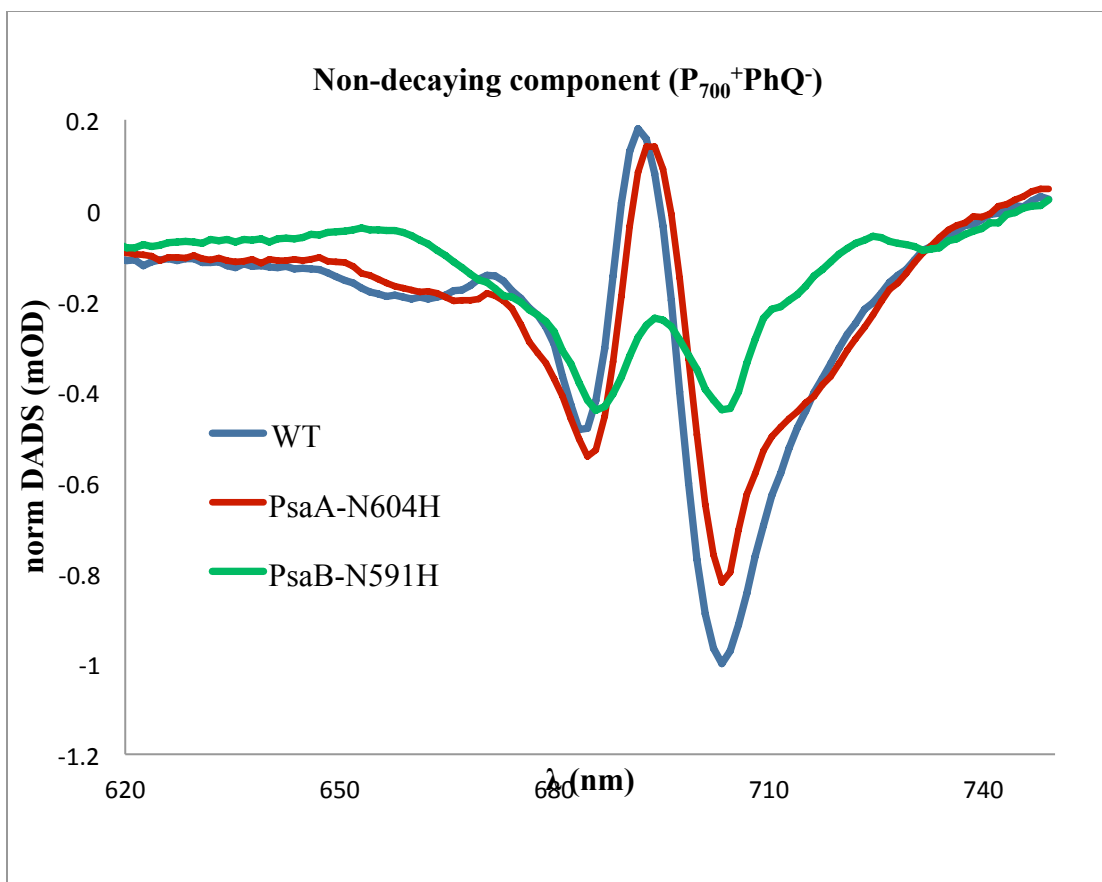
**Figure S4.6.** Spin polarized transient EPR spectra of Chl triplet states in the WT; PsaA-N604M; PsaB-N591M PsaA-N604H; PsaB-N591H mutants of *Synechocystis sp.* PCC 6803. The EAE polarization pattern is characteristic of the  $P_{700}^+A_1^-$  radical pair. Note the absence of both a spin polarized  $P_{700}$  triplet and an antenna Chl intersystem crossing triplet. The spectra were recorded at 80 K and extracted from the time/field datasets in a time window centered at 1  $\mu$ s after the laser flash.



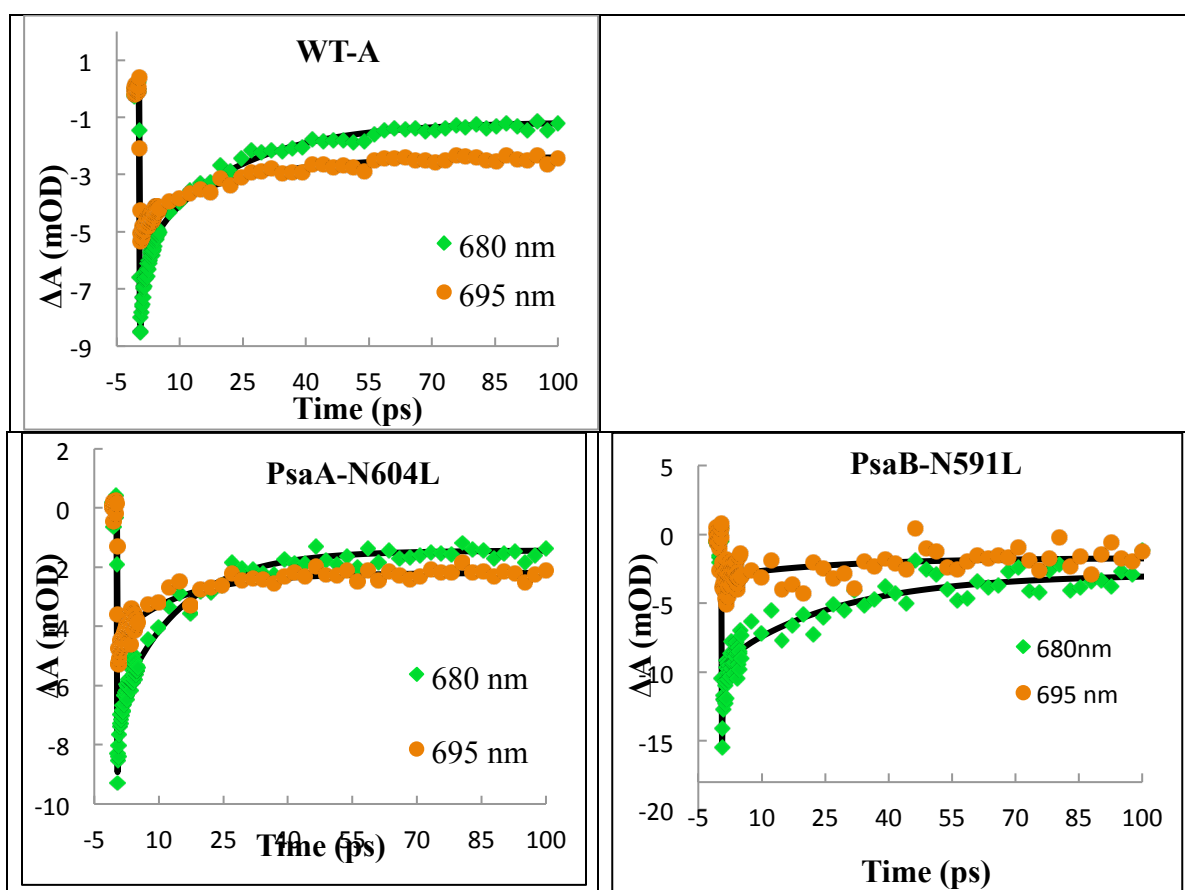
**Figure S4.7.** Transient absorption difference spectra of PSI trimers of PsaA-N604H and PsaB-N591H mutant particles from *Synechocystis* PCC 6803 obtained at different delay times after excitation at 700 nm.



**Figure S4.8.** Energy trapping component from DADS of WT; PsaA-N604H and PsaB-N591H mutant PSI of *Synechocystis sp.* PCC 6803. The spectra are normalized to the maximum amount of bleaching in WT.

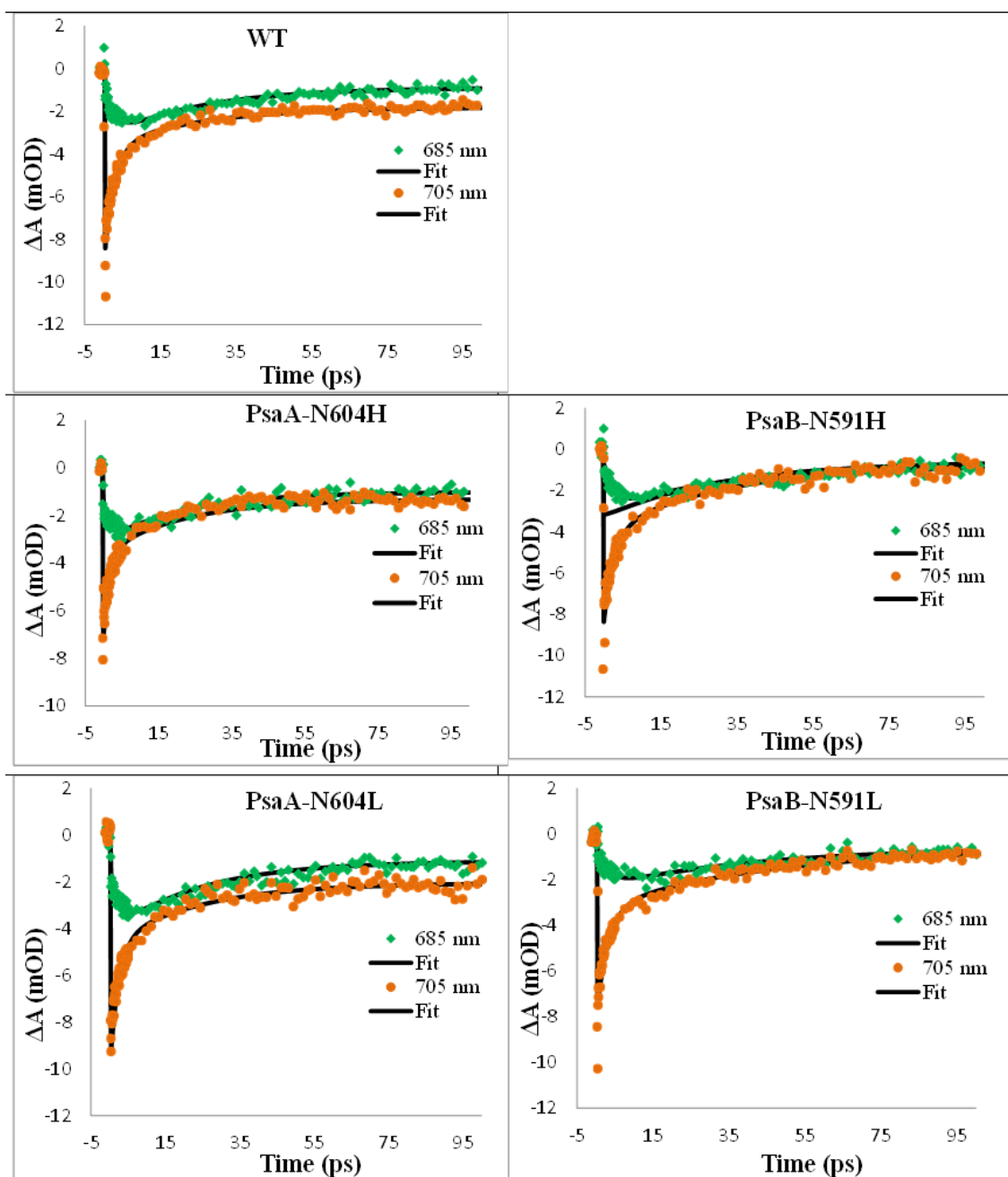


**Figure S4.9.** Long lived component from DADS of WT; PsaA-N604H and PsaB-N591H mutant PSI o *Synechocystis* sp. PCC 6803. The spectra are normalized to the maximum amount of bleaching in WT.

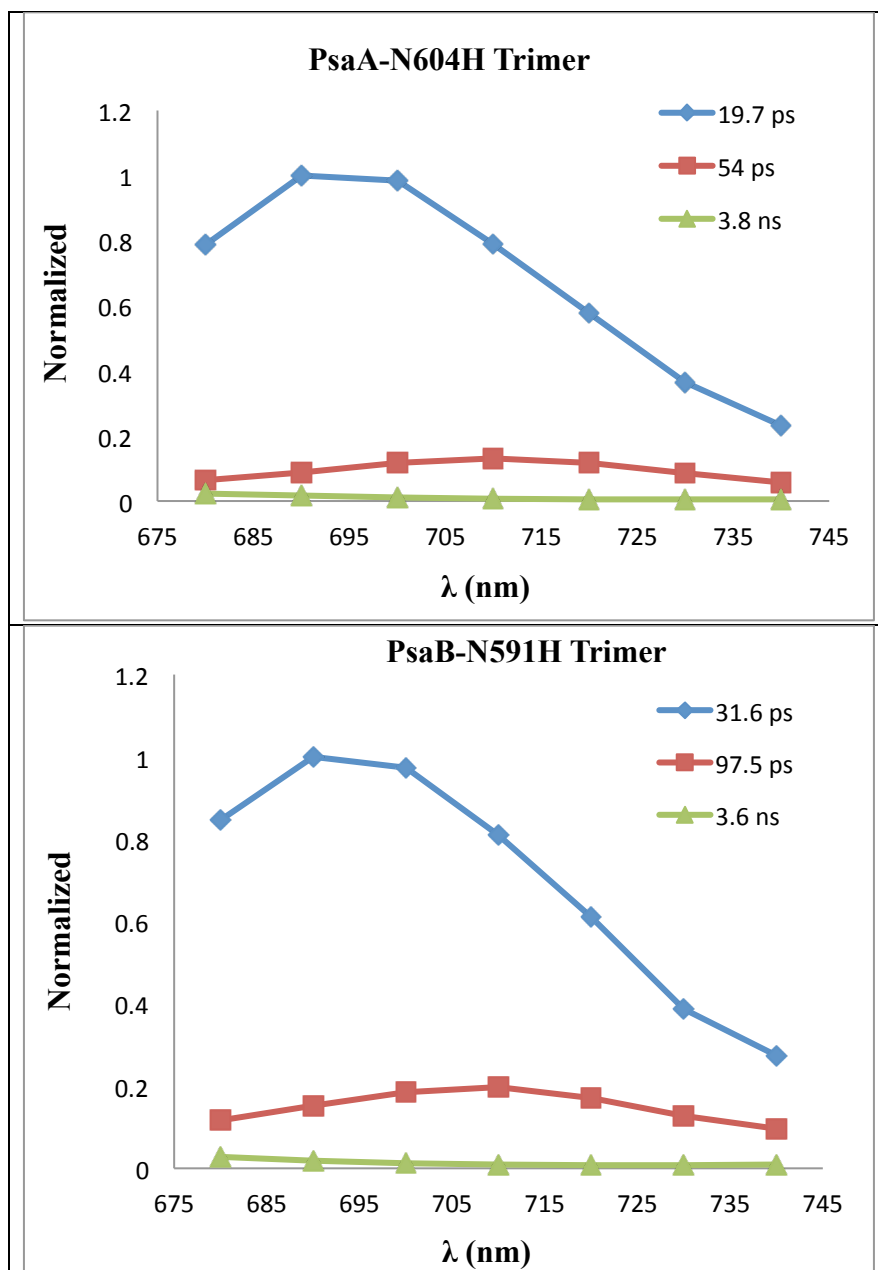


**Figure S4.10.** Kinetics of WT; PsaA-N604L and PsaB-N591L mutant PSI of *C. reinhardtii* at 680 nm and 695 nm. The kinetics are shown up to 100 ps post-pump flash.

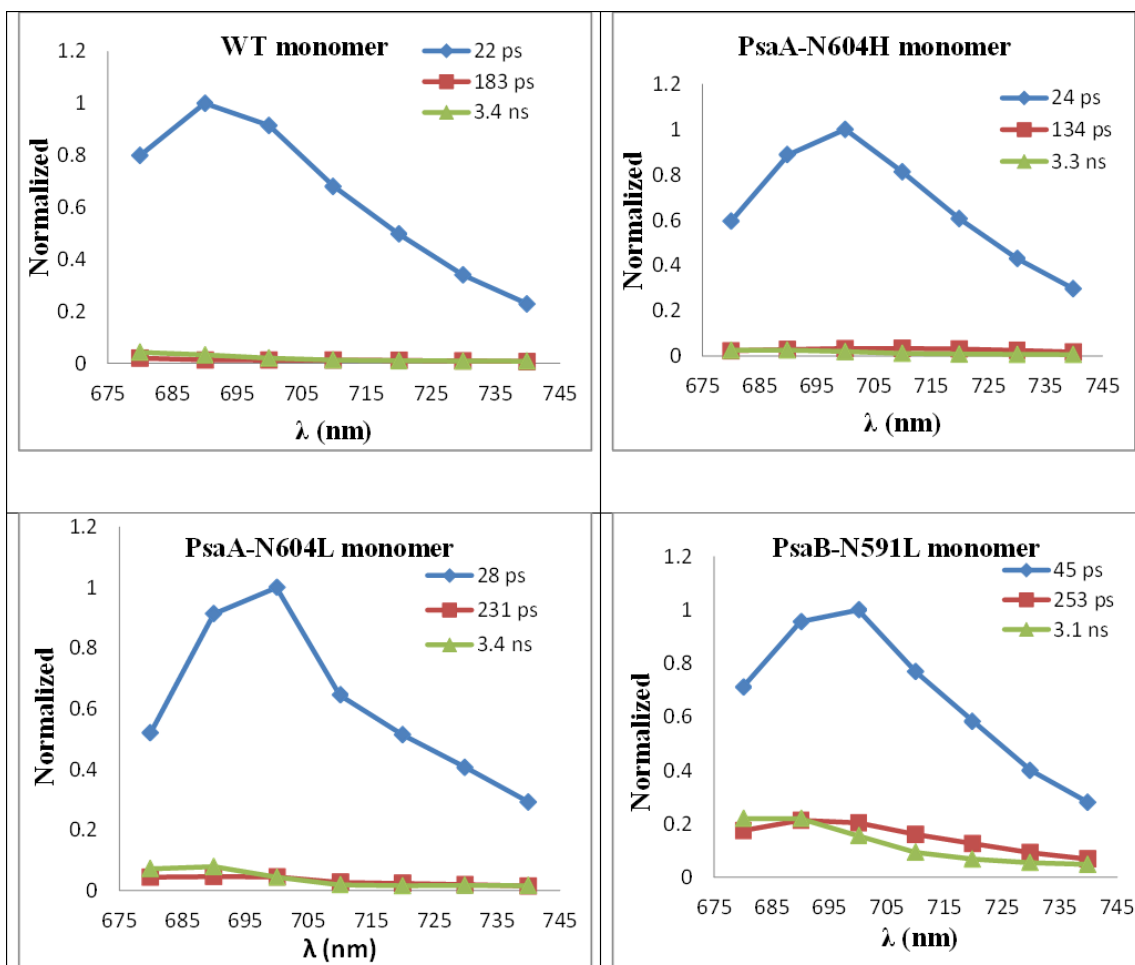




**Figure S4.11.** Kinetics of WT, PsaA-N604H and PsaB-N591H mutant PSI trimers from *Synechocystis sp.* PCC 6803 at 685 nm, 690 nm and 705 nm. The kinetics are shown up to 100 ps post-pump flash.



**Figure S4.12.** Decay associated fluorescence spectra (DAS) of PSI particles obtained from global analyses of PsaA-N604H and PsaB-N591H mutants of PSI trimers from *Synechocystis* sp. PCC 6803. The maximum peak of the fast energy trapping component was considered as 1 and the data was normalized to it.



**Figure S4.13.** Decay associated fluorescence spectra (DAS) of PSI particles obtained from global analyses of WT and PsaA-N604L and PsaB-N591L mutants of PSI monomers from *Synechocystis sp.* PCC 6803. The maximum peak of the fast energy trapping component was considered as 1 and the data was normalized to it.

## CHAPTER NO 5

### 5 SUMMARY

The experimental work presented in this dissertation showed the bidirectionality of electron transfer and the role of ec2 chlorophyll on each branch of PSI RC. In the classical model of CS,  $P_{700}$  is considered as a primary electron donor. However, mutagenesis studies and ultrafast transient spectroscopy predicted that the ec2 chlorophyll is the primary electron donor as  $P_{700}$  only affects the secondary electron transfer step. The ec2 cofactor although not directly linked to any protein residue, has a hydrogen bond between the water molecule coordinating the central magnesium ion of ec2 and the nearby asparagine residue. Secondly a methyl group of alanine is directed towards the ec2-ec3 chlorophyll pair. Due to the embedded nature of ec2 in the RC of PSI, its redox properties are have not been determined experimentally; however theoretical studies debated its role in energy trapping and ET.

In this work, a combined approach of mutation and various spectroscopic methods are used to unravel the properties of ec2 cofactor. In chapter 2, the effects of PsaA-A684 and PsaB-A664 mutants on charge separation are presented. Based on two independent methods for estimation of the level of PSI, the best transformants were selected for bidirectional ET study in vivo using transient absorption spectroscopy. The Ala to Asn mutant pair was chosen due to its PSI accumulation level and its effect on bidirectionality of ET. The PsaA-A684N has a profound effect on the charge separation in PSI. This mutation modulates the A-branch ec2 environment such that most of energy trapping and

subsequent ET events occurs on the B-side. This increase in CS on B-branch was first observed in ns-ms transient absorption spectroscopy where the amplitude and lifetime of the fast phase semiphylloquinone decay dominates while the slow phase representing A-branch ET is minor. The increased B-branch ET is also evident from the formation of  $P_{700}^{+}PhQ_B^{-}$  RP both at room and cryogenic temperature. The increase in the lifetime of excitation energy decay into the trapping form is present in both ultrafast transient absorption spectroscopy and time-resolved fluorescence. This increase in lifetime showed that the excitation energy visits the energy trap several times, causing slower kinetics but leaving the quantum yield of CS unaffected in PsaA-A684N and PsaB-A664N.

In chapter 3, the effects of PsaA-N604 and PsaB-N591 mutants from *C. reinhardtii* on bidirectionality of ET were discussed. Mutation near ec2 results in loss of phototrophic growth. The PsaA-N604H, PsaA-N604L, PsaB-N587H, PsaB-N5917L and PsaB-N591Y mutants decrease the quantum yield of CS. The observed decrease in stable CS is evident in both *in vivo* and *in vitro* analysis through ns-ms transient absorption spectroscopy. In the *in vitro* study, the amplitude of CS on the altered branch showed a decrease while the lifetimes of the two phases were not affected. The reduction in stable CS did not result in  $^3P_{700}$  from charge recombination. Transient EPR spectroscopy at room and cryogenic (80 K) temperature exhibited a decrease in the observable RPs formation as seen from a small signal to noise ratio. This reduction is apparent in the A-side (PsaB-N591) mutants. The ultrafast transient absorption spectroscopy also confirmed the decrease in amplitude of  $P_{700}^{+}PhQ^{-}$  in several mutants. The decrease in CS and wastage of excitation energy in the mutants were explained from decrease in the lifetime of energy trapping component in

time-resolved fluorescence. The decreases in lifetimes were described in terms of two paths of excitation energy decay that are in competition with one another. One route is the decay of excitation energy into charge separation and subsequent ET, while the other is a new channel of the energy decay through a rapid internal conversion process to the ground state. The fast decay of energy trapping component is dominant in PsaB-N591H, PsaB-N591L, and PsaB-N591Y whereas in PsaA-N604D, PsaA-N604H, PsaA-N604K and PsaA-N604L on the B-branch it is minor. The other unusual properties of these mutants include a red shift in the  $P_{700}$  difference spectra of PsaA-N604D and PsaB-N591D. Secondly introduction of a positively charged lysine residue (PsaA-N604K and PsaB-N591K) at the site of ec2 is rarely tolerated in a hydrophobic protein like PSI. It was speculated that unprotonated lysine ligates to ec2, therefore these two unusual properties were investigated by FTIR spectroscopy. The FTIR difference spectroscopy exhibited changes in several vibration bands of  $P_{700}$ . These shifts in vibration bands showed that the mutation also affected the upstream  $P_{700}$  chlorophyll spectral properties.

In chapter 4, a comparison of the PsaA-N604L and PsaB-N591L of *C. reinhardtii* mutants with its counterpart mutants (PsaA-N604L and PsaB-N591L) from *Synechocystis sp.* PCC 6803 is presented to get a clear picture of energy trapping and primary charge separation. The main difference in PSI between the two species is that in *C. reinhardtii* it is in monomeric form with nine Lhca attached to the internal antenna. Two of the Lhca have red chlorophylls that absorb at longer wavelengths. In *Synechocystis sp.* PCC 6803 PSI exists in trimeric form and has red chlorophylls inside the core antenna. Transient optical spectroscopy with time resolution of ns-ms showed that the Asn to Leu mutants

have a similar effect on the CS. These results also agree quantitatively at 480 nm and 820 nm, showing decrease in CS. The inhibition of stable CS at ec2 did not result in the formation of  $^3P_{700}$  in mutants of both the species. Transient EPR at room and low temperature also have the same reduction in RP formation as observed from S/N ratio in the Asn to Leu pair mutants. The  $^3P_{700}$  were also absent in wide scan EPR at cryogenic temperature. Ultrafast transient absorption spectroscopy of the mutant pair in the two species also agrees that mutations at ec2 causes a loss of excitation energy and it is more evident in the A-branch. In DADS of *Synechocystis sp.* PCC 6803 mutants there were new bleaching bands at the red side of the spectrum, which originates from the excited red chlorophylls. The lifetime obtained from decay associated spectra of transient fluorescence exhibited an increase in lifetime in *Synechocystis sp.* PCC 6803 mutants while it is decreases in *C. reinhardtii* mutants. These differences between the two species possibly arise from their structural variations.

The new channel of excitation energy can be explored further through target analysis of ultrafast transient absorption spectroscopic and time-resolved fluorescence data. In addition to the spectroscopic methods used here, 2D electronic spectroscopy and ultrafast visible pump infrared probe spectroscopy will unravel the excitation energy decay pathways and primary charge separation in these PSI mutants.

## REFERENCES

1. Blankenship, R. (2014) *Molecular Mechanisms of Photosynthesis*, 2nd ed., Wiley-Blackwell Publishing, Hoboken, NJ.
2. Scholes, G. D., Fleming, G. R., Olaya-Castro, A., and van Grondelle, R. (2011) Lessons from nature about solar light harvesting., *Nature Chemistry* 3, 763-774.
3. Melkozernov, A. N., Barber, J., and Blankenship, R. (2006) Light Harvesting in Photosystem I Supercomplexes., *Biochem.* 45.
4. R., C., and Van Amerongen, H. (2013) Light harvesting in photosystem I, *Photosynth Res* 116, 153-166.
5. Mozzo, M., Mantelli, M., Passarini, F., Caffarri, S., Croce, R., and Bassi, R. (2010) Functional analysis of Photosystem I light-harvesting complexes (Lhca) gene products of *Chlamydomonas reinhardtii*., *Biochem Biophys Acta* 1797.
6. Takahashi, Y., Yasui, T. A., Stauber, E. J., and Hippler, M. (2004) Comparison of the subunit compositions of the PSI-LHCI supercomplex and the LHCI in the green alga *Chlamydomonas reinhardtii*, *Biochem.* 43, 7816-7823.
7. Drop, B., Webber-Birungi, M., Fusetti, F., Kouril, R., Redding, K. E., Boekema, E. J., and Croce, R. (2011) Photosystem I of *Chlamydomonas reinhardtii* contains nine light-harvesting complexes (Lhca) located on one side of the core, *J Biol Chem* 286, 44878-44887.
8. Amunts, A., Toporik, H., Borovikova, A., and Nelson, N. (2010) Structure determination and improved model of plant photosystem I., *J. Biol. Chem.* 285, 3478-3486.
9. Amunts, A., and Nathan, N. (2009) Plant Photosystem I design in the light of evolution., *Structure* 17, 657-650.
10. Lucinski, R., Schmid, V. H., Jansson, S., and Klimmek, F. (2006) Lhca5 interaction with plant photosystem I., *FEBS Letters* 580, 6485-6488.
11. Müller, M. G., Slavov, C., Luthra, R., Redding, K. E., and Holzwarth, A. R. (2010) Independent initiation of primary electron transfer in the two branches of the photosystem I reaction center, *Proc Natl Acad Sci U S A* 107, 4123-4128.
12. Drop, B., Webber-Birungi, M., Yadav, S. K. N., Filipowicz-Szymanska, A., Fusetti, F., Boekema, E. J., and Croce, R. (2014) Light harvesting complex II (LHCII) and its supramolecular organization in *Chlamydomonas reinhardtii*., *Biochimica et Biophysica Acta (BBA)* 1837, 63-72.



13. Wientjes, E., van Amerongen, H., and Croce, R. (2013) Quantum yield of charge separation in photosystem II: functional effect of changes in the antenna size upon light acclimation, *J Phys Chem B* 117, 11200-11208.
14. Wientjes, E., Van Amerongen, H., and Croce, R. (2013) LHCII is an antenna of both photosystems after long term acclimation., *Biochim Biophys Acta (BBA) Bioenergetics* 1827, 420-426.
15. Liu, Z., Yan, H., Wang, K., Kuang, T., Zhang, J., Gul, L., An, X., and Chang, W. (2004) Crystal structure of spinach major light-harvesting complex at 2.72 °Å resolution., *Nature* 482, 287-292.
16. Busch, A., and Hippler, M. (2011) The structure and function of eukaryotic photosystem I., *Biochimica et Biophysica Acta (BBA) - Bioenergetics* 1807, 864-877.
17. Hippler, M., Biehler, K., Krieger-Liszkay, A., van Dillewijn, J., and Rochaix, J. D. (2000) Limitation in electron transfer in photosystem I donor side mutants of *Chlamydomonas reinhardtii*. Lethal photo-oxidative damage in high light is overcome in a suppressor strain deficient in the assembly of the light harvesting complex, *J Biol Chem* 275, 5852-5859.
18. Haldrup, A., Naver, H., and Scheller, H. V. (1999) The interaction between plastocyanin and photosystem I is inefficient in transgenic Arabidopsis plants lacking the PSI-N subunit of photosystem I., *Plant Journal* 17, 689-698.
19. Fischer, N., Boudreau, E., Hippler, M., Drepper, F., Haehnel, W., and Rochaix, J. D. (1999) A large fraction of PsuF is nonfunctional in photosystem I complexes lacking the PsuJ subunit, *Biochem.* 38, 5546-5552.
20. Jensen, P. K., Bassi, R., Boekema, E. J., Dekker, J. P., Jansson, S., Leister, D., Robinson, C., and Scheller, H. V. (2007) Structure, function and regulation of plant photosystem I., *Biochimica Biophysica Acta* 1767, 335-352.
21. Jordan, P., Fromme, P., Witt, H. T., Klukas, O., Saenger, W., and Krauss, N. (2001) Three-dimensional structure of cyanobacterial photosystem I at 2.5 Å resolution, *Nature* 411, 909-917.
22. Amunts, A., Drory, O., and Nelson, N. (2007) The structure of a plant photosystem I supercomplex at 3.4 Å resolution, *Nature* 447, 58-63.
23. Amunts, A., and Nelson, N. (2008) Functional organization of a plant Photosystem I: evolution of a highly efficient photochemical machine, *Plant Physiol Biochem* 46, 228-237.
24. Grotjohann, I., and Fromme, P. (2005) Structure of cyanobacterial photosystem I., *Photosynth Res* 85, 51-72.

25. Saito, K., and Ishikita, H. (2011) Cationic state distribution over the P700 chlorophyll pair of PSI., *Biophys J* 101, 2018-2025.
26. Krabben, L., Schlodder, E., Jordan, R., Carbonera, D., Giacometti, G., Lee, H., Webber, A. N., and Lubitz, W. (2000) Influence of the axial ligands on the spectral properties of P700 of photosystem I: a study of site-directed mutants, *Biochem.* 39, 13012-13025.
27. Lubitz, W., Lendzian, F., and Bittl, R. (2002) Radicals, radical pairs and triplet states in photosynthesis, *Acc Chem Res* 35, 313-320.
28. Giera, W., Ramesh, V. M., Webber, A. N., van Stokkum, I., van Grondelle, R., and Gibasiewicz, K. (2010) Effect of the P700 pre-oxidation and point mutations near A<sub>0</sub> on the reversibility of the primary charge separation in Photosystem I from *Chlamydomonas reinhardtii*, *Biochim Biophys Acta* 1797, 106-112.
29. Holzwarth, A. R., Muller, M. G., Niklas, J., and Lubitz, W. (2006) Ultrafast transient absorption studies on photosystem I reaction centers from *Chlamydomonas reinhardtii*. 2: mutations near the P700 reaction center chlorophylls provide new insight into the nature of the primary electron donor, *Biophys J* 90, 552-565.
30. Hooper, J. K., Eggink, L. L., and Shen, M. (2007) Chlorophylls, ligands and assembly of light harvesting complexes in chloroplasts., *Photosynth Res* 94.
31. Sun, J., Hao, S., Radle, M., Xu, W., Shelaev, I. V., Nadtochenko, V. A., Shuvalov, V. A., Semenov, A. Y., Gordon, H., Est, A. v. d., and Golbeck, J. H. (2014) Evidence that histidine forms a coordination bond to the A<sub>0A</sub> and A<sub>0B</sub> chlorophylls and a second H-bond to the A<sub>1A</sub> and A<sub>1B</sub> phylloquinones in M688H<sub>PSaA</sub> and MH668H<sub>PSaB</sub> variants of *Synechocystis* sp. PCC 6803., *Biochimica et Biophysica Acta (BBA) - Bioenergetics* 1837, 1362-1375.
32. Niedzwiecki, D. M., and Blankenship, R. E. (2010) Singlet and triplet excited state properties of natural chlorophylls and bacteriochlorophylls., *Photosynth Res* 106, 227-238.
33. Zazubovich, V., Matsuzaki, S., Johnson, T. W., Hayes, J. M., Chitnis, P. R., and Small, G. J. (2002) Red antenna states of photosystem I from cyanobacterium *Synechococcus elongatus*: a spectral hole burning study., *Chemical Physics* 275, 47-59.
34. Slavov, C., El-Mohsnawy, E., Rogner, M., and Holzwarth, A. R. (2009) Trapping kinetics in isolated cyanobacterial PSI complexes., *Chemical Physics* 357, 163-170.

35. Slavov, C., Ballottari, M., Morosinotto, T., Bassi, R., and Holzwarth, A. R. (2008) Trap-limited charge separation kinetics in higher plant photosystem I complexes, *Biophys J* 94, 3601-3612.
36. Karapetyan, N. V., Bolychevtseva, Y. V., Yurina, N. P., Terekhova, I. V., Shubin, V. V., and Brecht, M. (2014) Long-Wavelength Chlorophylls in Photosystem I of Cyanobacteria: Origin, Localization, and Functions., *Biochemistry (Moscow)* 79, 213-220.
37. Schlodder, E., Lendzian, F., Meyer, J., Cetin, M., Brecht, M., Renger, T., and Karapetyan, N. V. (2014) Long-wavelength limit of photochemical energy conversion in photosystem I, *J. Am. Chem. Soc.*
38. Schlodder, E., Vladimir V. Shubin, S., El-Mohsanavey, E., and Karapetyan, N. (2007) Steady state and transient polarized absorption spectroscopy of Photosystem I complex from the cyanobacteria *Arthrospira platensis* and thermosynechococcus elongatus., *Biochim. Biophys. Acta* 1767, 732-741.
39. Karapetyan, N. V. (2008) Protective dissipation of excess absorbed energy by photosynthetic apparatus of cyanobacteria: role of antenna terminal emitters., *Photosynth. Res.* 97, 195-204.
40. Schlodder, E., Cetin, M., Byrdin, M., Terekhova, I. V., and Karapetyan, N. V. (2005)  $P_{700}^{+}$  and  $^3P_{700}$  induced quenching of the fluorescence at 760 nm in trimeric Photosystem I complexes from the cyanobacterium *Arthrospira platensis*. , *Biochim. Biophys. Acta* 1706, 53-67.
41. Takahashi, H., Clowe, S., Wollman, F. A., Vallon, O., and Rappaport, F. (2013) Cyclic electron flow is redox-controlled but independent of state transition, *Nat Commun* 4, 1954.
42. Rochaix, J.-D. (2011) Regulation of photosynthetic electron transport., *Biochimica et Biophysica Acta (BBA)* 1807, 375-383.
43. Holzwarth, A. R., Muller, M. G., Niklas, J., and Lubitz, W. (2005) Charge recombination fluorescence in photosystem I reaction centers from *Chlamydomonas reinhardtii*, *J Phys Chem B* 109, 5903-5911.
44. Byrdin, M., Jordan, P., Krauss, N., Fromme, P., Stehlik, D., and Schlodder, E. (2002) Light harvesting in photosystem I: Modeling based on the 2.5-Å structure of photosystem I from *Synechococcus elongatus*, *Biophysical Journal* 83, 433-457.
45. Adolphs, J., Müh, F., Madjet, M. E.-A., Busch, M. S. a., and Renger, T. (2010) Structure-Based Calculations of Optical Spectra of Photosystem I Suggest an Asymmetric Light-Harvesting Process, *J. Am. Chem. Soc.* 132, 3331-3343.

46. Blankenship, R. E. (2014) *Molecular Mechanism of Photosynthesis*, 2nd ed., Wiley-Blackwell Publishing, Hoboken, New Jersey.
47. Moser, C. C., Anderson, J. L. R., and Dutton, P. L. (2010) Guidelines for tunneling in enzymes, *Biochim. Biophys. Acta* 1797, 1573-1586.
48. Sétif, P., and Brettel, K. (1993) Forward electron transfer from phyloquinone A<sub>1</sub> to iron-sulfur centers in spinach photosystem I, *Biochem.* 32, 7846-7854.
49. Joliot, P., and Joliot, A. (1999) In vivo analysis of the electron transfer within photosystem I: are the two phyloquinones involved?, *Biochem.* 38, 11130-11136.
50. Guergova-Kuras, M., Boudreaux, B., Joliot, A., Joliot, P., and Redding, K. (2001) Evidence for two active branches for electron transfer in photosystem I, *Proc Natl Acad Sci U S A* 98, 4437-4442.
51. Santabarbara, S., Reifschneider, K., Jasaitis, A., Gu, F., Agostini, G., Carbonera, D., Rappaport, F., and Redding, K. E. (2010) Interquinone electron transfer in photosystem I as evidenced by altering the hydrogen bond strength to the phyloquinone(s), *J Phys Chem B* 114, 9300-9312.
52. Srinivasan, N., Santabarbara, S., Rappaport, F., Carbonera, D., Redding, K., van der Est, A., and Golbeck, J. H. (2011) Alteration of the H-bond to the A(1A) phyloquinone in Photosystem I: influence on the kinetics and energetics of electron transfer, *J Phys Chem B* 115, 1751-1759.
53. Li, Y., van der Est, A., Lucas, M. G., Ramesh, V. M., Gu, F., Petrenko, A., Lin, S., Webber, A. N., Rappaport, F., and Redding, K. (2006) Directing electron transfer within Photosystem I by breaking H-bonds in the cofactor branches, *Proc Natl Acad Sci U S A* 103, 2144-2149.
54. Santabarbara, S., Kuprov, I., Poluektov, O., Casal, A., Russell, C. A., Purton, S., and Evans, M. C. (2010) Directionality of electron-transfer reactions in photosystem I of prokaryotes: universality of the bidirectional electron-transfer model, *J Phys Chem B* 114, 15158-15171.
55. van der Est, A., Chirico, S., Karyagina, I., Cohen, R., Shen, G., and Golbeck, J. (2010) Alteration of the Axial Met Ligand to Electron Acceptor A<sub>0</sub> in Photosystem I: An Investigation of Electron Transfer at Different Temperatures by Multifrequency Time-Resolved and CW EPR., *Appl Magn Reson* 37, 103-121.
56. Savitsky, A., Gupta, O., Mamedov, M., Golbeck, J., Tikhonov, A., Mobius, K., and Sememov, A. Y. (2010) Alteration of the axial ligand to electron acceptor A<sub>0</sub> in Photosystem I: Effect on the generation of P700+•A1-• radical pairs as studied by W-band transient EPR., *Appl Magn Reson* 37, 85-102.

57. Milanovsky, G. E., Ptushenko, V. V., Golbeck, J. H., Semenov, A. Y., and Cherepanov, D. A. (2014) Molecular dynamics study of the primary charge separation reactions in Photosystem I: Effect of the replacement of the axial ligands to the electron acceptor A<sub>0</sub>., *Biochimica et Biophysica Acta (BBA)* XXXX, XX-XX.
58. Käß, H., Fromme, P., Witt, H. T., and Lubitz, W. (2001) Orientation and electronic structure of the primary donor radical cation P700<sup>•+</sup> in photosystem I: A single crystals EPR and ENDOR study, *Journal of Physical Chemistry B* 105, 1225-1239.
59. Webber, A. N., and Lubitz, W. (2001) P700: the primary electron donor of photosystem I, *Biochim Biophys Acta* 1507, 61-79.
60. Li, Y., Lucas, M.-G., Konovalova, T., Abbott, B., MacMillan, F., Petrenko, A., Sivakumar, V., Wang, R., Hastings, G., Gu, F., van Tol, J., Brunel, L.-C., Timkovich, R., Rappaport, F., and Redding, K. (2004) Mutation of the Putative Hydrogen-Bond Donor to P700 of Photosystem I, *Biochem.* 43, 12634-12647.
61. Ishikita, H., Saenger, W., Biesiadka, J., Loll, B., and Knapp, E. W. (2006) How photosynthetic reaction centers control oxidation power in chlorophyll pairs P680, P700 and P870., *Proc Natl Acad Sci U S A* 103, 9855-9860.
62. Müller, M. G., Niklas, J., Lubitz, W., and Holzwarth, A. R. (2003) Ultrafast transient absorption studies on photosystem I reaction centers from *Chlamydomonas reinhardtii* I. A new interpretation of the energy trapping and early electron transfer steps in photosystem I, *Biophys J* 85, 3899-3922.
63. Ptushenko, V. V., Cherepanov, D. A., Krishtalik, L. I., and Semenov, A. Y. (2008) Semi-continuum electrostatic calculations of redox potentials in photosystem I., *Photosynth Res.* 97, 55-74.
64. Shelaev, I. V., Gostev, F. E., Mamedov, M. D., Sarkisov, O. M., Nadtochenko, V. A., Shuvalov, V. A., and Semenov, A. Y. (2010) Femtosecond primary charge separation in *Synechocystis* sp. PCC 6803 photosystem I, *Biochimica et Biophysica Acta (BBA)* 1797, 1410-1420.
65. Semenov, A. Y., Shelaev, I. V., Gostev, F. E., Mamedov, M. D., Shuvalov, V. A., Sarkisov, O. M., and Nadtochenko, V. A. (2012) Primary steps of electron and energy transfer in photosystem I: Effect of excitation pulse wavelength., 77, 1011-1020.
66. Donato, M. D., Stahl, A. D., Stokkum, I. H. M. V., Grondelle, R. V., and Groot, M. L. (2011) Cofactors involved in light driven charge separation in Photosystem I identified by subpicosecond infrared spectroscopy., *Biochem.* 50, 480-490.

67. Rappaport, F., Diner, B. A., and Redding, K. (2006) Optical measurements of secondary electron transfer in Photosystem I, In *Photosystem I: The Plastocyanin:Ferredoxin Oxidoreductase in Photosynthesis* (Golbeck, J., Ed.), pp 223-244, Kluwer Academic Publishers, Dordrecht.
68. Ramesh, V. M., Gibasiewicz, K., Lin, S., Bingham, S. E., and Webber, A. N. (2004) Bidirectional Electron Transfer in Photosystem I: Accumulation of A<sup>0</sup>- in A-Side or B-Side Mutants of the Axial Ligand to Chlorophyll A<sub>0</sub>, *Biochem.* **43**, 1369-1375.
69. Ramesh, V. M., Gibasiewicz, K., Lin, S., Bingham, S. E., and Webber, A. N. (2007) Replacement of the methionine axial ligand to the primary electron acceptor A(0) slows the A(0)(-) reoxidation dynamics in Photosystem I, *Biochim Biophys Acta* **1767**, 151-160.
70. Giera, W., Gibasiewicz, K., Ramesh, V. M., Lin, S., and Webber, A. (2009) Electron transfer from A<sub>0</sub> to A<sub>1</sub> in Photosystem I from *Chlamydomonas reinhardtii* occurs in both the A and B branch with 25-30-ps lifetime, *Phys Chem Chem Phys* **11**, 5186-5191.
71. Berthold, T., Gromoff, E. D. V., Santabarbara, S., Stehle, P., Link, G., Poluektov, O. G., Heathcote, P., Beck, C. F., Thurnauer, M. C., and Kothe, G. (2012) Exploring the Electron Transfer Pathways in Photosystem I by High-Time-Resolution Electron Paramagnetic Resonance: Observation of the B-side Radical Pair P<sub>700</sub><sup>+</sup>A<sub>1B</sub><sup>-</sup> in Whole Cells of the Deuterated Green Alga *Chlamydomonas reinhardtii* at Cryogenic Temperatures., *Journal of American Chemical Society* **134**, 5563-5576.
72. Milanovsky, G. E., Ptushenko, V. V., Golbeck, J. H., Semenov, A. Y., and Cherepanov, D. A. (2014) Molecular dynamics study of the primary charge separation reactions in Photosystem I: Effect of the replacement of the axial ligands to the electron acceptor A<sub>0</sub>., *Biochimica et Biophysica Acta (BBA) - Bioenergetics* **1837**, 1472-1483.
73. Picard, V., Ersdal-Badju, E., Lu, A., and Bock, S. C. (1994) A rapid and efficient one-tube PCR-based mutagenesis technique using *Pfu* DNA polymerase., *Nucl. Acids Res.* **22**, 2587-2591.
74. Gulis, G., Narasimhulu, K. V., Fox, L. N., and Redding, K. E. (2008) Purification of His(6)-tagged Photosystem I from *Chlamydomonas reinhardtii*, *Photosynth Res.*
75. Vassiliev, I. R., Jung, Y. S., Mamedov, M. D., Semenov, A., and Golbeck, J. H. (1997) Near-IR absorbance changes and electrogenic reactions in the microsecond-to-second time domain in Photosystem I, *Biophys J* **72**, 301-315.

76. Shinkarev, V. P., Vassiliev, I. R., and Golbeck, J. H. (2000) A kinetic assessment of the sequence of electron transfer from F-X to F-A and further to F-B in photosystem I: The value of the equilibrium constant between F-X and F-A, *Biophysical Journal* 78, 363-372.
77. Witt, H., Bordignon, E., Carbonera, D., Dekker, J. P., Karapetyan, N., Teutloff, C., Webber, A., Lubitz, W., and Schlodder, E. (2003) Species-specific differences of the spectroscopic properties of P700: analysis of the influence of non-conserved amino acid residues by site-directed mutagenesis of photosystem I from *Chlamydomonas reinhardtii*, *J Biol Chem* 278, 46760-46771.
78. Redding, K., MacMillan, F., Leibl, W., Brettel, K., Hanley, J., Rutherford, A. W., Breton, J., and Rochaix, J. D. (1998) A systematic survey of conserved histidines in the core subunits of Photosystem I by site-directed mutagenesis reveals the likely axial ligands of P700, *EMBO J* 17, 50-60.
79. Ramesh, V. M., Guergova-Kuras, M., Joliot, P., and Webber, A. N. (2002) Electron transfer from plastocyanin to the photosystem I reaction center in mutants with increased potential of the primary donor in *Chlamydomonas reinhardtii*, *Biochem.* 41, 14652-14658.
80. Xu, W., Chitnis, P. R., Valieva, A., van der Est, A., Brettel, K., Guergova-Kuras, M., Pushkar, Y. N., Zech, S. G., Stehlik, D., Shen, G., Zybailov, B., and Golbeck, J. H. (2003) Electron transfer in cyanobacterial photosystem I: II. Determination of forward electron transfer rates of site-directed mutants in a putative electron transfer pathway from A0 through A1 to FX, *J Biol Chem* 278, 27876-27887.
81. Muller, M. G., Lambrev, P., Reus, M., Wientjes, E., Croce, R., and Holzwarth, A. R. (2010) Singlet energy dissipation in the photosystem II light-harvesting complex does not involve energy transfer to carotenoids, *Chemphyschem* 11, 1289-1296.
82. van Stokkum, I. H. M., Larsen, D. S., and van Grondelle, R. (2004) Global and target analysis of time-resolved spectra, *Biochimica et Biophysica Acta (BBA) - Bioenergetics* 1657, 82-104.
83. Chauvet, A., Dashdorj, N., Golbeck, J. H., Johnson, T. W., and Savikhin, S. (2012) Spectral resolution of the primary electron acceptor A0 in Photosystem I, *J Phys Chem B* 116, 3380-3386.
84. Giera, W., Szewczyk, S., McConnell, M. D., Snellenburg, J. J., Redding, K. E., Grondelle, R. V., and Gibasiewicz, K. (2014) Excitation dynamics in Photosystem I from *Chlamydomonas reinhardtii*. Comparative studies of isolated complexes and whole cells., *Biochimica et Biophysica Acta (BBA)* 1837, 1756-1768.

85. van der Est, A., Valieva, A. I., Kandrashkin, Y. E., Shen, G., Bryant, D. A., and Golbeck, J. H. (2004) Removal of PsaF alters forward electron transfer in photosystem I: evidence for fast reoxidation of QK-A in subunit deletion mutants of *Synechococcus* sp. PCC 7002, *Biochem.* 43, 1264-1275.
86. Cohen, R. O., Shen, G., Golbeck, J. H., Xu, W., Chitnis, P. R., Valieva, A. I., van der Est, A., Pushkar, Y., and Stehlik, D. (2004) Evidence for asymmetric electron transfer in cyanobacterial photosystem I: analysis of a methionine-to-leucine mutation of the ligand to the primary electron acceptor A0, *Biochem.* 43, 4741-4754.
87. Byrdin, M., Santabarbara, S., Gu, F., Fairclough, W. V., Heathcote, P., Redding, K., and Rappaport, F. (2006) Assignment of a kinetic component to electron transfer between iron-sulfur clusters F<sub>X</sub> and F<sub>A/B</sub> of Photosystem I, *Biochim Biophys Acta* 1757, 1529-1538.
88. van der Est, A. (2009) Transient EPR: using spin polarization in sequential radical pairs to study electron transfer in photosynthesis, *Photosyn. Res.* 102, 335-347.
89. Boudreaux, B., MacMillan, F., Teutloff, C., Agalarov, R., Gu, F., Grimaldi, S., Bittl, R., Brettel, K., and Redding, K. (2001) Mutations in both sides of the photosystem I reaction center identify the phylloquinone observed by electron paramagnetic resonance spectroscopy, *J Biol Chem* 276, 37299-37306.
90. van der Est, A. (2006) Electron transfer involving phylloquinone in Photosystem I, In *Photosystem I: The Plastocyanin:Ferredoxin Oxidoreductase in Photosynthesis* (Golbeck, J., Ed.), Kluwer Academic Publishers, Dordrecht.
91. Pushkar, N. Y., Karyagina, I., Stehlik, D., Brown, S., and Est, A. v. d. (2005) Recruitment of a foreign quinone into the A<sub>1</sub> site of Photosystem I, *The Journal of Biological Chemistry* 280.
92. Niklas, J., Epel, B., Antonkine, M. L., Sinnecker, S., Pandelia, M. E., and Lubitz, W. (2009) Electronic structure of the quinone radical anion A1<sup>•-</sup> of photosystem I investigated by advanced pulse EPR and ENDOR techniques, *J Phys Chem B* 113, 10367-10379.
93. Kandrashkin, Y. E., Vollmann, W., Stehlik, D., Salikhov, K., and Van Der Est, A. (2002) The magnetic field dependence of the electron spin polarization in consecutive spin correlated radical pairs in type I photosynthetic reaction centers, *Molecular Physics* 100, 1431-1443.
94. Srinivasan, N., Karyagina, I., Bittl, R., van der Est, A., and Golbeck, J. H. (2009) Role of the hydrogen bond from Leu722 to the A1A phylloquinone in photosystem I, *Biochem.* 48, 3315-3324.



95. Carmieli, R., Mi, Q., Ricks, A. B., Giacobbe, E. M., Mickley, S. M., and Wasielewski, M. R. (2009) Direct measurement of photoinduced charge separation distances in donor-acceptor systems for artificial photosynthesis using OOP-ESEEM., *Journal of American Chemical Society* 131, 8372-8373.
96. Bittl, R., and Weber, S. (2005) Transient radical pairs studied by time-resolved EPR., *Biochimica et Biophysica Acta (BBA)* 1707, 117-126.
97. Bittl, R., and Zech, S. G. (2001) Pulsed EPR spectroscopy on short-lived intermediates in Photosystem I, *Biochim Biophys Acta* 1507, 194-211.
98. Santabarbara, S., Kuprov, I., Fairclough, W. V., Purton, S., Hore, P. J., Heathcote, P., and Evans, M. C. (2005) Bidirectional electron transfer in photosystem I: determination of two distances between P700<sup>+</sup> and A1<sup>-</sup> in spin-correlated radical pairs, *Biochem.* 44, 2119-2128.
99. Dzuba, S. A., Hara, H., Kawamori, A., Iwaki, M., Itoh, S., and Tsvetkov, Y. D. (1997) Electron spin echo of spin-polarized radical pairs in intact and quinone-reconstituted plant photosystem I reaction centers, *Chem. Phys. Lett.* 264, 238-244.
100. Santabarbara, S., Kuprov, I., Hore, P. J., Casal, A., Heathcote, P., and Evans, M. C. (2006) Analysis of the spin-polarized electron spin echo of the [P700<sup>+</sup> A1<sup>-</sup>] radical pair of photosystem I indicates that both reaction center subunits are competent in electron transfer in cyanobacteria, green algae, and higher plants, *Biochem.* 45, 7389-7403.
101. Frank, H. A., McLean, M. B., and Sauer, K. (1979) Triplet states in photosystem I of spinach chloroplasts and subchloroplast particles, *Proc Natl Acad Sci U S A* 76, 5124-5128.
102. Ramesh, V. M., Gibasiewicz, K., Lin, S., Bingham, S. E., and Webber, A. N. (2004) Bidirectional Electron Transfer in Photosystem I: Accumulation of A0<sup>-</sup> in A-Side or B-Side Mutants of the Axial Ligand to Chlorophyll A0<sup>+</sup>, *Biochem.* 43, 1369-1375.
103. Santabarbara, S., Heathcote, P., and Evans, M. C. (2005) Modelling of the electron transfer reactions in Photosystem I by electron tunnelling theory: the phylloquinones bound to the PsaA and the PsaB reaction centre subunits of PS I are almost isoenergetic to the iron-sulfur cluster F<sub>X</sub>, *Biochim Biophys Acta* 1708, 283-310.
104. Witt, H., Schlodder, E., Teutloff, C., Niklas, J., Bordignon, E., Carbonera, D., Kohler, S., Labahn, A., and Lubitz, W. (2002) Hydrogen bonding to P700: site-directed mutagenesis of threonine A739 of photosystem I in *Chlamydomonas reinhardtii*, *Biochem.* 41, 8557-8569.

105. Agalarov, R., and Brettel, K. (2003) Temperature dependence of biphasic forward electron transfer from the phylloquinone(s) A(1) in photosystem I: only the slower phase is activated, *Biochim. Biophys. Acta-Bioenerg.* 1604, 7-12.
106. Schlodder, E., Falkenberg, K., Gergeleit, M., and Brettel, K. (1998) Temperature dependence of forward and reverse electron transfer from A1- , the reduced secondary electron acceptor in photosystem I, *Biochem.* 37, 9466-9476.
107. Mula, S., Savitsky, A., Mobius, K., Lubitz, W., Golbeck, J., Mamedov, M. D., Semenov, A. Y., and Est, A. v. d. (2012) Incorporation of a high potential quinone reveals that electron transfer in Photosystem I becomes highly asymmetric at low temperature., *Photochemical and Photobiological Sciences* 11, 946-956.
108. Anna, J. M., Ostroumov, E. E., Maghlaoui, K., Barber, J., and Scholes, G. D. (2012) Two-Dimensional Electronic Spectroscopy Reveals Ultrafast Downhill Energy Transfer in Photosystem I Trimers of the Cyanobacterium *Thermosynechococcus elongatus*., *J. Phys. Chem. Lett.* 3, 3677-3684.
109. Bautista, J. A., Rappaport, F., Guergova-Kuras, M., Cohen, R. O., Golbeck, J. H., Wang, J. Y., Beal, D., and Diner, B. A. (2005) Biochemical and biophysical characterization of photosystem I from phytoene desaturase and zeta-carotene desaturase deletion mutants of *Synechocystis* sp. PCC 6803: Evidence for PsaA- and PsaB-side electron transport in cyanobacteria, *J Biol Chem* 280, 20030-20041.
110. Zybailov, B. L. (2003) Modified quinone acceptors in photosystem I., In *Biochemistry and Molecular Biology*, p 235, The Pennsylvania State University, College State Park.
111. Wang, R., Sivakumar, V., Li, Y., Redding, K., and Hastings, G. (2003) Mutation induced modulation of hydrogen bonding to P700 studied using FTIR difference spectroscopy, *Biochem.* 42, 9889-9897.
112. Wang, R., Sivakumar, V., Johnson, T. W., and Hastings, G. (2004) FTIR difference spectroscopy in combination with isotope labeling for identification of the carbonyl modes of P700 and P700+ in photosystem I, *Biophys J* 86, 1061-1073.
113. Santabarbara, S., Bailleul, B., Redding, K., Barber, J., Rappaport, F., and Telfer, A. (2012) Kinetics of phyllosemiquinone oxidation in the Photosystem I reaction centre of *Acaryochloris marina*, *Biochim Biophys Acta* 1817, 328-335.
114. Santabarbara, S., Jasaitis, A., Byrdin, M., Gu, F., Rappaport, F., and Redding, K. (2008) Additive effect of mutations affecting the rate of phylloquinone reoxidation and directionality of electron transfer within Photosystem I, *Photobiochemistry and Photobiology* 84, 1381-1387.

115. Luthra, R., Jasaitis, A., Rappaport, F., and Redding, K. (2007) Directionality in Photosystem I: A preliminary study of the PsaA-A684D mutant, *Photosynth Res* 91, 167-171.
116. Agalarov, R., Byrdin, M., Rappaport, F., Shen, G., Bryant, D., Est, A. v. d., and Golbeck, J. (2008) Removal of the PsaF Polypeptide Biases Electron Transfer in Favor of the PsaB Branch of Cofactors in Triton X-100 Photosystem I Complexes from *Synechococcus* sp. PCC 7002., *Photochem. Photobiol.* 84, 1371-1380.
117. Niklas, J., Gupta, O., Epel, B., Lubitz, W., and Antonkine, M. L. (2010) Investigation of the Stationary and Transient A(1) Radical in Trp --> Phe Mutants of Photosystem I, *Appl Magn Reson* 38, 187-203.
118. Est, A. v. d., (Ed.) (2006) *Electron Transfer Involving Phylloquinone in Photosystem I*, Vol. 24, Springer, Dordrecht, The Netherlands.
119. Golbeck, J., (Ed.) (2006) *Advances in Photosynthesis and Respiration. Photosystem I, the light driven plastocyanin: ferredoxin oxidoreductase.*, Vol. 24, Springer, Dordrecht, The Netherlands.
120. Hastings, G., Ramesh, V. M., Wang, R., Sivakumar, V., and Webber, A. (2001) Primary donor photo-oxidation in photosystem I: a re-evaluation of (P700(+)-P700) Fourier transform infrared difference spectra, *Biochem.* 40, 12943-12949.
121. Breton, J., Navedryk, E., and Leibl, W. (1999) FTIR study of the primary electron donor of photosystem I (P700) revealing delocalization of the charge in P700+ and localization of the triplet character in 3P700, *Biochem.* 38, 11585-11592.
122. Breton, J. (2001) Fourier transform infrared spectroscopy of primary electron donors in type I photosynthetic reaction centers, *Biochim Biophys Acta* 1507, 180-193.
123. Breton, J., Chitnis, P. R., and Pantelidou, M. (2005) Evidence for hydrogen bond formation to the PsaB chlorophyll of P700 in photosystem I mutants of *Synechocystis* sp. PCC 6803, *Biochem.* 44, 5402-5408.
124. Bender, S. L., and Barry, B. A. (2008) Light-Induced dynamics in photosystem I electron transfer., *Biophysical Journal* 95, 3927-3934.
125. Barth, A. (2000) The infrared absorption of amino acid side chains., *Prog. Biophys. Mol. Biol.* 74, 141-173.
126. Nie, B., Stutzman, J., and Xie, A. (2005) A Vibrational Spectral Marker for Probing the Hydrogen-Bonding Status of Protonated Asp and Glu Residues., *Biophys J.* 88, 2833-2847.

127. Kong, J., and Yu, S. (2007) Fourier transform infrared spectroscopic analysis of protein secondary structure., *Acta Biochimica et Biophysica Sinica* 39, 549-559.
128. Gunner, M. R., Mao, J., Song, Y., and Kim, J. (2006) Factors influencing the energetics of electron and proton transfers in proteins. What can be learned from calculations ?, *Biochim Biophys Acta* 1757, 942-968.
129. Barth, A. (2007) Infrared spectroscopy of proteins, *Biochimica et Biophysica Acta (BBA)* 1767, 1073-1101.
130. Ali, K., Santabarbara, S., Heathcote, P., Evans, M. C., and Purton, S. (2006) Bidirectional electron transfer in photosystem I: replacement of the symmetry-breaking tryptophan close to the PsaB-bound phylloquinone A1B with a glycine residue alters the redox properties of A1B and blocks forward electron transfer at cryogenic temperatures, *Biochim Biophys Acta* 1757, 1623-1633.
131. Melkozernov, A. N., Su, H., Lin, S., Bingham, S., Webber, A. N., and Blankenship, R. E. (1997) Specific mutation near the primary donor in photosystem I from *Chlamydomonas reinhardtii* alters the trapping time and spectroscopic properties of P700, *Biochem.* 36, 2898-2907.
132. Redding, K. (2008) Photosystem I, In *The Chlamydomonas Sourcebook* (Stern, D. B., Ed.), pp 541-572, Academic Press.
133. Heathcote, P., Muhiuddin, I., Rigby, S., Carter, S., Purton, S., Gu, F., Redding, K., and Evans, M. (2001) Evidence for two functional phylloquinones in Photosystem I from *Chlamydomonas reinhardtii*., In *PS2001 proceedings: 12th International Congress on Photosynthesis*, CSIRO Publishing, Brisbane.
134. Redding, K., and van der Est, A. (2006) The Directionality of Electron Transfer in Photosystem I, In *Photosystem I: The Plastocyanin:Ferredoxin Oxidoreductase in Photosynthesis* (Golbeck, J., Ed.), pp 413-437, Kluwer Academic Publishers, Dordrecht.
135. Santabarbara, S., Galuppini, L., and Casazza, A. P. (2010) Bidirectional electron transfer in the reaction centre of photosystem I, *J Integr Plant Biol* 52, 735-749.
136. Nelson, N., and Yocum, C. (2006) Structure and function of photosystems I and II., *Annu. Rev. Plant Biol.* 57, 521-565.
137. Giera, W., Ramesh, V. M., Webber, A. N., van Stokkum, I., van Grondelle, R., and Gibasiewicz, K. (2010) Effect of the P700 pre-oxidation and point mutations near A0 on the reversibility of the primary charge separation in Photosystem I from *Chlamydomonas reinhardtii*, *Biochimica et Biophysica Acta (BBA) - Bioenergetics* 1797, 106-112.

138. Donato, M. D., and Groot, M. L. (2014) Ultrafast infrared spectroscopy in photosynthesis, *Biochimica et Biophysica Acta (BBA)* XX, XX-XX.
139. van Stokkum, I. H., Desquillet, T. E., van der Weij-de Wit, C. D., Snellenburg, J. J., van Grondelle, R., Thomas, J. C., Dekker, J. P., and Robert, B. (2013) Energy transfer and trapping in red-chlorophyll-free photosystem I from *Synechococcus* WH 7803, *J Phys Chem B* 117, 11176-11183.
140. Kompanets, V., Shubin, V., Terekhova, I., Kotova, E., Kozlovsky, V., Novoderezhkin, V., Chekalin, S., Karapetyan, N., and Razjivin, A. (2014) Red chlorophyll excitation dynamics in *Arthrospira platensis* Photosystem I trimeric complexes as studied by femtosecond transient absorption spectroscopy., *FEBS (Fed. Eur. Biochem. Soc.) Lett.* 588, 3441-3444.
141. Xu, W., Chitnis, P., Valieva, A., van der Est, A., Pushkar, Y. N., Krzystyniak, M., Teutloff, C., Zech, S. G., Bittl, R., Stehlik, D., Zybailov, B., Shen, G., and Golbeck, J. H. (2003) Electron transfer in cyanobacterial photosystem I: I. Physiological and spectroscopic characterization of site-directed mutants in a putative electron transfer pathway from A0 through A1 to FX, *J Biol Chem* 278, 27864-27875.
142. Warren, P. V., Golbeck, J. H., and Warden, J. T. (1993) Charge recombination between P700<sup>+</sup> and A1<sup>-</sup> occurs directly to the ground state of P700 in a photosystem I core devoid of FX, FB, and FA, *Biochem.* 32, 849-857.
143. Nakamura, A., Suzawa, T., Kato, Y., and Watanabe, T. (2011) Species dependence of the redox potential of the primary electron donor p700 in photosystem I of oxygenic photosynthetic organisms revealed by spectroelectrochemistry, *Plant Cell Physiol* 52, 815-823.
144. McConnell, M. D., Cowgill, J. B., Baker, P. L., Rappaport, F., and Redding, K. E. (2011) Double reduction of plastoquinone to plastoquinol in photosystem 1, *Biochem.* 50, 11034-11046.
145. Mula, S., McConnell, M. D., Ching, A., Zhao, N., Gordon, H. L., Hastings, G., Redding, K. E., and van der Est, A. (2012) Introduction of a Hydrogen Bond between Phylloquinone PhQ(A) and a Threonine Side-Chain OH Group in Photosystem I, *J Phys Chem B* 116, 14008-14016.
146. Ratsep, M., Johnson, T. W., Chitnis, P. R., and Small, G. J. (2000) The red absorbing chlorophyll a antenna states of Photosystem I: A hole-burning study of *Synechocystis* sp PCC 6803 and its mutants., *J. Phys .Chem. B* 104, 836-847.
147. Dutta, P. K., Lin, S., Loskutov, A., Levenberg, S., Jun, D., Saer, R., Beatty, J. T., Liu, Y., Yan, H., and Woodbury, N. (2014) Reengineering the Optical Absorption

- Cross-Section of Photosynthetic Reaction Centers., *J. Am. Chem. Soc.* 136, 4599-4604.
148. Palsson, L. O., Flemming, C., Gobets, B., van Grondelle, R., Dekker, J. P., and Schlodder, E. (1998) Energy transfer and charge separation in photosystem I: P700 oxidation upon selective excitation of the long-wavelength antenna chlorophylls of *Synechococcus elongatus*, *Biophys J* 74, 2611-2622.
  149. Schlodder, E., Hussels, M., Cetin, M., Karapetyan, N. V., and Brecht, E. (2011) Fluorescence of the various red antenna states in photosystem I complexes from cyanobacteria is affected differently by the redox state of P<sub>700</sub>., *Biochimica et Biophysica Acta (BBA)* 1807, 1423-1431.